

Spatio-temporal variation in lesser sandeel growth
and demography: causes and consequences



Agnes Olin

July 2020

A thesis submitted in partial fulfilment for the
degree of Doctor of Philosophy
in the
Faculty of Science
Department of Mathematics and Statistics
University of Strathclyde

Copyright declaration

This thesis is the result of the author's original research. It has been composed by the author and has not been previously submitted for examination which has led to the award of a degree.

The copyright of this thesis belongs to the author under the terms of the United Kingdom Copyright Acts as qualified by University of Strathclyde Regulation 3.50. Due acknowledgement must always be made of the use of any material contained in, or derived from, this thesis.

“Tobis or not tobis.”
Popp Madsen, 1994

Abstract

In large parts of the north-east Atlantic, the lesser sandeel (*Ammodytes marinus*) is an important prey for seabirds, marine mammals and fish. *A. marinus* shows strong spatio-temporal variation in abundance and size, including a sustained decline in size in several locations in the North Sea. The variation in size has been hypothesised to be mainly driven by variability in food conditions, but exploring this hypothesis on a larger spatial scale has so far been hampered by the lack of zooplankton data of sufficient spatio-temporal and taxonomic resolution. Further, the extent to which the clear spatial structure in the sandeel population is reflected in the populations of their seabird predators is not clear. This thesis aims to address these gaps and contribute to the mechanistic understanding of bottom-up effects in the zooplankton-sandeel-seabird food chain. As declines in the abundance and size of sandeels as a result of changes in their zooplankton prey are thought to have played a large role in driving the dramatic declines of seabirds in large parts of north-east Atlantic, understanding drivers and bottom-up processes in this food chain is of large importance.

The thesis first addresses the lack of the kind of high-resolution zooplankton data required for exploring the role of food conditions in sandeel dynamics. For this purpose, an approach for the generation of prey fields from spatially aggregated Continuous Plankton Recorder data is developed. The generated prey fields are then used to examine spatio-temporal patterns in sandeel food conditions, focusing mainly on the North Sea and covering the time period 1975 to 2016. In the western North Sea, there have been clear declines in both the total amount of energy available to sandeels and the abundance of small copepods, which make up a large proportion of the sandeel diet. In terms of *Calanus* spp., which are also an important part of the sandeel diet, there was no clear change in abundances of *Calanus finmarchicus* in the examined locations, while abundances of *Calanus helgolandicus* showed a clear increase in most of the study area around 2000. The average prey size generally increased over time in the western North Sea, whereas it instead declined in the north-east. Further, due to the differences in the timing of the feeding seasons, it is clear that 0 group and 1+ group sandeels experienced different prey fields, with, for example, a larger abundance of smaller copepods during the 0 group feeding season.

To explore to what extent this variation in food conditions can explain spatio-temporal variation in sandeel size, a dynamic energy budget growth model is then developed. This model estimates size daily throughout the first sandeel growth season as a function of food conditions, temperature, light conditions as well as size at

and timing of metamorphosis. The model is run in six locations: southern Iceland, the Faroes, Shetland and three locations further south in the North Sea, including Dogger Bank, the Firth of Forth and the East Central Grounds. In the more southerly locations considered, model predictions agreed well with observations in terms of long-term mean lengths and spatial differences in length and the model also reproduced a previously observed decline in length in the north-western North Sea. Agreement with observations in the Faroes and Iceland was poorer. Food conditions played the main role in driving predicted variation in size, with *Calanus* spp. being particularly important. Timing of metamorphosis also had a substantial impact on predicted sandeel size. In contrast, the direct effect of temperature was negligible.

Finally, the thesis explores the extent to which spatial patterns in the sandeel population along the coast of the UK propagate up to their seabird predators. To do this, geographical patterns in the synchrony of breeding success in black-legged kittiwake (*Rissa tridactyla*) colonies are examined in areas where sandeels are an important part of the diet. The distance between colonies was a strong determinant of between-colony synchrony, with the scale of synchrony in kittiwake and sandeel populations being similar. Further, the colonies also formed clusters with synchronous breeding success with a clear spatial pattern, which generally aligned with the spatial structure of the kittiwakes' sandeel prey.

The results of the thesis thus suggest that food conditions play an important role in driving observed variation in sandeel size. This implies that past and ongoing climate change-driven changes in the sandeel prey field are likely to have a large impact on sandeel growth rates, with potential knock-on effects on demographic rates. Further, the results suggest that processes occurring at the level of the sandeel are reflected in the structure of the local kittiwake population, indicating that the sandeels are able to mediate changes occurring at lower trophic levels up to the level of their seabird predators.

Acknowledgements

Starting with the supervisors – Neil, I have really enjoyed working with you for the past three years and I hope I have been able to pick up at least some of your creativity and your much more elegant approach to modelling along the way. Peter, your impressive knowledge of sandeels has been incredibly useful throughout the project and I have always come back from our meetings in Aberdeen with a lot of useful input (and a renewed enthusiasm for sandeels!). Mike, being able to draw on your extensive experience in pretty much all areas of marine science has come in very handy and I am also grateful to you for often providing a more sceptical perspective on my work. Ruedi, throughout the past three years you have been endlessly supportive, always taking the time to respond to long emails, have multiple-hour meetings and read my drafts more carefully than I do myself. I also appreciate you making sure that I got to see some birds once in a while! I could not wish for better supervisors and I very much hope we will continue working together.

This thesis builds on data collected by a large group of people. I am very grateful to everyone who has contributed data to the Seabird Monitoring Programme, giving me a large amount of kittiwake data to play with. Will Miles and Martin Heubeck deserve a special mention for giving me access to the SOTEAG dataset which has provided fuel for several masters and side projects – always with very helpful input from both Will and Martin. Sarah Wanless and Francis Daunt have allowed me to use not only their kittiwake data, but also their sandeel dataset. They have also shared a lot of their long experience working with seabirds and sandeels – which I am very grateful for. I am also grateful to John Speakman for conducting the body composition analysis on the sandeels collected by the puffins. Sandeel data have also been provided by many other people – including Peter, Simon Greenstreet, Espen Johnsen, Valur Bogason and Helga Bára Mohr Vang. Mikael van Deurs deserves a special mention and has shared not only data on sandeel length and stomach content but also a lot of very useful feedback. Moving down the food chain – David Johns has been a great contact over at MBA, putting the CPR dataset together, answering my many questions about it and providing useful input throughout. Margarita Machairopoulou at Marine Scotland Science also provided some very helpful feedback on using the Stonehaven dataset. In addition to the people mentioned here I am aware that the datasets used in this thesis are the product of the communal effort of many lab technicians, field assistants, fishers and students – and I am grateful to each one.

The marine group at Strathclyde, and especially the Banas sub-group – Soizic, Euan, Laura, Hoa, Trevor, Paul, Fabian – has been a really great group to be part of for the last few years and I hope we will stay in touch. Alan – not only did you lay the whole foundation for my project, but you also provided great support in handing the work over as well as useful input throughout. Special thanks should also go to Fabian for saving me from spending days on Stack Overflow multiple times and for also being a meticulous proof-reader during the final stages. Finally, as part of the Strathclyde cluster, Linda, our runs have ensured I stayed sane during the PhD.

BAHCM has also been a great institute and community to be part of for the last three years. Diana, Hans, Marco, Katia, Sara, Michele – I am going to miss all the lunches, Friday night dinners and Wednesday coffees (and more recently awkward zoom workouts). You have made the whole experience a lot better and I hope you will all come visit in Stockholm. Teteh – I will miss you most of all, I cannot think of a better person to be locked into a flat with for several months.

My friends back home also deserve a mention – especially Frida who has received close to hour-by-hour updates during the last three years and always responded with consistent (but supportive) pessimism. Ellen, Ellinor and everyone else back in Stockholm – you have been there for much-needed breaks during holidays and phone calls. I also want to thank the Karlsö team – and especially Jonas and Aron – for giving me the opportunity to spend some of the best months of my PhD in the middle of a guillemot colony.

Finally, my family. Axel – you are a very tough act to follow, if I manage to do even half as well as you, I will be content. Pappa – you have not only been my personal illustrator for the past three years but also an avid postcard-writer, stats consultant and unwavering supporter throughout, and I cannot thank you enough. Mamma – I could not have asked for a better role model. You have taught me not only the greatness of Earl Grey, Ingvar Storm and programming but also that if a thing is worth doing, it is worth doing well (which I hope is at least vaguely reflected in my work).

Table of contents

Abstract	i
Acknowledgements	iii
Abbreviations	xiv
1 Introduction	1
1.1 Energy flow in marine ecosystems	1
1.2 Study system	4
1.2.1 <i>Ammodytes marinus</i>	5
1.2.2 Sandeels and zooplankton	9
1.2.3 Sandeels and seabirds	10
1.2.4 Bottom-up and top-down control in the zooplankton-sandeel-seabird food chain	11
1.2.5 Temporal changes in the study system	12
1.2.6 Understanding the dynamics of the sandeel food chain	15
1.3 Aim of thesis	17
1.3.1 Thesis synopsis	17

I	Spatio-temporal patterns in sandeel prey	19
2	Exploring spatio-temporal variation in lesser sandeel prey fields using Continuous Plankton Recorder data	20
2.1	Introduction	20
2.2	Continuous Plankton Recorder data	22
2.2.1	CPR sampling biases	23
2.3	Methods	28
2.3.1	Diet of post-metamorphic sandeels	28
2.3.2	Taxonomic groups included	29
2.3.3	Adjusting for clogging	30
2.3.4	Correction factors	30
2.3.5	Spatial aggregation of CPR data	36
2.3.6	Interpolation	37
2.3.7	Prey traits	40
2.3.8	Spatio-temporal variation in the sandeel prey field	46
2.4	Results	47
2.5	Discussion	54
2.5.1	Caveats of the approach	54
2.5.2	Spatio-temporal patterns in the sandeel prey field	55
2.5.3	Relationship between prey field characteristics and sandeel growth	57
2.5.4	Applicability to other species and life stages	58

II Exploring drivers of spatio-temporal variation in the growth of juvenile lesser sandeels using a dynamic energy budget model	60
3 Dynamic energy budget model description	61
3.1 Introduction	61
3.2 Model framework	64
3.2.1 Differences compared with the MacDonald model	66
3.3 Model equations and initial parameter values	69
3.3.1 Assimilated energy	74
3.3.2 Metabolic costs	88
3.3.3 Energy allocation	93
3.3.4 Translating structural and reserve energy into length and wet weight	97
3.4 Discussion	100
4 Drivers of spatio-temporal variation in the growth of juvenile lesser sandeels	104
4.1 Introduction	104
4.2 Methods	108
4.2.1 Model input	108
4.2.2 Initial conditions	111
4.2.3 Sandeel data	112
4.2.4 Tuning of handling time and capture success	112
4.2.5 Spatio-temporal variation in 0 group growth	114
4.2.6 Parameter sensitivity analysis	115
4.2.7 Drivers of variation in growth	116
4.3 Results	119

4.3.1	Spatio-temporal variation in 0 group growth	119
4.3.2	Parameter sensitivity analysis	122
4.3.3	Drivers of variation in growth	125
4.4	Discussion	130
4.4.1	Agreement between predictions and observations	130
4.4.2	Drivers of spatio-temporal variation in growth	133
4.4.3	Climate change-driven decreases in size	137
4.4.4	Future studies	137

III Spatio-temporal patterns in the dynamics of a sandeel predator in relation to the spatial structure of their sandeel prey **139**

5 Spatial synchrony of breeding success in the black-legged kittiwake (*Rissa tridactyla*) reflects the spatial dynamics of its sandeel prey **140**

5.1	Introduction	140
5.2	Methods	143
5.2.1	Kittiwake breeding success data	143
5.2.2	Synchrony in breeding success	143
5.2.3	Spatial patterns in synchrony	144
5.2.4	Inferring causes of synchrony	145
5.3	Results	148
5.3.1	Spatial patterns in synchrony	148
5.3.2	Inferring causes of synchrony	150
5.4	Discussion	154

IV	General discussion	158
6	Discussion and conclusions	159
6.1	Bottom-up energy flow in the sandeel food chain and its implications	160
6.1.1	Knock-on effects on sandeel demographic rates	163
6.1.2	Knock-on effects on seabirds	164
6.1.3	Implications for fisheries	166
6.2	How may sandeels be affected by projected environmental change? . .	167
6.2.1	Implications for seabirds	169
6.3	Implications for the understanding of other zooplankton-forage fish-seabird food chains	170
6.3.1	Other <i>Ammodytes</i> spp.	170
6.3.2	Lessons learnt about understanding variation in size and bottom-up effects in forage fish	171
6.4	Potential directions for future work	172
6.5	Conclusions	174
A	Appendix for Chapter 2	175
B	Appendix for Chapter 4	177
C	Appendix for Chapter 5	184
	Bibliography	191

List of figures

1.1	Study area with distribution of sandeel grounds.	5
1.2	Annual cycle of lesser sandeels.	6
1.3	Summary of drivers and processes in sandeel dynamics.	8
2.1	CPR samples within study area.	27
2.2	Spatial and temporal variation in CPR sampling frequency.	28
2.3	Location of Stonehaven site together with CPR samples used to develop correction factors.	31
2.4	Correlation between Stonehaven abundances and abundances in local CPR samples aggregated over different distances.	33
2.5	Example of CPR interpolation.	38
2.6	Map of available energy in sandeel prey.	49
2.7	Time series of available energy in sandeel prey.	49
2.8	Map of abundance of small copepods.	50
2.9	Time series of abundance of small copepods.	50
2.10	Map of abundance of <i>Calanus finmarchicus</i>	51
2.11	Time series of abundance of <i>Calanus finmarchicus</i>	51
2.12	Map of abundance of <i>Calanus helgolandicus</i>	52
2.13	Time series of abundance of <i>Calanus helgolandicus</i>	52
2.14	Map of abundance of average daily mean square root of prey image area.	53

2.15	Time series of abundance of average daily mean square root of prey image area.	53
3.1	Main variables and processes in DEB model.	65
3.2	Schematic representation of search rate.	80
3.3	Predicted and observed sandeel gut evacuation rate.	85
3.4	Observed sandeel gut contents as a function of length.	87
3.5	Summary of the key equations governing ingestion.	88
3.6	Predicted and observed sandeel standard metabolic rate.	91
3.7	Allocation to structural energy as a function of total energy.	96
3.8	Energy content predicted from length and weight compared to observed energy content.	99
4.1	Model locations and associated CPR samples.	111
4.2	Comparison of predicted and observed sandeel length.	120
4.3	Predicted growth curves for each model location.	122
4.4	Predicted length at overwintering for each model location.	123
4.5	Results of model parameter sensitivity analysis.	124
4.6	Model input versus predicted length.	126
4.7	Sensitivity of predicted length to environmental conditions.	128
4.8	Sensitivity of predicted length to initial conditions.	129
5.1	Maps of (a) study colonies, (b) colony pairs showing weaker/stronger synchrony than expected based on distance and (c) cluster structure.	147
5.2	Effect of distance on inter-colony synchrony.	148
5.3	Time series of breeding success in each cluster.	152
B.1	Sensitivity of length predictions to CPR correction factors	178

B.2	Sensitivity of length predictions to prey energy content.	179
B.3	Sensitivity of length predictions to prey size.	180
C.1	Effect of sample size on estimated breeding success synchrony.	186
C.2	Determination of the value of k to use for clustering.	187
C.3	Effect of distance on inter-colony synchrony based on r	189
C.4	Maps of (a) colony pairs showing weaker/stronger synchrony than expected based on distance and (b) cluster structure based on r	190

List of tables

2.1	CPR abundance categories.	23
2.3	CPR correction factors.	35
2.4	Prey trait values.	41
3.1	DEB model variables and parameter values.	70
4.1	Comparison of predicted and observed sandeel length.	121
4.2	Relative impact of drivers on predicted length.	134
5.1	Results of fuzzy clustering of kittiwake breeding success.	151
5.2	Weights for alternative models explaining synchrony.	153
A.1	Corresponding CPR and Stonehaven taxa.	175
B.1	Prey search classes.	177
B.2	Result of models of environmental input versus predicted length.	180
C.1	Number of overlapping estimates of breeding success in two consecutive years for all colony pairs.	185
C.2	Final synchrony cluster structure for each algorithm.	188

Abbreviations

CI	Confidence interval
CPR	Continuous Plankton Recorder
DEB	Dynamic energy budget
ECG	East Central Grounds
DVM	Diel vertical migration
GAM	Generalised additive model
ICES	International Council for the Exploration of the Sea
SDA	Specific dynamic action
SMR	Standard metabolic rate
SSB	Spawning-stock biomass

Chapter 1

Introduction

1.1 Energy flow in marine ecosystems

Energy can be considered as the common, critical currency in ecology and understanding energy flows between trophic levels has been a long-standing quest in ecology (Odum 1968). In marine ecosystems, three types of control on energy flow are generally recognised: bottom-up control (producer-driven dynamics, increases at lower trophic levels result in increases at upper trophic levels), top-down control (predator-driven dynamics, increases at upper trophic levels result in decreases at lower trophic levels) and wasp-waist control (dominant mid-trophic species exerts bottom-up control on upper trophic levels and top-down control on lower trophic levels) (Cury et al. 2003). While bottom-up control is thought to generally be the main governing mechanism in marine ecosystems, different types of control will likely act at the same time, and their importance may vary over time and space (Cury et al. 2003). It is also increasingly recognised that trophic interactions are more complex than mere responses to changes in abundance of adjacent trophic levels, and that predators may also respond to changes in species composition, phenology or prey size (e.g. Ljungström et al. 2020; Österblom et al. 2008; Régnier et al. 2019; Scopel et al. 2019). If a system is bottom-up controlled, understanding how predators respond to spatio-temporal variation in prey dynamics is of key importance, especially in the light of current global environmental change, where many of these prey populations may be changing rapidly (e.g. Poloczanska et al. 2013; Richardson 2008).

In marine food webs, the mid-trophic position is often occupied by small, pelagic forage fish, which play a key role in the transfer of energy from plankton to upper trophic levels occupied by piscivorous fish, marine mammals, squid and seabirds (Engelhard et al. 2014; Pikitch et al. 2014). The fitness of these top predators has repeatedly been found to be strongly related to the abundance and quality of the forage fish available (e.g. Cury et al. 2011; Engelhard et al. 2013, 2014; Scopel et al. 2019). Forage fish are also commercially valuable as many of the piscivorous fish preying on them are important fisheries species, resulting in forage fish contributing around 20% of the global value of marine fisheries (Pikitch et al. 2014). In light

of this, and even more so considering the dramatic declines in many populations of both forage fish and their predators (e.g. Hutchings et al. 2010; Paleczny et al. 2015), understanding the dynamics of forage fish, and how these dynamics are reflected in predator populations, is of key importance. Previous research suggests that the dynamics of forage fish are governed by multiple drivers. Most of the mortality appears to be the result of predation, although mortality from fisheries can sometimes be substantial (e.g. Engelhard et al. 2014). However, while in some cases this predation may result in top-down control, forage fish populations are often found to be mainly bottom-up controlled (e.g. Ayón et al. 2008; Boldt et al. 2019; Engelhard et al. 2014).

This bottom-up control means that understanding the dynamics of the zooplankton, and the interactions between zooplankton and forage fish, is key. Again, this may go beyond a simple response to variation in abundances, and instead aspects such as size (e.g. Ljungström et al. 2020) or temporal variability in availability (e.g. Boldt et al. 2019) may be more important for determining fish ingestion rates. However, not only food conditions will determine net rates of energy acquisition of forage fish. For example, metabolic costs are strongly related to temperature in fish (Clarke and Johnston 1999) such that higher temperatures result in greater energetic losses. Other less obvious aspects of the environment may also be important, such as light conditions in the case of visually foraging fish (Aksnes 2007; Ljungström et al. 2020; van Deurs et al. 2015; Varpe and Fiksen 2010). Further, as body size and energy reserves are related to both mortality (e.g. Sogard 1997) and productivity (e.g. Barneche et al. 2018) in fish, identifying not only drivers of variation in net energy gain but also how this is divided between growth, energy reserves and reproduction will improve the understanding of drivers of both abundance and size of forage fish.

All these variables that impact forage fish dynamics are likely to show considerable spatial variation, which may also be reflected in spatial variability in the populations of forage fish predators. For example, spatial variation in the local abundance of forage fish, thought to be the result of variation in environmental conditions as a result of different upwelling dynamics, was found to result in spatial variation in the diet of rhinoceros auklets (*Cerorhinca monocerata*) in the California Current System, which in turn affected chick growth (Thayer and Sydeman 2007). On top of spatial variation, drivers of forage fish dynamics are also likely to show considerable temporal variation, and many, such as zooplankton dynamics (Richardson 2008) and ocean temperatures (Belkin 2009), are changing as a result of climate change. Due to this sensitivity to rapidly changing environmental conditions, it is not surprising that forage fish have been demonstrated to display all three “universal responses” to climate change (see Daufresne et al. 2009): a decline in body size (e.g. Baudron et al. 2014; Daufresne et al. 2009) as well as shifts in distribution and phenology (Poloczanska et al. 2013). These temporal changes are also likely to propagate up to the level of their predators. For example, a temperature-driven shift to a forage fish community dominated by species of low energy density in the Gulf of Maine appears to have resulted in reduced breeding success in several seabird species (Scopel et al. 2019).

Understanding the dynamics of bottom-up effects in the zooplankton-forage fish-top predator food chain is thus important, but how to approach this is not always straightforward due to the complexity of the system. Temporal correlations are often used to try to understand trophic interactions in marine food webs. However, as responses to lower trophic levels may not be a simple positive response to abundances, identifying these relationships may require considering more complex responses. For example, Ljungström et al. (2020) found that the response of herring (*Clupea harengus*) intake rates to the size distribution of the available prey was much stronger than the response to the abundance of prey. This means that while no traditional bottom-up association between zooplankton and herring abundances may necessarily be found, herring are nonetheless responding to changes occurring at lower trophic levels. Further, improving the understanding of these trophic interactions is often hindered by a lack of data. Lower trophic levels often have to be reduced to rough estimates of biomass, or even represented by environmental proxies such as temperature (e.g. Frederiksen et al. 2007a, 2006), which may make it difficult to identify these complex interactions. Another complication is that several drivers may interact, making relationships even more difficult to identify. For example, temperature may have a positive effect on growth of forage fish through increased intake rates when food is abundant, but may instead have a negative effect through increased metabolic costs when food is scarce (e.g. Brodersen et al. 2011). The consequence of this is that the impact of a single driver can potentially not be identified unless the interacting driver is also accounted for. Finally, another important point is that even when clear associations between variables are found, this does not necessarily mean that these variables are directly related. For example, even if a positive correlation between temperature and seabird breeding success is detected, this does not mean that there is a direct effect of temperature on seabirds, but the relationship might instead act through the seabirds' forage fish prey (e.g. Frederiksen et al. 2007a). Understanding the mechanisms through which these indirect relationships are acting is important for being able to extrapolate findings to other locations and time periods. As such, an improved mechanistic understanding of trophic interactions in marine food chains is crucial, especially in this time of rapid environmental change.

1.2 Study system

This thesis focuses on parts of the north-east Atlantic where the lesser sandeel (*Ammodytes marinus*, hereafter generally referred to as ‘sandeel’), a small, pelagic planktivorous fish, occupies a key role in the food web, providing an important food source for several marine top predators (e.g. Engelhard et al. 2014). The study area includes large parts of the North Sea, as well as the coasts of the Faroes and southern Iceland (see Figure 1.1), with a particular focus on the western and northern North Sea. While there are several species of forage fish in this region, *A. marinus* is the principal prey species for many species of seabirds, marine mammals and piscivorous fish (Engelhard et al. 2014). Seabirds are particularly dependent on sandeels as prey (Engelhard et al. 2014). Both seabird breeding success (Christensen-Dalsgaard et al. 2018a; Rindorf et al. 2000; Vigfúsdóttir 2012) and survival (Oro and Furness 2002) have repeatedly been linked to sandeel availability and energy content. It has been hypothesised that declines in the energy content and abundance of *A. marinus* have contributed to the widespread decline in many species of seabirds along the North Sea coast (MacDonald et al. 2015). These declines are in turn hypothesised to result from temperature-driven changes in the sandeel zooplankton prey base, as well as potentially also direct effects of temperature on the sandeels (MacDonald et al. 2015).

In this section, *A. marinus* and the drivers of its population dynamics are introduced in more detail. This is followed by a synthesis of the links between *A. marinus* and both its zooplankton prey and its seabird predators, as well as a discussion of bottom-up and top-down control in the sandeel food chain. The section finishes with a discussion on how the ecosystem on which the sandeel depends has changed, and is expected to continue to change.



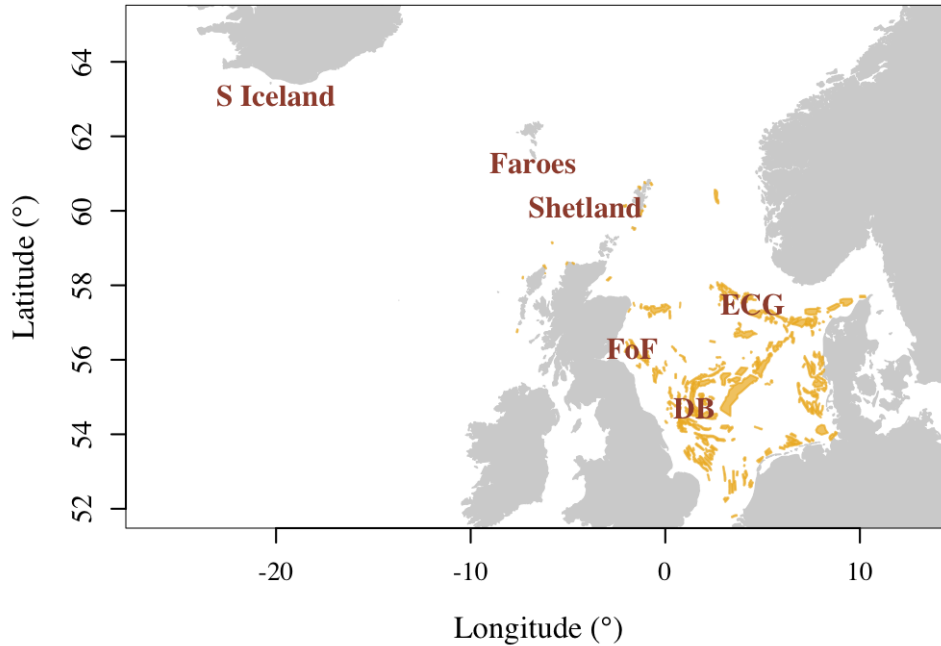


Figure 1.1: Study area with lesser sandeel grounds marked in yellow (Jensen et al. 2011 and data provided by Marine Scotland Science). Mapped grounds are limited to locations where more complete data exist as a result of fisheries (Faroese and Icelandic waters have never been fished). Locations regularly used in the text are also marked out (FoF = Firth of Forth, DB = Dogger Bank, ECG = East Central Grounds).

1.2.1 *Ammodytes marinus*

A. marinus is part of the sandeel family (Ammodytidae). There are six recognised species of the genus *Ammodytes*, all inhabiting the oceans of the Northern Hemisphere, where they often constitute an important prey for seabirds, marine mammals and piscivorous fish (Reay 1970; Robards et al. 1999a). As both the English and scientific names imply (ammos = sand, dytes = diver), sandeels, which all lack swim bladders, spend much of their time burrowed in sandy substrates (Reay 1970).

1.2.1.1 Habitat and life cycle

A. marinus occurs from the northern coast of Russia into the Barents Sea, down along the coast of Norway and into the North Sea, as well as along the coasts of the Faroes and Iceland, and into the western Baltic Sea (Robards et al. 1999a). It has very specific habitat preferences, favouring hydrodynamically active regions (Tien et al. 2017) of 30–70 m depth and medium to coarse sand (Holland et al. 2005; Wright et al. 2000). During the summer feeding season, they spend the night burrowed into the sand, but during winter they remain buried in the sand throughout day and night. The timing of overwintering varies, but generally occurs from around June–October to March–April, depending on age (Reeves 1994). A diagram of the annual cycle of the sandeel is shown in Figure 1.2.

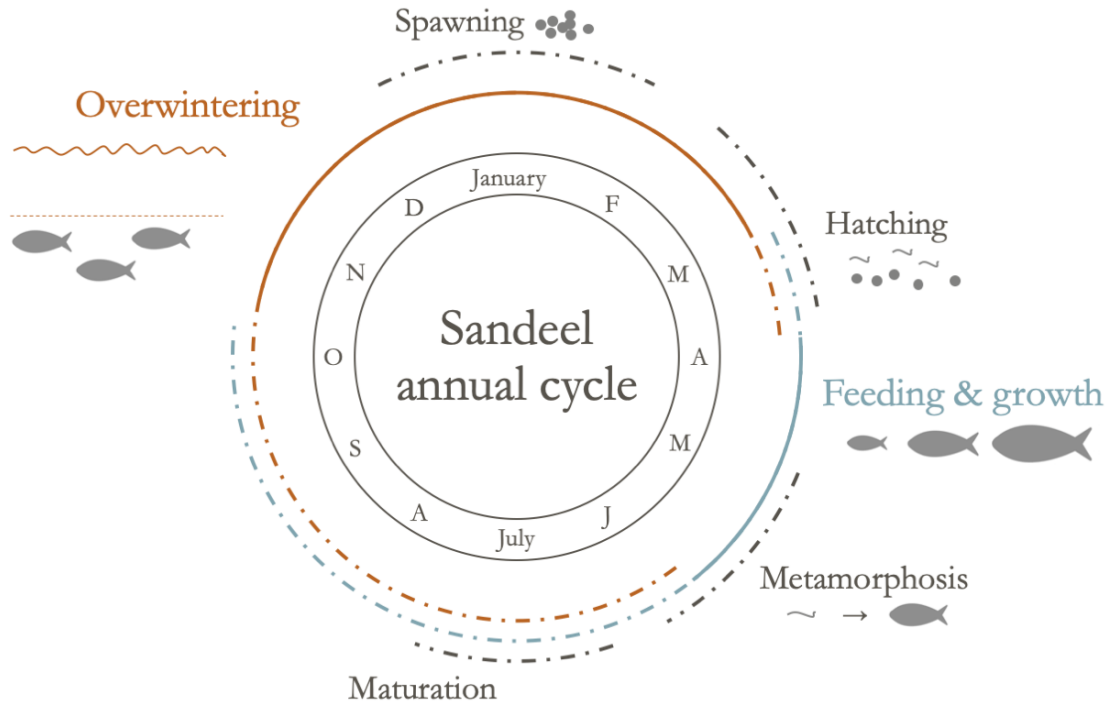


Figure 1.2: Annual cycle of lesser sandeels. Dot-dash lines indicate inter-individual and inter-annual variability. Grey lines = reproductive processes, red lines = overwintering, blue lines = feeding and growth.

Sandeels live up to around 9 years of age (Macer 1966), but due to high mortality rates, the age distribution is strongly skewed towards younger age classes (e.g. Cook 2004). They normally mature at an age of 1–2 years (Boulcott et al. 2007) and spawning usually takes place between December and February (Bergstad et al. 2001; Macer 1966) when the sandeels briefly emerge before returning to burrow in the substrate. The eggs are demersal and usually hatch in February–March (Wright and Bailey 1996). Following this, the larvae drift passively with the prevailing currents (e.g. Christensen et al. 2008; Gurkan et al. 2013; Jensen 2000; Proctor et al. 1998). They then metamorphose in around May–June at a size of roughly 35–55 mm (Jensen 2000; Régnier et al. 2017; Wright and Bailey 1996). After metamorphosing and settling, sandeels are highly sedentary, usually only moving a few kilometres from their nightly burrowing habitat (Engelhard et al. 2013; Johnsen et al. 2017; van der Kooij et al. 2008).

1.2.1.2 Population dynamics

Several processes govern sandeel dynamics, which in turn govern the energy available to upper trophic levels (Figure 1.3). Inter-annual variability in recruitment, which is substantial, is generally the main driver of variation in sandeel abundance (e.g. ICES 2017; Poloczanska et al. 2004). The maturation rate, which determines the number of spawners, is strongly related to size (Bergstad et al. 2001; Boulcott and Wright 2008; Boulcott et al. 2007) as well as rate of energy acquisition (Boulcott and Wright 2008). Following maturation, the sandeels continuously allocate resources

to gonad development from their energy reserves, which they have accumulated during summer, with most investment occurring after the sandeels have initiated overwintering (Bergstad et al. 2001; Boulcott and Wright 2008). The total amount of energy allocated to gonads depends on the size of the energy reserves built up during summer and the energy lost from reserves through metabolic maintenance costs during gonad development (Wright et al. 2017a). When the metabolic rate increases at higher temperatures, sandeels seem to prioritise survival and thus reduce gonad investment (Wright et al. 2017a). Gonad investment will determine fecundity, which explains why fecundity is related to size (Bergstad et al. 2001; Boulcott and Wright 2008, 2011), but gonad investment will also impact the timing of spawning (Boulcott et al. 2017; Wright et al. 2017b). Together with a temperature-dependent incubation period (Régnier et al. 2018), the timing of spawning, which is asynchronous and often protracted (Boulcott et al. 2017; MacDonald et al. 2019a), will determine timing of hatching, which often shows large intra- and inter-annual variability (MacDonald et al. 2019a; Régnier et al. 2017; Wright and Bailey 1996). Loss rates during the incubation phase are largely unknown.

The growth patterns of the subsequent larval phase will depend on the temperature and prey the larvae are exposed to while drifting with the currents (Christensen et al. 2008; Gurkan et al. 2013). Several studies suggest that food conditions during the early larval stages are a key determinant of recruitment (Arnott and Ruxton 2002; Régnier et al. 2017; van Deurs et al. 2009), likely through their effect on larval growth rates, and subsequent effects on size-selective mortality. While the yolk-sac provides a bit of a buffer, hatching within two weeks of peak food production may be necessary to obtain sufficient food resources for surviving the early larval period (Régnier et al. 2018). Further, successfully drifting to a location of suitable habitat at the time of metamorphosis may be another key determinant of recruitment, suggesting that current patterns will be important (Christensen et al. 2008; Proctor et al. 1998). The advective regime may also be important through its effect on larval food conditions by controlling the retention of prey close to sandeel grounds (Henriksen et al. 2018). In addition, several studies have found a negative relationship between recruitment and 1 group abundance (Arnott and Ruxton 2002; Lindegren et al. 2017; van Deurs et al. 2009), which has been suggested to act through cannibalism (Arnott and Ruxton 2002; Eigaard et al. 2014; Lynam et al. 2013), disruption of the demersal eggs when adult sandeels are burrowing (Arnott and Ruxton 2002) and/or competition for food or habitat (Arnott and Ruxton 2002; Lindegren et al. 2017; van Deurs et al. 2009). Finally, several studies have reported a correlation between winter temperature and recruitment (Arnott and Ruxton 2002; Lindegren et al. 2017; van Deurs et al. 2009). It is unclear what exact mechanism might generate this correlation, as temperature may have direct impacts on reproductive investment (Wright et al. 2017a), timing of spawning (Wright et al. 2017b), incubation period (Régnier et al. 2018) and larval growth (Christensen et al. 2008), but may also be related to food conditions (Régnier et al. 2017).

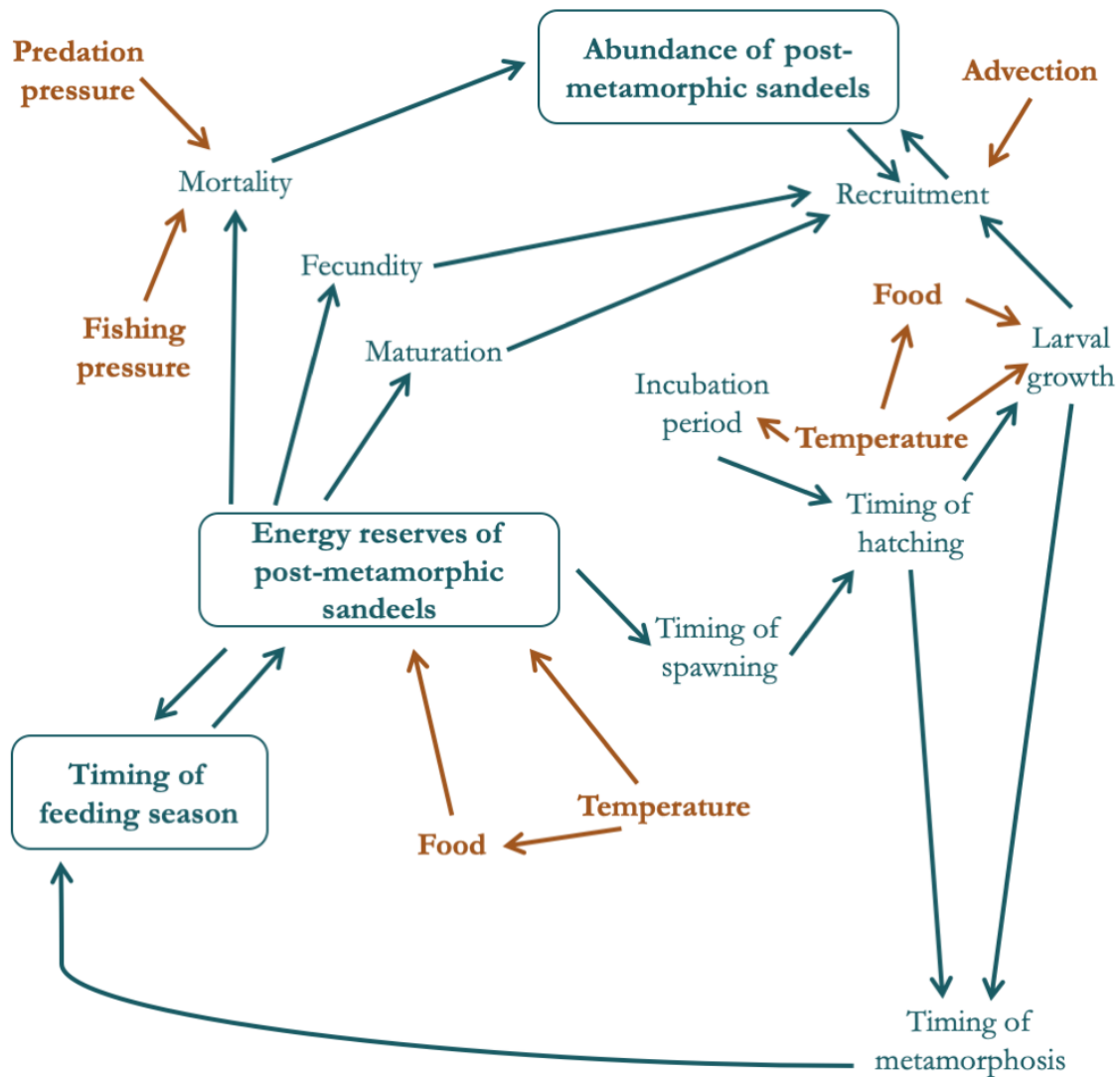


Figure 1.3: Main known drivers and processes in sandeel dynamics determining the energy available to upper trophic levels. Blue text and arrows = sandeel demographic processes. Red text and arrows = environmental drivers. Blue boxes = determinants of energy availability to upper trophic levels.

Once the sandeels have metamorphosed, the size at and timing of which vary depending on timing of hatching and the larval growth period (Régnier et al. 2017; Wright and Bailey 1996), they settle and begin feeding together with older sandeels. As such, the timing of metamorphosis will to a large extent determine when 0 group sandeels become available to predators in a particular sandeel ground, whereas recruitment will determine the number available. At the time of 0 group settlement, the 1+ group sandeels will likely have been present and feeding for 1–2 months already (Reeves 1994). The timing at which the 1+ group sandeels become available to predators will depend on when they emerge from overwintering, and it is still unknown what drives this. It is possible that the sandeels use temperature, light or other environmental drivers as a cue (Winslade 1974a,b). Both 0 group and 1+ group sandeels will then continue feeding, being available to predators in the water column during the day, until they initiate overwintering. When overwintering is

initiated varies between age groups and years (Bergstad et al. 2002; Reeves 1994), likely as a result of variability in energy reserves (MacDonald et al. 2018; van Deurs et al. 2011a), but it is possible that environmental conditions also play a role.

During the feeding season, environmental conditions and the abundance and composition of prey will impact intake rates and growth (Eliassen 2013; MacDonald et al. 2018; van Deurs et al. 2015, 2014). This variation in growth and energy acquisition will have knock-on effects not only on maturation rates, fecundity and timing of spawning as discussed above, but also on starvation mortality (MacDonald et al. 2018), further strengthening the link between sandeel energy reserves and demographic rates. While starvation mortality can be substantial in some years (MacDonald et al. 2018), the greatest source of mortality is likely predation, primarily from fish (Furness 2002). Further, where fishing occurs, this will also introduce additional mortality (Furness 2002). Finally, density-dependent effects will also impact mortality, through, for example, increased competition for food or habitat, although different density-dependent mechanisms appear to largely cancel each other out (Rindorf et al. 2019).

1.2.1.3 Spatial structure and connectivity

An important feature of sandeel dynamics is the clear spatial structure. As a result of their preferred habitat being patchily distributed, sandeels are patchily distributed themselves (see Figure 1.1). Further, the patterns of larval dispersal, which is the main source of connectivity between sandeel sub-populations, also introduces a spatial structure (Wright et al. 2019). Some sub-populations are strongly connected, whereas other regions show high levels of larval retention, resulting in more isolated sub-populations (Christensen et al. 2008; Wright et al. 2019). The resulting spatial structure is reflected in studies of otolith chemistry (Gibb et al. 2017; Wright et al. 2018), to some degree in genetic studies (Jiménez-Mena et al. 2020) as well as in the degree of synchrony in abundances between sub-populations (Wright et al. 2019). Sandeels may also show asynchronous variation in abundances at smaller scales of just a few kilometres (Jensen et al. 2011). Spatial variability in environmental conditions is also likely to contribute to the asynchronous dynamics, as well as the clear spatial variation in size (Bergstad et al. 2002; Boulcott et al. 2007; Rindorf et al. 2016).

1.2.2 Sandeels and zooplankton

Food conditions are important for sandeel dynamics both at the larval stage and after metamorphosis. At the larval stage, copepod nauplii, copepod eggs and appendicularians make up the main part of the sandeel diet (Economou 1991; Ryland 1964). Again, the temporal match of hatching and food abundance is an important determinant of recruitment, with *Calanus* copepods potentially playing a particularly important role (Arnott and Ruxton 2002; Régnier et al. 2017; van Deurs et al. 2009; but see Henriksen et al. 2018). Beyond the larval stage, copepods are the main food source (Eliassen 2013; Godiksen et al. 2006; Macer 1966; Roessingh 1957; van Deurs et al. 2014), but the sandeels also feed on appendicularians (Gómez García et

al. 2012; van Deurs et al. 2010), cladocerans (Roessingh 1957), krill (Godiksen et al. 2006), amphipods, mysids (Eigaard et al. 2014), crustacean larvae (Eliassen 2013), polychaetes (Macer 1966) and their larvae (Eliassen 2013) as well as fish eggs (Rankine and Morrison 1989; Roessingh 1957) and larvae (Eigaard et al. 2014; Godiksen et al. 2006; Rankine and Morrison 1989; Roessingh 1957). As with larval sandeel, the abundance and composition of zooplankton consumed by adult sandeels have been related to growth and demographic rates. Eliassen (2013) and MacDonald et al. (2019b) both found a positive relationship between zooplankton biomass and sandeel size. Similarly, MacDonald et al. (2018) found that food availability had a large impact on growth, with knock-on effects on starvation mortality. Their study also pointed to the importance of the type of prey available, with variation in the abundance of large copepods having a larger impact on sandeel growth than variation in the abundance of small copepods. This aligns with the finding that sandeels feeding on larger copepods (mainly *Calanus* spp.) tend to show higher consumption rates than those feeding on smaller ones (van Deurs et al. 2014). Modelling results have suggested that this mainly results from the sandeels, which are visual foragers (Winslade 1974c), being able to detect larger copepods from further away (van Deurs et al. 2015). As such, the abundance and composition of zooplankton play a large role in the growth and demographic rates of sandeels, and thus also the energy available to upper trophic levels.

1.2.3 Sandeels and seabirds

The timing, energy content and abundance of sandeels available to their seabird predators during the breeding season will vary over space and time, which may impact seabird breeding success. As 0 group sandeels are often used to feed chicks, the agreement of the timing of appearance of 0 group sandeels in the water column and the timing of chick energy demand may affect chick-rearing success (Wright and Bailey 1993). On the Isle of May in the north-western North Sea, the difference between the timing of peak chick energy demand and the date when 0 group sandeels reach a specified threshold size has increased since the early 1980s, although this mismatch does not seem to have had a negative impact on the seabirds yet (Burthe et al. 2012). Further, while some seabird species, such as European shags (*Phalacrocorax aristotelis*), are able to extract sandeels from the sand (Watanuki et al. 2008), the initiation of overwintering generally makes sandeels unavailable for most foraging seabirds, meaning that the timing of overwintering may also be important. This mechanism likely explains the negative impact of early overwintering in local sandeels on seabird breeding success at the Isle of May (Rindorf et al. 2000).

The energy content of individual sandeels varies between years (Wanless et al. 2018), which may also impact seabird breeding success (Frederiksen et al. 2006). In 2004, the energy content of sandeels in the Firth of Forth was exceptionally low, and this coincided with widespread seabird breeding failure (Wanless et al. 2005). Species that are single-prey loaders, such as common guillemots (*Uria aalge*), seem to be more sensitive to variability in energy content than species such as black-legged kittiwakes (*Rissa tridactyla*, hereafter ‘kittiwake’), which feed their chicks through regurgitation (Frederiksen et al. 2006).

Studies of sandeel diet also show that there is clear inter-annual variability in the amount of sandeels eaten by seabirds (Wanless et al. 2018). To a large extent, this likely reflects variation in the abundance of sandeels in the water column (e.g. Bailey et al. 1991; Daunt et al. 2008). However, it may also reflect variability in the accessibility of sandeels to the seabirds, as well as the foraging behaviour of the birds. Sandeel abundance may show fine-scale horizontal variation (e.g. van der Kooij et al. 2008; Wright and Bailey 1993), which will impact accessibility to the seabirds as well as foraging costs. The vertical distribution of sandeels also varies (Freeman et al. 2004; Johnsen et al. 2017; Wright and Bailey 1993), which may explain why diving species of seabirds sometimes have higher levels of sandeel in their diet compared to surface-feeding species (e.g. Chivers et al. 2012). Seabirds also show some behavioural flexibility in their response to food conditions, such as switching prey, or adjusting foraging range and time as their prey become more scarce (e.g. Suryan et al. 2000). This will also impact the relationship between sandeel dynamics and seabird breeding success, and may contribute to the variability in the amount of sandeels consumed by seabirds. Due to differences in foraging costs, time budgets, foraging ranges, diving ability and ability to switch diets, different species of seabirds are likely to respond differently to changes in the sandeel populations (e.g. Furness and Tasker 2000).

1.2.4 Bottom-up and top-down control in the zooplankton-sandeel-seabird food chain

While sandeels are evidently responding to variability in their zooplankton prey, and variability in sandeel populations is in turn important for their seabird predators, it is still not fully clear to what extent the zooplankton-sandeel-seabird food chain is top-down versus bottom-up controlled and how this may vary over time and space. Several studies have found positive relationships between biomass/abundance of zooplankton and biomass/abundance of sandeels (Arnott and Ruxton 2002; Eliasen 2013; Frederiksen et al. 2006), indicative of bottom-up control. Again, the sandeels may also show more complex responses to their zooplankton prey. For example, sandeel intake and growth rates are also related to the size composition of available prey (MacDonald et al. 2018; van Deurs et al. 2015, 2014). However, this trophic link does not seem to solely be subject to bottom-up control, as sandeels also are able to exert top-down control on their zooplankton prey (Jacobsen et al. 2019). Further, sandeels may themselves also be subject to top-down control. In Shetland, sandeel and herring have been found to show mirrored, opposite trends in abundance, which could suggest top-down control by herring (Frederiksen et al. 2007b). Whiting (*Merlangius merlangus*) and mackerel (*Scomber scombrus*) have also been suggested to exert top-down effects on sandeels in the North Sea (Lynam et al. 2017; MacDonald 2017). In addition, fisheries constitute another source of top-down control (Lynam et al. 2017). However, while fisheries appear to have a minor impact on sandeel abundances, this is generally thought to be smaller than the impact of environmental variability (Greenstreet et al. 2006; Poloczanska et al. 2004). Any effect of fisheries is likely to be larger in older age groups, with variation in 0 group abundance mainly driven by environmentally controlled variability in recruitment (Greenstreet et al. 2006). While it thus seems as if predators can exert top-down

control on sandeels, this trophic link also seems to be subject to bottom-up control (Engelhard et al. 2014). Along these lines, several positive correlations have been found between sandeel biomass/abundance and seabird survival and breeding success (Daunt et al. 2008; Eliassen 2013; Frederiksen et al. 2006; Oro and Furness 2002). As with the sandeels, the relationship between the seabirds and their prey may be more complex, for example may the breeding success of some species of seabird depend more strongly on the size of the sandeels rather than their abundance (Frederiksen et al. 2006).

As such, the evidence to date supports the presence of bottom-up control in the zooplankton-sandeel-seabird food chain, but also occasionally top-down effects, which are likely to vary in strength over time and space (Frederiksen et al. 2007b). Either way, it is clear that the adjacent trophic levels in this food chain are strongly linked. As such, improving the understanding of drivers of each component of the food chain and how interactions result in the propagation of impacts up through the food chain is of large importance, especially in the light of the marked temporal changes occurring in the surrounding environment and at all trophic levels.

1.2.5 Temporal changes in the study system

The study system has seen substantial changes over the last few decades. The North Sea is one of the most rapidly warming oceans (Belkin 2009), and temperatures are predicted to continue to increase (Schrum et al. 2016). Similarly, temperatures are rapidly increasing on the Icelandic and Faroese shelves (Belkin 2009). These temperature changes may have direct impacts on several physiological rates in sandeels (van Deurs et al. 2010; Wright et al. 2017a), but are also likely to impact lower trophic levels (Edwards et al. 2020; Richardson 2008). In addition to changes in temperature, currents are also expected to change as a result of climate change (Holt et al. 2018), which could alter larval transport patterns and may also impact the planktonic food of the sandeel. For example, the population of *C. finmarchicus* in the North Sea is replenished each year through advective transport from more northerly waters (Heath et al. 1999), and these currents are likely to show reduced power in the coming decades (Holt et al. 2018). Hydrodynamic changes are also likely to impact the underwater light conditions in the study area, where increased wave action has led to an increase in suspended particulate matter (Wilson and Heath 2019), which is likely to have contributed to the increase in turbidity that has been observed in the North Sea (Capuzzo et al. 2015; Dupont and Aksnes 2013). This may have resulted in a reduced ability of the sandeels to detect their prey (van Deurs et al. 2015).

1.2.5.1 Phytoplankton and zooplankton

Likely as a result of these physical changes as well as changes in nutrient input (Capuzzo et al. 2018), primary productivity has changed over time. On the scale of the north-east Atlantic, primary productivity has increased, although trends vary between regions (Edwards et al. 2020). In the North Sea, primary productivity has declined since the late 1980s (Capuzzo et al. 2018). Phenological shifts have also

occurred in the phytoplankton, with dinoflagellates generally showing earlier phenology (which is in line with the general pattern of phytoplankton, Poloczanska et al. 2013), while diatoms have shown shifts in both directions (Edwards and Richardson 2003). The species composition has also changed, including a marked decline in dinoflagellates in large parts of the North Sea (Edwards et al. 2020), and in general, a move towards smaller phytoplankton, which is likely to have impacted food conditions for the zooplankton (Schmidt et al. 2020).

Accordingly, large changes have also been observed in the zooplankton, the food of the sandeel. In general, there has been a decrease in the abundance of cold-water zooplankton species and an increase in the abundance of warm-water zooplankton species in the North Sea and up towards the Faroes (Alvarez-Fernandez et al. 2012; Beaugrand 2004). As part of this shift from cold-water to warm-water species, there has been a marked shift in dominance from *C. finmarchicus* to *Calanus helgolandicus* since the 1960s (Edwards et al. 2020). Both species are important food sources for the sandeel (Eliassen 2013; MacDonald 2017; van Deurs et al. 2014). In contrast, no clear temporal trend in the abundance of *C. finmarchicus* seems to have occurred in Iceland (Gislason et al. 2014) and the abundance of *C. helgolandicus* remains low (Bonnet et al. 2005). Multiple other sandeel prey groups have also changed over time, including a decline in krill (Beaugrand et al. 2003) and fish larvae (Capuzzo et al. 2018) in the North Sea since the late 1980s. Observed temporal trends in the zooplankton are not uniform, but instead there is clear spatial variability. While the average size of zooplankton is declining in the northern North Sea, it is increasing in the southern North Sea (Pitois and Fox 2006). This trend towards an increased size in the south is likely driven by a decline in the abundance of small species rather than an increase in larger species (Capuzzo et al. 2018; Pitois and Fox 2006). Most of the temporal changes in the zooplankton are not linear but are instead often associated with regime shifts. In the greater North Sea, a cold-episodic event in the late 1970s was followed by a shift to a warmer regime in the late 1980s, which was in turn followed by a shift occurring around the year 2000 which also involved an increase in temperature, as well as a change in current patterns (Alvarez-Fernandez et al. 2012; Beaugrand et al. 2008). The shift occurring in the late 1980s was associated with a sharp shift in the relative abundance of warm-water and cold-water copepods, while the one occurring around the year 2000 involved a decline in the abundance of neritic copepod species and fish larvae (Alvarez-Fernandez et al. 2012). Both shifts thus had a large impact on species making up the majority of the sandeel diet. In addition to changes in abundance and distribution, changes in phenology have also been observed. For example, long-term monitoring at Stonehaven on the east coast of Scotland has shown an extension of the *C. helgolandicus* growing season since the start of monitoring in the late 1990s (Edwards et al. 2020).

1.2.5.2 Sandeel predators and fisheries

In addition to changes in the zooplankton prey of the sandeels, changes have also occurred in the populations of their predators. The vast majority of predation on sandeels comes from piscivorous fish (Furness 2002) and this source of mortality has increased over time, at least in the southern North Sea (ICES 2017), and may be likely to continue to increase as the stocks of previously over-fished predators, such

as herring, recover (Frederiksen et al. 2007b). Fisheries introduce further mortality and the fishing pressure on sandeels in the North Sea increased greatly from the 1950s to the end of the century (Furness 2002). Fishing mortality shows inter-annual variation, but there was a clear reduction in fishing effort in the northern North Sea in the early 2000s following the introduction of greater precautionary measures (ICES 2020a,b,c), which was partly in response to concerns regarding the impact of fisheries on sandeel-eating seabirds (Greenstreet et al. 2006). In Shetland, the fishery has not operated since 2006 (ICES 2017). Sandeels have never been exploited commercially in the Faroes (Eliassen 2013) or Iceland (Vigfúsdóttir 2012).

1.2.5.3 Sandeel abundance, size and phenology

Likely due to a combination of the described factors, marked spatio-temporal variation has been observed in several aspects of sandeel dynamics. Since 2011, ICES has produced annual age-based assessments for four stock assessment areas in the North Sea using catch-at-age data and research survey indices. In the south-western North Sea, which includes Dogger Bank (see Figure 1.1), both spawning-stock biomass (SSB) and recruitment were higher in the 1980s and 1990s compared to recent decades (ICES 2020c). Similar drops in SSB around 2000 were observed in the north-eastern North Sea (which includes the East Central Grounds, see Figure 1.1) and the north-western North Sea (which includes the Firth of Forth, see Figure 1.1) (ICES 2020a,b). In the latter case, this also coincided with a period of very low recruitment (ICES 2020b). Following this drop however, there has been a number of strong year-classes, which is also reflected in the SSB estimates. In Shetland, SSB data suggest an increase from the mid-1970s to the mid-1980s, followed by a decline until the early 1990s and a partial recovery thereafter (Cook 2004; Poloczanska et al. 2004). Annual Marine Scotland Science trawl surveys indicated a further decline in recruitment in the early 2000s before the survey ended in 2007. In the Faroes, data are only available on 0 group sandeels, which show large variability but no clear long-term trend (Eliassen 2013; Jacobsen et al. 2019). Finally, in Iceland, no long-term datasets from direct sandeel sampling are available. However, one dataset on the proportion of haddock (*Melanogrammus aeglefinus*) with sandeels in their stomachs covering the years 1997 to 2012 suggests a decline from the 1990s to the early 2000s, with generally low values since then (Lilliendahl et al. 2013).

In addition to variation in abundance, sandeels show clear inter-annual variability in size (e.g. Jacobsen et al. 2019; Wanless et al. 2018), as well as long-term trends in some locations. For instance, at Dogger Bank, the length of 1+ group sandeels increased from 1975 until the late 1980s before starting to decline (although larger values were again observed in the late 2000s, van Deurs et al. 2014). Further, in the Firth of Forth, the length of 0 group and 1+ group sandeels dropped by Atlantic puffins (*Fratercula arctica*, hereafter ‘puffin’) on the Isle of May when mistnetted after coming in from a foraging trip has also declined over time since the start of measurements in 1975 (Wanless et al. 2018). Based on a comparison between new field samples and historical data, it has also been concluded that sandeel growth rates were higher in several fishing grounds in the North Sea in the 1960s and late 1970s compared to in the late 1990s (Bergstad et al. 2002). Similarly, in the Faroes, sandeels have been found to be smaller in recent years (Jacobsen et al. 2019).

Finally, in terms of phenology, the timing of spawning (Régner et al. 2019), hatching (Régner et al. 2019; Wright and Bailey 1996), metamorphosis (Jensen 2000; Régner et al. 2017; Wright and Bailey 1996) and overwintering (MacDonald 2017; Reeves 1994) varies between years, but there are only a few sufficiently long time series that can be used to explore whether any systematic changes have occurred. However, in those that do exist there is no evidence of any long-term trends. Time series of estimated spawning and hatching timing in the Firth of Forth from 2000 to 2016 did not show any clear trends (Régner et al. 2019). Further, based on an examination of samples of sandeel larvae mainly from the North Sea, no clear temporal trends in the timing of larval emergence were observed (Lynam et al. 2013).

1.2.5.4 Seabirds

Along with the changes in sandeel populations, there have also been several changes in the populations of sandeel-eating seabirds. Long-term data from the Isle of May (Wanless et al. 2018, source for all diet information in the following section) suggest that the amount of sandeel in the seabird diet varies between years, and so does the ratio of 1+ to 0 group sandeels in the diet for those species feeding on both, such as kittiwakes and puffins. The longest time series available from the Isle of May is from puffins (1973-present), which shows a shift from a clupeid-dominated to a sandeel-dominated diet occurring in the first few years of the time series. Thereafter, the proportion of sandeel in seabird diets has generally remained high, although with a distinct temporary drop in the early-to-mid-1990s in all monitored species. A lower proportion of sandeel in the diet of most of the species has also been observed since the early 2000s, in particular in common guillemots and European shags. These trends are not necessarily driven by changes in the local sandeel populations but could also be driven by, for example, variation in the abundance of alternative prey. In addition to changes in diet, the colony sizes and breeding success of several species of sandeel-eating seabirds have declined in large parts of the study area (Fauchald et al. 2015; JNCC 2016; MacDonald et al. 2015). However, these trends vary strongly over space and between species (JNCC 2016; MacDonald et al. 2015). While they are likely the result of multiple factors, declines in sandeel energy content and abundance are thought to have contributed to the observed trends (Fauchald et al. 2015; MacDonald et al. 2015).

1.2.6 Understanding the dynamics of the sandeel food chain

To understand the impact of past changes on the sandeel food chain, and predict the impact of further changes, a clear understanding of interactions between trophic levels, as well as of the impact of external drivers, is necessary. A substantial body of work have already contributed much to this understanding, but there are still gaps in our knowledge.

As described in Section 1.2.2, sandeels may respond not only to general changes in the prey biomass (Eliassen 2013; MacDonald et al. 2019b), but may also be sensitive to, for example, size (MacDonald et al. 2018; van Deurs et al. 2015, 2014) or timing of prey availability (van Deurs et al. 2010). As such, to explore the inter-

action between sandeels and their prey, zooplankton data of high taxonomic and within-season temporal resolution may be needed. However, this type of data are often not available. This means that rougher metrics with low taxonomic and temporal resolution have to be used, which could potentially hinder the identification of existing relationships (e.g. Rindorf et al. 2016). When higher-resolution data are available, they may be restricted to a specific location (e.g. MacDonald et al. 2018) and therefore not useful for understanding larger-scale variation.

It is also clear that the mechanisms connecting trophic levels are complex and that relationships are not consistently found across space and time. One study that examined the relationship between kittiwake breeding success and winter temperatures and stratification, as a proxy for sandeel availability, at several colonies around the British Isles, found that relationships varied widely between colonies (Carroll et al. 2015). This variability likely results from the chain of links between the sandeel proxy and kittiwake breeding success being a product of interactions and indirect effects, meaning that depending on local conditions, different relationships may be found. This highlights the importance of a mechanistic understanding of the processes involved, which is necessary if findings are to be extrapolated to other time periods and locations. Using mechanistic modelling may thus be a useful way forward for teasing apart the impact of different drivers and identifying interactions between drivers. Due to the relationship between sandeel size and demographic rates (Bergstad et al. 2001; Boulcott and Wright 2008, 2011; Boulcott et al. 2007; MacDonald et al. 2018; van Deurs et al. 2011a), mechanistic growth models may be particularly useful for understanding spatio-temporal variation in sandeel dynamics. As both abundance and size of sandeels may impact the fitness of their predators (e.g. Engelhard et al. 2014; Frederiksen et al. 2006; Rindorf et al. 2000), the output of growth models are directly relevant for understanding the energy available to upper trophic levels. While previous foraging and growth modelling approaches have provided valuable insight into drivers of variation in growth (MacDonald et al. 2018; van Deurs et al. 2015), they have been limited in their spatial and temporal extent and there is still a lack of understanding of what has driven the observed strong variation in sandeel size over time (Jacobsen et al. 2019; van Deurs et al. 2014; Wanless et al. 2018) and space (Bergstad et al. 2002; Boulcott et al. 2007; Rindorf et al. 2016).

The clear spatial variation in sandeel size (Bergstad et al. 2002; Boulcott et al. 2007; Rindorf et al. 2016), alongside spatial independence in abundance (Wright et al. 2019), is likely to also be reflected in the populations of their predators. Indeed, previous studies by Furness et al. (1996) and Frederiksen et al. (2005) suggested that in the British Isles, the spatial pattern in the breeding success of kittiwakes - which are particularly sensitive to variation in sandeel populations (Furness and Tasker 2000) - mirrored the spatial structure of the surrounding sandeel populations. However, these studies were based on a very coarse understanding of sandeel spatial dynamics. This understanding has since been much improved (see Wright et al. 2019 in particular), but it is unclear whether the spatial pattern in kittiwake breeding success reflect this refined structure.

1.3 Aim of thesis

The aim of this thesis is to contribute to the mechanistic understanding of bottom-up effects in the zooplankton-sandeel-seabird food chain. Specifically, objectives include:

1. Improving the understanding of spatio-temporal variation in sandeel food conditions in the study area.
2. Quantifying the relative importance of drivers of spatio-temporal variation in sandeel size by further developing and applying a mechanistic growth model.
3. Exploring to what extent spatial structure at the level of the sandeels may be reflected in the breeding success of sandeel-eating kittiwakes.

1.3.1 Thesis synopsis

To address the lack of sandeel prey data of sufficient temporal, spatial and taxonomic resolution, the thesis starts at the lowest trophic level in the zooplankton-sandeel-seabird food chain and describes an approach for creating daily sandeel prey fields based on Continuous Plankton Recorder data (Chapter 2). Using the generated prey fields, the chapter then explores the question of how sandeel food conditions - in terms of total energy availability, prey size, and abundance of some key prey types - have varied over time and space in the North Sea since the mid-1970s.

To explore to what extent this variation in food conditions can explain spatio-temporal variation in sandeel size, a dynamic energy budget (DEB) growth model is then developed, which estimates size daily throughout the first sandeel growth season as a function of food conditions, temperature, light conditions as well as size at and timing of metamorphosis. The model, which is described in Chapter 3, draws on the DEB model developed by MacDonald et al. (2018) but improves its generality to make it possible to run it in more locations and time periods, partly by incorporating components from the sandeel foraging model developed by van Deurs et al. (2015).

In Chapter 4, the model is then run in six locations: southern Iceland, the Faroes, Shetland and three locations further south in the North Sea: Dogger Bank, the Firth of Forth and the East Central Grounds. The chapter explores the role of food conditions (as based on prey fields developed in Chapter 2), temperature, light conditions as well as size at metamorphosis and timing of metamorphosis in explaining observed spatio-temporal variation in size, and what the impact of some expected future changes in these variables may be.

The thesis finishes at the top of the food chain by exploring the extent to which spatial patterns in the sandeel population along the coast of the UK propagate up to their kittiwake predators (Chapter 5). Specifically, the chapter examines whether the spatial patterns of inter-colony synchrony in kittiwake breeding success reflect the spatial structure of their sandeel prey. If the patterns are aligned, this would suggest that processes occurring at the level of the sandeel act to structure the populations of their predators. This chapter is published in *Marine Ecology Progress Series* (see Olin et al. 2020). Slight modifications have been made to the published version to better align it with the format of the thesis.

Finally, in Chapter 6, the implications of the findings for the understanding of sandeel-mediated bottom-up effects in the north-east Atlantic are discussed, with a particular focus on seabirds. Further, the impact of potential future environmental change is discussed, as well as what the findings contribute to the understanding of dynamics of other *Ammodytes* spp. and forage fish-mediated bottom-up effects in general.

Part I

Spatio-temporal patterns in sandeel prey

Chapter 2

Exploring spatio-temporal variation in lesser sandeel prey fields using Continuous Plankton Recorder data

2.1 Introduction

Forage fish have repeatedly been found to be mainly bottom-up regulated, so that the dynamics of the fish (abundance, size, condition) are strongly related to those of zooplankton biomass/density (e.g. Ayón et al. 2008; Boldt et al. 2019). While the abundance of prey is undoubtedly important, the response of the fish to the prey field is often more complex than that. Prey traits, such as size, will impact the ability of the fish to detect and successfully capture a given prey type, and may also determine whether they would actively select this prey type (Eggers 1977). As such, the composition of the prey field will be important for intake rates. In addition to the abundance and type of prey, the time at which the prey becomes available is also important. For example, that the end of the larval yolk-sac period and peak availability of larval prey coincide has long been recognised as a key determinant of fish recruitment, as it regulates growth rates, which has knock-on effects on starvation and predation rates (Cushing 1990; Durant et al. 2007; Hjort 1914). The abundance, composition and phenology of the prey are all likely to show marked spatio-temporal variation. Average abundances and long-term trends for a given taxon may vary on relatively small spatial scales, such as in different parts of the North Sea (Pitois and Fox 2006), which will impact spatio-temporal patterns in both abundance and composition. The timing of seasonal peaks also varies by both taxon and location, again on relatively small scales such as in the shelf waters off western UK (McGinty et al. 2011).

This means that to fully characterise the important aspects of the forage fish prey field, zooplankton data of high taxonomic, temporal and spatial resolution are required. This resolution may vary between different zooplankton datasets. Longer-

term zooplankton sampling schemes can roughly be sorted into point samples of high temporal resolution, and larger scale surveys with a wide spatial extent but poorer temporal resolution (Everett et al. 2017). While the former may be better at capturing variation in phenology, the latter will be necessary for understanding larger-scale dynamics, and the two thus complement each other (Ostle et al. 2017). Within these two types of sampling schemes, there are several different sampling techniques, including different types of nets, optical plankton counters, bioacoustic approaches as well as the Continuous Plankton Recorder (CPR), a device towed after ships sampling plankton with continuously moving bands of silk. The different sampling techniques have different strengths and inherent biases, for example will data obtained from bioacoustic approaches have very high spatial and temporal resolution, but very coarse taxonomic resolution, and no one technique will be optimised in all respects (Everett et al. 2017). In addition to using field samples to characterise prey fields for forage fish, these can also be generated using models (as in e.g. Gurkan et al. 2013). However, while these, depending on the model, can be produced with the spatio-temporal resolution needed, they will represent idealised conditions rather than actual conditions, and they may also have quite poor taxonomic resolution. As such, it is often a challenge to obtain forage fish prey field data with sufficient spatio-temporal and taxonomic resolution that can be used in statistical approaches or mechanistic models to pinpoint drivers of forage fish dynamics.

In lesser sandeels (*Ammodytes marinus*, hereafter ‘sandeel’), food conditions have long been hypothesised to be behind the clear spatial variation in size (Bergstad et al. 2002; Boulcott et al. 2007; Macer 1966). However, while food conditions have been shown to be linked to temporal variation in size (Eliassen 2013; MacDonald et al. 2018; MacDonald et al. 2019b), it is not clear what role they play in the observed spatial variation. Rindorf et al. (2016) explored this question, but found no relationship between sandeel growth and the metric used to represent food conditions - average abundance of copepod and proto-zooplankton between March and June based on model predictions. The authors suggested that the lack of a relationship may have been down to the data not capturing variation in the shape and timing of the zooplankton peak, which will be important as the degree of match between the sandeel foraging window and peak availability of zooplankton is a key determinant of fitness in post-metamorphic sandeels (van Deurs et al. 2010). It is also possible that a better taxonomic resolution is required. While the diet of lesser sandeels consists mainly of copepods (Eliassen 2013; Godiksen et al. 2006; Macer 1966; Roessingh 1957; van Deurs et al. 2014), they also feed on wide variety of other prey types, which may at times dominate the diet (e.g. Gómez García et al. 2012; van Deurs et al. 2010). The prey composition is important as the type of prey available has been suggested to be linked to growth rates, in particular through a positive effect of a larger proportion of large *Calanus* copepods (MacDonald et al. 2018; van Deurs et al. 2015, 2014). As such, to capture the aspects of the prey field that drive variation in intake rates and subsequent growth, it may be necessary to consider a prey field with high taxonomic and within-season temporal resolution. Further, prey fields would need to match the scale of the observed spatial variation in sandeel size (see Bergstad et al. 2002; Boulcott et al. 2007; Rindorf et al. 2016) in order to further explore the hypothesis that food conditions are behind the observed variation.

This chapter describes the development of an approach for generating sandeel prey fields of high taxonomic, temporal and spatial resolution from CPR zooplankton data. The focus is on the greater North Sea and the area up towards the Faroes and Iceland, an area where sandeels play an important role in the food web and that is also quite well covered in terms of CPR transects. The purpose is to fill a gap by creating a dataset with the resolution needed to examine the relationship between food conditions and sandeel growth on a larger spatial scale. To this end, the generated prey fields are used in Chapter 4 as input for a sandeel growth model to determine whether variation in food conditions can explain the observed variation in size. Further, in this chapter they are used to explore the question of how sandeel food conditions - in terms of total energy availability, prey size, and abundance of some key prey types - vary over time and space.

First, in Section 2.2, the CPR dataset is introduced in more detail and some of the potential biases in this dataset are discussed. Then, a review of studies on sandeel diet is presented (Section 2.3.1). Based on these studies, taxonomic groups sampled by the CPR that match the sandeel diet are identified. As a result of some of the biases in the CPR dataset, the abundances estimated by the CPR may be quite different from actual abundances for some taxa. For this reason, correction factors are developed with the help of data from the Stonehaven point-based sampling scheme (Bresnan et al. 2015) to correct for some of the sampling efficiency issues. While there are published correction factors for some CPR taxa (see Pitois and Fox 2006), the ones develop here add to previous work by also accounting for variation in sampling efficiency due to diel vertical migration. Following this, the methods used to translate CPR samples into prey fields are outlined. Briefly, these involve temporal interpolation of spatially aggregated data on scales over which plankton dynamics are considered to be sufficiently coherent. Then, collated information on size, weight and energy content for each taxon is presented. Finally, spatio-temporal patterns in characteristics of the lesser sandeel prey field thought to be important to sandeel growth conditions (total available energy, abundance of different copepod groups, average prey image area) are presented.

2.2 Continuous Plankton Recorder data

As part of the large-scale CPR sampling scheme, the CPR is towed behind “ships of opportunity” along commercial routes, thus providing good coverage of large parts of the study area, which is heavily trafficked. The CPR is towed at a depth of between 2 and 10 m (average 6.7 m), collecting plankton in the water entering the 1.27×1.27 cm square opening using continuously moving bands of silk filter with a mesh size of approximately 270 μm (Warner and Hays 1994). The speed at which the silk moves is adjusted to the speed at which the ship travels, so that 10 cm of silk (one sample) corresponds to 10 nautical miles (18.72 km) of tow (Reid et al. 2003a). Each sample takes around 15–30 minutes to collect (Everett et al. 2017). As the CPR is towed through the water, the continuously moving filter silk is wound together with covering silk and collects in the rear of the CPR where it is fixed with buffered formaldehyde. Once the tow is complete, it is hauled and transported to the laboratory facilities to be processed (Reid et al. 2003a).

The samples are then analysed using a method that has remained unchanged since 1958 (see Richardson et al. 2006 for details). First, the silk is divided into individual samples corresponding to 10 nautical miles. Then, the green colouration (which is a proxy for phytoplankton abundance) is assessed in relation to standard pantone colour charts. After this, the abundances of various plankton taxa are determined. Depending on the length of the silk, either all or alternate sections are examined. The assessment of zooplankton abundance is done in two stages. First, a ‘traverse’ count is conducted. Here, the silk is placed under $48\times$ magnification and a traverse of both the filter silk and the covering silk is conducted, during which around $1/50$ of the silk is viewed. For the traverse, all zooplankton are identified and counted, with the focus being on <2 mm organisms. Second, an ‘eye count’ is made, where all larger (>2 mm) zooplankton on the filtering and covering silks are removed, identified and counted. Following this, counts are sorted into abundance categories (see Table 2.1). Each category has an accepted midpoint, which is lower than the arithmetic mean, reflecting the fact that the abundances are generally skewed towards lower values. This categorical system is a trade-off between numerical accuracy and speed of processing and has been found to only result in a small (4%) underestimate of average abundances (Clark et al. 2001). For taxa counted with the traverse method, values are then multiplied by 50 in order to obtain the total abundance for a section of silk.

Table 2.1: Abundance categories used when processing CPR zooplankton data.

Number counted	Category	Accepted midpoint
0	0	0
1	1	1
2	2	2
3	3	3
4–11	4	6
12–25	5	17
26–50	6	35
51–125	7	75
126–250	8	160
251–500	9	310
501–1000	10	640
1001–2000	11	1300
2001–4000	12	2690

2.2.1 CPR sampling biases

The CPR data, as with all forms of zooplankton sampling, contain several sources of bias. This means that the data as they are should be interpreted more as a form of semi-quantitative abundance index, rather than a representation of absolute abundances. Comparisons with other plankton samplers have found that while showing similar seasonal and, to a lesser degree, inter-annual variation in overall plankton abundance, absolute estimates of abundance tend to differ, with the CPR often

producing lower estimates when compared to samples based on larger net samplers with a finer mesh (Batten et al. 2003; Clark et al. 2001; John et al. 2001; Kane 2009). For example, a spatially matched comparison with the net-based Dove time series from the western North Sea found that while the Dove time series caught 4500 individuals m^{-3} on average, the CPR only caught 293 individuals m^{-3} on average (Clark et al. 2001). Furthermore, as the type and impact of different sources of bias may vary between different taxa (Richardson et al. 2004), this means that changes in community composition are not straightforward to assess (Clark et al. 2001; John et al. 2001; Kane 2009). Different sources of bias are discussed in the following sections.

2.2.1.1 Variation in sampling volume

As plankton accumulates in the CPR, it becomes clogged. This will reduce the amount of water filtered, which is important as estimated plankton densities depend on the volume filtered (Batten et al. 2003). However, even at maximum clogging, the volume filtered is only reduced by 20% and the effect on estimated abundances is very small compared to the observed variation in abundances (John et al. 2002). Similarly, another study concerning phytoplankton found that any bias introduced by clogging is not a dominating driver of observed patterns (Barton et al. 2013). In addition, it is possible to some extent to correct for this by adjusting the sampled volume based on the estimated extent of clogging (see Section 2.3.3).

2.2.1.2 Vertical distribution and diel vertical migration

Zooplankton are generally not evenly distributed throughout the water column, which means that the samples collected by the CPR may not necessarily be representative of average densities as integrated over the whole water column, as only one depth is sampled (on average 6.7 m, but it has been suggested that the vessel towing the CPR may generate mixing down to 15 m, Everett et al. 2017, or potentially even deeper, David Johns, pers. comm.). For many taxa, peak densities are often found below the sampling depth of the CPR (Batten et al. 2003). The fact that the vertical distribution of a given taxon may vary with stage, sex, time of day, season, weather conditions and location, and that the patterns of this will vary with taxon (Lalli and Parsons 1997), also means that the relationship between the abundance sampled by the CPR and the abundance integrated over the whole water column will not be constant. Further, if the depth distribution is fully below the sampling depth, this may mean that CPR does not detect the presence of the taxon at all.

Still, correlations between CPR abundance estimates and abundance estimates based on sampling from the whole water column are often positive and strong (e.g. Clark et al. 2001; John et al. 2001; Kane 2009), suggesting that CPR estimates are representative of abundances deeper down. One study looking specifically at how CPR data collected for *Calanus finmarchicus* corresponded to abundances integrated over the whole water column found that the abundances sampled at the depth of the CPR were generally highly correlated with abundances at greater depths (Hélaouët et al. 2016). Still, it should be recognised that the relationship between abundances at the

CPR sampling depth and abundances as integrated over the whole water column may vary, and that this variation may to some degree be systematic, for example as a function of water depth.

One source of systematic variation in the depth of peak zooplankton density in relation to the CPR sampling depth is diel vertical migration (DVM) (Richardson et al. 2006), which generally involves a movement of zooplankton up towards shallower depths at sunset and a return towards deeper depths at sunrise. DVM behaviour tends to differ between taxa, some even showing reversed migration under certain conditions, and it may also differ depending on environmental conditions (see e.g. Irigoien et al. 2004). As such, the relationship between abundances measured by the CPR and average abundances integrated over the whole water column may differ between day and night, but the magnitude of this difference will depend on the taxon and environmental conditions. Some of this variation will be systematic, where, for example, the strength of DVM may vary systematically over the year (e.g. Beare and McKenzie 1999a), but there will also be more complex and unpredictable sources of variation. The presence of DVM means that if CPR samples used are not equally distributed between day and night, this could thus introduce a bias, which is not always accounted for (but see e.g. Beaugrand et al. 2001).

2.2.1.3 Small zooplankton slipping through mesh

Another bias is introduced by the fact that the relatively large mesh size may lead to certain taxa slipping through the mesh. It has been found that samplers with smaller mesh sizes than the CPR generally catch larger abundances of small zooplankton such as *Oithona* spp. (e.g. Batten et al. 2003; Clark et al. 2001; John et al. 2001; Kane 2009; Thompson et al. 2012). Experiments in which different zooplankton assemblages were poured through the CPR also confirmed that while around 98% of large copepods were retained, for smaller species such as *Oithona* spp. only around 40% were retained (Batten et al. 2003). In reality, even fewer are likely retained as the pressure exerted is increased when the CPR is towed. At the same time, increased clogging may act to reduce effective mesh size (Batten et al. 2003). Smaller taxa, such as *Oithona* spp., present further problems in that they can be difficult to identify and this may be further exacerbated by them, together with other soft-bodied taxa, being damaged by the double-silk winding method (Hunt and Hosie 2003; Kane 2009), potentially introducing further bias (Richardson et al. 2004).

2.2.1.4 Gear avoidance

On the other side of the spectrum, for larger zooplankton for which mesh size is not an issue, discrepancies between estimates from CPR samples and other samplers are likely the result of active avoidance (e.g. Batten et al. 2003; Clark et al. 2001; Kane 2009; Richardson et al. 2004). Avoidance is related to the speed of the device and the mouth area (Richardson et al. 2004). While the speed at which the CPR is towed is relatively high, the opening is small, which could allow some taxa to escape (Clark et al. 2001).

2.2.1.5 Spatio-temporal pattern in samples

One distinctive feature of the CPR data is the uneven distribution of samples as a result of the set-up, where the sampler is towed along certain shipping routes. This results in clear spatial patterns in sampling frequency (Figure 2.1) but also in temporal patterns as shipping routes have a fixed timetable, which introduces a temporal structure to the data. Furthermore, as shipping routes may change or be cancelled, this can lead to gaps in the data or variation in the sampling frequency over time (Figure 2.2).

This spatio-temporal structure is important to consider when trying to infer patterns from CPR data. In addition to large-scale spatio-temporal patterns, zooplankton are inherently patchy in time and space. This patchiness occurs on several scales. Any patchiness on a finer spatial scale than the length of one sample (18.72 km) will be averaged out. However, patchiness occurs on larger scales too. A transect study in the northern North Sea, conducted during the latter part of the spring bloom, found that patchiness occurred on multiple scales (Mackas et al. 1985). On top of finer scale variability, the transect first covered a ~ 25 km section with lower abundances, followed by a section of around equal length with higher abundances. This larger-scale patchiness would not be averaged out in the CPR samples. The study also highlights that this patchiness may vary with taxon, with higher trophic levels showing more fine-scale patchiness. Whether the CPR samples inside or outside a high-density patch will have a large impact on the estimated abundance and will determine to what degree a sample is representative of a larger area.

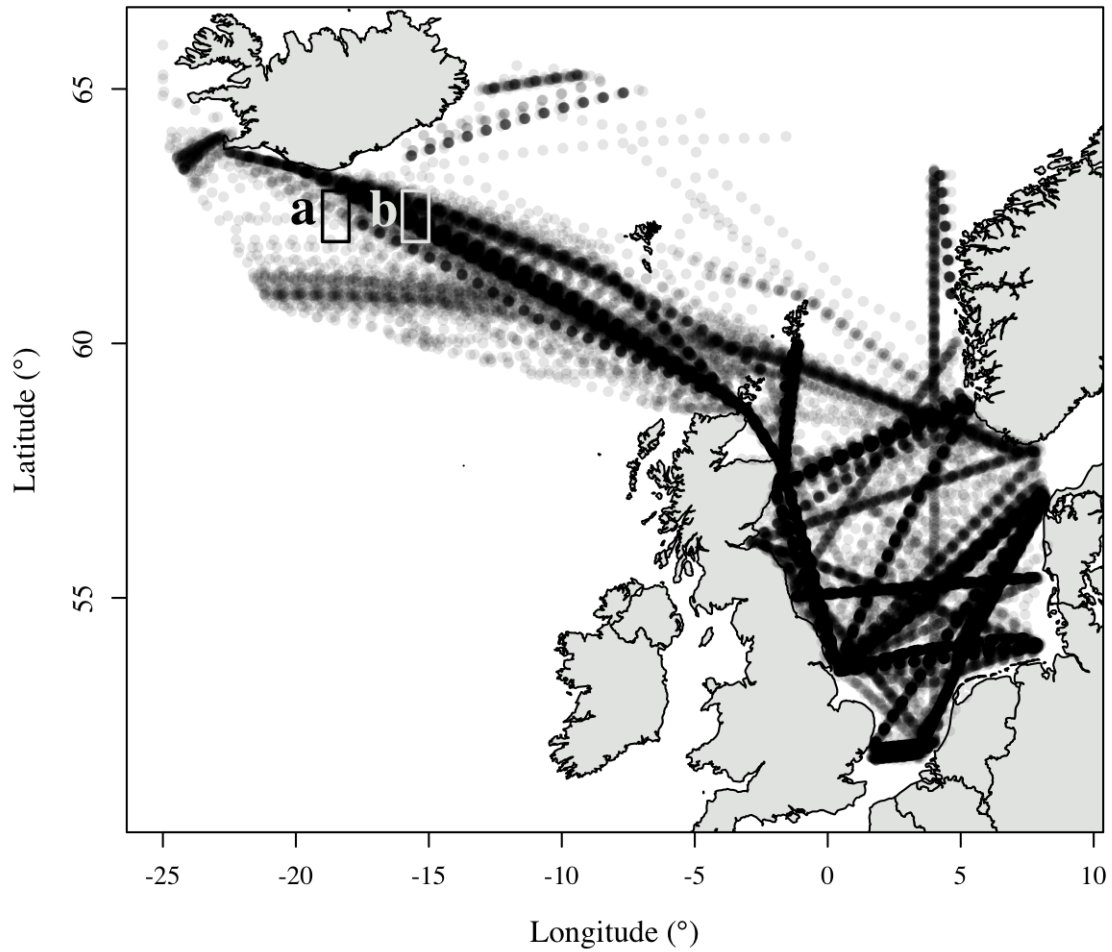


Figure 2.1: Translucent markers show CPR samples between 1975 and 2016 within the study area. The rectangles (a) and (b) show the locations of the rectangles used in Figure 2.2.

2.2.1.6 Abundance categories

As described, abundances are recorded as one of 13 abundance categories (Table 2.1). This system, as compared to recording actual abundances, may also introduce some issues. For example, as the classes increase in size, where the last class encompasses all values between 2000 and 4000, this means that it can be difficult to detect changes in areas of high density (Beare and McKenzie 1999b).

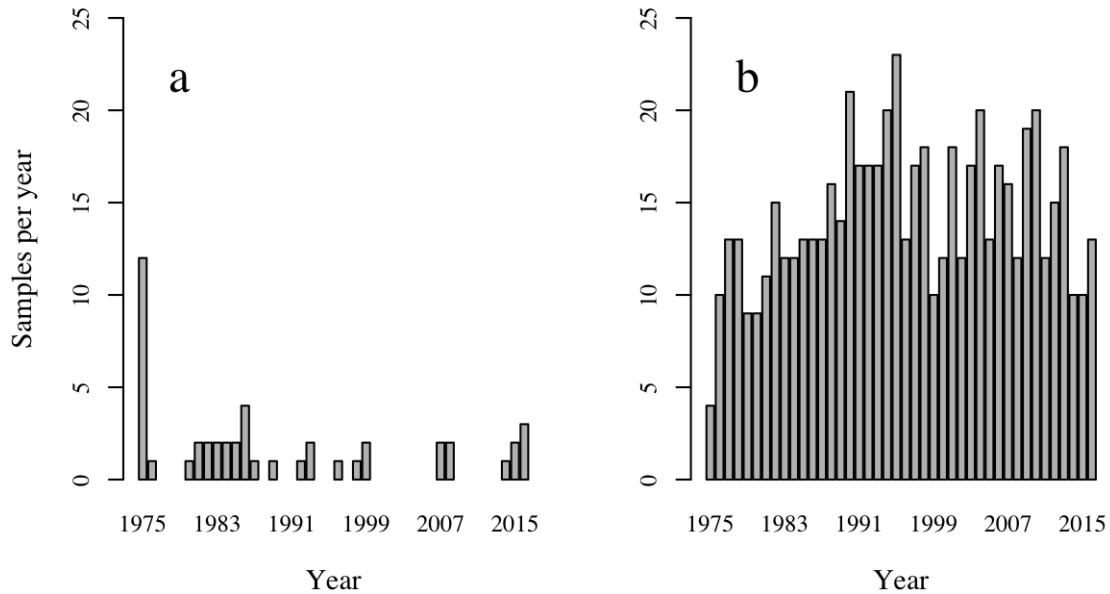


Figure 2.2: Example of spatial and temporal variation in CPR sampling frequency, showing number of samples per year, based on the rectangles (a) and (b) as indicated in Figure 2.1.

2.3 Methods

2.3.1 Diet of post-metamorphic sandeels

To determine which taxonomic groups from the CPR data should be included in the generated prey fields, a review of published diet studies was conducted. Copepods have repeatedly been pointed out as an important prey item for post-metamorphic sandeels. One study from the southern North Sea found copepods of the genus *Temora* to be the most common prey item, while *Calanus* copepods occurred in 30% of the sampled stomachs and copepods of the genus *Pseudocalanus* were present at lower numbers (Macer 1966). Another early study conducted outside the Dutch coast identified copepods of the genera *Pseudocalanus*, *Paracalanus* and *Temora* (Roessingh 1957). Later studies at Dogger Bank have pointed to copepod species of the genus *Calanus*, in particular *Calanus finmarchicus*, as the most important prey item (van Deurs et al. 2014). *Calanus finmarchicus* was also found to be dominant in a study conducted outside the coast of northern Norway (Godiksen et al. 2006). Sandeel stomachs sampled from the Faroe shelf contained the copepods *Calanus finmarchicus*, *Temora longicornis* and *Pseudocalanus* sp. Finally, a study in the Firth of Forth found *Temora longicornis* and *Acartia clausi* as well as other unidentified copepods in the sampled sandeel stomachs (Gómez García et al. 2012).

In addition to copepods, other crustaceans including krill (Godiksen et al. 2006) amphipods, mysids (Eigaard et al. 2014) as well as crustacean larvae (Eliassen 2013) are also part of the diet. Fish larvae have also been found repeatedly in sandeel stomachs (Eigaard et al. 2014; Godiksen et al. 2006; Rankine and Morrison 1989) and may be underestimated as a prey item as they are rapidly digested and may thus not be detected at the time of sampling (Christensen 2010; Godiksen et al.

2006). Fish eggs have also been found in sampled stomachs (Rankine and Morrison 1989; Roessingh 1957). Further, appendicularians were found to be the dominant prey item at the survey in the Firth of Forth (Gómez García et al. 2012) and has also been found to be the dominant prey of sandeel at other sampling sites in the North Sea (van Deurs et al. 2010). Finally, cladocerans (*Podon* and *Evadne* spp., Roessingh 1957) as well as polychaetes (Macer 1966) and their larvae (Eliassen 2013) have been found in sampled stomachs. It should be noted that as the prey available to sandeels will vary over time and space, these surveys should be thought of as snapshots of stomach content and may as such not necessarily be representative of diet in the long term. Still, taken together, these studies should provide a good idea of the range of prey consumed by the sandeel.

2.3.2 Taxonomic groups included

All taxonomic groups that were considered to be part of the sandeel prey base (as based on the review above in Section 2.3.1) and that were present in at least 5% of the CPR samples within the study area (see Figure 2.1) were included. These taxa included the copepod groups *Acartia* spp., *Calanus finmarchicus*, *Calanus helgolandicus*, *Calanus* I–IV, *Centropages typicus*, *Metridia lucens*, *Oithona* spp., *Parapseudocalanus* spp. and *Temora longicornis*. In terms of other crustaceans, this included Euphausiacea and the amphipod group Hyperiidea, and for crustacean larvae, this included copepod nauplii and Decapoda larvae. Appendicularia, fish eggs, fish larvae as well as the cladocerans *Evadne* spp. and *Podon* spp. were also included. Even though they did not fulfill the criterion for inclusion, *Centropages* spp. and *Calanus* V–VI were also included, as they, respectively, represent individuals of the *Centropages* and *Calanus* genera that could not be identified to species levels, and *Calanus finmarchicus*, *Calanus helgolandicus* and *Centropages typicus* did meet the criterion. As the group *Centropages* spp. may also include unidentified *Centropages hamatus*, this species was also included, even though it fell just short of the 5% threshold. Taxonomic details of the groupings used in the CPR dataset are provided by Richardson et al. (2006).

This final dataset, which spans the years 1975–2016, covers all the taxonomic groups that make up the vast majority of sandeel prey (see Section 2.3.1). However, it may still be that it excludes prey items that could potentially be locally important in some years. For example, it does not include polychaete larvae, which was reported in sampled stomachs by Eliassen (2013), although only found in 3 years out of 5, making up 5–20% of the diet. However, this potential reduction in prey availability is balanced against the benefit a simpler dataset with less uncertainty, as each prey group requires correction factors and prey characteristics to be determined, which both introduce uncertainty. Furthermore, since the abundance criterion for inclusion was generous, it does not have a big impact on total abundances.

2.3.3 Adjusting for clogging

To translate the raw data, which are in the format of abundance per 10 nautical miles, into individuals m^{-3} , each abundance estimate was divided by the filtered volume. The filtered volume was estimated from an empirical relationship between phytoplankton abundance (indicated by silk colour) and filtered volume estimated by a flowmeter, where $\text{volume filtered} = 3.19 - 0.07 \times \text{colour index}$ (John et al. 2002).

2.3.4 Correction factors

As a result of the various biases outlined above in Section 2.2.1, the raw CPR data are not equivalent to absolute average abundances. While all plankton samplers have inherent biases (Owens et al. 2013) some of the issues of the CPR, such as small zooplankton slipping through the mesh, may be reduced in other samplers. As such, in order to produce something more similar to absolute abundances, CPR samples can be compared with data collected by other plankton samplers to develop correction factors that can be used to bring CPR samples up to a similar level. While applying these correction factors will not result in “true” estimates for a given location and time point, for example as a result of variation in the vertical distribution in relation to the depth of the CPR, the resulting estimated long-term average may be more similar to the true long-term average. It was assumed that abundances averaged over the whole water column are sufficiently representative of sandeel feeding conditions as sandeels are generally present throughout the water column during the day (Freeman et al. 2004; Johnsen et al. 2017) and generally forage in areas with stronger currents (Tien et al. 2017) that are thus well-mixed.

Data from the Stonehaven sample site in the north-western North Sea (57°N 2.1°W , see Figure 2.3) were used to develop the correction factors. Zooplankton abundance estimates collected weekly at this site since 1997 were obtained from Marine Scotland Science (2018), but the copepod nauplii data were provided separately by Margarita Machairopoulou. The sampling site is located 5 km offshore to reduce the freshwater influence from rivers (Bresnan et al. 2015) and due to strong tidal currents, thermal stratification is minimal (Bresnan et al. 2009). Zooplankton samples are collected by vertical hauls from a depth of 45 m, which is close to the total depth of 48 m (Bresnan et al. 2015). The sampler used is a 40 cm diameter bongo net with a 200 μm mesh (Bresnan et al. 2015). Several of the biases present in the CPR dataset are reduced in the Stonehaven dataset. The vertical haul from close to the seabed means that variation in the vertical distribution of the zooplankton (including as a result of DVM) is not going to impact the abundance estimates. Further, the small mesh size of the bongo net means that small zooplankton are less likely to pass through the mesh, whereas the larger diameter reduces the ability of larger zooplankton to escape. However, the slower speed at which it is towed, compared to the CPR, may enhance the ability of larger zooplankton, such as krill, to escape.

In order to create correction factors, taxonomic groups in the CPR and Stonehaven samples had to be matched up (see Table A.1 in Appendix A). If one CPR taxon corresponded to multiple groups in the Stonehaven dataset, these were added

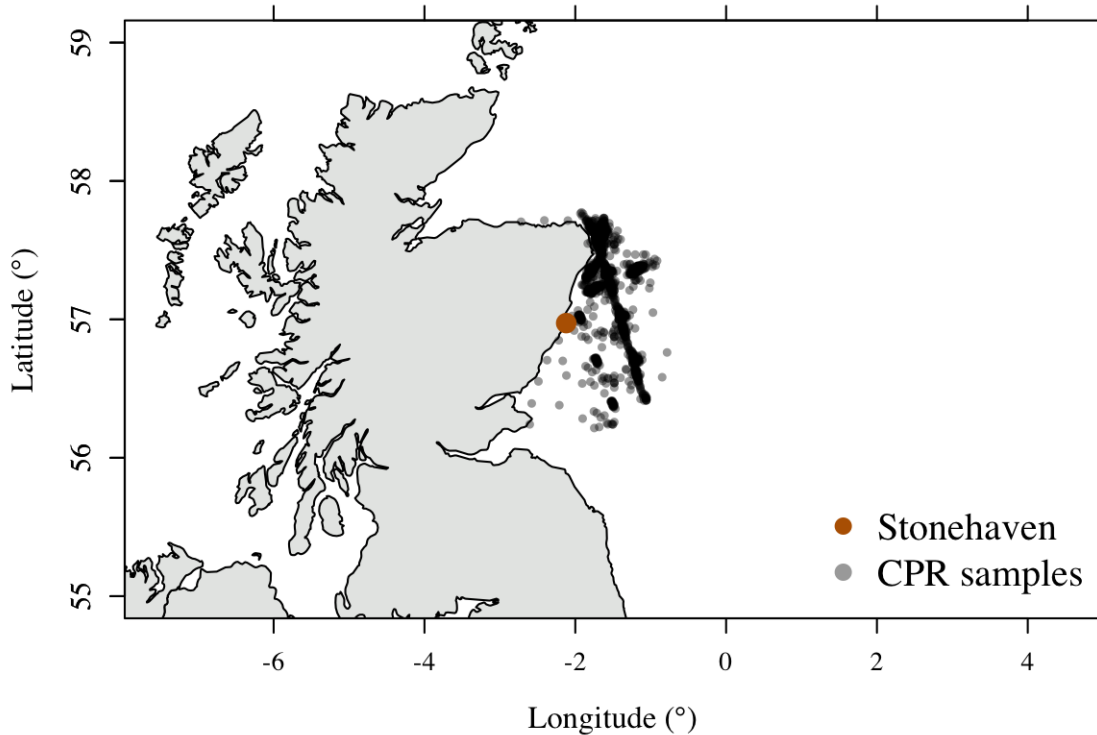


Figure 2.3: Location of the Stonehaven sample site is indicated by the red point. Translucent black markers show CPR samples used to develop the correction factors.

up. While the categories were matched up as closely as possible, there may sometimes be certain discrepancies due to, for example, age categories being handled differently. It should be noted that the CPR copepod categories generally refer to adult copepods (V–VI), unless otherwise noted (*Calanus* I–IV) (Richardson et al. 2006). One exception is the *Para-Pseudocalanus* spp. This category includes adults of *Paracalanus* and *Pseudocalanus* spp., but may also include other unidentifiable small copepods, including juveniles (Richardson et al. 2006). This is reflected in the groupings for this category (see Table A.1 in Appendix A, based on pers. comm. Margarita Machairopoulou). For the *Centropages* categories (*Centropages hamatus*, *Centropages typicus* and *Centropages* spp.), these were all grouped and a single correction factor was calculated. For *Calanus* V–VI, which includes unidentifiable *Calanus* V–VI, a correction factor was not calculated but instead the average of the correction factors for *Calanus finmarchicus* and *Calanus helgolandicus* was used, as this category likely represents a mix of these two species in the study area.

Following this, a subset of the CPR data which corresponded to the Stonehaven dataset in location and time span was created. This subset had to provide a large enough sample size for the CPR data, but still display as similar plankton dynamics to Stonehaven as possible. The waters surrounding the Stonehaven sampling site display mixed hydrodynamic regimes, which may impact the plankton dynamics (Capuzzo et al. 2018) and could possibly mean that measurements at Stonehaven are not very representative of dynamics in a larger area. To determine how similar the dynamics in the CPR data are to those measured at Stonehaven, the correlation between monthly averages were assessed (Pearson correlation r). The arithmetic

mean was calculated for a given year-month combination if there were at least 3 samples per month, for both the Stonehaven dataset and the CPR dataset separately. The area used to aggregate CPR data was centred on the Stonehaven sampling site, where the radius was incrementally increased by 1 km from 50 km (16 year-month combinations with data from both sources) to 200 km (142 year-month combinations with data from both sources). The distances were calculated using the function *spDistN1* in the package *sp* (Bivand et al. 2013; Pebesma and Bivand 2005) in R 3.5.2 (R Core Team 2018, used for all analyses in this chapter), where distances are measured as Great Circle (WGS84 ellipsoid) distances. The approach of aggregating data over circular areas centred on Stonehaven is based on the idea that samples closer in space are likely to be more similar. However, it may be that greater coherence is achieved by using samples that are located further away, but in locations that are hydrodynamically similar. Based on this idea, an alternative approach where data were aggregated over an area which corresponded roughly to the permanently mixed and intermittently stratified coastal waters along the Stonehaven coast and up into the Moray Firth as based on Figure 1a in Capuzzo et al. (2018) was also used (132 year-month combinations with data from both sources). The results can be seen in in Figure 2.4.

It was clear that below around 75 km, estimated correlation strengths were quite variable, likely due to the smaller sample sizes. Further, it was clear that the different taxa displayed quite different patterns in how the strength of the correlation changed with increasing radius used for the area of aggregation. The strength of the correlation based on data following the coastline as compared to aggregating data based on a maximum radius also differed between taxa, but did not generally result in greater correlations than using circular areas centred on Stonehaven. While no distance was optimal for all taxa, somewhere between 80–100 km appeared to work well for most (ignoring distances below 75 km where estimates were more variable). As some taxa showed an increase in correlation strength between 80 and 100 km and others a decrease, a value of 90 km was chosen as a compromise (it should also be noted that correction factors as developed below based on either a 80 km or a 100 km radius gave similar results). This is well within previously used distances that achieved coherence between local point-samples and CPR samples (discussed in Section 2.3.5). From this area, all CPR samples from years for which sampling in Stonehaven was run (1997–2016) were extracted.

Next, the CPR samples were sorted into night and day samples in order to be able to develop correction factors that accounted for any possible impact of DVM. To do this, the function *getSunlightTimes* from the R-package *suncalc* (Thieurmél and Elmarhraoui 2019) was used to calculate the timing of sunrise and sunset for each day. Samples collected post-sunrise and pre-sunset were classified as day samples and samples collected post-sunset and pre-sunrise were classified as night samples. To account for DVM, separate correction factors were then calculated for day and night samples for all taxa apart from the fish eggs, which were not expected to undergo DVM as, unlike the other taxa, they are not capable of independent movement. While not all other taxa may undergo any substantial DVM, assuming that they do will not have a great impact on the results as it just means that the estimated correction factors for day and night samples will be similar.

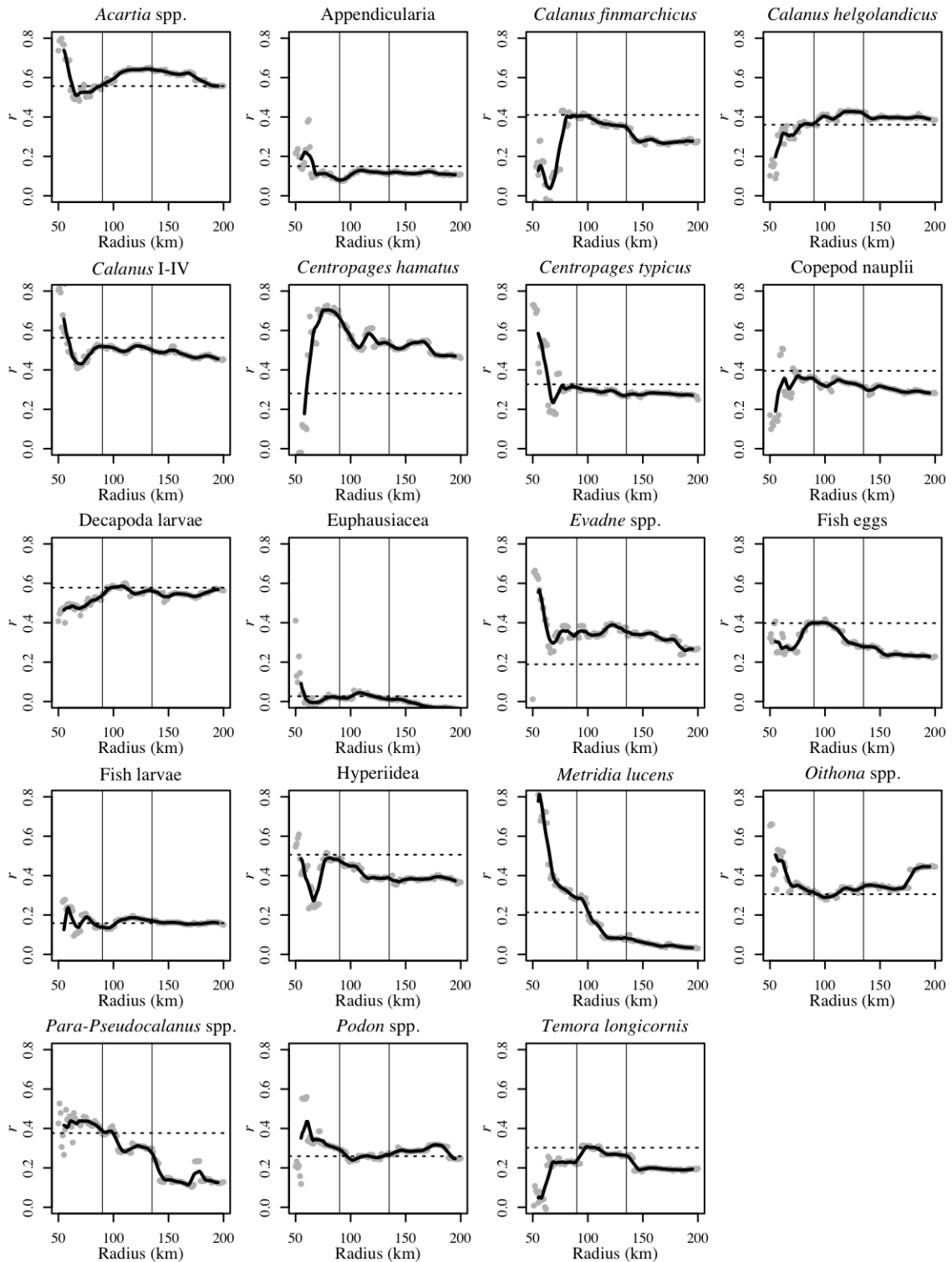


Figure 2.4: Correlations between time-matched monthly average abundances at Stonehaven and in the CPR dataset as aggregated for different radii around the Stonehaven sampling site. Grey markers show the estimated correlations and the black full line shows the moving average based on a 10 km window. Horizontal dotted line shows correlation strength based CPR data aggregated over coastal waters that are hydrodynamically similar to those at Stonehaven. Vertical lines show final aggregation radii of 90 km for the development of correction factors (see Section 2.3.4) and 135 km for generating prey fields (see Section 2.3.5).

To reduce any impact of seasonal or long-term trends, the samples were matched up in terms of their temporal spread so that the proportional contribution of each year-month combination was the same for both the Stonehaven dataset and the CPR datasets (this was done separately for the night and day datasets). If there was a higher proportion of Stonehaven samples than CPR samples for a given year-month combination, the samples collected closest in time to the CPR samples were used so that there was an equal proportion of samples. Similarly, if there was a higher proportion of CPR samples than Stonehaven samples for a given year-month combination, the samples collected closest in space to the Stonehaven sampling site were used so that there was an equal proportion of samples. For each taxon the correction factor was then calculated as the long-term mean abundance in the Stonehaven samples divided by the long-term mean abundance in the CPR samples. This was done separately for day and night samples. However, for fish eggs, that do not undergo DVM, all data were pooled instead.

As expected based on DVM behaviour, the estimated correction factors for day samples (when the plankton are more likely to be below the sampling depth of the CPR) were larger than the corresponding night correction factors (except for fish larvae where they were the same) and were generally within the range of previously estimated values (Table 2.3). However, it should be noted that some of these previous estimates showed large variation between different studies and were also not available for all taxa. When the estimated correction factor did not fall within the previously observed range, the discrepancy was generally not large, especially in relation to the range of values estimated from previous studies. While the estimated correction factors will be dependent on local plankton dynamics, as well as the distribution of CPR samples (which clearly are not uniformly distributed, see Figure 2.3), this similarity with previous estimates suggest that the estimated correction factors can be applied more generally. However, it should still be remembered that their validity may vary, for example as a result of spatial patterns in DVM.

While the approach worked well for most taxa, this was not the case for Euphausiacea. Euphausiacea are well-known to be particularly difficult to sample, showing high levels of gear avoidance (Wiebe et al. 1982). This can also be seen in Table 2.3, where some previous studies have estimated correction factors below zero, which is also what was found when using the data from Stonehaven. For this reason, estimates from studies aimed at quantifying the degree of undersampling of Euphausiacea (Sameoto et al. 1993; Wiebe et al. 2013) were used to develop correction factors for this taxon, resulting in a correction factor of 10 for day samples and 4 for night samples. While these studies were based on samplers with a larger opening, it seems as if for krill there is a trade-off between aperture opening and the ability of the krill to detect and avoid the sampler (Wiebe et al. 1982), suggesting that these values may be representative for the CPR as well.

Table 2.3: Final correction factors for each taxon based on the values calculated from the Stonehaven and CPR datasets, or previous work in the case of Euphausiacea (c.f. = correction factor). The number of samples used to calculate the correction factors are given in brackets after each estimate. Previously published CPR correction factors/ratios are also presented. These include estimates for day and night separately (as provided by Michael Heath) with the first value based on data from the L4 station in Plymouth (same as in John et al. 2001) and the second based on data from Stonehaven, as well as published estimates from Clark et al. (2001), John et al. (2001), and Kane (2009), in which night and day samples are considered together.

Taxon	c.f. day	c.f. night	Heath day	Heath night	Clark	John	Kane
<i>Acartia</i> spp.	21.9 (584)	11.3 (464)	3.8, 72.7	3.8, 23.1	13.2	2.3	-
<i>Appendicularia</i>	12.7 (688)	7.3 (537)	7.3, 15.4	7.7, 6.9	10.1	-	13.8
<i>Calanus finmarchicus</i>	22.9 (688)	4.1 (537)	-, 13.4	-, 4.1	2.8	2.1	2.2
<i>Calanus helgolandicus</i>	9.1 (688)	6.9 (537)	4.3, 4.9	3.8, 5.4	2.8	2.1	-
<i>Calanus</i> V–VI	16.0 (688)	5.5 (537)	-, -	-, -	-	-	-
<i>Calanus</i> I–IV	5.8 (688)	3.5 (537)	-, 2.3	-, 2.6	-	-	-
<i>Centropages hamatus</i>	5.2 (689)	3.1 (537)	0.2, 221.3	0.1, 332.0	-	0.95	-
<i>Centropages typicus</i>	5.2 (689)	3.1 (537)	0.8, 0.9	0.8, 0.6	0.8	0.95	1.6
<i>Centropages</i> spp.	5.2 (689)	3.1 (537)	-, -	-, -	-	-	-
Copepod nauplii	18.8 (632)	14.2 (480)	-, -	-, -	-	-	-

Decapoda larvae	16.9 (689)	9.7 (537)	9.2, 16.9	5.5, 10.8	-	-	7.7
Euphausiacea	10.0	4.0	0.9, 4.9	0.4, 1.2	-	-	2.1
<i>Evadne</i> spp.	18.0 (632)	13.0 (480)	22.3, 12.5	40.5, 11.3	18.2	-	-
Fish eggs	6.0 (889)	6.0 (889)	-, -	-, -	-	-	-
Fish larvae	1.4 (689)	1.4 (537)	-, -	-, -	-	-	5.8
Hyperiid	9.5 (632)	4.4 (480)	3.7, 12.5	2.9, 5.3	-	-	18.1
<i>Metridia lucens</i>	17.5 (584)	1.6 (464)	65.2, 15.4	5.1, 1.8	-	20.0	12.0
<i>Oithona</i> spp.	127.0 (446)	83.3 (336)	58.5, 148.7	60.0, 76.1	47.5	43.3	-
<i>Parapseudocalanus</i> spp.	18.3 (689)	8.7 (537)	21.8, 46.7	15.6, 21.9	15.8	8.1	-
<i>Podon</i> spp.	6.4 (689)	3.6 (537)	9.4, 9.6	13.2, 9.9	5	-	-
<i>Temora longicornis</i>	15.6 (584)	6.8 (464)	27.5, 24.8	10.3, 25.6	12.3	14.9	-

2.3.5 Spatial aggregation of CPR data

To create time series of prey fields, the CPR data were aggregated over space and then interpolated (interpolation is described in the next section - Section 2.3.6). The larger the area used for aggregation is, the more samples there are within each year, which leads to more robust estimates. Further, using a larger area also means that more years will have sufficient samples, resulting in a more complete series of prey fields. However, increasing the size of the area may mean that locations where dynamics are different from those at the focal location are included. Previous studies interpolating CPR data have used quite large radii (463 km, Beaugrand et al.

2000; 277.8 km, Pitois and Fox 2006). One study found high consistency, although variable between taxa, between local samples with high temporal resolution and CPR data averaged over a relatively large area (around 150 km maximum) (John et al. 2001), which suggests that using larger areas to develop representative estimates is appropriate. Another study comparing data from a fine-scale sampling station with CPR data collected from around 120 km around found that while the correlation in estimated monthly abundances often was poor, inter-annual variation and average annual cycles were similar (Clark et al. 2001). A similar study found that while the timing of spring and autumn peaks estimated by CPR data aggregated up to 3° from the focal site matched those estimated by fine scale sampling relatively well, the best match was achieved by using data within 1/4° (~30 km) of the sampling station (Ostle et al. 2017). However, John et al. (2001) got a very good agreement in the timing of peaks in spite of using a larger area. Finally, a study by Defriez et al. (2016) looked at the relationship between distance and correlation in the annual abundance of different zooplankton taxa sampled by the CPR aggregated by 1° by 1° grid cells, finding that this relationship varied between taxa, and in some cases between time periods. In general, there seemed to be a steeper decline with distance up to 200 km for the studied taxa consumed by sandeels, although in some cases, correlations remained above zero beyond this.

Based on Figure 2.4, taxa showed different patterns in how the strength of the correlation between monthly averages at Stonehaven and monthly averages based on the CPR data changes as the CPR data were aggregated over increasingly large areas. However, most taxa show weaker correlations as the size of the area increases. Based on the observation that several taxa that are important in the sandeel diet (*Calanus finmarchicus*, *Calanus helgolandicus*, *Para-Pseudocalanus* spp. and *Temora longicornis*, see Section 2.3.1) seem to show a steeper drop in the strength of correlation after 135 km, this was chosen as the radius used for interpolation. While correlations were stronger for shorter distances (which is why a distance of 90 km was used for calculating the correction factors), this would mean that prey fields could only be generated for very well-sampled areas. As such, the limit of 135 km is the result of a trade-off between coherence in dynamics and sample size. Compared to previous studies as outlined in the preceding paragraph, this threshold is well within distances for which coherent dynamics between the CPR and independent samples have been found previously.

Again, for aggregating areas, distances were calculated using the function *spDistN1* in the R-package *sp* (Bivand et al. 2013; Pebesma and Bivand 2005), where distances are measured as Great Circle (WGS84 ellipsoid) distances.

2.3.6 Interpolation

To obtain daily values, interpolation was carried out on a yearly basis. CPR transects are generally run on a monthly basis, so this is the smallest temporal unit that can be used for aggregating CPR data (Beare et al. 2003). Based on this idea, the samples were sorted into 12 equally sized sampling intervals for a given year and location. For each sampling interval, the arithmetic mean was calculated (see

next paragraph for a discussion on why the mean was used to represent the central tendency). This mean was then associated with the midpoint of each sampling interval and values between each midpoint were obtained through interpolation. This method ensured that the date of sampling would not introduce a bias in the phenological patterns. For the interpolation, piece-wise cubic Hermite interpolation with the function *pchip* in the R-package *signal* (Signal Developers 2014) was used. This type of interpolation preserves monotonicity, so that values will always be within the range of the two observations between which values are interpolated. Compared to linear interpolation, it has the benefit of providing smooth estimates around interpolation points, rather than sharp spikes. The method is described in Fritsch and Carlson (1980) and an example can be seen in Figure 2.5. Interpolation was only carried out if there were at least 3 samples per sampling interval during the period of interest (in this case, the sandeel feeding season). If the period of interest started before the midpoint of a given sampling interval, the previous sampling interval also had to have at least 3 samples, as this sampling interval will also impact the interpolated values in the first half of the next sampling interval. The threshold of 3 samples was the result of a trade-off between making estimates more robust and maximising the number of years for which daily time series could be produced.

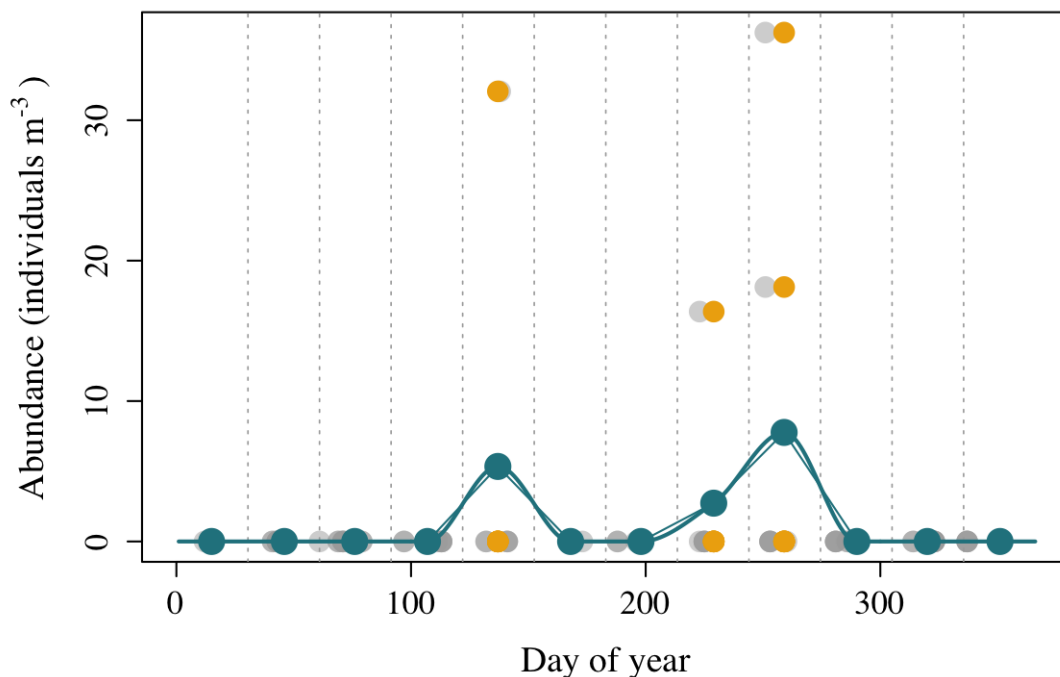


Figure 2.5: Example of interpolation of abundance estimates. The dotted vertical lines delineate the standardised sampling intervals. The grey dots show the raw CPR estimates of *Evadne* spp. abundance in the year 2016 in a 90 km radius around Stonehaven (see Section 2.3.4). The yellow markers show the same raw CPR estimates standardised to the midpoint of each sampling interval. The blue markers show the mean value in each sampling interval (the mean of the values shown by the yellow markers). The thick blue line shows interpolated values, using piece-wise cubic Hermite interpolation. Linearly interpolated values are also shown for reference with a thinner line.

The choice of using the arithmetic mean to represent the central tendency of a sampling interval is not a given. Within each sampling interval there may be a lot of variability. Prey fields are patchy, and since sandeels tend to show limited horizontal movement (Engelhard et al. 2008; Johnsen et al. 2017; van der Kooij et al. 2008), they are reliant on the patches that pass over their feeding grounds. This means that the spatial patchiness of zooplankton will translate into temporal patchiness for a given location, with the characteristics of this patchiness depending on the size of the patch and the advection speed. The impact of this patchiness on sandeel intake rate depends to a large extent on how the sandeels respond to the prey field. If they would be limited by their ability to process the prey, either by the time it takes to catch the prey or by their stomach capacity, then the patchiness is important. If prey availability is the main limiting factor, then patchiness is less important. For example, if there is a peak one day and low abundances one day, sandeels that are limited by stomach capacity or handling time might not be able to make full use of the peak day as their intake is capped. As such, intake would be lower than if they were feeding on the same total abundances averaged over two days. If instead the sandeels would be limited by availability, then total intake would be similar to intake based on abundances averaged over two days. In general, sandeel stomachs are most of the time well below maximum capacity (see Figure 3.4), suggesting that they are most often not limited by stomach capacity. In terms of handling times, the length of handling time that was found to introduce a limitation on intake based on a sandeel bio-energetic model (van Deurs et al. 2014), is greater than the handling times observed in an experimental setting (Christensen 2010; Winslade 1974b). However, even if they are not limited by stomach space or handling time in a strict sense, there are still other processes that may reduce the ability of the sandeels to make full use of the prey field, such as the small-scale patchiness in the prey field resulting in the sandeels most of the time being exposed to below-average abundances (see further discussion in Section 3.3.1.1).

Still, it seems as if in most cases, sandeels will be limited by prey availability. This means that the total intake based on prey abundances averaged over time is likely to be similar to total intake based on actual abundances for each day. For this reason, the arithmetic mean was used in the interpolation. However, it should be noted that in some cases the sandeels may be limited by stomach capacity or handling time, which may be particularly likely if zooplankton occur at extreme values, and in this case, the food that the sandeels are able to ingest over the whole season may be overestimated as a result of ignoring this patchiness. Further, sandeels do not feed in proportion to prey availability, but are instead selective (see Section 3.3.1), meaning that the composition of the prey field also matters. The composition of the prey field will also vary between days but when abundances are averaged over time, the temporal resolution of this variation in composition is decreased, which may also be a further reason why the response to a patchy prey field is different from the response to smoothed averages.

A further adjustment which has been adopted previously when spatially interpolating CPR data (Beaugrand et al. 2001, 2000; Pitois and Fox 2006) is to give samples closer to the focal point a larger weight when calculating the mean. While this may be a good idea when looking at large-scale spatial patterns in the data, it also re-

sults in the mean being very sensitive to variation in close-by samples which could be the result of patchiness, but also things like variation in sample depth or variation in flow rates, and may for this reason introduce a lot of noise. Using several samples from a relatively small area and giving all samples equal weight was therefore thought to be a more robust approach in this case, where samples were considered on a year-by-year basis.

2.3.7 Prey traits

Not only the abundance of zooplankton but also their size, weight and energy density are important as they will determine the ability of the sandeels to detect and catch the prey and how much energy ingested prey will provide. This information was thus collated for each taxon, sourcing values from the literature (see Table 2.4). While there is likely variation within prey types as a result of some groups containing several different species which may be of different sizes (Richardson et al. 2006) and within species as a result of variation over time and life stages (e.g. Bottrell and Robins 1984) or over space (Dessier et al. 2018), only one value was assumed for each prey type for simplicity.

For the total length of copepods the values reported by Richardson et al. (2006) were used and the length-weight relationship reported in this study was also used to estimate the wet weight for all copepods, whereas length and weight for other taxa were sourced independently. Energy densities were sourced independently for all taxa. Relationships presented by Kiørboe (2013) were used to translate reported carbon and dry weights into wet weights, apart from in the case of fish eggs, when information from Riis-Vestergaard (2002) was used. To translate reported carbon weights into energy, it was assumed that the energy density of carbon is 46 kJ g^{-1} (Salonen et al. 1976).

Table 2.4: Total length (mm), wet weight (mg) and energy density (J g wet weight⁻¹) of all taxonomic groups along with the source of the values. Copepod length and weight values were derived from Richardson et al. (2006), as described in the text.

Taxon	Total length (mm)	Wet weight (mg)	Energy density (J g wet weight⁻¹)
<i>Acartia</i> spp.	1.15	0.11	3500 Laurence (1976)
Appendicularia	1 <i>Oikopleura dioica</i> and <i>Fritillaria borealis</i> are the only indigenous appendicularians in the North Sea and both have a trunk length of around 1 mm (van Couwelaar 2003).	0.77 King et al. (1980), Hopcroft et al. (1998)	330 King et al. (1980), Hopcroft et al. (1998)
<i>Calanus finmarchicus</i>	2.70	0.64	4400 Laurence (1976)
<i>Calanus helgolandicus</i>	2.68	0.63	4400 Laurence (1976)
<i>Calanus</i> I-IV	1.65	0.23	3800 Campbell et al. (2001)
<i>Calanus</i> V-VI	2.48	0.54	4400 Laurence (1976)
<i>Centropages hamatus</i>	1.30	0.14	3400 Laurence (1976)
<i>Centropages typicus</i>	1.55	0.20	3600 Laurence (1976)
<i>Centropages</i> spp.	1.63	0.22	3500 Laurence (1976), mean of densities for <i>Centropages hamatus</i> and <i>Centropages typicus</i> .

Copepod nauplii	0.19 It is assumed that the nauplii of <i>Acartia clausi</i> are representative as this is the most common copepod species to occur in the dataset. Nauplii of <i>A. clausi</i> are around 0.19 mm (Hay et al. 1991). This is similar to the length of many other copepod taxa, but shorter than some, such as <i>Calanus</i> spp (0.41 mm, Hay et al. 1991).	0.0029 Hay et al. (1991)	1500 Tanskanen (1994)
Decapoda larvae	0.9 Polybiinae is the most common group of decapod larvae in the CPR dataset, with the most common species being part of the infraorder Brachyura (Lindley et al. 2010). In surveys around the coast of the UK in spring/summer, the size of Brachyuran larvae was around 0.9 mm (Lindley 1998).	0.46 Lindley (1998)	3200 Lindley (1998)

Euphausiacea spp.	17 <i>Thysanoessa inermis</i> is the most common species of Euphausiacea in most of the study area, although <i>Meganyctiphanes norvegica</i> is more common further north (Lindley 1977). A survey in the northern North Sea during April–June found adult <i>T. inermis</i> to be around 17 mm (Lindley and Williams 1980). A survey in the NE Atlantic in August/September found most <i>M. norvegica</i> to be around 15 mm long (Lindley et al. 1999).	56 Harvey et al. (2012)	4500 Kulka and Corey (2006)
<i>Evadne</i> spp.	0.5 The most common <i>Evadne</i> spp. in the North Sea is <i>Evadne nordmanni</i> (Gieskes 1971), which has a size of around 0.5 mm (Bainbridge 1958).	0.021 Rodhouse and Roden (2007)	4400 Rodhouse and Roden (2007)

Fish eggs	1 As herring (<i>Clupea harengus</i>) larvae are the most commonly found fish larvae in the CPR samples (Edwards et al. 2011), it is assumed that herring eggs are the best represented fish eggs as well. Herring eggs have a diameter of 1 mm (Stroud 2011).	1.6 Hempel and Blaxter (1967)	1300 Riis-Vestergaard (2002)
Fish larvae	12 12 mm is the average length of fish larvae in CPR samples from the NE Atlantic, with most of the larvae found in the study area being clupeids, followed by Ammodytidae larvae (Edwards et al. 2011).	2 Ehrlich et al. (1976)	2000 Arrhenius and Hansson (1996)
Hyperiidia spp.	16 The most common species in this taxon in the study area is <i>Themisto compressa</i> (at the time <i>Parathemisto gracilipes</i> , McHardy 1970). A survey in the NE Atlantic in July found a range of sizes with 16 mm being mid-range (Williams and Robins 1979).	32 Williams and Robins (1979)	2900 Williams and Robins (1979)
<i>Metridia lucens</i>	2.27	0.45	3100 Lindley et al. (1997)
<i>Oithona</i> spp.	0.68	0.036	2500 Uye (1982)

<i>Para- Pseudo- calanus</i> spp.	0.70	0.038	3400 Laurence (1976)
<i>Podon</i> spp.	1 The species <i>Podon leuckartii</i> and <i>Podon intermedius</i> are the most common in the study area (Gieskes 1971). Both are around 1 mm in size (van Couwelaar 2003).	0.21 Uye (1982)	4400 Uye (1982)
<i>Temora longicornis</i>	1	0.08	3000 Laurence (1976)

The prey image area (the area of the prey item as viewed by the sandeel) was also calculated. The square root of the image area will be directly related to the detection distance (and thus search rate) of the sandeel (see van Deurs et al. 2015 and Equation 3.9). It was assumed that appendages, such as legs or antennae, are generally not visible. For copepods it was assumed that the image area is an ellipse with length equal to the copepod prosome length and width equal to half the prosome length (see van Deurs et al. 2015). For prosome lengths it was assumed that this was 75% of total length (Razouls et al. 2020). For appendicularians it was assumed that only the trunk is visible, and that the trunk is an ellipse with the width being half the length. For crustacean larvae, cladocerans (*Evadne* and *Podon* spp.) and fish eggs, the simplifying assumption that these are all circular was made, with the measured length being their diameter. For fish larvae, the formula from Langsdale (1993) was used to calculate image area. For Euphausiacea and Hyperiidea spp., an elliptical shape was assumed with width 1/8 (based on images in Conti et al. 2005) and 3/11 (based on images in Kraft et al. 2013) of length, respectively.

2.3.8 Spatio-temporal variation in the sandeel prey field

Having developed methods for correcting abundances and creating daily interpolated time series for locations with sufficient coverage, this was now paired with the prey trait information to explore the spatio-temporal variation in some of the characteristics of the prey field hypothesised to be important for sandeel growth. Based on the finding that sandeel size is related to zooplankton biomass (Eliassen 2013; MacDonald et al. 2019b), patterns in average daily total energy (kJ m^{-3}) were examined. Further, as small copepods (defined as having a prosome length of less than 1.3 mm based on van Deurs et al. 2013) make up the main part of the diet in at least some locations and years (Macer 1966; Roessingh 1957), the average abundance of small copepods (*Acartia* spp., *Oithona* spp., *Para-Pseudocalanus* spp. and *Temora longicornis*) m^{-3} was also examined. Variation in the abundance of *Calanus* has also been pointed out as an important driver of growth (Bergstad et al. 2002; MacDonald et al. 2018; van Deurs et al. 2014) and so the abundance of *Calanus finmarchicus* m^{-3} and the abundance of *Calanus helgolandicus* m^{-3} were examined too. Finally, as it has been hypothesised that prey size may also be important through its effect on detection distance (van Deurs et al. 2015), the average daily mean square root of prey image area (mm), which is directly proportional to prey detection distance, was also examined.

The dataset (1975–2016, see Figure 2.1 for spatial extent) was split into three equally sized time periods (1975–1988, 1989–2002, 2003–2016), and a gridded map was produced for each time period. Two different sandeel feeding seasons were considered, a 1+ group feeding season (day 80–165, van Deurs et al. 2013) and an 0 group feeding season (day 141–212, Jensen 2000; Régnier et al. 2017; van Deurs et al. 2011a; Wright and Bailey 1996, see Section 4.2.2). The timing of these seasons may vary between years, and potentially also over space, due to variation in the date of metamorphosis (e.g. Régnier et al. 2017) or the timing of initiation and termination of overwintering (e.g. Reeves 1994), but these standardised seasons should provide an idea of general patterns. To produce the maps, data within a radius of 135 km (see Section 2.3.5) were aggregated for each time period and grid point (based on a grid of 0.25° latitude \times 0.5° longitude as the length of one latitude is roughly double that of one longitude at this latitude). Interpolation was then carried out for each year for which there were sufficient data during the feeding season, considering each age group separately. If there were sufficient data in at least 5 years during the time period, the interpolated data were subset according to the feeding season for each age group and the quantities of interest were calculated based on these datasets. For the average daily total energy, the daily abundances of each taxon were multiplied by the energy content of each taxon and these were then added up for all taxa and the average over the feeding season was calculated. It should be noted that this is not equivalent to ingested energy but only captures the amount available. For the abundance of small copepods, *Calanus finmarchicus* and *Calanus helgolandicus*, the average daily abundance over the feeding season was calculated (and added together in the case of small copepods). Finally, the average daily mean square root of prey image area was calculated by multiplying the daily abundances of each taxon by the square root of image area of each taxon, summing for all taxa, and then dividing by the total abundance of all taxa and calculating the average over the feeding season.

A simple exploration of temporal trends was also carried out. To do this, time series for four different areas which are well-covered by CPR transects and also contain sandeel grounds in which there is some knowledge of sandeel size and dynamics were examined: the Firth of Forth (56.3°N 2°W) in the north-western North Sea (roughly the location of Wee Bankie, Greenstreet et al. 2006), Dogger Bank (54.7°N 1.5°E) in the central-western North Sea (roughly location of North-West Rough, Boulcott et al. 2007; Rindorf et al. 2016), East Central Grounds (ECG, 57.6°N 4°E) in the north-eastern North Sea (based on location in Bergstad et al. 2002, see also Johannessen and Johnsen 2015) and Shetland (59.8°N 1.3°W), north of mainland UK (slightly south of an aggregation of sandeel grounds in southern Shetland, Wright and Bailey 1993). Locations further north were not included due to poor CPR coverage. As before, time series of prey fields were generated based on interpolation of an area with a 135 km radius.

For each location, generalised additive models (GAMs) were fitted using the function *gam* in the R-package *mgcv* (Wood 2011), with the response variable being the average value for each of the prey field variables (total energy, abundance of small copepods, *Calanus finmarchicus* and *Calanus helgolandicus* and average square root of image area), year as a smooth term and feeding season (1+ group/0 group) as a factor. The models were fitted with an identity link function, using generalised cross-validation to estimate the smoothing parameter. The adequacy of the smooths were assessed by checking for patterns in the residuals using the function *gam.check*. A confidence level of 0.05 was used to evaluate the presence of temporal trends and the difference between the feeding seasons.

2.4 Results

The characteristics of the sandeel prey field showed marked spatio-temporal variation. In terms of the average daily total energy (kJ m^{-3}) in sandeel prey, this varied over space (Figure 2.6), with generally higher concentrations closer to the coast. Further, there were clear declines in average daily total energy during the 0 group feeding season in Dogger Bank ($p < 0.01$) and the Firth of Forth ($p < 0.01$) as well as during the 1+ group feeding season in the Firth of Forth ($p < 0.01$) (Figure 2.7). The decline in the Firth of Forth was more rapid until around 2000, before levelling off, whereas in Dogger Bank declines were more rapid in the latter part of the time series. The other locations showed inter-annual variation, which was particularly marked in the ECG, but no clear temporal pattern (p all ≥ 0.08). The amount of energy available was greater during the 0 group feeding season in Dogger Bank and Shetland ($p < 0.01$), but not in the Firth of Forth ($p = 0.50$) or the ECG ($p = 0.93$).

Small copepods were more abundant further south within a given time period (Figure 2.8). In terms of temporal changes, they showed declines in Dogger Bank (1+ group: $p < 0.01$; 0 group: $p < 0.01$) and the Firth of Forth (1+ group: $p < 0.01$; 0 group: $p < 0.01$) (Figure 2.9). The declines were particularly marked during the 0 group feeding season. No clear temporal patterns were seen in the ECG or Shetland (p all ≥ 0.18). In all locations, there was a greater abundance of small copepods during the feeding season of the 0 group as compared to the feeding season of the 1+ group ($p < 0.01$).

The two species of *Calanus* copepods examined, *C. finmarchicus* and *C. helgolandicus*, showed different spatio-temporal patterns (Figure 2.10 and Figure 2.12). *C. finmarchicus* showed a clear spatial pattern with the highest abundances in the north-eastern part of the North Sea, off the coast of Norway. Spatial variation was not as marked in *C. helgolandicus*, but it is clear that abundances were low in the north up towards Iceland. There were no clear temporal trends in *C. finmarchicus* (p all ≥ 0.06 , Figure 2.11). *C. helgolandicus* has instead shown a clear increase over time in the Firth of Forth (1+ group: $p < 0.01$; 0 group: $p = 0.04$), ECG (1+ group: $p = 0.01$; 0 group: $p = 0.01$) and Shetland (1+ group: $p = 0.04$; 0 group: $p < 0.01$), as well as during the 1+ group feeding season in Dogger Bank ($p = 0.04$), but not the 0 group feeding season ($p = 0.75$). The increases in all locations seem to have mainly occurred after around 2000 (Figure 2.13). Abundances did not differ between the two feeding seasons in *C. finmarchicus* (p all ≥ 0.18) or *C. helgolandicus* (p all ≥ 0.10) in the examined locations. Even after increasing in more recent years, the peak abundances in *C. helgolandicus* were lower than peak abundances of *C. finmarchicus*. *C. helgolandicus* only made it over 100 individuals m^{-3} in a few years in the ECG and Shetland, whereas *C. finmarchicus* were repeatedly present in multiple hundreds in the ECG.

In general, the average daily mean square root of prey image area was largest in the far north, up towards Iceland (Figure 2.14). In terms of temporal trends, there was an increase over time during the 1+ group feeding season in Dogger Bank ($p < 0.01$), the Firth of Forth ($p = 0.04$) and Shetland ($p = 0.03$), as well as a decrease in the ECG during the 1+ group feeding season ($p < 0.01$) (Figure 2.15). Apart from this, there were no clear trends (p all ≥ 0.08). Values were larger during the 1+ group feeding season than the 0 group feeding season in the ECG ($p < 0.01$) and Dogger Bank ($p = 0.03$), but showed no difference in the Forth of Forth ($p = 0.08$) or Shetland ($p = 0.49$).

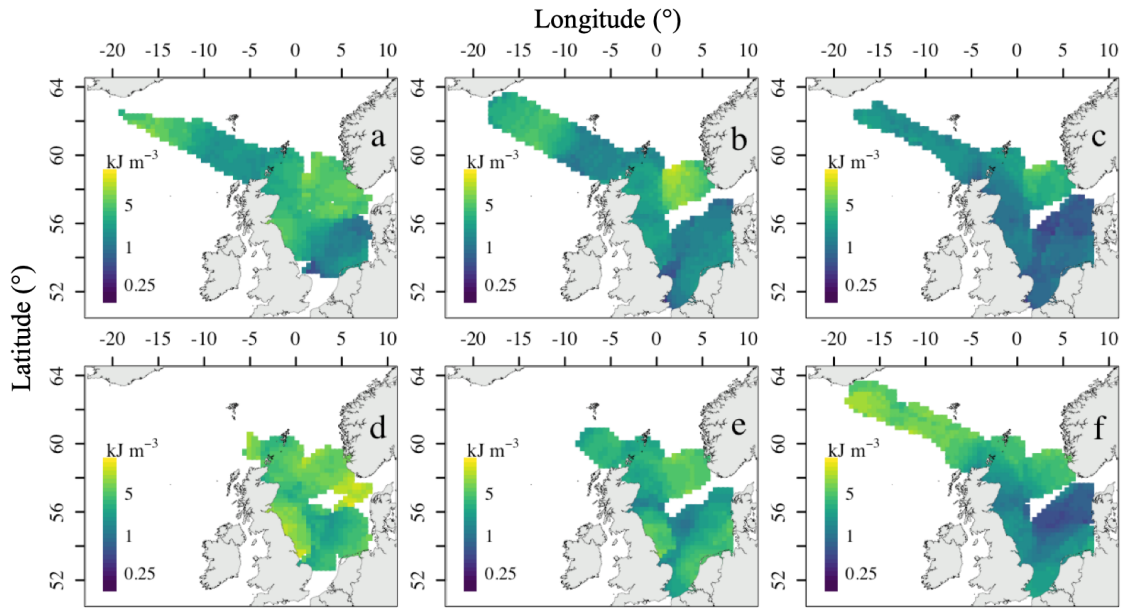


Figure 2.6: Average daily **total energy** (kJ m^{-3} , \log_{10} -scale) during the feeding season of 1+ group sandeels (a–c, day 80–165) and 0 group sandeels (d–f, day 141–212) for 1975–1988 (a,d), 1989–2002 (b,e), 2003–2016 (c,f).

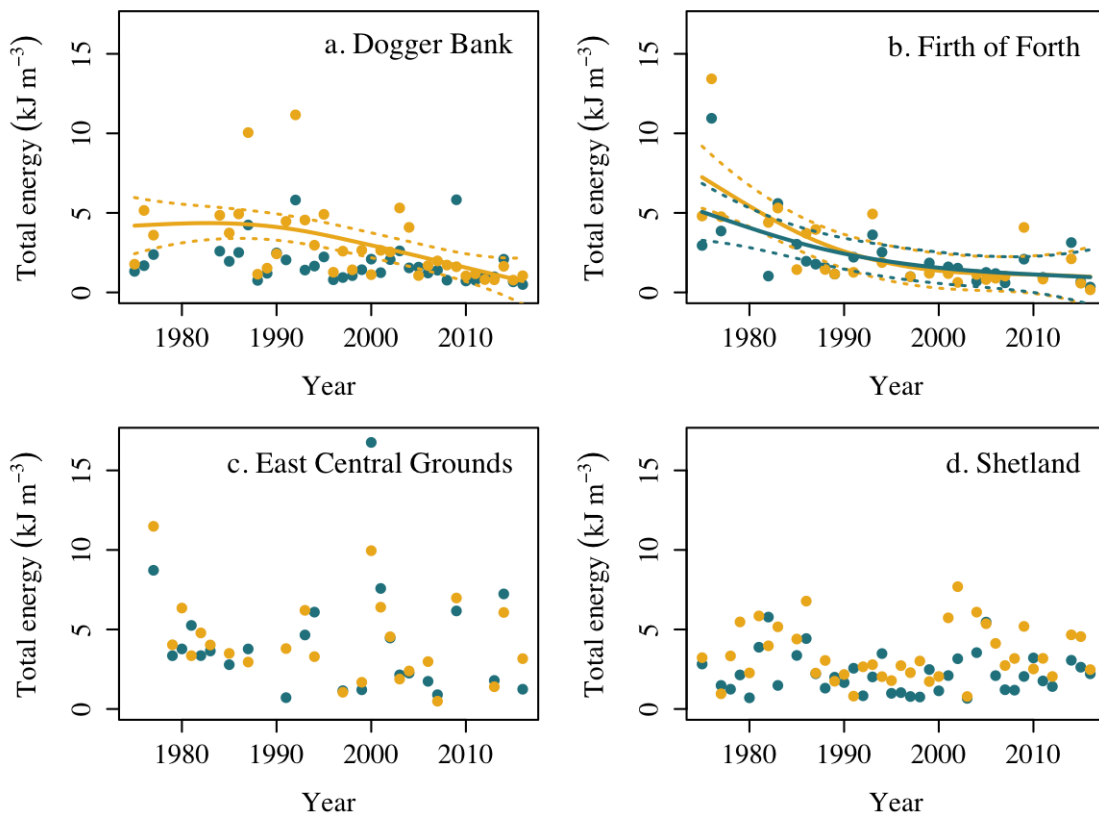


Figure 2.7: Changes in average daily **total energy** (kJ m^{-3}) over time. Blue and yellow markers denote averages during the 1+ group (day 80–165) and 0 group (day 141–212) feeding seasons, respectively. Lines show GAM predictions (if $p < 0.05$), with dotted lines indicating the 95% confidence interval.

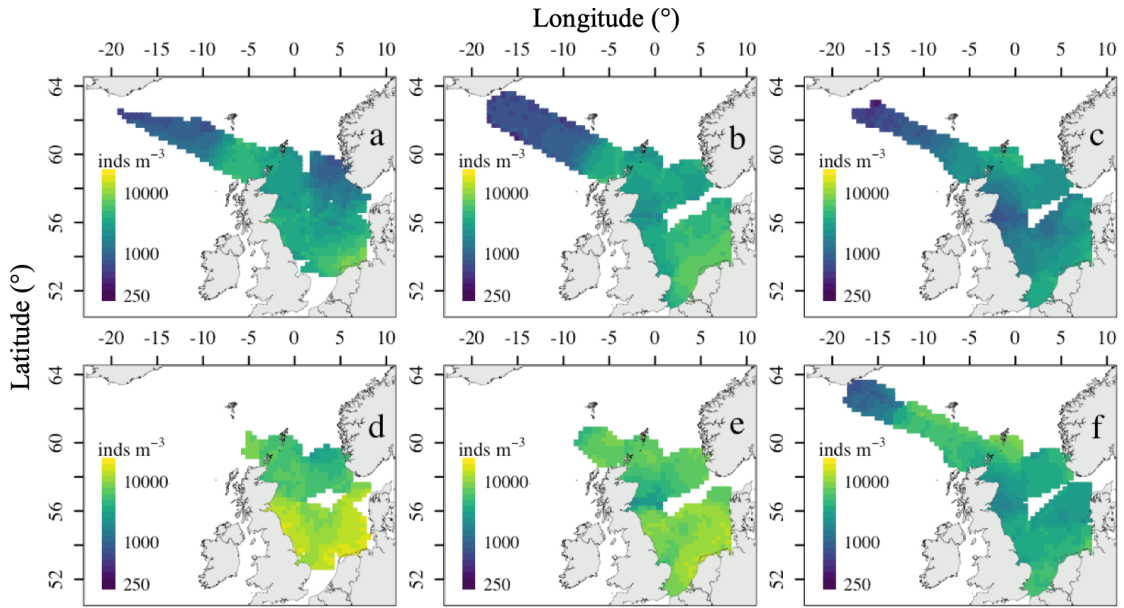


Figure 2.8: Average daily **abundance of small copepods** m^{-3} (\log_{10} -scale) (*Acartia* spp., *Oithona* spp., *Para-Pseudocalanus* spp. and *Temora longicornis*) during the feeding season of 1+ group sandeels (a–c, day 80–165) and 0 group sandeels (d–f, day 141–212) for 1975–1988 (a,d), 1989–2002 (b,e), 2003–2016 (c,f).

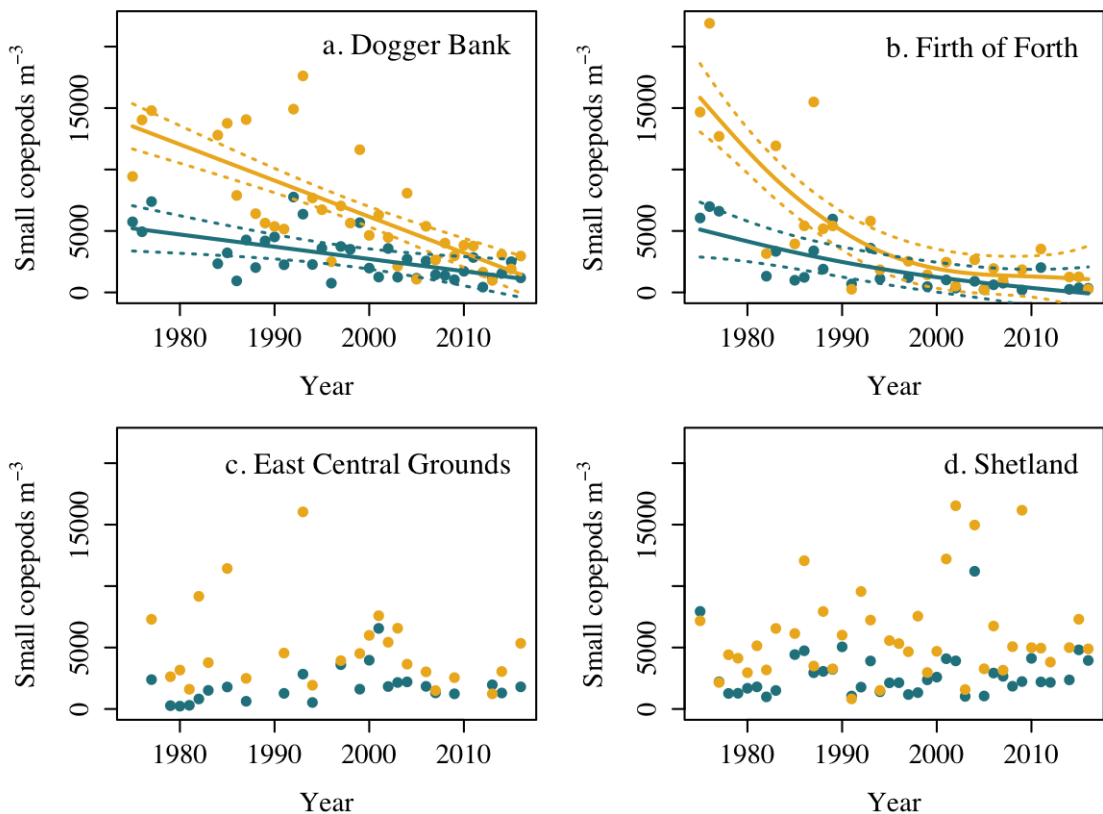


Figure 2.9: Changes in the average daily **abundance of small copepods** m^{-3} (*Acartia* spp., *Oithona* spp., *Para-Pseudocalanus* spp. and *Temora longicornis*) over time. Blue and yellow markers denote averages during the 1+ group (day 80–165) and 0 group (day 141–212) feeding seasons, respectively. Lines show GAM predictions (if $p < 0.05$), with dotted lines indicating the 95% confidence interval.

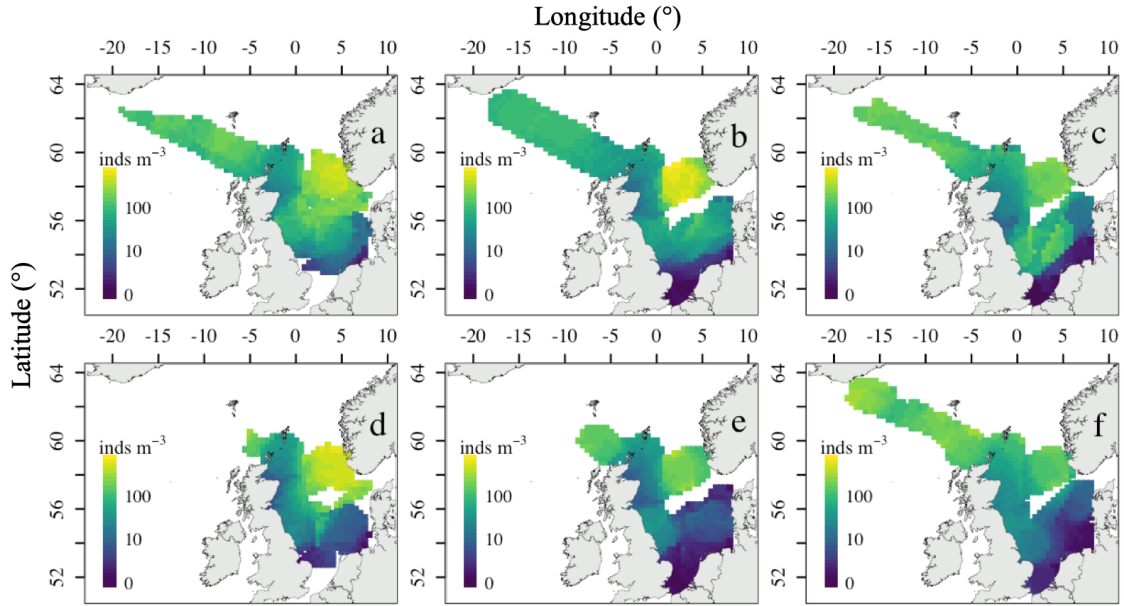


Figure 2.10: Average daily abundance of *Calanus finmarchicus* m^{-3} (\log_{10} -scale) during the feeding season of 1+ group sandeels (a–c, day 80–165) and 0 group sandeels (d–f, day 141–212) for 1975–1988 (a,d), 1989–2002 (b,e), 2003–2016 (c,f).

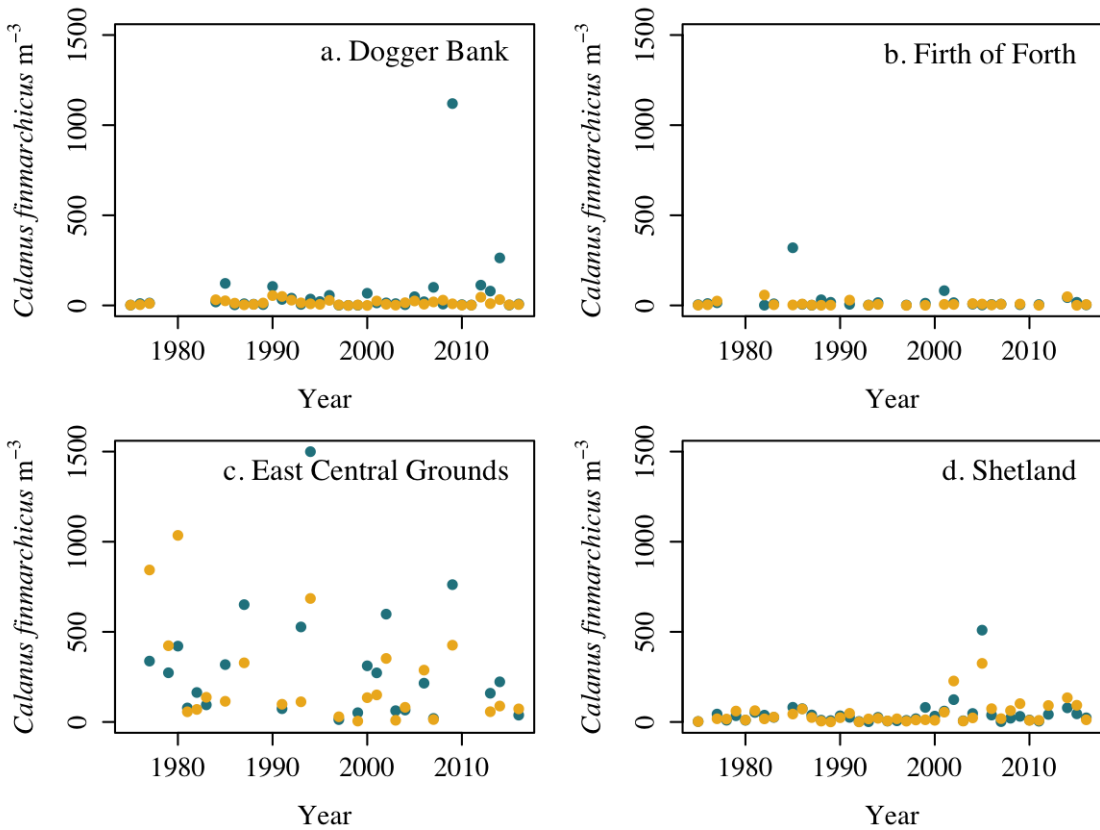


Figure 2.11: Changes in the average daily abundance of *Calanus finmarchicus* m^{-3} over time. Blue and yellow markers denote averages during the 1+ group (day 80–165) and 0 group (day 141–212) feeding seasons, respectively.

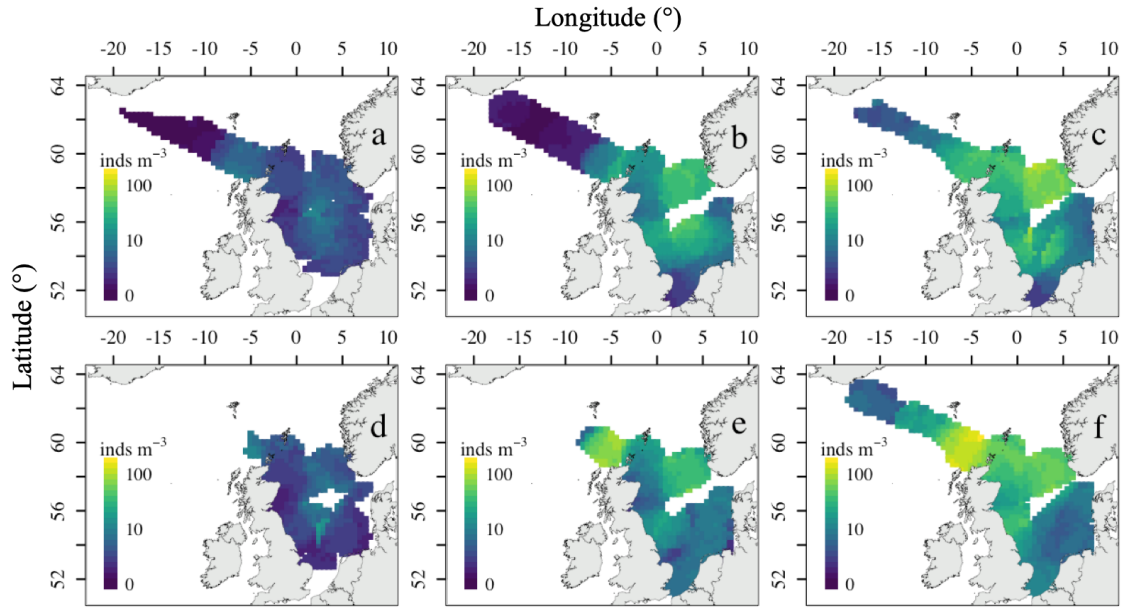


Figure 2.12: Average daily abundance of *Calanus helgolandicus* m^{-3} (\log_{10} -scale) during the feeding season of 1+ group sandeels (a–c, day 80–165) and 0 group sandeels (d–f, day 141–212) for 1975–1988 (a,d), 1989–2002 (b,e), 2003–2016 (c,f).

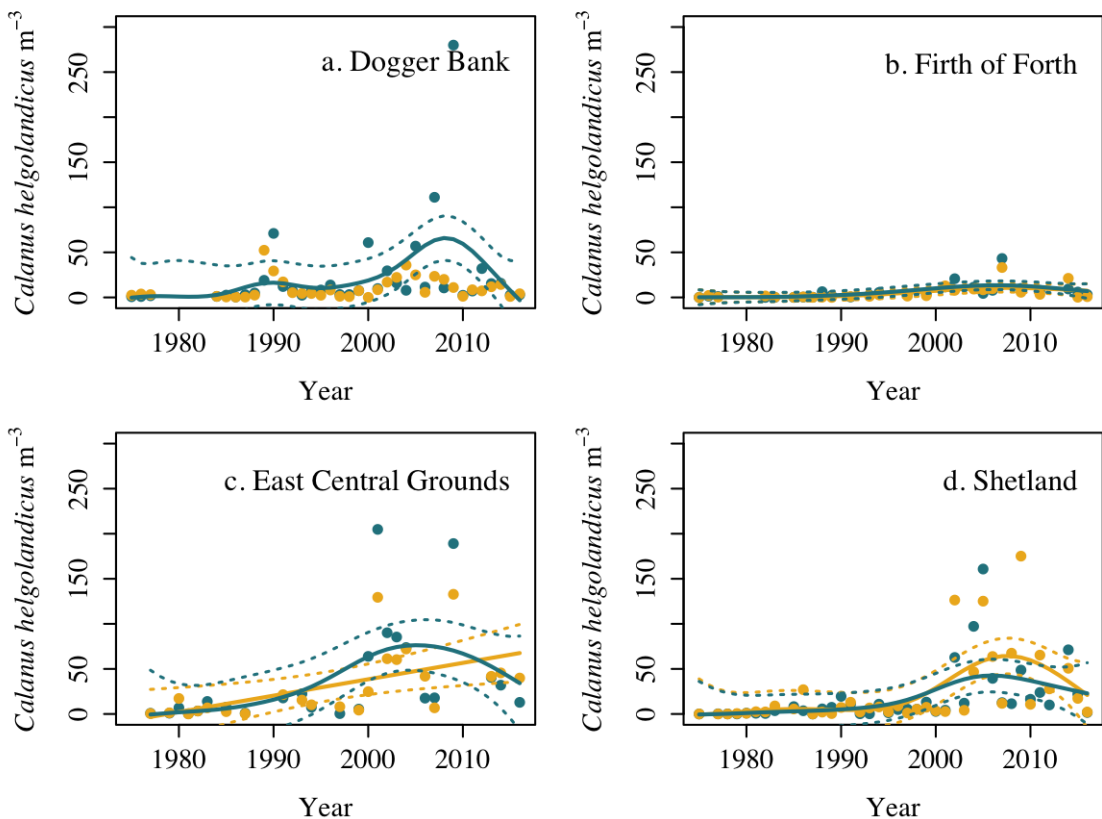


Figure 2.13: Changes in the average daily abundance of *Calanus helgolandicus* m^{-3} over time. Blue and yellow markers denote averages during the 1+ group (day 80–165) and 0 group (day 141–212) feeding seasons, respectively. Lines show GAM predictions (if $p < 0.05$), with dotted lines indicating the 95% confidence interval.

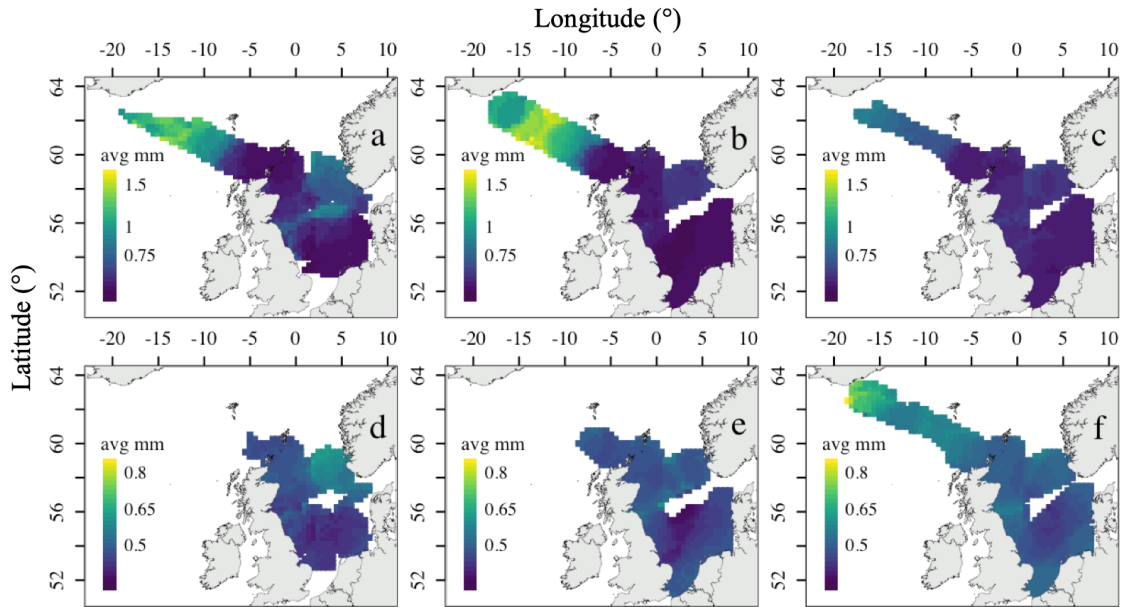


Figure 2.14: Average daily mean **square root of prey image area** (mm) (\log_{10} -scale) during the feeding season of 1+ group sandeels (a–c, day 80–165) and 0 group sandeels (d–f, day 141–212) for 1975–1988 (a,d), 1989–2002 (b,e), 2003–2016 (c,f). Note the different scales of 1+ group and 0 group feeding seasons.

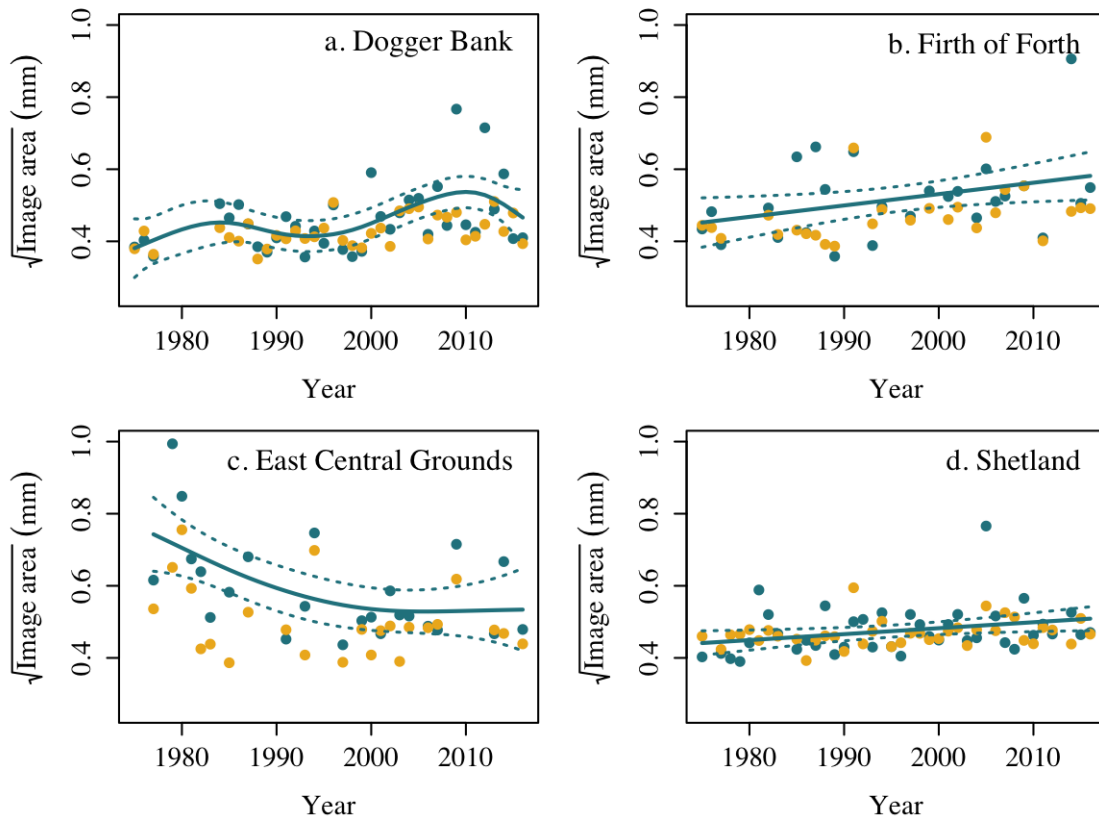


Figure 2.15: Changes in average daily mean **square root of prey image area** (mm) over time. Blue and yellow markers denote averages during the 1+ group (day 80–165) and 0 group (day 141–212) feeding seasons, respectively. Lines show GAM predictions (if $p < 0.05$), with dotted lines indicating the 95% confidence interval.

2.5 Discussion

This chapter has described an approach for using CPR data to create daily sandeel prey fields through temporal interpolation of spatially aggregated data corrected for taxon-specific sampling efficiency. It was clear that the sandeel prey field shows marked spatio-temporal variation. In the western North Sea, there have been marked declines both in the total amount of energy available, especially during the 0 group feeding season, and in the abundance of small copepods, with abundances decreasing by more than 50% during the 0 group feeding season. In terms of *Calanus* spp., there was no clear change in *Calanus finmarchicus* over time but a clear spatial pattern with peak abundances in the north-east, while *Calanus helgolandicus* showed a clear increase in most of the study area around 2000 but a less marked spatial pattern. The average prey size generally increased over time in the western North Sea, whereas it instead declined in the north-east. Further, due to the differences in the timing of the feeding seasons, it was clear that 0 group and 1+ group sandeels were exposed to different prey fields, with, for example, a larger abundance of smaller copepods during the 0 group feeding season.

2.5.1 Caveats of the approach

While the described method goes a long way to producing prey fields of the necessary resolution, there are still a number of caveats to be considered. For example, while the similarity of the estimated correction factors with previously estimated correction factors (see Table 2.3) suggests that they should be applicable to other areas, it is still likely that local characteristics of the sampling site and the surrounding CPR samples will have affected the estimates. Further, there will also be systematic variation in these correction factors that are not accounted for, such as spatial variation in DVM behaviour (e.g. Irigoien et al. 2004). However, considering the number and complexity of sources of variation, trying to account for these in a robust manner would be difficult and would potentially be more likely to introduce bias. The impact of the choice of correction factors when using the generated sandeel prey fields to predict sandeel growth is considered further in Section 4.2.6.

In addition to being used to develop correction factors, the Stonehaven sample site was also used to inform the scale used for aggregating data before interpolation. Here again, it is possible that local conditions may have led to a final threshold that is not representative of a larger area. But then, again, previous studies based on other locations suggest that the dynamics captured by the CPR and local point samples are similar when aggregating data over larger areas than those used here (Clark et al. 2001; John et al. 2001; Ostle et al. 2017). Still, the spatial aggregation step could likely be improved. Plankton dynamics do not change linearly over space, and taking this into account will help to define areas with more homogenous plankton dynamics over which to aggregate the CPR data. For example, McGinty et al. (2011) combined satellite chlorophyll measurements and cluster analysis to define areas that showed similar plankton dynamics, and then examined trends in the CPR data within these areas, whereas Capuzzo et al. (2018) instead aggregated CPR data over previously defined hydrodynamic regions in the North Sea.

It may also be worth to consider whether it would be possible to better take into account the irregular spatial distribution of CPR samples. If data are aggregated based on a circular area around a focal point as now, then if a transect runs through the edge of this area, this is likely to make up the majority of the data points, meaning that the average value is more representative of the location through which the transect runs than the midpoint of the aggregation area. As such, it should potentially be considered whether the spatial structure of the transects should in some way be reflected in the spatial aggregation method.

Further, in addition to the distinctive spatial structure of the CPR data, there is also a temporal structure as a result of the transects being monthly. In the current approach, samples are standardised to the middle of each monthly sampling interval in order to minimise the bias introduced by variation in sampling dates. This means that abundance peaks will be forced to artificially occur in the middle of each month. In addition to the artificial timing of the peaks, the smooth curves between the monthly averages are also not very representative of actual conditions as patchiness in the plankton is likely to introduce substantial variation between days. As discussed in Section 2.3.6, the impact of patchiness on sandeel intake rates may depend on to what degree the fish are limited by handling time/stomach space or prey availability, but either way, it will have a large impact on the abundance and composition of available prey on a given day. In a further extension of the approach presented here, patchy time series could be simulated by drawing from a defined distribution based on the interpolated daily time series presented here, where the scale of the patchiness could potentially be informed by bioacoustic data (see Godø et al. 2014). Finally, the way the data are interpolated also introduce an artificial shape to abundance peaks in the form of an even increase from the previous month and an even decline to the next month, whereas in reality the peak could be narrower, or broader.

In terms of trait values, it has been assumed here that a single average value for each prey type is representative, but actually these values could show large variation over space and time (e.g. Bottrell and Robins 1984). This could have a large impact on, for example, the total amount of energy available, or the size distribution of the prey field. The impact of prey trait values on sandeel growth is explored further in Section 4.2.6.

2.5.2 Spatio-temporal patterns in the sandeel prey field

There was clear spatio-temporal variation in the sandeel prey field. The following discussion focuses mainly on the North Sea as coverage was inconsistent further north. However, there were some clear patterns in the prey fields extending further north consisting of lower levels of small copepods and *C. helgolandicus*, relatively high levels of *C. finmarchicus* and a large average prey image area. This aligns well with previous observations of an increase in the size of copepods up towards the Faroes and Iceland (Beaugrand et al. 2008). There was no clear pattern in average total energy availability.

Now, focusing on the North Sea and starting with the average total energy contained in sandeel prey, this has declined over time in several locations. This aligns with previous studies, also based on corrected CPR data, finding an overall decline in zooplankton biomass in the North Sea (Pitois and Fox 2006). The temporal patterns in total energy that were observed in Dogger Bank and the Firth of Forth were to a large extent driven by the abundance of small copepods, which also showed a decline over time in these locations. This aligns with previously observed negative trends in the abundance of small zooplankton in the North Sea (Capuzzo et al. 2018). Small copepods were more abundant in the south, which also agrees with previous observations (Beaugrand et al. 2008). The abundance of the larger copepod *C. finmarchicus* showed a different spatial pattern, with the highest concentration in the north-eastern North Sea, which aligns with previous studies (Edwards et al. 2020). While *C. finmarchicus* showed clear inter-annual variation, previously reported negative trends (Reid et al. 2003b) were not visible in the areas examined. The finding that *C. helgolandicus* has increased over time does however align with previous findings (Reid et al. 2003b), and is in line with a range expansion at its northern limits (Bonnet et al. 2005). The more southerly distribution of *C. helgolandicus* also agrees with previous observations (Bonnet et al. 2005).

Finally, in alignment with the decline in small copepods (and thus an increase in the proportion of larger prey), the average square root of the prey image area (which is directly related to prey detection distance and thus search rate for foraging sandeels) has increased over time in Dogger Bank and the Firth of Forth. This aligns with a previously observed increase in the average dry weight of individual zooplankton in the southern North Sea (Pitois and Fox 2006). However, in the northern North Sea the same study observed the opposite pattern, which also aligns with the results from the ECG in this study. In Shetland, an increase was also observed although in this case it seems to have been driven by an increase in the abundance of larger prey types, rather than a decrease in small prey types.

It was also clear that 1+ group and 0 group sandeels are exposed to different prey fields. The abundance of small copepods was higher during the 0 group feeding season in all locations, and so was the total energy m^{-3} in Dogger Bank and Shetland. No clear differences between the seasons were found for *C. finmarchicus* or *C. helgolandicus*. The lack of difference in the abundance of *C. finmarchicus* was somewhat surprising considering that the timing of peak abundance is generally observed to occur at a time that better aligns with the timing of the 1+ group feeding season (Planque and Fromentin 1996). The lack of a difference between the feeding seasons in the abundance of *C. helgolandicus* fit better with previous observations of a less marked spring peak (Planque and Fromentin 1996). Finally, the average square root of the prey image area was found to be larger during the 1+ group feeding season. This aligns with the observation that sandeels tend to eat larger copepods in spring (1 April–15 May) as compared to early summer (15 May–30 June) (van Deurs et al. 2013).

These marked differences in the prey fields mean that spatio-temporal trends in the plankton observed here and elsewhere are likely to have different impacts on the intake rate and growth potential of 0 group and 1+ group sandeels. For example, the observed decline in small copepods in some locations (Figure 2.9, Capuzzo et al. 2018) is likely to have had a larger impact on the 0 group as compared to the 1+ group. Many studies on growth in lesser sandeels have naturally focused on 1+ group sandeels (e.g. Bergstad et al. 2002; Rindorf et al. 2016), as these are the ones mainly caught by the fisheries. However, considering how different the prey fields appear to be, one cannot necessarily assume that good growth conditions for 1+ group sandeels equate to good growth conditions for 0 group sandeels in the same location. The clear differences between the feeding seasons found here point to the importance of delineating time windows based on the timing of the feeding seasons, rather than using more coarse, seasonally aggregated data.

2.5.3 Relationship between prey field characteristics and sandeel growth

The generated prey fields can be matched up with some previous predictions of the impact of various aspects of the prey field on sandeel growth patterns. Based on previous studies (Bergstad et al. 2002; Boulcott et al. 2007; Rindorf et al. 2016), both 0 group and 1+ group sandeels in the Firth of Forth show relatively slow growth rates, with higher growth rates observed at Dogger Bank and even higher still at the ECG. The slow growth rates in the Firth of Forth have been hypothesised to be the result of the poorer food conditions (Boulcott et al. 2007), and the observed spatial growth patterns do align quite well with the spatial pattern in energy availability found here (Figure 2.6), although patterns differ between time periods. Further, the decline in energy availability seen at Dogger Bank and the Firth of Forth (Figure 2.7) align with observed declines in sandeel size at both locations (van Deurs et al. 2014; Wanless et al. 2018). Again, the decline in energy availability at Dogger Bank and Firth of Forth was to a large extent driven by a decline in small copepods, especially during the 0 group feeding season. It is worth to note here that the contribution of small copepods to total energy availability was 36% and 47% higher during the feeding season of 1+ group and 0 group sandeels, respectively, when using the corrected dataset as compared to the uncorrected dataset. As such, the correction factors have a large impact on the observed patterns (echoing findings of Pitois and Fox 2006), and likely contribute to creating a more representative prey composition.

In addition to biomass, it has been showed previously that the abundance of *Calanus* spp. could have a large impact on intake and growth rates (MacDonald et al. 2018; van Deurs et al. 2014). Along these lines, it has been suggested that a difference in the abundance of *C. finmarchicus* could potentially explain why sandeels tend to be smaller in Shetland than in the north-eastern North Sea (Bergstad et al. 2002). Indeed *C. finmarchicus* is more abundant in the north-east compared to Shetland (Figure 2.10). A decline in the abundance of *C. finmarchicus* has also been hypothesised to be behind a decline in the size of 1+ group sandeels at Dogger Bank (van Deurs et al. 2014). However, this decline is not clear in this dataset.

Looking at a subset of the generated prey fields aligning well in space and time with the data used to construct the trend in sandeel size in van Deurs et al. (2014), there was no clear decline in *C. finmarchicus*, and values were generally low. As noted by the authors of the study, Dogger Bank is close to the southern border of the *C. finmarchicus* distribution, whereas the references used for the decline of *C. finmarchicus* (Beaugrand 2004; Beaugrand et al. 2003; Planque and Fromentin 1996) were based on a much larger area, which included the north-east where the decline has been more prominent (Edwards et al. 2020). This suggests that caution is needed when using trends based on larger areas to explain an observed pattern as these trends are likely to be driven mainly by regions of high abundance. However, while there was no clear decline in *C. finmarchicus*, there has been a marked decline in total energy availability at Dogger Bank (Figure 2.7) driven to a large extent by a decline in small copepods, which could potentially have contributed to the observed decline in size.

Finally, it has been suggested that the prey size composition is important for intake rate through the impact on detection distance (van Deurs et al. 2015). However, the patterns in average prey image area observed here do not fully match observed patterns of size, with the average image area increasing in both Dogger Bank and the Firth of Forth (Figure 2.14), whereas sandeel size has decreased in both these areas (van Deurs et al. 2014; Wanless et al. 2018). The increase in average prey image area in these areas is to a large extent driven by a decrease in the abundance of small copepods rather than an increase in large copepods, which might explain why the expected alignment of patterns in sandeel size and average image area is not seen. This points to the importance of considering several different aspects of the prey field together.

2.5.4 Applicability to other species and life stages

A lack of prey field data of high temporal and taxonomic resolution is not a sandeel-specific problem. With minor modifications, for example modifying the temporal extent of the feeding season, the prey fields generated here for the sandeel may be directly applicable to other planktivores in the north-east Atlantic which feed on a similar prey base (see e.g. Raab et al. 2012). As such, some of the observed changes in the prey base may also have impacted other planktivores in this region, where several species of fish have declined in size over time (Baudron et al. 2014). For species with a different prey base, the approach can be adapted by removing or adding taxa (for a comprehensive list of taxa, see Richardson et al. 2006), although adding taxa would require developing additional correction factors.

Further, while the focus here was on the food of post-metamorphic sandeels, the methods could also be useful for developing prey fields for larval sandeels. Copepod eggs, copepod nauplii and appendicularians make up the main part of the sandeel larvae diet, with a shift towards larger prey such as adult copepods as the larvae grow (Economou 1991; Ryland 1964). All of these prey groups are counted in CPR samples, although due to the large mesh size of the CPR, a large proportion of copepod nauplii and eggs may go undetected. One of the most important determinants

of recruitment is the extent to which sandeel hatching and larval food availability coincide (Régner et al. 2017). While the method described here is not sensitive to fine-scale temporal variation in larval food phenology, a study in the north-western North Sea found that the phenology of larval food show variation of more than a month (Régner et al. 2017) - a scale of variation which would be picked up by this approach. As such, examining spatio-temporal variation in the abundance, composition and phenology of sandeel larval food could give an even more complete understanding of food conditions of the sandeel throughout its life.

Part II

Exploring drivers of
spatio-temporal variation in the
growth of juvenile lesser sandeels
using a dynamic energy budget
model

Chapter 3

Dynamic energy budget model description

3.1 Introduction

Understanding energy flows at an individual level has implications for the understanding of processes at a multi-trophic scale. The energy contained in a single organism will equal energy input minus energy output, where the input to a large extent will be dependent on the energy available at lower trophic levels. Within the organism, some of the ingested energy will have to be used for maintenance, while the rest will be allocated to growth, energy reserves, and reproduction. Investment into growth and energy reserves may impact survival rates through size-selective predation mortality (e.g. Sogard 1997) and starvation (e.g. MacDonald et al. 2018), respectively, while investment into reproduction will be related to reproductive success (e.g. Barneche et al. 2018). This means that the net energy uptake and how it is allocated has consequences not only for the energy contained in a single individual, but also the number of individuals in a population. Together, this will determine the energy available to upper trophic levels. As such, understanding what drives variation in net energy gain and its allocation at an individual level is of key importance, in particular as many of these rates are directly related to environmental variables, such as temperature, that are likely to change rapidly in the future.

In this vein, much work has gone into the field of bioenergetics - the study of how ingested energy is partitioned into losses, reproduction and growth (Ney 1993; Winberg 1960). In animals, energy available for growth and, if reproductively active, investment into gonads, is equal to the consumed energy minus metabolic costs of maintenance, activity, digestion and synthesis of new tissue, as well as losses from nitrogenous excretion and egestion (faeces). This balance equation can be solved for any of its constituent parameters when the others are known, but is most commonly solved for consumption or energy available for growth (Ney 1993). However, to fully understand how the energy available for growth translates into changes in the size and energy density of an individual, the processes governing how this net energy intake is allocated between growth, energy reserves and reproduction also

need to be considered. Often bioenergetic models stop at estimating growth potential, but in some cases they may be coupled with a growth model to produce growth curves (e.g. Hayes et al. 2000). One framework in which energy intake and losses can be combined with allocation processes to model growth is dynamic energy budget (DEB) models, in which allocation to energy reserves, structural growth and reproduction is explicitly modelled (Kooijman 2000; Lika and Nisbet 2000). DEB models can range from highly general and somewhat abstract models based on first principles to species-specific models that build more heavily on traditional bioenergetic studies (Nisbet et al. 2012) and have been shown to be able to predict observed spatio-temporal patterns in growth when forced with real-world data (Thomas et al. 2011). They have been proven useful in understanding the impact of environmental conditions, mainly in the form of temperature and food conditions, on growth (e.g. MacDonald et al. 2018; Ren and Ross 2001) and have also been used to predict the impact of projected changes in environmental conditions (e.g. Maar et al. 2015; MacDonald et al. 2018). As net energy intake and how it is allocated is generally linked to a host of demographic rates, DEB models can also be used to study the impact of environmental conditions on key vital rates such as reproduction (e.g. Pecquerie et al. 2009) and mortality (e.g. MacDonald et al. 2018). As such, they are a useful tool for exploring environmental drivers of spatio-temporal variation in growth and demographic rates as well as for predicting the impact of environmental change on these rates. The model output is directly related to the energy available to upper trophic levels, making DEB models ideal for studying bottom-up energy flow and predicting how changes at lower trophic levels result in knock-on effects on predators.

Several studies have taken a bioenergetic approach to understanding variation in growth and consumption in sandeels. In the south-western North Sea, several bioenergetic modelling studies of *Ammodytes marinus* have been conducted, looking at the optimal timing of overwintering (van Deurs et al. 2010), the energetic cost of overwintering (van Deurs et al. 2011a) the efficiency of converting energy contained in copepods into energy contained in sandeels (van Deurs et al. 2013) as well as the impact of prey size on ingested energy (van Deurs et al. 2015). At Georges Bank in the western Atlantic Ocean, an energy budget of *Ammodytes dubius* was developed which primarily aimed to estimate food consumption (Gilman 1994). None of these studies explicitly modelled the growth of the sandeels, focusing instead on drivers and consequences of energy intake and loss. MacDonald et al. (2018) considered not only energy gains and losses in their model of *A. marinus* in the north-western North Sea, but instead developed a DEB model that also included the allocation of net energy gain to growth, energy reserves and reproduction. This model produces growth curves of a daily resolution in response to temperature and food availability, and also models the consequences of growth conditions on overwintering starvation mortality. However, this model relies on large amounts of data to estimate location-specific fitting parameters (such as “background food availability”) and also requires size measurements from field surveys to define starting conditions, hindering its application in more data poor regions or time periods. As such, it cannot be directly employed to understand the observed variation in size in *A. marinus* over space and time.

Here, a highly modified, more general version of the *A. marinus* DEB model developed by MacDonald et al. (2018) is described, which covers only the first growing season but can be run in all locations and years where environmental input data are available. This enables the exploration of drivers of the clear spatio-temporal variation in size observed in *A. marinus* (e.g. Bergstad et al. 2002; Boulcott et al. 2007; Rindorf et al. 2016; van Deurs et al. 2014; Wanless et al. 2018) on a larger scale.

Differences in food conditions have long been hypothesised to be behind this observed spatial variation in growth (Bergstad et al. 2002; Boulcott et al. 2007; Macer 1966), but a study aiming to pinpoint drivers of the observed spatial variation in growth did not identify an effect of prey availability (Rindorf et al. 2016). However, the absence of a relationship could have been the result of a lack of resolution in the prey data used (Rindorf et al. 2016), suggesting that the role played by food conditions is still not clear. Further, variation in ingestion rates and size has also been related to temperature (Rindorf et al. 2016; Winslade 1974b), light conditions (van Deurs et al. 2015; Winslade 1974a) and pre-metamorphic phenology (Frederiksen et al. 2011; MacDonald et al. 2019a), but the relative contribution of these factors to variation in size, and how they may interact with the impact of food conditions, remains yet to be fully understood. Using the model described in this chapter, the impact of these variables are explored further in Chapter 4, with a particular focus on how ongoing changes in these variables may impact the growth of juvenile sandeels. Understanding drivers of growth in juveniles is particularly important, as this is likely to impact rates of mortality from starvation (MacDonald et al. 2018) and potentially also predation (Sogard 1997). Further, there is no information to suggest that responses to the prey field as well as metabolic rates would not be similar for 0 group and 1+ group, meaning that inferences regarding drivers of growth to a large extent apply to 1+ group sandeels too.

This chapter describes the full model formulation as well as the sourcing of parameter values. Model validation and a parameter sensitivity analysis is carried out in Chapter 4. The model can be considered as a type of net-production DEB model, but the individual sub-components are approached in the more parameter-heavy species-specific spirit of traditional bioenergetic models. In particular, based on the observation that the characteristics of available food is a major determinant of intake rates and growth rates (MacDonald et al. 2018; van Deurs et al. 2015, 2014) and several lines of evidence suggesting that the composition of ingested food does not show a simple proportional relationship with available food in *A. marinus* (Christensen 2010; Eliassen 2013; Godiksen et al. 2006; Gómez García et al. 2012), particular attention is paid to the modelling of ingestion. Much of this builds on the work of van Deurs et al. (2015), which focuses on the visual aspect of foraging and the importance of light conditions, but it also draws upon advancements in optimal foraging (Visser and Fiksen 2013) and empirical observations from experiments and field studies (e.g. Christensen 2010; Godiksen et al. 2006). In addition to ingestion, the model also includes metabolic costs, which builds on new experimental work in *A. marinus* (see Wright et al. 2017a), as well as how net assimilated energy is allocated between structural growth and reserves. Not all processes incorporated into the model will necessarily be important drivers of growth, but the approach taken

here is to have the complexity reflect the current understanding of *A. marinus* biology and to then critically assess the model to determine what processes appear to be the main drivers of growth, and where key knowledge gaps lie (see Chapter 4).

3.2 Model framework

The model is constructed around two state variables: reserve energy R (kJ) and structural energy S (kJ). Reserve energy represents the part of the sandeel that can be remobilised to meet metabolic costs when ingested energy is not enough. Structural energy represents the part of the sandeel that cannot be remobilised and includes parts of the sandeels such as skeletal tissue and organs. The model applies to both sexes, as *A. marinus* appears to be sexually monomorphic in all aspects other than their reproductive organs (Reay 1970).

The model framework can be seen in Figure 3.1. The basic structure of the model is based around the allocation of net energy gain (assimilated energy minus metabolic costs) to reserve energy and structural energy. The assimilated energy A (kJ day⁻¹) is the energy that is available to the sandeel based on ingested food, after accounting for assimilation efficiency. The model assumes that metabolic costs M (kJ day⁻¹) are subtracted from assimilated energy and that if the assimilated energy is not enough to meet metabolic costs (i.e. if net energy gain is negative), the rest is subtracted from reserves. If net energy gain is instead positive, a certain proportion f_S is allocated to structural energy and the rest $(1 - f_S)$ is allocated to reserve energy, making it a form of net-production DEB model (Lika and Nisbet 2000). The net-production model was chosen because it is known that *A. marinus* does not allocate energy to structural energy when energy intake is zero (length stays constant when no feeding occurs, e.g. Boulcott and Wright 2008). This is captured by the net-production model but not the more common κ -rule DEB model in which a fixed fraction of reserves is continuously allocated to maintenance and growth (Kooijman 2000).

The model starts just after metamorphosis, the timing of which is defined by previous observations (see Section 4.2.2). It is run until mid-September, but for the purposes of comparison with field data, it is generally assumed that overwintering, and thus the cessation of feeding and growth, occurs on 1 August (MacDonald 2017; van Deurs et al. 2011a). The model does not include overwintering or maturation. Model time steps are daily, based on the idea that environmental conditions may show important variation on this time scale. However, as in van Deurs et al. (2015), feeding is modelled on an hourly time-scale. The model requires several types of input. This includes temperature T (°C), which impacts both metabolic rates and intake rates through its effect on assimilation and digestion rates, as well as food abundance $\sum n_k$ (where n_k is the individuals m⁻³ of prey type k), which impacts ingestion rate. Each prey type also have associated trait values which impact intake rate. As sandeels are visual feeders, meaning that light conditions will be important (van Deurs et al. 2015), several types of input relating to light conditions are also included. These include day length h_{day} (h), which controls the number of hours available for feeding, average daylight surface irradiance I_0 (W m⁻²), which determines light levels, as well

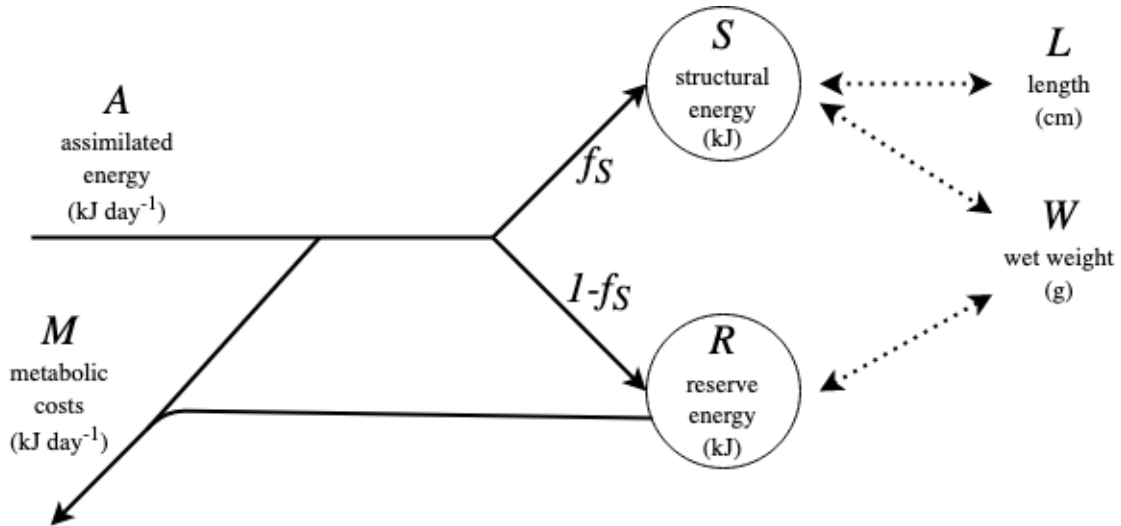


Figure 3.1: State variables and main processes included in the dynamic energy budget model. Solid arrows represent energy flows. The dotted arrows represent the relationship between the state variables (S and R) and sandeel length L and wet weight W .

as the beam attenuation coefficient a_b (m^{-1}) and the diffuse attenuation coefficient a_d (m^{-1}), which govern how light is scattered and absorbed when travelling down through the water and are related to the turbidity of the water (Devlin et al. 2009). The sources of input data used to later run the model are described in Chapter 4. The output of the model is daily reserve and structural energy, estimated at the end of the day. As these are quantities that are not measured in the field, a way in which to translate these into length L (cm) and wet weight W (g) and vice versa is also described below.

The model is implemented in C, based on an adaptation of the code for the model presented in MacDonald et al. (2018). However, R 3.5.2 (R Core Team 2018) was used for model fitting when parameters were estimated from data in this chapter, and was also used for visualisation.

3.2.1 Differences compared with the MacDonald model

As mentioned, the model presented here builds on a previous model developed by MacDonald et al. (2018) (in this section referred to as the MacDonald model), but several differences exist between the two models. To start, the models cover different parts of the sandeel life cycle. The model presented here starts at metamorphosis, making it possible to explore the impact of variation in date of metamorphosis on predicted growth. The MacDonald model has so far used year-specific size and abundance data as initial conditions, meaning that the start date of the model in a given year thus depends on the dates for which data are available, which is generally in June. However, this is just a difference in the initial conditions used, and not a difference in terms of model structure. Further, while the MacDonald model covers the full post-metamorphic life-cycle, the model presented here only covers the first growth season, as the interest here was mainly in processes that drive growth. For the same reason, the model presented here only tracks changes in growth while the MacDonald model also tracks changes in abundance.

In terms of the modelling of growth during the feeding season, the overall structure of the models are very similar, both using structural energy S and reserve energy R as state variables. The models build on the same sub-processes (ingestion, metabolism and allocation of net energy gain) and both incorporate a way in which to translate the state variables into weight and length to be able to make use of field data more easily. However, within this structure, differences exist in how these sub-processes are modelled.

In general, the governing principles of ingestion are largely similar in the two models, although the ways in which these have been incorporated are different. In both models, larger sandeels are assumed to have higher ingestion rates. In the MacDonald model, this is represented by a general weight-scaling factor, assuming that intake scales with the surface area of the sandeel. In the model presented here, the benefit of a larger body size is instead reflected in several sub-processes (faster swimming, a larger stomach and better visual capacity). This was done so that empirically observed processes and parameter values could be more directly incorporated into the model. Further, in both models it is assumed that sandeels feed selectively. In the MacDonald model, this is represented by attack rates for different prey groups (large copepods, small copepods and “background food”), which are all fitting parameters. The abundance of “background food” is also a fitting parameter. In this model, selectivity is instead the result of several explicit sub-processes: prey size-dependent encounter and capture success rates as well as different preferences for different prey groups based on an optimal foraging approach. This made it possible to incorporate previously measured relationships and parameter values in a more direct manner. Further, it accounts for the fact that attack rates are not static but dynamic, and may depend on, for example, the presence and the relative abundance of alternative prey types (e.g. Christensen 2010; Sekiguchi 1977) as well as visual conditions (e.g. van Deurs et al. 2015; Varpe and Fiksen 2010). To a large extent, this extension was based on the foraging model presented by van Deurs et al. (2015). However, the model presented by van Deurs et al. (2015) was also extended to account for variation in capture success, as well as switching between several prey types.

The MacDonald model and the model presented here are similar in that they both assume that at large prey densities, the sandeels will be limited by their ability to process the food, rather than encounter rates. Processing of food involves the capture, ingestion and digestion of food. The limitation introduced by finite gut space and temperature-dependent digestion rates (see van Deurs et al. 2015) is incorporated into both models. One simplification in the model presented here is that an increased ingestion rate in response to poor body condition is not included. This was included in the MacDonald model based on observations in other species as well as the observation that the condition of sandeels improve rapidly following overwintering (Hislop et al. 1991; Rindorf et al. 2016). However, it may be that the rapid increase in condition following overwintering is instead the result of good food conditions and an increased allocation to reserves (which are both represented in the model formulated here). Based on this, in conjunction with there being no information available on this process in any closely related species, this process was not included. One process which was included in the model presented here but not in the MacDonald model is the assumption that sandeels do not forage when prey abundance is particularly low, which was included based on experimental observations (van Deurs et al. 2011b; Winslade 1974c). Finally, both models include a temperature-dependent assimilation efficiency based on measurements from *A. dubius* (Larimer 1992). However, the model presented here also includes losses from nitrogenous excretion, as these can also be non-negligible (Elliott 1976; Jobling 1993).

Differences between the two models in terms of how metabolism and the allocation of net energy gain are modelled are arguably smaller. The standard metabolic rate is modelled in the same way, although parameter values have been partially updated as new data have become available from experiments on *A. marinus* (Wright et al. 2017a). In terms of metabolic costs of activity, these are in the MacDonald model assumed to be equal to the standard metabolic rate when the sandeel is active, so that the total metabolic costs are doubled. The validity of this assumption, which can be traced back to van Deurs et al. (2015), is not clear. Further, this assumption implies that the response of activity costs to changes in temperature and body mass are similar, which is generally not the case (e.g. Brett 1965; Brett and Groves 1979; Dwyer and Kramer 1975). For this reason, activity costs were here instead based on measurements of *A. tobianus* (see van Deurs et al. 2010). Finally, metabolic costs of processing food and synthesising tissue are not included in the MacDonald model, but were included in the model presented here as they can make up a substantial part of metabolic costs (Jobling 1981; Secor 2009). In terms of the allocation of net energy gain to structural and reserve energy, this is approached similarly in the two models, where allocation to structural energy is a function of both size and condition. However, the exact form differs slightly and was here informed by the relationship between total energy ($R + S$) and S in an empirical dataset. Finally, in terms of how R and S are translated into length and weight, the overall approach is similar between the two models and parameter values are also similar. However, some of the parameter values were updated based on a detailed dataset on *A. marinus* body composition so that all values were derived from *A. marinus* data, which was not the case in the MacDonald model.

As such, while the overall structure is similar, there are differences between the two models in how sub-processes are modelled. In general, the adjustments to the MacDonald model were made with generality in mind. The structure of the MacDonald model is certainly general, but the model relies on several fitting parameters including “background food availability” and attack rates for different prey types, which may all be expected to vary over space and time depending on, for example, prey composition and abundance. However, in most locations and time periods there are not enough sandeel data to estimate these parameter values. This motivated a more complex model in which these quantities are functions of local conditions and reflect the biological understanding of how the sandeels respond to these conditions. Further, the more complex structure is also a result of breaking processes, in particular ingestion, down into tractable sub-processes which correspond more directly to processes as they are measured in the field or in laboratory experiments. This means that parameters can be related to a specific measurable process rather representing composite effects, such as the overall effect of size on ingestion rates in the MacDonald model. This makes the link connecting models with experimental work and field studies more intuitive, and means that the results of the sensitivity analysis (see Section 4.2.6) can be directly used to identify single parameters for which the uncertainty is large, and design experiments to target those. In addition to these ideas of generality and tractable sub-processes, modifications were also made based on identified processes that were not included in the MacDonald but that may be important for the sandeel energy budget, such as losses due to nitrogenous excretion or metabolic costs from processing food, or based on new research that has emerged since the development of the MacDonald model (such as measurements of metabolic rates in *A. marinus*, see Wright et al. 2017a). The model here thus introduces adjustments, and in some cases further complexity, to achieve a better understanding of sub-processes that govern growth. The MacDonald model instead achieves not only an understanding of drivers of growth but also the consequences of variation in growth on overwinter mortality and gonad investment. The two models thus complement each other.

3.3 Model equations and initial parameter values

Net energy gain is the assimilated energy A (kJ day^{-1}) minus metabolic costs M (kJ day^{-1}). If net energy gain ($A - M$) is negative, any outstanding metabolic costs are paid from reserve energy R . If it is positive, it will be divided between reserve energy R and structural energy S . Reserve energy R (kJ) thus changes as follows:

$$\frac{dR}{dt} = A - M - \frac{dS}{dt} \quad (3.1)$$

If net energy gain $A - M$ is positive, a proportion f_S dependent on current values of R and S is allocated to structural energy S (kJ):

$$\frac{dS}{dt} = f_S[A - M]^+ \quad (3.2)$$

where $[A - M]^+ = \max(0, A - M)$. Both Equation 3.1 and Equation 3.2 are discretised assuming daily time steps.

In the following sections, each sub-process of the model is covered in turn, describing both the governing equations and parameter values. Model quantities and parameter values are summarised in Table 3.1. For each parameter, lower and upper uncertainty boundaries for the parameter sensitivity analysis (Chapter 4) are also defined.

Table 3.1: Model variables and parameter values. All parameters were rounded to two significant digits, unless this was not a sufficient level of precision in relation to the magnitude of uncertainty. For parameter values, associated uncertainty ranges are included in brackets. Sources of parameter values are described in the text. d.l. = dimensionless, b.l. = body length.

Name	Description	Value	Unit
State variables			
R	Reserve energy	-	kJ
S	Structural energy	-	kJ
Translated state variables			
W	Wet weight of sandeel	-	g
L	Length of sandeel	-	cm
Input variables			
T	Temperature	-	°C
$\sum n_k$	Food abundance for each prey type k	-	ind m ⁻³
E_k	Energy content of prey type k , see Chapter 2	-	kJ
ψ_k	Image area of prey type k , see Chapter 2	-	m ²
L_k	Length of prey type k , see Chapter 2	-	mm
h_{day}	Hours of daylight	-	h
I_0	Average surface irradiance during hours of daylight	-	W m ⁻²
a_d	Diffuse attenuation coefficient	-	m ⁻¹
a_b	Beam attenuation coefficient	-	m ⁻¹

Assimilated energy

A	Assimilated energy	-	kJ day^{-1}
h_{active}	Number of hours in a day available for feeding	-	h
i_h	Energy intake during a given hour	-	kJ h^{-1}
i_{max}	Maximum energy intake without gut space limitation	-	kJ h^{-1}
ϵ	Assimilation efficiency	-	d.l.
p_c	Proportion of time spent in search class c	-	d.l.
$\lambda_{k,L,I}$	Search rate for prey type k , length L , light conditions I	-	$\text{m}^3 \text{h}^{-1}$
$D_{k,L,I}$	Detection distance for prey type k , length L , light conditions I	-	m
γ_L	Visual sensitivity for a sandeel of length L	-	d.l.
I_z	Ambient irradiance at feeding depth z	-	W m^{-2}
ϕ_k	Capture probability for prey type k	-	d.l.
g	Gut content	-	g
d	Digestion rate	-	g h^{-1}
δ_{food}	Energy density of ingested prey mix (g wet weight $^{-1}$)	-	kJ g^{-1}
g_{max}	Maximum gut content	-	g
α_ϵ	Faecal loss coefficient	0.82 (0.73; 0.91)	d.l.
β_ϵ	Faecal loss temperature scaling factor	$7.6 (7.5; 7.7) \times 10^{-3}$	d.l.
U_ϵ	Nitrogenous excretion loss coefficient	$5.1 (2.0; 12) \times 10^{-2}$	d.l.
h_e	Effective handling time (see Chapter 4)	-	h
v	Swimming speed	1.5 (0.5; 2.0)	b.l. s^{-1}
C	Prey contrast	0.23 (0.20; 0.26)	d.l.
D_{frac}	Fraction of L equal to detection distance with no light limitation	1/2 (1/3; 1)	d.l.
K_D	Light saturation	3.5 (2.0; 5.0)	$\mu\text{E m}^{-2} \text{s}^{-1}$
z	Feeding depth	30 (0; 70)	m
b	Capture probability decline rate (see Chapter 4)	-	d.l.
m	Capture probability sigmoidal midpoint (see Chapter 4)	-	d.l.

α_{dig}	Digestion coefficient	$3.5 (3.0; 4.0) \times 10^{-2}$	d.l.
β_{dig}	Digestion scaling factor	$5.4 (5.1; 5.7) \times 10^{-2}$	d.l.
δ^*	Energy density reference prey (g wet weight ⁻¹)	4.4 (3.9; 4.9)	kJ g ⁻¹
α_{gut}	Maximum gut size coefficient	$1.7 (1.6; 2.0) \times 10^{-3}$	d.l.
β_{gut}	Maximum gut size scaling factor	2.3 (2.2; 2.4)	d.l.

Metabolic

costs

M	Total daily metabolic costs	-	kJ day ⁻¹
M_{SMR}	Standard metabolic rate	-	kJ day ⁻¹
M_{feed}	Metabolic activity costs	-	kJ day ⁻¹
M_{SDA}	Metabolic costs from processing food	-	kJ day ⁻¹

α_{met}	SMR coefficient	$4.5 (2.5; 6.5) \times 10^{-3}$	d.l.
β_{met}	Metabolic weight scaling factor	0.65 (0.51; 0.79)	d.l.
Q_{10}	Temperature effect on SMR	3.1 (1.5; 3.4)	d.l.
F	Feeding costs	$3.4 (3.0; 3.8) \times 10^{-3}$	kJ g ⁻¹ h ⁻¹
ζ_{SDA}	Cost of processing food	0.16 (0.016; 0.59)	d.l.

Allocation

f_S	Proportion of net energy gain allocated to structural energy	-	-
α_{alloc}	Allocation coefficient	0.43 (0.42; 0.44)	d.l.
β_{alloc}	Allocation scaling factor	-0.09 (-0.10; -0.08)	d.l.

Translation

δ_S	Structural energy density (g dry weight ⁻¹)	19.2 (19.0; 19.4)	kJ g ⁻¹
δ_R	Reserve energy density (g dry weight ⁻¹)	27 (25; 29)	kJ g ⁻¹
α_{dry}	Structural dry weight coefficient	1.7 (1.6; 1.9) × 10 ⁻⁴	d.l.
β_{dry}	Structural dry weight scaling factor	3.27 (3.22; 3.33)	d.l.
ω_{SDW}	Structural dry to wet weight conversion factor	5.7 (4.7; 6.9)	d.l.
ω_{RDW}	Reserve dry to wet weight conversion factor	3.9 (3.2; 4.6)	d.l.

3.3.1 Assimilated energy

The way in which assimilated energy is modelled draws heavily on the *A. marinus* foraging model presented by van Deurs et al. (2015). As in the model by van Deurs et al. (2015), feeding is modelled with hourly time steps. This is done so that gut fullness, and its impact on intake, can be tracked on a relevant time-scale during the hours of feeding. Feeding occurs during the day, with surveys suggesting that the sandeels migrate up from their nightly burrowing habitat as light levels increase in the morning (Freeman et al. 2004; Johnsen et al. 2017; Wright and Bailey 1993). Experimental observations in the closely related *Ammodytes tobianus* seem to suggest that individuals emerge at around the same time, but that emergence is gradual and that feeding does not begin immediately (van Deurs et al. 2011b). Field observations of *A. marinus* also seem to suggest that school formation is an extended process (Embling et al. 2008) and, in addition, that the sandeels also move from their nightly burrowing habitat to deeper grounds before starting to forage (Engelhard et al. 2008; van der Kooij et al. 2008). The patterns of descent are less clear. While some surveys have found that *A. marinus* cease feeding at sunset (Freeman et al. 2004; Johnsen et al. 2017), other studies have observed the sandeels to descend well before sunset (Wright and Bailey 1993). In an experimental setting, activity patterns tend to be strongly linked to light levels (*A. marinus*: Winslade 1974a; Wright et al. 2000; *A. tobianus*: van Deurs et al. 2011b), but in the field, presence in the water column is likely the result of a trade-off between increased feeding opportunities and increased predation risk (van Deurs et al. 2010) as well as energetic costs, which are large in sandeels as they lack swim bladders (Reay 1970). This means that the sandeels might descend while light levels are still sufficient for foraging. Both experimental observations from *A. tobianus* (van Deurs et al. 2011b) and field surveys of *A. marinus* (Freeman et al. 2004) suggest that descent is even more gradual and less synchronised than the morning ascent, indicating that the sandeels may individually adjust the length of time they stay up. It may be that they are adjusting the length of the foraging period to their own energetic state, which could explain why the smaller 0 group sandeels often feed for longer (Wright and Bailey 1993). Further, while the majority of sandeels will be in the water column feeding during the day, some may be burrowed into the sand (Mackinson 2007). However, as predation pressure may be particularly strong during ascent and descent (Engelhard et al. 2008) and as their foraging habitat is not directly over their burrowing habitat (Engelhard et al. 2008; van der Kooij et al. 2008), they are unlikely to re-burrow repeatedly during the day.

Based on this, the total number of hours available to the sandeel for active foraging for a given day, h_{active} (h), was considered to be the total number of hours of daylight h_{day} (h) minus one hour for school aggregation in the morning and one hour for school disintegration at night (see van Deurs et al. 2011b), including movement to and from foraging grounds (Engelhard et al. 2008; van der Kooij et al. 2008). While sandeels may descend earlier (Wright and Bailey 1993), assuming that sandeels are in the water column through all hours of daylight was justified by several studies finding that descent occur at sunset (Freeman et al. 2004; Johnsen et al. 2017) and the finding that 0 group sandeels often feed for longer (Wright and Bailey 1993). Daylight was defined as occurring from sunrise to sunset, rounded to a whole number.

Further, experimental observations of *A. marinus* (Winslade 1974c) and *A. tobianus* (van Deurs et al. 2011b) suggest that sandeels do not forage when prey is absent. Based on these observations, it is assumed that no feeding occurs on days when prey abundances are so low that the daily ingested energy would be lower than the metabolic costs associated with feeding and processing the food (M_{feed} and M_{SDA} , see Equation 3.19 and Equation 3.20). On such days, it is assumed that the sandeels stay buried, do not feed, and do not pay the metabolic costs associated with feeding and processing food. It is unclear how well this translates into field conditions. For this reason, the impact of this assumption on predicted size is explored in Section 4.2.6. Incorporating this assumption, total assimilated energy A (kJ day^{-1}) for a given day is then obtained by adding up the ingested energy for each hour of feeding:

$$A = \begin{cases} \epsilon \sum_{h=1}^{h_{active}} i_h, & \epsilon \sum_{h=1}^{h_{active}} i_h - (M_{feed} + M_{SDA}) > 0 \\ 0, & \epsilon \sum_{h=1}^{h_{active}} i_h - (M_{feed} + M_{SDA}) \leq 0 \end{cases} \quad (3.3)$$

where i_h (kJ h^{-1}) is the energy ingested during a given hour, h_{active} (h) is the total number of hours feeding, M_{feed} (kJ day^{-1}) and M_{SDA} (kJ day^{-1}) are the metabolic costs associated with feeding and food processing, respectively, and ϵ the assimilation efficiency.

The assimilation efficiency is the proportion of energy from ingested food remaining after faecal losses and nitrogenous excretion (Jobling 1993). Faecal losses have been estimated in the closely related *A. dubius* and is positively related to temperature (Gilman 1994, based on measurements from Larimer 1992). However, there are no measurements of nitrogenous excretion in any species of sandeels, and it is unknown how it responds to for example temperature (which is often found to have a positive impact on excretion rates, see e.g. Elliott 1976). As such, it is assumed that a constant proportion U_ϵ of ingested energy is lost to nitrogenous excretion. Combining the two types of losses, the following equation for ϵ is obtained:

$$\epsilon = (\alpha_\epsilon + \beta_\epsilon T) - U_\epsilon \quad (3.4)$$

where T is temperature ($^\circ\text{C}$), and α_ϵ , β_ϵ and U_ϵ are constants. Parameter values for α_ϵ and β_ϵ were obtained from Gilman (1994), based on measurements on *A. dubius* from Larimer (1992). No uncertainty estimates are provided in the study, and uncertainty ranges were instead based on the magnitude of uncertainty of previous estimates of temperature effects on faecal losses in another species of small planktivorous fish, the minnow (*Phoxinus phoxinus*) (Cui and Wootton 1988). For U_ϵ , this varies between species and depends on intake and temperature (Elliott 1976), but in absence of any information on any closely related species, it is, as mentioned, assumed to be constant. The value of U_ϵ was based on an estimate from the study on minnows (Cui and Wootton 1988), but a wide uncertainty range from 2% (Cui and Wootton 1988) to 12% (Elliott 1976) was used based on estimates from other species of fish.

i_h , the energy ingested during a given hour, is limited by the available prey as well the gut capacity. Gut capacity limits how much food can actually be eaten whereas the potential maximum intake rate i_{max} is determined by the response of the sandeels to the daily prey field, disregarding the limitation introduced by finite gut space. Here, the potential maximum intake rate i_{max} is described first, followed by the limitation introduced by limited gut capacity.

3.3.1.1 Maximum intake rate i_{max} and prey selection

Aspects of selectivity

A. marinus feed on several different taxa of zooplankton (see Section 2.3.1 for a summary). These prey types differ in their size and energy content, and this variation will likely determine the profitability of these prey types to the sandeel, as well as the sandeel's ability to detect and catch them. Based on simultaneous sampling of *A. marinus* gut contents and zooplankton, it is clear that the sandeels do not feed in proportion to the availability of different prey types (Eliassen 2013; Godiksen et al. 2006; Gómez García et al. 2012) but instead show some form of selectivity. Observations of other species of the same genus also seem to suggest that they feed selectively (Scott 1973; Sekiguchi 1977; but see Purcell and Sturdevant 2001). It should be noted that selectivity here refers to any difference between the composition of prey ingested and prey in the environment, not necessarily active selection. Eggers (1977) identified three processes of selectivity in planktivorous fish: (1) prey size-dependent detection rates, (2) prey type-dependent capture probability and (3) active selection of more profitable prey. As sandeels are visual foragers (Winslade 1974c), prey size-dependent detection rates likely constitute an important process. The finding that within prey types, the individuals found in *A. marinus* guts are generally larger than individuals sampled in the water column (Godiksen et al. 2006) could provide some support for this form of passive selection. In terms of capture probability, it is clear that capture probability given detection in *A. marinus* is not 1 (Christensen 2010), but little is known of the regulating mechanisms. Based on studies of other planktivorous fish (e.g. Butler and Pickett 1988; Folkvord and Hunter 1986; Fuiman 1989; Luecke et al. 1990; Margulies 1989; Rice et al. 1987), it appears as if the capture probability is dependent on the ratio between prey and predator size, generally following a sigmoidal relationship (Pepin et al. 1987). In *A. marinus*, this is supported by the finding that larger individuals tend to consume larger prey (Eigaard et al. 2014; van Deurs et al. 2014).

Finally, experimental observations have found that *A. marinus* feeding on small copepods almost immediately switched to feeding solely on herring (*Clupea harengus*) larvae when these were introduced into the tank (Christensen 2010). The observation that no more copepods were consumed once the sandeel had switched to larvae and that feeding on larvae was associated with a different swimming speed and technique suggests that this was an active switch to another prey type, rather than being driven by differences in detectability or catchability. What drove the switch is not clear, but considering that the average weight of the copepods in the experiment was a tenth of the weight of each herring larva, the larvae are likely to be the more profitable prey in terms of total energy content. This active switching behaviour is to some extent also supported by observations based on field gut sam-

pling. In *A. marinus* guts, different prey types are often found in distinct clumps (Eigaard et al. 2014; Godiksen et al. 2006) and prey size distribution tends to show larger between-gut than within-gut variation (van Deurs et al. 2014). This could suggest that the sandeels focus on one type of prey at the time. However, spatial patchiness in the prey field is also likely to play a role. Another source of support for active switching behaviour is evidence suggesting that the sandeels develop a search image while foraging. In the experiment by Christensen (2010), *A. marinus* preying on herring larvae were found to also attack inanimate elongate objects, such as dust particles, which they did not do when feeding on copepods. Furthermore, based on the finding that krill (*Thyssaneosssa* sp.) and capelin (*Mallotus villosus*) larvae were found in distinct clumps in the sampled guts, while copepods formed separate clumps, Godiksen et al. (2006) suggested that the sandeels are using the larger size and darkly pigmented eyes of the krill and capelin larvae to form a distinct search image, which differs from the one used when feeding on copepods. As such, the evidence seem to suggest that the sandeels show some form of active switching behaviour, but it is not known what triggers a switch.

Maximum intake rate i_{max}

As in van Deurs et al. (2015), the functional response to the prey field is modelled as a Holling type II response (Holling 1959), which is based on a mechanistic understanding of predator-prey interactions and allows all sub-processes to be incorporated in a transparent manner. Into this functional response, the three forms of prey selectivity described by Eggers (1977) are incorporated, including a prey size-, sandeel size- and light-dependent detection distance ($D_{k,L,I}$, which determines search rate), a prey size-dependent capture probability ϕ_k and finally, active switching behaviour. To incorporate this switching behaviour, each prey type is sorted into a search class c , in which all prey types are assumed to have a common search image that is distinct from the other search classes. The sandeel only focuses on one search class at a time. As it is not known what may trigger a switch between search classes, the parsimonious assumption advocated by Visser and Fiksen (2013) is followed, where it is assumed that the predator base their switching behaviour on the profitability of the different prey search classes. The profitability of each search class is based on the energy intake rate when feeding in this search class, and is as such determined by a combination of abundance, capture rate and the energy contained in each prey type. One could either assume that the fish would spend the whole foraging period in the most profitable search class, or that they allocate time in proportion to profitability (see Visser and Fiksen 2013). Based on the observation that sandeel guts tend to contain a mix of prey types (Eigaard et al. 2014; Godiksen et al. 2006) and experimental studies of other species of planktivorous fish showing that the fish allocate their foraging time in proportion to profitability (Crowder 1985; Werner and Hall 1974), it is assumed here that the proportion of time spent in each search class p_c each day is in proportion to the profitability of that search class. While behaviour such as swimming speed is likely to differ between prey search classes (for example, sandeels have been observed to swim faster when feeding on fish larvae as compared to small copepods, see Christensen 2010) there is not enough information to incorporate this, and it is thus assumed that behaviour is the same in each search class. Within a given search class c , the maximum amount of energy

$i_{max,c}$ (kJ h⁻¹) that can be ingested during one hour, disregarding the limitation from finite gut space, thus follows:

$$i_{max,c} = \frac{\sum_k \lambda_{k,L,I} \phi_k n_k E_k}{1 + \sum_k h_e \lambda_{k,L,I} \phi_k n_k} \quad (3.5)$$

where $\lambda_{k,L,I}$ (m³ h⁻¹) is the prey size-, sandeel size- and light-dependent search rate (see Equation 3.8), ϕ_k is the prey size-dependent capture probability (see Equation 3.12), n_k (individuals m⁻³, assuming an even distribution) and E_k (kJ) are the abundance and energy content of prey type k , respectively, and h_e is the effective handling time (h, but generally on the scale of seconds).

In foraging models, handling time tends to reflect the time taken to pursue and capture the prey, as well as the time taken to ingest and digest prey. As the limitation introduced by digestion time is handled separately here, in this model, handling time does not include digestion time. Observations of *A. marinus* by Christensen (2010) found that the sandeels caught 1–2 small copepods per seconds while Winslade (1974b) observed that sandeels caught on average 0.7–1.5 copepod nauplii per second. No average is given for sandeels feeding on herring larvae in the study by Christensen (2010), but it is stated that as a maximum rate, one sandeel caught 12 larvae in less than 10 seconds. As such, there does not appear to be a strong difference in the handling time for different prey types, and it is thus assumed to be constant for all prey types. It is possible that it could be longer for larger, more mobile prey, which are more likely to be pursued again if the initial attack failed (Christensen 2010), but the effect of this on energy intake is probably to a large extent soaked up by the size-dependent capture probability.

However, these measurements may not necessarily translate very well to the field. For example, prey used in experimental studies may not be as active as in field conditions (Pepin et al. 1987). As such, appropriate handling time values for field conditions are highly uncertain. Further, the fine-scale patchiness of plankton (Lalli and Parsons 1997; Owen 1989) in combination with the schooling behaviour of the sandeel may mean individual sandeels are only temporarily exposed to higher prey densities, during which they may be handling time-limited, but most of the time they will be exposed to below-average abundances. The sandeels may also have to engage in predator avoidance behaviour (e.g. Pitcher and Wyche 1983), further reducing the time available for foraging. To account for these time limitations, an *effective* handling time is considered, which represents not only the time it takes for the sandeel to capture and ingest a given prey, but which represents a general limitation on sandeel ingestion rate, rendering intake rates a saturated function of prey abundance. As there are no data that can inform the value of this parameter, it is tuned against size data in Section 4.2.4.

Again, it is assumed that the sandeels spend time in each search class c in proportion p_c to the profitability of that search class, which is calculated as follows:

$$p_c = \frac{i_{max,c}}{\sum_c i_{max,c}} \quad (3.6)$$

where $i_{max,c}$ (kJ h^{-1}) is the maximum potential energy ingested during one hour spent feeding in search class c . It should be noted here that as digestion is modelled as a separate process, differences in digestion rates are not included when determining profitability. It has been argued that differences in digestive quality (amount of energy that can be assimilated per unit of digestion time) could be an important, often overlooked, process that should be incorporated into models based on optimal foraging (e.g. Fall and Fiksen 2019, and references therein). However, while selectivity based on digestive quality has been suggested to occur in some cases (e.g. Gill and Hart 1998) other studies have shown that pre-digestive traits are more important for prey selection in fish (Kaiser et al. 1992) and when incorporated into a foraging model of the Atlantic cod (*Gadus morhua*), a non-selective model better predicted diet than the model which incorporated selection based on digestive quality (Fall and Fiksen 2019). As such, while it is recognised that selectivity based on digestive quality could be an important process in some cases, it is not included in this model. This is further supported by observations of *A. marinus* guts during the feeding season showing that they are often well below maximum capacity (see Figure 3.4), suggesting that digestive quality is likely to be a less important driver of selectivity.

Finally, i_{max} (kJ h^{-1}), the total amount of energy that can be ingested during an hour, is calculated as follows:

$$i_{max} = \sum_c p_c i_{max,c} \quad (3.7)$$

where p_c is the proportion of time spent in each search class and $i_{max,c}$ (kJ h^{-1}) is the maximum amount of energy that can be ingested in a given hour in a given search class, assuming continuous feeding. Note again that this is the potential maximum intake rate and that this may be modified by the available gut space (Section 3.3.1.2).

Search rate $\lambda_{k,L,I}$

For the search rate $\lambda_{k,L,I}$ ($\text{m}^3 \text{h}^{-1}$), this is a function of the prey size-, sandeel size- and light-dependent detection distance $D_{k,L,I}$ (see the following section, Equation 3.9) and the length of the sandeel L , as this determines speed:

$$\lambda_{k,L,I} = D_{k,L,I}^2 \pi v L \quad (3.8)$$

where $D_{k,L,I}$ (m) is the detection distance, v is the swimming speed (body lengths

per hour) and L (m) is sandeel length. vL provides the speed in m h^{-1} . The equation assumes a cylindrical search space with a cross-section of $D_{k,L,I}^2\pi$ where the radius is equal to the detection distance $D_{k,L,I}$ (thus assuming that the angle of the visual field is 90°). By multiplying this with the swimming speed, the volume searched per hour ($\text{m}^3 \text{h}^{-1}$) is obtained (see Figure 3.2 for a schematic representation). This is a common model of planktivorous fish foraging (e.g. Eggers 1977), and is also used in the van Deurs et al. (2015) model.

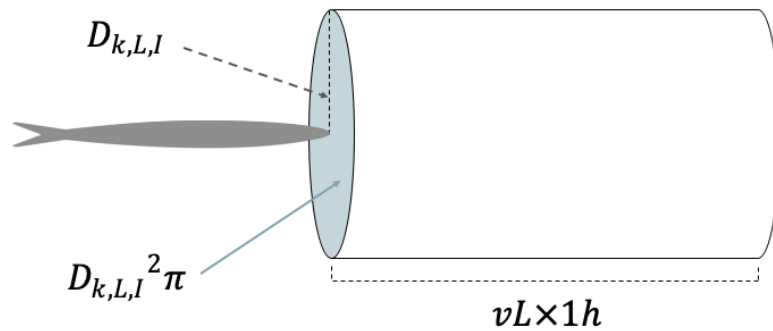


Figure 3.2: Schematic representation of search rate $\lambda_{k,L,I}$ (see Equation 3.8). $D_{k,L,I}$ (m) = prey detection distance, v (body lengths per hour) = swimming speed and L (m) = sandeel length. The depicted cylinder is equal to the volume searched in one hour.

The equation further assumes that swimming speed is a linear function of length, which is generally the case in fish (e.g. Blaxter and Dickson 1959). It may be that this assumption is not fully appropriate for schooling fish, such as sandeels, as each individual will have to adjust their speed to that of their neighbours. However, there is some suggestion that sandeel schools are sorted by size (found in both *A. marinus* by Johnsen et al. 2009 and in *Ammodytes americanus* by Meyer et al. 1979), and as such, the restriction introduced by schooling may be reduced, and the assumption of a linear increase with length may be reasonable. Further, swimming speed may vary depending on type of prey being pursued (Christensen 2010), but not enough information is available to incorporate this in a robust manner here. As such, a constant swimming speed was assumed. As no average speed has been reported for *A. marinus*, the average speed of *A. tobianus* (van Deurs et al. 2010) was used, which is within the range of values observed for *A. marinus* (Christensen 2010). Upper and lower boundaries were obtained from Christensen (2010).

Detection distance $D_{k,L,I}$

In terms of the detection distance $D_{k,L,I}$ (m), this is, as in van Deurs et al. (2015), dependent on prey size, sandeel size and light conditions. It is based on the model of visual range in fish developed by Aksnes and Utne (1997), and modelled as follows:

$$D_{k,L,I}^2 \exp(a_b D_{k,L,I}) = C \psi_k \gamma_L \frac{I_z}{K_D + I_z} \quad (3.9)$$

where a_b is the beam attenuation coefficient (input to the model, dependent on turbidity), C is the prey contrast, ψ_k (m^2) is the image area of a given prey type, γ_L is the sandeel length-dependent visual sensitivity of sandeels (see Equation 3.10), K_D ($\mu\text{E m}^{-2} \text{s}^{-1}$) is the light saturation of detection distance and I_z (W m^{-2}) the ambient irradiance (see Equation 3.11). The equation is solved through iteration, based on an adaptation of the Fortran code presented in the supplementary materials of Ljungström et al. (2020). It requires the estimation of two parameters - C and K_D . Prey contrast C is the ratio of prey radiance and background radiance, and will depend on the colour and brightness of the prey as well as visual conditions (Utne-Palm 1999). Measurements of transparent copepods at wavelengths corresponding to those of *A. marinus* habitat (see Utne-Palm 1999) were used to define the nominal value of C , with measured standard deviations providing the uncertainty range. It should be noted however that while a constant contrast was assumed for all prey types, it is likely to show some variation between prey types or even within prey types, where, for example, it has been found that copepods with a larger clutch are more likely to get predated upon (Svensson 1995). The light saturation parameter K_D ($\mu\text{E m}^{-2} \text{s}^{-1}$), which accounts for the fact that detection distance does not increase linearly with irradiance, has been estimated experimentally based on several species of fish (Aksnes and Utne 1997). The range of estimated values was used here to define lower and upper boundaries to this value, and the midpoint of the range was used as the nominal value.

Visual sensitivity γ_L is calculated based on the distance at which prey is detected when there is no light limitation (i.e. $I_z/(K_D + I_z) = 1$, notice the relationship between Equation 3.10 and Equation 3.9). Here, this was done using experimental observations by Christensen (2010) of foraging sandeels under well-lit conditions. It is assumed that visual sensitivity scales with body size, as is generally observed in planktivorous fish (e.g. Miller et al. 1993) and often included in this type of fish foraging model (e.g. Ljungström et al. 2020; Varpe and Fiksen 2010, as well as van Deurs et al. 2015). Visual sensitivity γ_L is thus calculated as follows:

$$\gamma_L = \frac{(D_{frac}L)^2}{C\psi_{ref}} \quad (3.10)$$

where L (m) is sandeel length, $D_{frac}L$ (m) is the measured detection distance (thus assuming detection distance at no light limitation scales with body length and is a constant fraction of the body length), C is the prey contrast and ψ_{ref} (m^2) is the prey image area of the experimental prey used when measuring detection distances.

For the herring larvae used in the study by Christensen (2010) (which had a length of around 7 mm at the reported average weight based on the length-weight relationship in Fossum 1996), it was observed that the sandeels reacted to the larvae at around one-half to one-third and at a maximum one whole of the sandeel body length. To calculate γ_L for a given sandeel of length L , D_{frac} takes on the nominal value of 0.5, C is the constant prey contrast and ψ_{ref} is the image area of 7 mm fish larvae (see Langsdale 1993 for how to calculate the image area of herring larvae based on their length). For the uncertainty range for D_{frac} , one-third is used as the lower limit and 1 was used as the upper limit based on the observations from Christensen (2010).

Ambient irradiance I_z

The ambient irradiance I_z (W m^{-2}) is calculated as follows:

$$I_z = I_0 e^{-a_d z} \quad (3.11)$$

where I_0 (W m^{-2}) is the surface irradiance on a given day (average irradiance during the foraging period, which is input to the model), a_d (m^{-1}) is the diffuse attenuation coefficient (also model input, dependent on turbidity) and z (m) is the foraging depth. For the foraging depth z a value of 30 m as in van Deurs et al. (2015) was used, which also seems to align with observations of *A. marinus* schools in the water column (Embling et al. 2008; Johnsen et al. 2009). While it is possible that feeding depths could vary over space and time as a result of, for example, the sandeels adjusting to the depth of maximum prey concentrations (see e.g. Wright and Bailey 1993), there is not enough information to incorporate this. Based on the observation that sandeels are distributed all through the water column during the day (e.g. Freeman et al. 2004; Johnsen et al. 2017), 0 (feeding at the surface) and 70 m (upper limit of optimal habitat depths, Wright et al. 2000) were used as the lower and upper limits, respectively.

Capture probability ϕ_k

In planktivorous fish, it has repeatedly been found that larger prey items are more difficult to capture (e.g. Folkvord and Hunter 1986; Fuiman 1989; Margulies 1989). This likely contributes to the finding that the average size of prey in sandeel guts is only slightly greater than the average size of prey in the water column (Godiksen et al. 2006), in spite of greater encounter rates for large prey types (see van Deurs et al. 2015 and preceding paragraphs) and potentially also an active preference for larger prey (Christensen 2010). To account for the reduced capture success of larger prey types, capture probability is a function of prey size in the model. This relationship is often found to be nonlinear (Folkvord and Hunter 1986; Fuiman 1989), generally following a sigmoidal relationship (Pepin et al. 1987). Further, it is often found that larger predators have a larger capture success (Mills et al. 1984; Pepin et al. 1987). While larger larval sandeel catch larger prey (Simonsen et al. 2006), and this also to some extent occurs in post-metamorphic sandeel too (Eigaard et al. 2014; van Deurs et al. 2014), the effect in post-metamorphic sandeel is very small (an increase in average prey size by 0.027 mm per 1 cm increase, van Deurs et al. 2014). For this reason,

the sigmoidal relationship from (Pepin et al. 1987) was adopted, but the effect of sandeel size was ignored:

$$\phi_k = \left(1 - \frac{1}{1 + \exp(-b \times \ln(L_k/10 - m))} \right) \quad (3.12)$$

where L_k is the size (mm) of prey type k and b and m are constants. This results in a close-to-guaranteed success when targeting small prey, and then a sigmoidal decline as prey becomes larger. b controls the steepness of the decline whereas m controls the point at which the decline occurs.

Since no data exist on species closely related to *A. marinus* and the relationship may vary greatly between species (Luecke et al. 1990), b and m were tuned against the ratio of the size of consumed prey and the size of prey available in the water column as based on the data presented by Godiksen et al. (2006). This is done in Section 4.2.4.

It should be noted that the assumption that capture probability depends solely on prey length is a simplification. Capture probability may vary depending on, for example, the amount of “practice” a fish has had with a certain prey type (e.g. Confer and Blades 1975) or size-independent escape probabilities (e.g. Link 1996). However, experimental results show that within prey species (e.g. Folkvord and Hunter 1986; Fuiman 1989; Margulies 1989) and also across species (e.g. Link 1996) prey size appears to be a good proxy for the ability of the prey to escape.

3.3.1.2 Gut fullness and realised intake rate i_h

Finite gut space puts an ultimate limit on the amount of food a sandeel can ingest, which will depend on the rate of ingestion and digestion, as well as maximum gut capacity. In order to incorporate this limitation into the model, gut content is tracked in terms of wet weight and it is then assumed that intake cannot be greater than what fills the remaining space. The weight rather than energy content is tracked as it is the size of the gut that is limiting, not the amount of energy it can contain (it is assumed that weight and volume are proportional based on water content of zooplankton generally being high, e.g. Kiørboe 2013).

Gut content g (g) changes as follows:

$$\frac{dg}{dt} = \frac{i_h}{\delta_{food}} - d \quad (3.13)$$

where gut content increases with ingested food i_h (kJ h^{-1}) - as this is measured in terms of energy, this is divided by the energy density of the food δ_{food} ($\text{kJ g wet weight}^{-1}$) to obtain ingested food in terms of wet weight - and decreases with digested food d (g h^{-1}). In the model, changes in gut content are discretised assuming hourly time steps.

Digestion

Based on observations in *Ammodytes* spp. (Mackinson 2007; Sun et al. 2010; van Deurs et al. 2010), and as is generally the case in fish (e.g. Andersen 1999; Elliott 1991), digestion is modelled as an exponential process. In addition, as is again observed both in *Ammodytes* spp. (van Deurs et al. 2010) and other species of fish (e.g. Andersen 2001; Elliott 1991), the rate increases with temperature. Further, prey energy density is a key control on digestion rates in fish (Andersen 1999, 2001), with the rate decreasing with increased energy density. This was included in the foraging model of *A. marinus* by van Deurs et al. (2015), where digestion rates were assumed to be inversely proportional to the energy density of the prey. The presence and type of exoskeleton of the prey can also impact digestion rates (Andersen 1999, 2001) which is likely why fish larvae have been found to be digested faster than copepods in *A. marinus* (Christensen 2010; Eigaard et al. 2014). However, there is not enough information of how this would impact the digestion rates for various types of prey to incorporate this into the model. Two studies of *Ammodytes* spp. have found digestion rates to vary depending on prey type (Ciannelli 1997; Sun et al. 2010), but it is unclear what drove the variation between prey types. The study by Sun et al. (2010) found that the smaller of the two prey types studied was digested faster, but as other aspects differed between the prey types, it is difficult to know whether size, which generally has a small impact on digestion rate (Andersen 1999), was the driving factor. In the study by Ciannelli (1997), the fish were fed a mix of prey types, which again makes it difficult to determine what may have driven the variation. Finally, when the impact of other potential drivers of digestion rate such as meal size (Elliott 1991; Garber 1983) and predator size (Garber 1983) have been examined in fish, effects have generally been small or non-existent, and none of these were thus included. As such, the digestion rate d (g h^{-1}) was modelled as in van Deurs et al. (2015):

$$d = \alpha_{dig} \exp(\beta_{dig}T) \frac{\delta^*}{\delta_{food}} g \quad (3.14)$$

Where α_{dig} and β_{dig} are constants, T ($^{\circ}\text{C}$) is temperature, δ^* ($\text{kJ g wet weight}^{-1}$) is the energy density of the prey used when experimentally measuring digestion rates, δ_{food} ($\text{kJ g wet weight}^{-1}$) is the overall energy density of prey in the gut and g is the gut content (g). There are published observations on gut evacuation in *A. marinus* (Mackinson 2007), but as the temperature and prey energy density were not reported, this information could not be used for parameterisation (but see comparison in next paragraph). Instead α_{dig} , β_{dig} and δ^* were taken straight from van Deurs et al. (2015), which is in turn based on observations of *A. tobianus* (van Deurs et al. 2010). The study does not present an uncertainty range for the estimates. For the uncertainty of α_{dig} and β_{dig} , previous studies in fish digestion estimating the same relationship with temperature (Persson 1979, 1981, 1982) found that the 95% confidence interval for α_{dig} was up to around 15% of the nominal value, whereas for β_{dig} it was up to around 5% of the nominal value, and this was used here to define the range of uncertainty. The uncertainty (standard deviation) in the energy density δ^* of the prey (*Artemia salina*) used in the study by van Deurs et al. (2010) was obtained from Verkuil et al. (2006) (same source as in van Deurs et al. 2015).

Observations of *A. marinus* gut evacuation (Mackinson 2007) were compared to model predictions to determine whether Equation 3.14 seems to capture *A. marinus* digestion rates well. The observations were based on sandeels caught in the south-western North Sea in June and then kept in a tank, with 10 sandeels sampled each hour to measure gut contents. For input, the temperature for mid-June for the centre of the sampling area in Mackinson (2007) (based on data from Copernicus Climate Change Service C3S 2017) and prey energy density for the typical sandeel diet in this area around this time (van Deurs et al. 2013) were used. This resulted in a good fit with observations (Figure 3.3a). Observations of *Ammodytes personatus* feeding on adult and nauplii of *Artemia salina* (from Sun et al. 2010) were also compared to model predictions. Reported energy densities, temperature, initial stomach content and sandeel size from Sun et al. (2010) were used as input. This also seemed to suggest that predictions were similar to observations (Figure 3.3b). However, while digestion rates are predicted to be slower for nauplii than adults based on the higher energy content, this is not what was observed. It is possible that other differences, such as the digestibility of the exoskeleton, could explain this difference. As such, the predicted digestion rates appear reasonable, although it points to some uncertainty in the impact of prey traits on digestibility.

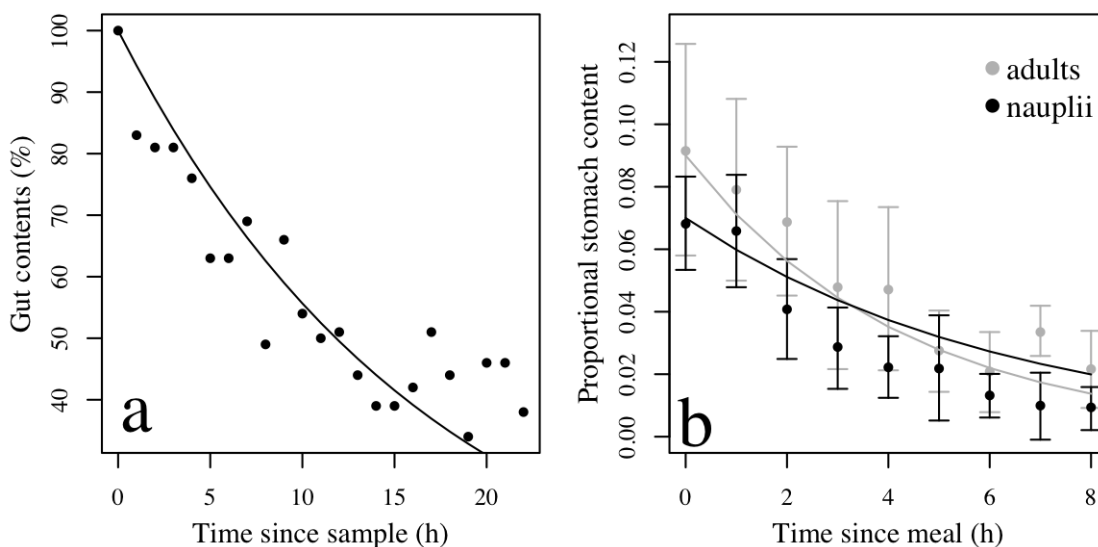


Figure 3.3: (a) Model predictions as compared to measurements from *A. marinus* (Mackinson 2007). Markers show relative stomach content at sequential intervals following sampling in the field. Lines show corresponding model predictions based on Equation 3.14. (b) Model predictions as compared to measurements from *A. personatus* (Sun et al. 2010). Markers with associated error bars are taken from estimates of relative gut content (wet weight of food divided by wet weight of sandeel) at sequential intervals following a meal, feeding on adults (grey) and nauplii (black) of *Artemia salina*. Lines show corresponding model predictions based on Equation 3.14.

It is assumed that digestion occurs continuously, both during the feeding period and during the night. Anything left in the gut after a night of burrowing is carried through to the next feeding period, acting as a limitation on intake. This is based on experimental observations of *A. tobianus* showing that when food was very abundant, there was generally food left in the gut the next morning (van Deurs et al.

2011b). In the field, guts collected first thing in the morning have been found to be empty (Wright and Bailey 1993), but this may be expected as food is likely to be more scarce than in the experimental setting.

Maximum gut size

Based on the finding that the maximum gut size g_{max} (g) in fish is well described by a power function of length (Pirhonen et al. 2019), it was modelled as follows:

$$g_{max} = \alpha_{gut} L^{\beta_{gut}} \quad (3.15)$$

where L (cm) is sandeel length and α_{gut} and β_{gut} are constants. To estimate the maximum gut size, data collected in the North Sea (mostly south-western, but also central-eastern) in 4 years were used (see e.g. van Deurs et al. 2014; 2006 N = 1153, 2007 N = 63, 2009 N = 711, 2010 N = 216). As a starvation period could potentially impact gut size (e.g. Krogdahl and Bakke-McKellep 2005), only gut samples collected during the feeding period were included (April–October). The parameters of the relationship were estimated by fitting a linear model between \log_{10} -transformed gut wet weight and \log_{10} -transformed length data (N = 7053, Figure 3.7b, $\log_{10}(\text{gut weight}) = -3.6 + 2.3\log_{10}(L)$, $R^2 = 0.34$). As log-transformations cannot be used for zero-values, these were not included (0.4% of samples). This provided the value for β_{gut} , with the associated 95% confidence interval, which describes the relationship between stomach content and length. Assuming that this is also representative for maximum content, α_{gut} was estimated by finding the value of α_{gut} for which 99% of data points fell below the estimated relationship (99 rather than 100% was used to reduce the impact of outliers and potential erroneous measurements). The lower and upper uncertainty limits were obtained by repeating this procedure using the limits 98.5% and 99.5%. It should be noted that this approach rests on the assumption that sandeels with completely full stomachs are represented in the sample. The resulting relationship and confidence limits can be seen in Figure 3.4.

Realised intake rate

The gut content at a given time determines the realised intake rate during a given hour i_h (kJ h^{-1}). This is included in the model in the following fashion:

$$i_h = \begin{cases} i_{max}, & (g_{max} - g)\delta_{food} \geq i_{max} \times (1\text{h}) \\ (g_{max} - g)\delta_{food}/(1\text{h}), & (g_{max} - g)\delta_{food} < i_{max} \times (1\text{h}) \end{cases} \quad (3.16)$$

where g_{max} (g) is the maximum gut content, g (g) is the current gut content, δ_{food} ($\text{kJ g wet weight}^{-1}$) is the energy density of gut contents (and ingested food) and i_{max} (kJ h^{-1}) is the maximum energy intake when there is no limitation from gut capacity. As such, the sandeels feed at maximum rate i_{max} when the difference between maximum gut size g_{max} and the actual gut content g is larger than what can be ingested in an hour ($i_{max} \times (1\text{h})$). If there is not enough space to feed at max capacity, it is assumed that the sandeels feed at a rate which corresponds to

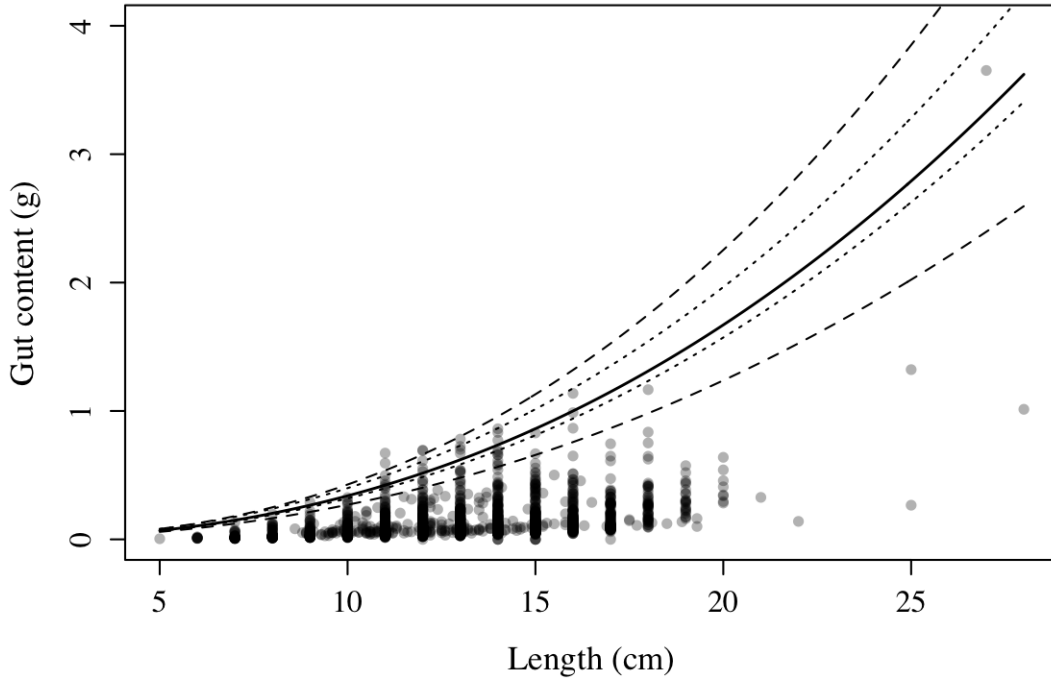


Figure 3.4: Total length of sandeels against wet weight of gut contents. Full line shows prediction of maximum gut size from Equation 3.15. Dotted line shows uncertainty in α_{gut} and dashed line shows uncertainty in β_{gut} .

the remaining gut space (weight) being filled up. Since g_{max} and g are measured in terms of wet weight (g) this is then translated into the unit of ingestion (kJ) by multiplication with the prey energy density δ_{food} (kJ g wet weight⁻¹).

As such, the intake decreases as gut contents near full capacity. However, it is possible that feeding rate would start to decrease even at below full capacity as a result of increased satiation. A potential decrease in feeding rate as a response to increased satiation has been suggested to occur in *A. marinus* (Winslade 1974b), *Ammodytes hexapterus* (now recognised as *Ammodytes personatus*, von Biela et al. 2019) (Cianelli 1997) and *A. tobianus* (see supplementary information in van Deurs et al. 2010, where it was suggested that the oesophagus constituted a digestive bottleneck), but there is not sufficient information to include this effect in the model in a robust way. However, if food is highly abundant and the sandeels are limited by gut capacity then this response to satiation is included, and if food is well below capacity, which is likely to mostly be the case in the field (see Figure 3.4), satiation is not likely to have a large impact on intake. Still, at intermediate abundances it is possible that omitting the effect of satiation on intake could lead to a slight overestimation of intake.

3.3.1.3 Summary of assimilated energy

Again, to calculate the total assimilated energy A , the realised intake rate per hour i_h is then added up for all hours of feeding and multiplied with assimilation efficiency ϵ , given that this is greater than metabolic feeding costs (see Equation 3.3). The equations governing ingestion are summarised in Figure 3.5.

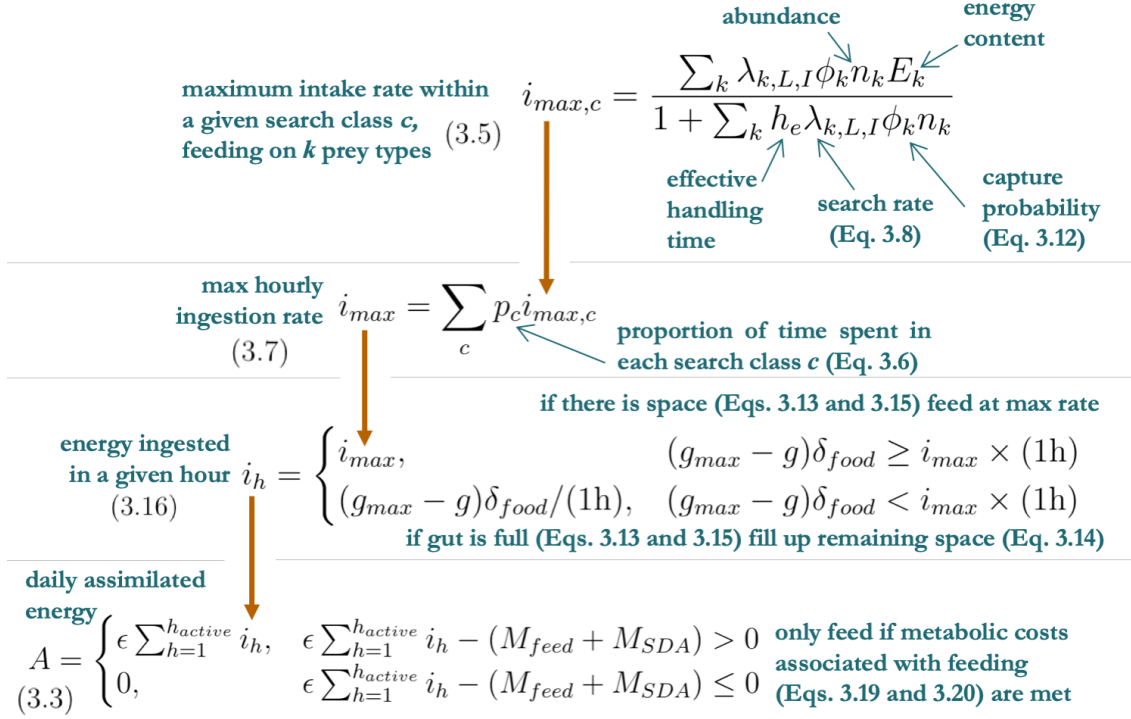


Figure 3.5: Summary of the key equations governing ingestion and how they fit together. See respective equation for details and units.

3.3.2 Metabolic costs

Sandeels have to pay multiple types of costs which contribute to the total metabolic rate. This includes the standard metabolic rate (SMR), which is the energy required to cover basic maintenance at virtually zero activity (no swimming, feeding, digestion, growth or reproductive investment). Further, when feeding, costs associated with feeding behaviour as well as processing of ingested food, including synthesising tissue, often referred to as specific dynamic action, have to be accounted for too. Together, these make up the total metabolic costs M (kJ day^{-1}):

$$M = M_{SMR} + M_{feed} + M_{SDA} \quad (3.17)$$

where M_{SMR} (kJ day^{-1}) represents the energy needed to cover basic maintenance at zero activity for the full 24 hours, M_{feed} (kJ day^{-1}) the additional cost of activity on days when the sandeels are foraging and M_{SDA} (kJ day^{-1}) the cost associated with processing food and synthesising tissue after feeding.

3.3.2.1 Standard metabolic rate SMR

The standard metabolic rate M_{SMR} (kJ day^{-1}) in fish is generally found to vary with body size and temperature (Clarke and Johnston 1999), and so it was assumed that in sandeels it also takes on the commonly observed relationship:

$$M_{SMR} = \alpha_{met} W^{\beta_{met}} Q_{10}^{T/10} \quad (3.18)$$

where α_{met} is a constant, W (g) is sandeel wet weight, β_{met} is the metabolic weight-scaling exponent, T ($^{\circ}\text{C}$) is temperature and Q_{10} represents the rate of change as temperature increases by 10°C . Three constants thus need to be estimated to calculate M_{SMR} . These include the weight-scaling exponent β_{met} , the temperature effect Q_{10} and the scaling factor α_{met} . Luckily, studies of SMR have been conducted on several species of *Ammodytes*, including *A. hexapterus* (now recognised as *A. personatus*, which is used hereafter, von Biela et al. 2019) (Quinn and Schneider 1991), *A. tobianus* (van Deurs et al. 2010) as well as *A. marinus* (Wright et al. 2017a). All studies used overwintering sandeels, and Quinn and Schneider (1991) also included sandeels collected during the summer feeding period ('summer acclimatised').

In general, β_{met} , the weight-scaling exponent, varies between around 0.65-0.95 in fish (Clarke and Johnston 1999). β_{met} has previously been estimated to be 0.65 for *A. personatus* (MacDonald 2017, based on values from summer acclimatised sandeels in Quinn and Schneider 1991), which is thus at the lower end of the spectrum. While observations exist of SMR for sandeels of different wet weights for *A. marinus* (Wright et al. 2017a, additional unpublished data), this dataset contained too much noise to estimate β_{met} (see Figure 3.6), and thus the value from Quinn and Schneider (1991) was used here. However, considering that this value was unusually low, and in addition, this relationship may vary even within species depending on experimental conditions (Jobling 1993), a wide uncertainty range based on estimates from other species of fish from Clarke and Johnston (1999) was used, with an upper bound equal to the average value based on the examined studies (0.79), and a symmetrical lower bound (0.51), which was slightly larger than the smallest value reported in fish.

In terms of Q_{10} , the median value based on 14 examined studies in fish was reported to be 2.4, ranging from 0.45 to 3.41 (Clarke and Johnston 1999). In *A. personatus*, Q_{10} has been estimated to be 1.46 in overwintering sandeels and 1.80 in summer acclimatised sandeels (Quinn and Schneider 1991) and thus sits comfortably within this range. In *A. tobianus*, the relationship between temperature and SMR, unlike what is commonly observed (Clarke and Johnston 1999), appears to be linear (van Deurs et al. 2011a). It is clear, however, that the increase in SMR as based on the same increase in temperature is larger in *A. tobianus* than in *A. marinus* (see supplementary material in Wright et al. 2017a). Finally, Q_{10} in overwintering *A. marinus* has been estimated to be 3.1 (Wright et al. 2017a), which, while only based on two temperature treatments, is thus within the previously observed range in fish (Clarke and Johnston 1999). As such, the value is considered to be plausible and is used as the nominal value. Considering that the value is close to the upper limit of

the range of values previously observed, an asymmetrical uncertainty interval with the value from overwintering *A. personatus* (Quinn and Schneider 1991) forming the lower bound and 3.4 (largest previously observed value in fish, Clarke and Johnston 1999) forming the upper bound.

The dataset from Wright et al. (2017a) was used to estimate α_{met} . First, the measured oxygen consumption rates ($\text{g O}_2 \text{ g fish}^{-1} \text{ h}^{-1}$) were converted into energy depletion rates (kJ day^{-1}). The rate of oxygen release will depend on the substrate that is being metabolised. Here, a conversion factor of 13.6 kJ g^{-1} was used based on fish metabolising mainly fat and some protein (Brett and Groves 1979). Then, to estimate α_{met} , $\alpha_{met} = M_{SMR} / (W^{\beta_{met}} Q_{10}^{T/10})$ was calculated for each fish in the experiment ($N = 16$) and the average was taken. The standard deviation was used to estimate a lower and upper bound to this scaling. Finally, observations on *A. personatus* suggest that there is a 17% reduction in oxygen consumption during winter, and this was evident in both of the temperature treatments (Quinn and Schneider 1991). The authors suggested that this could represent an adaptive shift to seasonal conditions, as the sandeels spend most of the winter immobile. Assuming that this increase in metabolic rate during the summer also applies to *A. marinus*, α_{met} was multiplied by $1/(1-0.17)$ to obtain the final nominal value, and the same was done for the lower and upper bounds.

While it is clear that the metabolic rates predicted based on Equation 3.18 do not capture the all the variation in the data from Wright et al. (2017a), the absolute values appear plausible (Figure 3.6). Variation in SMR between individuals is common, and might be caused by a range of things such as genotype, maternal effects or early-life conditions (Burton et al. 2011) and it is outside the scope of this model to capture the range of this variation. However, it should be noted that this variation can impact the fitness of the individual (Burton et al. 2011).

3.3.2.2 Metabolic costs of feeding

Swimming is an energetically costly activity (Brett and Groves 1979; Jobling 1993), with the energetic cost determined by swimming speed (Jobling 1993) as well as fish size and to some degree temperature (Brett and Groves 1979). The effects of temperature and size on active metabolic rate are not necessarily the same as their effect on SMR (e.g. Brett 1965; Brett and Groves 1979; Dwyer and Kramer 1975). Determining the cost of activity is difficult and often a large source of uncertainty in bioenergetic modelling (Ney 1993). Activity costs have not been measured in *A. marinus*, and in general there is a lack of studies on swimming energetics of pelagic, schooling species (Behrens et al. 2006). However, swimming costs have been measured in the closely related *A. tobianus* through measuring oxygen consumption of individuals swimming at a constant temperature at a constant speed of 1.5 body lengths per second (van Deurs et al. 2010). The measured oxygen consumption was translated into the energetic cost per gram of fish per hour, and the estimated standard metabolic rate at the same temperature was subtracted to obtain the energetic cost of swimming. This assumes no impact of temperature on activity cost, which is likely an oversimplification (see e.g. Brett 1965; Dwyer and Kramer 1975), but considering the wide inter-specific range of relationships between active

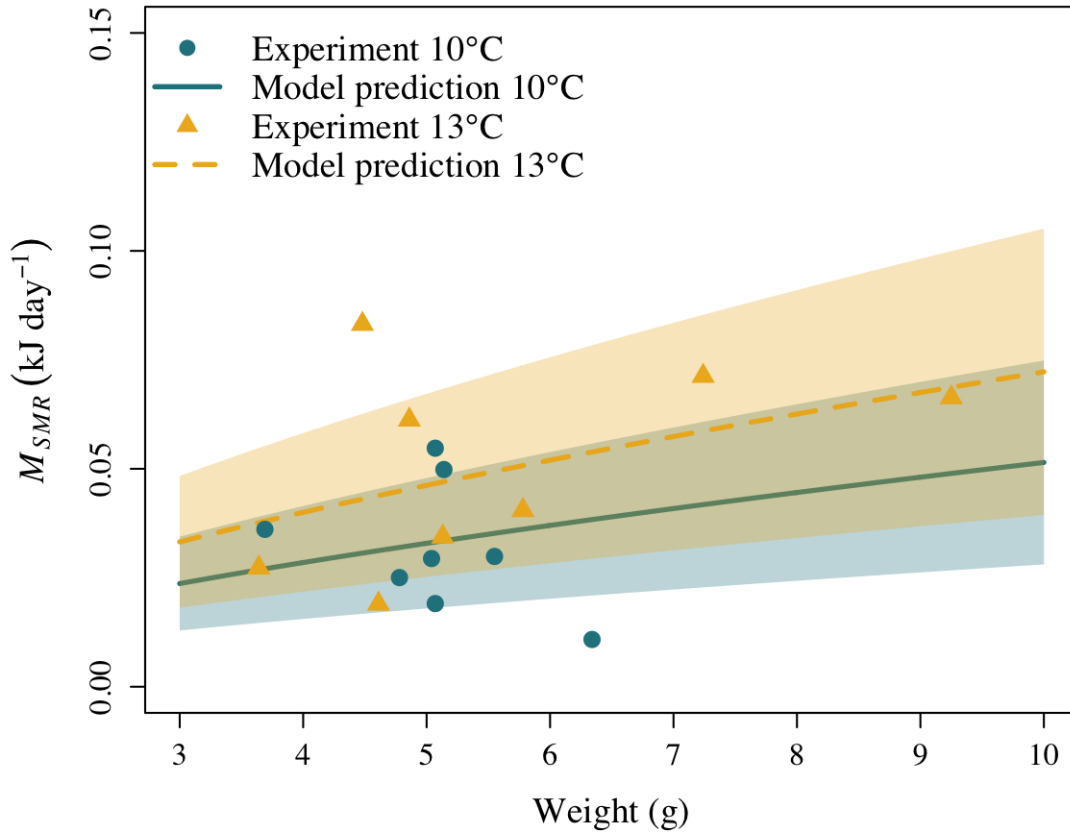


Figure 3.6: Markers show measured oxygen consumption from Wright et al. (2017a) based on the two temperature treatments in the study, 10°C (blue circles) and 13°C (yellow triangles), translated into energy depletion rates. Lines show corresponding predictions for M_{SMR} based on Equation 3.18 for the two different temperature treatments 10°C (blue full line) and 13°C (yellow dashed line). The shaded areas are based on the lower and upper range of α_{met} . It should be noted that the predictions are based on α_{met} without the 17% increase in metabolic rate in summer acclimatised sandeels incorporated (see Section 3.3.2.1), as the sandeels in the experiment were overwintering sandeels.

metabolic rate and temperature (see Fig. 2 in Brett 1965) and in absence of any information on similar species, this is likely the most parsimonious assumption. The assumption of activity costs scaling linearly with mass also appears to be valid - if adding estimated costs of SMR as based on Equation 3.18 for 10°C (temperature in experiment by van Deurs et al. 2010) to estimated activity costs, this results in a weight-scaling exponent β_{met} of around 0.95, which fits with the expected increase in β_{met} during activity (Brett 1965). As no other studies have been conducted on any closely related species and the relationship from van Deurs et al. (2010) has provided plausible output when used in a bioenergetic model of *A. marinus* in the same study, the same relationship was also used here to estimate swimming costs. As such, M_{feed} (kJ day⁻¹) can be estimated as follows:

$$M_{feed} = FWh_{day} \quad (3.19)$$

where F ($\text{kJ g}^{-1} \text{h}^{-1}$) is the cost of feeding per gram of fish per hour, W (g) is sandeel wet weight, and h_{day} (h) is the total number of hours of daylight. It was thus assumed that the costs are paid both when feeding (h_{active}) as well as the two hours used for ascent and descent. The estimate of F from van Deurs et al. (2010) was adopted here as the nominal value. While metabolic costs vary with swimming speed in fish (Behrens et al. 2006; Jobling 1993), Equation 3.19 assumes a constant speed of 1.5 body lengths per second based on this being the average swimming speed of *A. tobianus*. This was also the speed assumed in this study (Equation 3.8), but again, it might vary depending on, for example, prey type (Christensen 2010), which could have consequences for energetic costs.

The estimated swimming cost in capelin, also a pelagic schooling species, of $200 \text{ mg O}_2 \text{ kg}^{-1} \text{ km}^{-1}$ (Behrens et al. 2006), translated into the same units as F (assuming a speed of 1.5 body lengths per second and a capelin of a length corresponding to the midpoint of the range used in the experiment), gives a value of 0.0029, which is similar but slightly lower than F (0.0034). It may be expected that values are higher in sandeels as they lack a swimbladder and thus have to expend more energy to stay clear of the seabed (Reay 1970). As such, F seems like a plausible value. As no uncertainty range is provided in van Deurs et al. (2010), the variation in the estimates of swimming costs in capelin is used to define this range (standard deviation = 11% of the estimates), based on Behrens et al. (2006).

3.3.2.3 Specific dynamic action

It is commonly observed that the metabolic rate in fish increases after a meal, which reflects the energetic cost of processing food and synthesising new tissue, referred to as specific dynamic action (SDA) (Jobling 1981; Secor 2009). The most important drivers of variation in SDA are the amount and type of food ingested (Secor 2009). No relevant observations of SDA exist for any species closely related to *A. marinus*. For this reason, the simplifying assumption was made that SDA is proportional to the energy content of the meal (which seems to work relatively well in fish, Secor 2009), so that M_{SDA} (kJ day^{-1}) is calculated as follows:

$$M_{SDA} = \zeta_{SDA} \frac{A}{\epsilon} \quad (3.20)$$

where A (kJ day^{-1}) is the assimilated energy, ϵ is the assimilation efficiency (where A/ϵ is equal to total ingested energy during the day, before accounting for assimilation efficiency), and ζ_{SDA} is the SDA coefficient. As there are no measurements on closely related species, the average value based on a large range of studies of fish presented in Secor (2009) is used and a wide uncertainty interval based on the range of values observed in fish is adopted.

3.3.3 Energy allocation

Each day, if the net assimilated energy ($A - M$) is positive, a proportion f_S of this is allocated to structural energy S , while the rest is allocated to reserves. In basic DEB models, it is assumed that a fixed fraction of either reserve energy (Kooijman 2000) or net assimilated energy (Lika and Nisbet 2000) is allocated to structural energy (i.e. growth). However, it is possible that organisms may modulate their allocation in response to their state (e.g. Lika and Nisbet 2000). Observations in *A. marinus* (Hislop et al. 1991) and other species of the same genus (Danielsen et al. 2016; Robards et al. 1999b; Sekiguchi et al. 1976) suggest that allocation to growth (i.e. allocation to structural energy S) decreases as the sandeel increases in size. This also aligns with experimental observations of other juvenile fish (Hurst and Conover 2003; Post and Parkinson 2001). Further, it is also possible that allocation rules may depend on the size of the reserve in relation to total energy content, so that re-building reserves is prioritised after a period of starvation (e.g. Broekhuizen et al. 1994). This is supported by experimental observations of the fast recovery of body composition when re-feeding fish following a period of starvation (Xie et al. 2001; Zhu et al. 2005), although allocation to structural energy may also occur before body composition is recovered (see review in Jones 2001). An observed rapid increase in lipid content in *A. marinus* following a winter of no feeding (Hislop et al. 1991; Rindorf et al. 2016) suggests that replenishing reserves is a priority for sandeels in poor condition. Finally, reproduction will also impact energy allocation, but this is not relevant in this case as the model only covers the first growing season. However, it should be noted that in some locations where growth rates are high, a small proportion of sandeels may mature at age 0 (Boulcott et al. 2007), which would impact energy allocation patterns.

The way in which allocation to S changes as the sandeel increases in size can be derived from the relationship between structural energy and total energy across individuals in a population. As structural energy by definition cannot decrease, the derivative of the relationship between total energy and structural energy represents how structural energy increases as total energy increases, which is equivalent to the proportion allocated to structure. f_S can thus be expressed as:

$$f_S = \frac{\frac{dS}{dt}}{\frac{d(R+S)}{dt}} = \frac{dS}{d(R+S)} \quad (3.21)$$

where S (kJ) is structural energy and R (kJ) is reserve energy. This means that if the relationship between S and total energy content $S + R$ is estimated, the derivative of this relationship will be f_S . To estimate the shape and parameter values for this relationship, two different datasets were used. The first one is based on data collected from *A. marinus* dropped by Atlantic puffins (*Fratercula arctica*, hereafter ‘puffin’) on the Isle of May in the north-western North Sea when mistnetted after coming in from a foraging trip (see e.g. Wanless et al. 2018). Length is measured just after collection. Wet weight is estimated based on dry weight and energy density (see Hislop et al. 1991). This dataset included 236 0 group individuals collected in the years 1996 (N = 1), 2006 (N = 50), 2010 (N = 89) and 2015 (N = 96) from 1 June to

26 July, including lengths between 3.2 and 9.9 cm. The second dataset included *A. marinus* data collected from trawl and dredge surveys conducted in late May and in June (see MacDonald 2017 for a description), also in the north-western North Sea. For the survey data, these included a total of 6819 0 group sandeels ranging from 2.5 to 9.5 cm, collected during the years 2000 (N = 615), 2001 (N = 415), 2002 (N = 2389), 2003 (N = 2143), 2005 (N = 779), 2006 (N = 23) and 2009 (N = 455). Based on lengths and wet weights for each individual, structural and reserve energy were estimated for each individual in both datasets, as described in Section 3.3.4.

Based on these data, the relationship between total energy and structural energy seems to be well captured by a power function, which produced a smaller mean squared error than a linear relationship, and seemed to work better for small values (see Figure 3.7a). To fit the power function, a linear model was fit to \log_{10} -transformed structural energy S and \log_{10} -transformed total energy content $S+R$ for both datasets together (N = 7053, Figure 3.7b, $\log_{10}(S) = -0.33 + 0.91\log_{10}(R+S)$, $R^2 = 0.83$). The parameters for the allocation function were then obtained by taking the derivative of the estimated parameters.

This means that f_S is modelled as:

$$f_S = \alpha_{alloc}(R + S)^{\beta_{alloc}} \quad (3.22)$$

where α_{alloc} and β_{alloc} are the estimated constants (β_{alloc} being negative), R (kJ) is reserve energy and S (kJ) is structural energy. The uncertainty of α_{alloc} and β_{alloc} was represented by their 95% confidence intervals (see Figure 3.7c). Parameter estimates were slightly different when considering the puffin and survey datasets separately, where the 95% intervals did not overlap and the relationship based on the puffin dataset suggested a more dramatic decline in allocation to structural energy over time (Figure 3.7a). It is not clear what may have driven this difference, potentially it is a result of there generally being little overlap between the years, and the years displaying slightly different body composition (see Fig. 10b in Wanless et al. 2018). In general, inter-annual variation in sandeel size estimates based on survey and puffin data align well (Wanless et al. 2004). The final parameters are to a larger extent driven by the survey data, due to the larger sample size.

This covers the idea that allocation changes as sandeels grow in size, but does not capture the idea that the allocation strategy changes after reserves have been depleted. To incorporate this, the idea that the relationship between S and $R + S$ in Figure 3.7b can be interpreted as the ideal ratio between S and $R + S$ is used. When the net assimilated energy is positive, the sandeel will continue to follow this ideal ratio as it grows. However, if net assimilated energy is negative, the outstanding metabolic costs will be paid from the reserves and the individual will start to deviate from the ideal ratio. Based on the observation of *A. marinus* that re-building reserves seems to be a priority for sandeels after a winter of no feeding (Hislop et al. 1991; Rindorf et al. 2016), and experimental observations of fish re-building body composition after a period of starvation (Xie et al. 2001; Zhu et al. 2005), it is assumed that once food availability increases again, the sandeels first allocate net energy gain only to reserves in order to shift back towards the ideal ratio. As such, f_S is adjusted as follows:

$$f_S = \begin{cases} \alpha_{alloc}(R + S)^{\beta_{alloc}}, & R + (A - M) \times (1\text{day}) > R_{pre} \\ 0, & R + (A - M) \times (1\text{day}) \leq R_{pre} \end{cases} \quad (3.23)$$

where α_{alloc} and β_{alloc} are constants (same as in Equation 3.22), S (kJ) is structural energy, R (kJ) is reserve energy and $A - M$ is net assimilated energy (kJ day⁻¹). R_{pre} (kJ) is the reserve energy before the period of starvation (i.e. the value of R that corresponds to the ideal reserve ratio for the current value of S). R_{pre} is obtained from the relationship between S and $R + S$, which follows the ideal reserve ratio (Figure 3.7b, remember that α_{alloc} and β_{alloc} come from the derivative of this relationship). R_{pre} (kJ) can thus be calculated as follows:

$$R_{pre} = \left(\frac{S(\beta_{alloc} + 1)}{\alpha_{alloc}} \right)^{1/(\beta_{alloc} + 1)} - S \quad (3.24)$$

where α_{alloc} and β_{alloc} are constants and S (kJ) is structural energy.

The form of Equation 3.23 means that if adding the net assimilated energy $A - M$ to reserves R still does not bring the reserves up to pre-starvation levels (or brings it up exactly to pre-starvation levels), all should be allocated to reserves ($f_S = 0$). If adding the net assimilated energy $A - M$ to reserves R brings reserves up to above pre-starvation levels, allocation follows Equation 3.22. This means that there may be some allocation to structural energy before body composition is restored, which fits with previous observations of post-starvation allocation in fish (see review in Jones 2001).

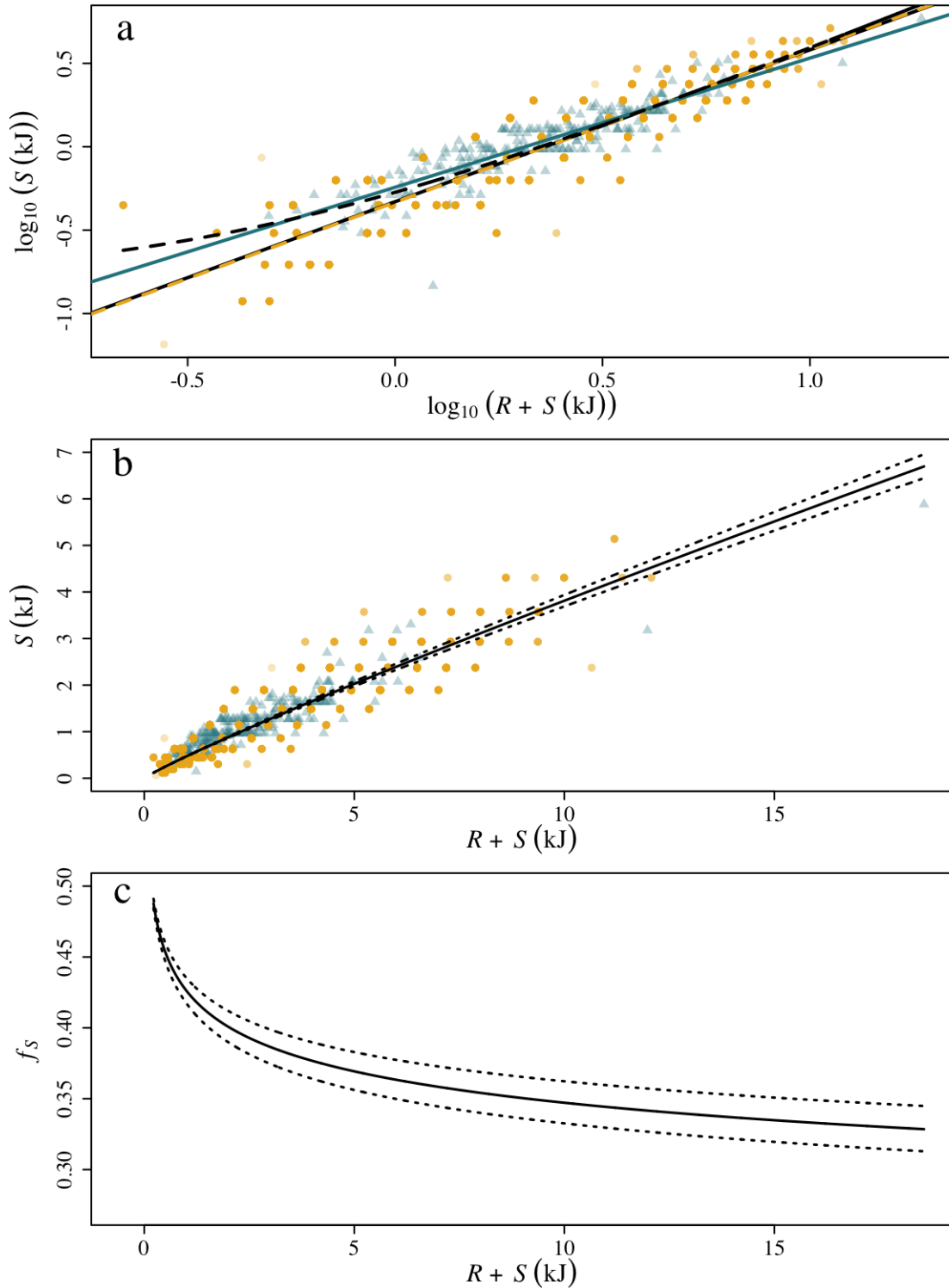


Figure 3.7: (a) \log_{10} of $R + S$ plotted against \log_{10} of S , yellow circles = survey data, blue triangles = Isle of May puffin dataset. Linear relationship between the logarithmically transformed variables based on survey dataset (yellow dashed line), puffin data (blue full line) and full dataset (full black line), dashed black line = linear relationship between the untransformed variables based on full dataset. (b) Relationship between $R + S$ and S , yellow circles = survey data, blue triangles = Isle of May puffin dataset. Full line = fitted logarithmic relationship, dotted lines = 95% confidence interval. (c) Relationship between $R + S$ and f_S , the proportion of net energy gain allocated to structural energy S , as in Equation 3.22. Dotted lines = 95% confidence interval.

3.3.4 Translating structural and reserve energy into length and wet weight

Again, in order to be able to use field data, a way to translate between measuring sandeels in terms of reserve energy R and structural energy S and measuring sandeels in terms of length L and wet weight W is needed. Structural energy S (kJ) is directly related to length L by a power function (see Broekhuizen et al. 1994) as follows:

$$S = \alpha_{dry} L^{\beta_{dry}} \times \delta_S \quad (3.25)$$

where α_{dry} and β_{dry} are constants governing the translation of length into structural dry weight (g), L (cm) is sandeel length and δ_S is structural energy density (kJ g dry weight⁻¹).

Reserve energy R (kJ) is instead a function of both length and wet weight:

$$R = \delta_R \times \frac{W - \omega_{SDW} \times \alpha_{dry} L^{\beta_{dry}}}{\omega_{RDW}} \quad (3.26)$$

where L (cm) is sandeel length, W (g) is sandeel wet weight, ω_{SDW} and ω_{RDW} are constants for translating dry weights into wet weights for S and R , respectively, α_{dry} and β_{dry} are constants governing the translation of L into structural dry weight (g) and δ_R is the reserve energy density (kJ g dry weight⁻¹).

To estimate the parameters for these relationships, the puffin dataset as described in Section 3.3.3 was used again. This dataset does not only provide information on the length and weight of sandeels, but also body composition. After collection, the sandeels are dried to a constant weight, providing total dry weight. This dry weight is then partitioned into fat dry weight, protein dry weight and ash dry weight (see Wanless et al. 2005 for methods). In order to calculate the total energy content of each individual sandeel, protein dry mass is multiplied by the energy density of protein (23.7 kJ g⁻¹, Crisp 1971) and the fat dry mass multiplied by the energy density of fat (39.6 kJ g⁻¹, Crisp 1971) and the two are added together. This approach shows good agreement with data from bomb calorimetry (Hislop et al. 1991). To estimate wet weight, a previously published relationship between energy density and water content was used (Hislop et al. 1991). As such, data on protein, fat, ash and energy content, dry weight, wet weight and length are available. For estimating the parameter values, the data were divided into a training set ($N = 186$) and a test set ($N = 50$), where the test set was chosen by stratified random sampling, so that the set contained data in proportion to the representation of the different years in the dataset, but was random within years.

First, the parameters for Equation 3.25 were estimated. To do this, the structural dry weight of each individual in the dataset was first estimated, where it was assumed that structural dry weight is made up of ash as well as non-remobilisable protein content. It was assumed that the individuals in the dataset that contained the minimum amount of protein for their length have used up their reserves and that the remaining protein is only non-remobilisable protein. So, to estimate the relationship between length and non-remobilisable protein, a quantile regression

of \log_{10} -transformed length and protein dry weight using the function rq from the R-package *quantreg* (Koenker 2018) was fitted, setting τ to 0 (meaning that 100% of data fall above the estimated relationship). This relationship ($N = 186$, $\log_{10}(\text{structural protein dry weight}) = -3.8 + 3.2\log_{10}(L)$) was then used to predict non-remobilisable protein for each sandeel based on their length, which was then added together with the ash dry weight to obtain structural dry weight for each sandeel. The parameters α_{dry} and β_{dry} (Equation 3.25) were then estimated by fitting a relationship between \log_{10} -transformed structural dry weight and \log_{10} -transformed length ($N = 186$, $\log_{10}(\text{structural dry weight}) = -3.77 + 3.27\log_{10}(L)$, $R^2 = 0.99$). The 95% confidence intervals of the parameters were used as a measure of uncertainty. It should be noted that this approach rests on the assumption that there are sandeels in the dataset that are close to starvation (i.e. made up of only structural energy).

To obtain structural energy S (kJ) from length, the structural energy density δ_S (kJ g dry weight $^{-1}$) also had to be estimated. Based on the assumptions as described above, all structural energy will be contained in the non-remobilisable protein. As such, the structural energy S of each sandeel was estimated by multiplying the predicted non-remobilisable protein with the energy density of protein (23.7 kJ g $^{-1}$, Crisp 1971). To obtain δ_S , S was divided by the sum of non-remobilisable protein dry weight and ash dry weight for each sandeel and the mean was taken. Uncertainty was estimated as the standard deviation.

All parameters for translating length into structural energy have thus been estimated, but several parameters from Equation 3.26 remain, including the energy density of reserves (δ_R). R of each sandeel in the dataset was estimated by multiplying the fat content of each sandeel with the energy density of fat (39.6 kJ g $^{-1}$, Crisp 1971), and multiplying the remobilisable protein (total protein minus non-remobilisable protein) with the energy density of protein (23.7 kJ g $^{-1}$, Crisp 1971) and adding the two together:

$$R = 39.6 \times \text{fat dry weight} + 23.7 \times \text{reserve protein dry weight} \quad (3.27)$$

δ_R was then estimated by dividing the estimated R by the estimated reserve dry weight (fat dry weight plus remobilisable protein dry weight) for each sandeel and taking the mean. Again, uncertainty was represented by the standard deviation.

Finally, to estimate how both structural and reserve dry weights translate into wet weights (ω_{SDW} and ω_{RDW}), the general approach outlined in MacDonald et al. (2018) was followed, making use of a published relationship between the proportion of wet weight made up of fat and the proportion of wet weight made up of water in *A. marinus* (Hislop et al. 1991):

$$\text{proportion fat} = 64.094 - 0.777 \times \text{proportion water} \quad (3.28)$$

As it was assumed that all fat is part of the reserve energy, the proportion of fat can be set to 0 in this equation in order to estimate the proportion of water in a sandeel with no reserves (i.e. made up completely of structural energy). This makes it possible to estimate ω_{SDW} :

$$\omega_{SDW} = \frac{1}{1 - (0.64094/0.777)} \quad (3.29)$$

ω_{RDW} was then estimated by calculating reserve wet weight by subtracting structural wet weight (which can be estimated using ω_{SDW} and the previously estimated structural dry weight) from total wet weight and dividing this by the sum of fat dry weight and remobilisable protein dry weight. Individuals that contained no reserves were excluded from the calculation. The standard deviation was again used as a measure of uncertainty. As expected, ω_{RDW} was smaller than ω_{SDW} , as sandeels lose water as they gain fat (Hislop et al. 1991). As no uncertainty range was provided in Hislop et al. (1991) to use for ω_{SDW} , the magnitude of uncertainty as calculated for ω_{RDW} was used.

Having estimated all parameter values, the ability to translate length and wet weight into structural and reserve energy was then tested by comparing the summed predictions of S and R based on Equation 3.25 and Equation 3.26 with the measured total energy content of the sandeels in the dataset. Doing this for the data used to develop the equations, the training set, the correlation strength was estimated to be 0.99 ($p < 0.001$, $N = 186$, Figure 3.8a). Doing the same for the test data, a correlation strength of 0.97 was obtained ($p < 0.001$, $N = 50$, Figure 3.8b).

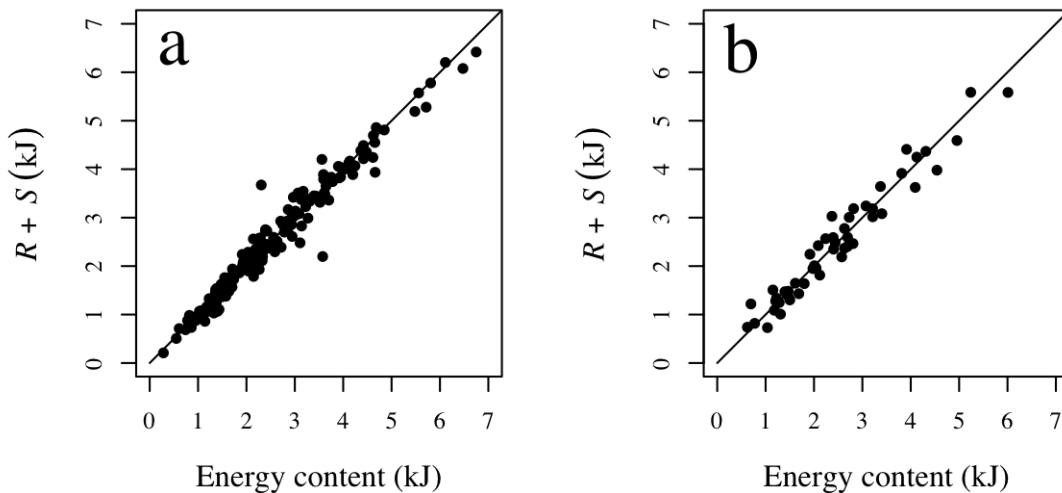


Figure 3.8: Summed predicted R and S based on Equation 3.25 and Equation 3.26 against measured total energy content for sandeels in the training set (a) and the test set (b), with 1:1 lines included.

3.4 Discussion

This chapter has described a DEB model for the first-year growth of *A. marinus*, including energy intake, energy loss, the allocation of net energy gain to growth and reserves, and how the state variables, structural energy S and reserve energy R , can be translated into length and wet weight, and thus compared with field measurements. As with all bioenergetic models, this model includes several sources of uncertainty. The final model output will depend on decisions regarding what processes are included, how these processes are represented in the model (e.g. linear or nonlinear relationships) and the parameter values that govern these processes, which all introduce uncertainty. Here, some of the decisions made in the formulation of this model and their potential impact on model output are discussed.

The right level of complexity in bioenergetic models, or any model for that matter, is not obvious. Erring both on the side of simplicity, potentially making unjustifiably simple assumptions regarding fish bioenergetics, or on the side of complexity, introducing a host of parameters requiring estimation, may both result in large errors (Ney 1993). What level of complexity is used, or in other words, what processes are included in a model, will depend on several things. One of these is what processes are included in previous, similar models. In this case, the DEB model by MacDonald et al. (2018) and the foraging model by van Deurs et al. (2015), which both in turn draw on previous models (e.g. Broekhuizen et al. 1994 and Varpe and Fiksen 2010, respectively), have clearly had a large impact on model formulation. Making use of previous models comes with the benefit of drawing on decades of thought and validation, but it should be recognised that they may also come with unjustified complications or simplifications that need to be critically evaluated.

In addition to the structure of previous models, the current level of understanding of sandeel biology also has a large impact on which processes are included in the model. However, this level of understanding may not necessarily be in line with the understanding needed to capture the key processes governing variation in growth. For example, Christensen (2010) observed large variation in sandeel behaviour (swimming speed, technique) depending on prey type, but since this was only based on two types of prey, this is not enough information to be able to infer what this may mean for the full range of prey consumed. However, this variation in behaviour, which included a four-fold change in speed, could potentially have a large impact on intake rates. The impact of the level of current biological knowledge on model formulation does not apply only to sandeel-specific knowledge. For example, Gliwicz et al. (2018) recently identified a positive effect of temperature on detection distance in two species of planktivorous fish, with an increase of 10°C leading to a doubling of the encounter rate. If this is a general phenomenon, this could have a major impact on intake rates, but has not been included in foraging models to date.

Finally, what processes are included in models will also be a result of what is *thought* to be important, and in particular what is thought to be important in the context of the questions being asked. In this model particular attention was paid to the processes governing intake, as food conditions have repeatedly been linked to size in *A. marinus* (e.g. Eliassen 2013; MacDonald et al. 2018; van Deurs et al. 2015,

2014) and other *Ammodytes* spp. (e.g. Nishikawa et al. 2020; Robards et al. 2002; von Biela et al. 2019). Based on Eggers (1977) and observations in sandeels (see Section 3.3.1.1), the model included a prey and sandeel size-dependent search rate, a prey size-dependent capture probability and active selection of profitable prey, and in addition to this, the limitation introduced from limited gut space. It could be argued that this model is likely to be unnecessarily complex. However, it may be preferable to start at this level of complexity, including all the key processes that are thought to be important, and then critically examine model output and its sensitivity to parameter values (which is done in Chapter 4). Based on this examination, the most salient processes can be picked out. If, instead, one focuses on only one process, it is possible that the results will point to the importance of this process, just as a result of the way it is coded into the model. For example, the model by van Deurs et al. (2015) focused on the impact of prey size on detection distance and its consequences for intake rate, not accounting for the fact that in addition to longer detection distances, an increase in size likely also leads to a decrease in capture probability. This study concluded that prey size is a major driver of variation in intake rates through its impact on detection rate. This may very well be the case, and the model predictions do align well with observed size (van Deurs et al. 2015), but assuming a constant capture rate is likely unrealistic and probably means that the positive effect of size on intake rate is overestimated. As such, complexity may be preferred if it gives a fairer representation of potentially important processes. Still, it is possible that all the additional complexity here is not necessary, and, again, after assessing the model behaviour in the next chapter, it will be important to consider whether a simpler model could capture the salient processes sufficiently well. In general, the model formulation and critical examination should be viewed as a learning process, directing attention to what seems to be the most crucial processes.

It could be argued that the largest simplification in this model is the simplified environment. In the model, the sandeel is considered largely as an independent entity - only interacting with their prey, but not with conspecifics or any other species, such as predators. However, all of these interactions may impact both intake rates and metabolic costs. Sandeels form schools, which may impact a range of processes. For example, intake rate has been found to be impacted by schooling behaviour via a disadvantage for individuals at the back of the school through individuals at the front of the school consuming the available prey (Eggers 1976). Non-sandeel competitors could also impact the fine-scale availability of prey, which will impact the experienced prey field for individual sandeels. However, positive relationships between size and abundance in sandeels (e.g. Eliassen 2013) seem to suggest that a common response to food availability and environmental conditions is a stronger driver of variation than competition, at least from conspecifics (but see Bergstad et al. 2002).

The assumption of a homogeneous prey field is also an important oversimplification. This is a common assumption in this type of foraging model, but in reality, plankton will be patchily distributed within the water column (e.g. Lalli and Parsons 1997). This patchiness may occur on fine spatial scales (Owen 1989), and may impact the intake rate of the fish (e.g. Gliwicz and Maszczyk 2016). Depending on the spatial extent of the patch, this, in combination with the schooling behaviour of the sandeel, may lead to a reduced intake rate as the individual sandeels may only be exposed to the high-density patches for a short amount of time, but most of the time experience below-average abundances. This effect was part of the motivation for the inclusion of an “effective handling time”, but it should be noted that depending on the patchiness of the prey field and the size of the school, the impact of this effect may vary and is thus not fully represented by a single parameter.

In terms of predators, they are also likely to impact the behaviour of the sandeels. While some predators are able to capture sandeels while buried in the sand (e.g. Watanuki et al. 2008), the risk of predation (as well as fishing mortality) will be greatly increased while present in the water column (as well as when leaving and entering the sand, Engelhard et al. 2008; Hobson 1986). As such, there is a trade-off between maximising energy intake by being present in the water column for longer and reducing predation risk by spending as little time in the water column as possible (van Deurs et al. 2010). It is thus possible that the presence of predators may impact the length of the foraging period, which will impact both intake rate and costs. Further, the change in schooling behaviour when predators are present (e.g. Meyer et al. 1979; Pitcher and Wyche 1983) could introduce increased activity costs.

In addition to these simplifications regarding interactions with other species, the environment is also simplified in terms of physical representation, which now only includes light conditions and temperature. For example, tidal movements may impact the rate of advection of zooplankton into the foraging area (Embling et al. 2008), which might affect intake rates. Further, it is possible that oxygen conditions could impact energetic costs, for example through changed activity patterns, which has been suggested could be the case for *A. tobianus* (Behrens et al. 2010). However, this is probably less likely to impact *A. marinus*, which inhabit more hydrodynamically active waters (Tien et al. 2017).

In addition to decisions regarding which processes are included, decisions regarding *how* they are included also need to be made, which will also introduce uncertainty (Ney 1993). For example, following Clarke and Johnston (1999), it was assumed that the effect of temperature on SMR could be represented by a Q_{10} -relationship, but as there were only two temperature treatments in the experiment on *A. marinus* (Wright et al. 2017a), and this relationship appears to be linear in *A. tobianus* (van Deurs et al. 2011a), this is far from certain. Decisions regarding how model processes are represented are similar to the decisions regarding what processes are included, and the two are interlinked. As such, similarly, the mathematical form of the included processes also depends on previous model formulation, the biological knowledge of the process, and how important the process is thought to be. Here, choices were based on either previously established forms (e.g. formulations for standard metabolic rate,

the model of visual foraging), biological observations (e.g. assuming that intake is zero when prey abundances are not sufficient for meeting metabolic feeding costs) or derived from data (e.g. the allocation of net assimilated energy to structural energy as a function of total energy content). When relationships are derived from data, this relies on the data being representative of the sandeels as a whole. For example, in the formulation of the allocation equations, this assumed that the dataset contained sandeels of representative body composition.

Finally, on top of decisions regarding which processes are included and their functional shape, values are needed for each parameter. This model includes 29 parameters. About half of those are based on data from *A. marinus*, and a further 8 are based on other *Ammodytes* spp. Only 4 parameters are based on studies of other species of fish, which were mostly other small planktivorous fish. As such, unjustified borrowing of parameter values from other species (see Ney 1993) should not be a large problem in this model. Further, when values were adopted from other species, a wide uncertainty interval was used, and the impact can be assessed in the sensitivity analysis (see Chapter 4). However, even when measurements existed from *A. marinus*, there could still be a lot of variability in these estimates, such as the ones related to standard metabolic rate (Figure 3.6). Again, when this was the case, wide uncertainty intervals were adopted, so that the impact of this uncertainty on model output could be explored. One further issue is that even when a process can be well measured with little uncertainty in an experimental setting, these values are not necessarily representative of field conditions. For example, plankton used in experiments may be in poorer condition than their wild counterparts, meaning that capture probability and handling times may be overly optimistic (Pepin et al. 1987). Further, even when field data are available, these may not be representative of the full set of conditions. For example, both the formulation of energy allocation and the translation equations relied on the data used being representative of sandeels more broadly. As such, there are many reasons for why parameter values may be inaccurate or unrepresentative, and it will be crucial to examine the results of the sensitivity analysis in the next chapter carefully to determine how much trust can be put in the values of parameters that appear to have a particularly large impact on model output.

To sum up, the formulated DEB model can be criticised for being parameter-heavy with many sources of uncertainty. However, it is argued here that this complexity, which is formulated to reflect the current understanding of sandeel biology and drivers of spatio-temporal variation in sandeel growth, in combination with a critical examination of the output and its sensitivity to parameter values, will help to identify important processes that drive observed growth patterns. Further, this can also help to guide future modelling efforts, suggesting what simplifications may be justified, and where key knowledge gaps lie.

Chapter 4

Drivers of spatio-temporal variation in the growth of juvenile lesser sandeels

4.1 Introduction

Climate change is expected to have pervasive impacts on marine ecosystems. This can act on species through direct physiological effects of changed climatic conditions, but also through indirect effects mediated by interacting species (e.g. Sydeman et al. 2015). Species higher up in the food web, such as seabirds and marine mammals, will likely be hardest hit by indirect effects through changes in their food supply, whereas species at intermediate trophic positions may be impacted by both direct physiological effects, as well as changes at lower trophic levels (Sydeman et al. 2015). In many marine ecosystems, these intermediate trophic positions are occupied by forage fish. As the climate warms, increased temperatures may impact forage fish directly via physiological rates, but they are also likely to be affected by changes in their zooplankton, which is expected to respond strongly to climate change (Poloczanska et al. 2013; Richardson 2008). Both of these effects will then be transferred up the food chain to top predators. Understanding the mechanisms of how forage fish are impacted by climate and other environmental change and how this gets transferred up the food chain is thus of key importance, especially in light of the rapid declines observed in many top predator populations (e.g. Hutchings et al. 2010; Paleczny et al. 2015; Sydeman et al. 2015).

As temperatures have increased, forage fish in various systems have decreased in size (e.g. Baudron et al. 2014; Daufresne et al. 2009). A decline in size is one of the three so-called “universal responses” to climate change, in addition to changes in phenology and distribution (Daufresne et al. 2009; Sheridan and Bickford 2011). It has been suggested that the observed size declines in ectotherms, which includes most fish, could be the result of direct effects of temperature, for example through warmer temperatures resulting in increased metabolic rates, leaving less resources to allocate to growth (Sheridan and Bickford 2011). Further, another possibility is

that temperature-driven changes in food conditions have led to a decline in size (Gardner et al. 2011). In addition to changes in zooplankton phenology, abundance and distribution (Poloczanska et al. 2013; Richardson 2008), this may also include a reduction in zooplankton size, both at the community level and within prey types (Daufresne et al. 2009). This results in less energy contained in each individual prey item but may also impact intake rates in visually foraging fish through the effect on prey detection distances (Ljungström et al. 2020; van Deurs et al. 2015). This may be exacerbated by the shift to more turbid waters observed in several mid-latitude locations (Capuzzo et al. 2015; Dupont and Aksnes 2013), which may to some extent also be climate change-driven (Capuzzo et al. 2015). Further, another mechanism which could result in a decline in size on a given date is phenological shifts. If there would be a delay in, for example, the timing of hatching of fish larvae, this would mean that the larvae start growing at a later date, and could also result in a mismatch with prey, both with the consequence of a decline in length-at-date. Finally, it is also possible that increased fishing pressure may have contributed to some of the observed declines in forage fish size by introducing selection for smaller body sizes. However, this mechanism is not sufficient for explaining at least some of the observed rates of decline in forage fish size (Baudron et al. 2014). Whatever the cause, declines in forage fish size are likely to have knock-on effects on both demographic rates and the energy available to upper trophic levels, and as such, understanding the driving mechanisms is of large importance (Ohlberger 2013; Sheridan and Bickford 2011).

However, understanding underlying mechanisms is not always straightforward. For example, while temperature and forage fish growth may be found to correlate, this could largely be the result of temperature effects on the food source, rather than direct temperature effects. Further, it is also possible for temperature and food effects to interact, so that temperature has a positive effect when food is abundant, but a negative effect when food is scarce (e.g. Brodersen et al. 2011). One useful approach to start teasing these effects apart is through the use of mechanistic models of growth, which incorporate metabolic costs and intake rates and how they depend on temperature and food conditions (Gardner et al. 2011). These can also be used to understand spatial variation in growth, and how local conditions may determine observed trends in size, where responses to increased temperatures may vary spatially as a result of different baseline conditions (Ohlberger 2013).

Like many other species of forage fish, lesser sandeels (*Ammodytes marinus*, hereafter 'sandeel') have also shown a negative temporal trend in several locations (van Deurs et al. 2014; Wanless et al. 2018). In the Firth of Forth in the north-western North Sea, the decline in sandeel size from the mid-1970s to 2015 resulted in a 70 and 40% decline in the energy content of 0 group and 1+ group sandeels, respectively, which is likely to have had a large impact on the seabirds relying on sandeel as prey during the breeding season (Wanless et al. 2018). This negative effect may be exacerbated by the impact of sandeel size on demographic rates and phenology (Boulcott and Wright 2011; Boulcott et al. 2007; MacDonald et al. 2018), which will also impact the availability of the sandeels to breeding seabirds at the time of their highest energy demand. Further, in addition to temporal trends, sandeel size also shows clear spatial variation (Bergstad et al. 2002; Boulcott et al. 2007; Rindorf et

al. 2016). This likely contributes to observed spatial variation in sandeel maturation rates (Boulcott et al. 2007) and fecundity (Boulcott and Wright 2011) as well as the strong spatial variation in seabird breeding success (e.g. Fauchald et al. 2015; JNCC 2020).

Several factors have been suggested to drive variation in the length and energy content of sandeels. One obvious candidate is food conditions, which has long been proposed as the main driver of observed spatial patterns in sandeel size (Bergstad et al. 2002; Boulcott et al. 2007; Macer 1966). In line with this, previous work suggests that sandeel ingestion and growth rates are related to both total food availability (Eliassen 2013; MacDonald et al. 2019b), and the type of prey available (in particular variability in the abundance of large prey types such as *Calanus* copepods) (MacDonald et al. 2018; van Deurs et al. 2015, 2014). Sandeel food conditions show clear spatial variation (see Chapter 2) and in addition, the prey available to North Sea sandeels has also changed markedly over time, with a decline in the total energy available in several sandeel grounds (see Figure 2.7), a change in the size composition (Pitois and Fox 2006, Figure 2.15) and a shift from cold-water *Calanus finmarchicus* to warm-water *Calanus helgolandicus* (Edwards et al. 2020). Further, the phenology of several sandeel prey species is shifting too as a response to increasing temperatures (Richardson 2008). This could potentially have negative effects on the sandeels if it results in a mismatch of food availability and the sandeel foraging window (see van Deurs et al. 2010). As sandeels are visual foragers (Winslade 1974c), visual conditions may modify the response to the prey field, with knock-on effects for ingestion rates (van Deurs et al. 2015). Turbidity has increased in large parts of the sandeel's range (Capuzzo et al. 2015), but as these trends are reported on a larger scale, changes in sandeel grounds are unclear. Further, cloud cover, which will also impact light conditions for foraging sandeels, is also changing as a result of climate change (May et al. 2016).

In addition to food and light conditions, temperature has also been linked to sandeel growth. In the North Sea, the body condition and mean length-at-age of sandeels have been found to be higher on warmer grounds (Rindorf et al. 2016), whereas Eliassen (2013) found that length and condition of sandeels were lower following a warm winter. A study of the closely related *Ammodytes hexapterus* (now recognised as *Ammodytes personatus*, von Biela et al. 2019) found that in the same location, there was a positive relationship between temperature and growth, whereas when compared across space, growth rates were higher in colder regions (Robards et al. 2002). This all points to how correlations between temperature and sandeels are the result of multiple mechanisms, including direct temperature effects on sandeels (e.g. Winslade 1974b; Wright et al. 2017a, see Chapter 3 for details), temperature effects on their zooplankton prey (Richardson 2008) as well as interactive effects between food and temperature (MacDonald et al. 2018). As such, the impact of the rapidly rising temperatures in the north-east Atlantic (see Belkin 2009) is still unclear.

In terms of environmental influences on growth, it is also important to consider timing. Pre-metamorphic processes will determine the time at which the sandeels settle and begin feeding with older age groups, and potentially also at what size (Jensen 2000; Régnier et al. 2017; Wright and Bailey 1996). It is unclear how much of the

observed variation in post-metamorphic size can be attributed to pre-metamorphic processes, such as timing of hatching and larval growth, and how much can be attributed to post-metamorphic processes (Frederiksen et al. 2011; MacDonald et al. 2019a). The relative importance of these processes needs to be clarified in order to predict how sandeel size will be impacted by projected temperature-driven changes in pre-metamorphic processes, including an increased mismatch between the timing of hatching and larval prey availability (Régnier et al. 2019). This increased mismatch will likely result in a reduction in larval growth rates, which may result in sandeels metamorphosing later. This not only means that the sandeels start their growing season later, but could potentially also lead to an increased mismatch with the timing of post-metamorphic food availability, likely with detrimental consequences for the sandeels (van Deurs et al. 2010).

In this chapter, potential drivers of variation in the growth of juvenile lesser sandeels are explored, focusing on the impact of food conditions, temperature, light conditions as well as metamorphosis timing and size. To this end, the dynamic energy budget (DEB) model described in Chapter 3 is (1) first run on the prey fields developed in Chapter 2 for several locations in the north-east Atlantic and the resulting predictions of sandeel length are compared to spatially and temporally matched observational length data. If predictions and observations agree, this suggests that the model captures at least some of the processes that have resulted in the observed spatio-temporal variation and can thus be used to tell us something about drivers of the observed variation. Then, the model is (2) subjected to a parameter sensitivity analysis, which will indicate which model mechanisms have the largest impact on predicted size and where the major sources of uncertainty lie. Finally, the model is (3) used to examine the roles food conditions, temperature, light conditions as well as the role of timing of and size at metamorphosis play in driving growth.

The study will help to understand drivers of variation in sandeel growth, with a particular focus on drivers that have and are expected to continue to change rapidly. It only considers growth during the sandeel's first feeding season, which is arguably the most important to understand due to its strong link with overwinter mortality (MacDonald et al. 2018) and the importance of 0 group sandeels as prey during the seabird chick-rearing period (e.g. Lewis et al. 2001). Further, in a qualitative sense, many of the findings will also apply to 1+ group sandeels as the response of ingestion rates and metabolic rates to food conditions and temperature are likely to be similar.

4.2 Methods

The DEB model, which is described in detail in Chapter 3, runs with daily time steps and models changes in reserve energy R (energy that can be remobilised to meet metabolic costs) and structural energy S (energy that cannot be remobilised, such as skeletal tissue) through the processes of feeding, metabolic costs as well as energy allocation rules. R and S can also be translated into length and weight so that the output can be compared to field data. The model is run from metamorphosis (see Section 4.2.2) until mid-September (day 250), but reported predictions generally refer to the beginning of August (day 212, day_{OW} from hereon), which roughly aligns with the initiation of overwintering (MacDonald 2017; van Deurs et al. 2011a).

While the model itself is coded in C, all data processing, output visualisation and analyses presented in this chapter were conducted in R 3.5.2 (R Core Team 2018), apart from surface irradiance which was calculated using a Fortran subroutine as published in the supplementary materials of Ljungström et al. (2020).

4.2.1 Model input

The model requires three kinds of input - prey fields, temperature and light conditions. Here the input data are first described generally, before the data for specific locations are described.

In terms of the prey field, this includes daily abundances (n_k) for each considered prey type k (individuals m^{-3}), as well as values for the energy content (E_k , kJ), prey image area (ψ_k , m^2) and length (L_k , mm). The daily abundances were based on CPR data, using the methods of spatial aggregation, temporal interpolation and correction for sampling efficiency outlined in Chapter 2. As described in Section 2.3.2), the prey types considered included the copepod groups *Acartia* spp., *Calanus finmarchicus*, *Calanus helgolandicus*, *Calanus* V–VI, *Calanus* I–IV, *Centropages typicus*, *Centropages hamatus*, *Centropages* spp., *Metridia lucens*, *Oithona* spp., *Para-Pseudocalanus* spp., *Temora longicornis* and copepod nauplii as well as the non-copepod groups Euphausiacea, Hyperiidia, Decapoda larvae, Appendicularia, fish eggs, fish larvae, *Evadne* spp. and *Podon* spp. Energy content, prey image area and length for each prey type can be found in Table 2.4.

Each prey type also needs to be assigned to a search class. Search classes are explained in further detail in Section 3.3.1.1, but, in brief, capture the assumption that the sandeels will only focus on one search class of prey types at a time, spending time in each search class in proportion to its profitability. Within each search class, prey types are similar and it would be expected that the sandeels use a common search image for these prey types. While behaviour, such as swimming speed, is likely to vary between search classes, not enough information is available to incorporate this and it is assumed that behaviour is the same for all search classes. To delineate the different search classes, previous studies of *A. marinus* were used. Observations of foraging sandeels that were first feeding on *Acartia* spp., which have a length of around 1.15 mm (Richardson et al. 2006), found that the sandeels switched to feeding

solely on herring (*Clupea harengus*) larvae (7mm) when these were introduced, while completely ignoring the copepods (Christensen 2010). As such, these prey types are part of different search classes. This is supported by Eigaard et al. (2014) finding that sandeel larvae (minimum length 12 mm) and copepods (no reported length) were found in distinct clumps in sandeel guts sampled in the field (suggesting that they only fed on one at a time). Further, Godiksen et al. (2006) found that krill (6 mm) and capelin larvae (18.3 mm) were clumped together, and suggested that this may be because the sandeel develop a common search image based on the larger size and darkly pigmented eyes. Copepods (2.5 mm) occurred in separate clumps. This suggests that fish larvae and large crustaceans are part of the same search class, and that large copepods are part of a separate search class. Finally, van Deurs et al. (2014) found that individual sandeel stomachs tended to contain either copepods smaller than 1.3 mm or copepods larger than 1.3 mm, suggesting that these size groups belong to different search classes. Together, this suggests three prey search classes: small (<1.3 mm) copepods (search class A), large (>1.3 mm) copepods (search class B) and finally fish larvae and other large crustaceans (search class C). Other small prey types such as cladocerans (all smaller than 1.3 mm) were grouped with the small copepods (search class A). The search class assigned to each prey type along with the justification can be found in Table B.1 in Appendix B. It should be noted that while the study by Christensen (2010) suggests that active switching does occur, at least between copepods and fish larvae (which is supported by Eigaard et al. 2014; Godiksen et al. 2006, although fine-scale spatial distribution may also have contributed to the clumping of prey types in sandeel stomachs), the distinction between the copepod groups based on the study by van Deurs et al. (2014) is less clear. For this reason, the impact on model output of considering search classes A and B as a single search class, as well as the impact of assuming no active switching at all, is examined in Section 4.2.6.

The model also requires daily estimates of temperature (T , °C). Temperature data were obtained from the ERA5 Climate Reanalysis, providing hourly sea surface temperature with a 31×31 km resolution (Copernicus Climate Change Service C3S 2017). The hourly data were averaged to daily values. While these values refer to surface temperature, it is assumed that they are representative of the temperatures experienced by the sandeels throughout the water column. This is justified by the fact that sandeels tend to occur in hydrographically dynamic areas (Tien et al. 2017), where temperatures are largely homogeneous throughout the water column. For example, a survey which measured both bottom and surface temperatures during late spring at sandeel grounds at Dogger Bank in the south-western North Sea, found the maximum difference to be 1.2°C (van der Kooij et al. 2008).

Finally, the model requires input in the form of light conditions, including the total number of hours of daylight (t_{day} , sunrise to sunset, rounded to a whole number), average surface irradiance during hours of daylight (I_0 , W m^{-2}), the diffuse attenuation coefficient (a_d , m^{-1}) and the beam attenuation coefficient (a_b , m^{-1}). t_{day} , which is a function of latitude and day of the year, was obtained using the function *daylength* in the R-package *geosphere* (Hijmans 2017). I_0 was calculated using a Fortran subroutine as published in the supplementary materials of Ljungström et al. (2020). I_0 is a function of cloud cover, which was generally assumed to be constant

at 0.75 based on a rough estimate of the average value during summer in the study area (Giggenbach et al. 2010). a_d and a_b measure how light dissipates with water depth, which will depend on the turbidity of the water, increasing with dissolved organic matter, suspended particulate matter and live organic matter (e.g. Devlin et al. 2009). As such, these parameters vary seasonally and over space (e.g. Capuzzo et al. 2013) and may also show temporal trends (Capuzzo et al. 2015; Dupont and Aksnes 2013). As there was not sufficient information to incorporate this variability, constant values were assumed. The choice of a_d was based on observations from hydrodynamic regions corresponding to sandeel habitat (see supplementary materials in Capuzzo et al. 2018). A value of around 0.1 seemed to be representative of the long-term average and was assumed for the parameter a_d here. For the beam attenuation coefficient, a_b , this can be approximated by a linear relationship with a_d ($a_b = 5a_d - 0.08$, Shannon 1975, applicable for $0.11 \leq a_b \leq 1.6$). The impact of the choice of a_d (and associated changes in a_b) as well as cloud cover on model predictions was investigated for a range of values (Section 4.2.7).

4.2.1.1 Location-specific input

To be able to compare model output with empirical data, the model was run in six locations (see Figure 4.1) where prior knowledge of sandeel growth is available. This included Dogger Bank (54.7°N 1.5°E) in the central-western North Sea (roughly location of North-West Rough, see Boulcott et al. 2007; Rindorf et al. 2016), Firth of Forth (56.3°N 2°W) in the north-western North Sea (roughly the location of Wee Bankie, see Greenstreet et al. 2006), East Central Grounds (ECG, 57.6°N 4°E) in the north-eastern North Sea (based on location in Bergstad et al. 2002, see also Johannessen and Johnsen 2015), Shetland (59.8°N 1.3°W), north of mainland UK (slightly south of an aggregation of sandeel grounds in southern Shetland, Wright and Bailey 1993), southern Faroes (59.8°N 6.8°W, towards the southern end of the Faroe shelf, where sandeel densities are high, Jacobsen et al. 2019) and southern Iceland (63.3°N 20°W, close to the sandeel grounds corresponding to sample site 3 in Lilliendahl et al. 2013).

The CPR data were, as described in Chapter 2, aggregated over a 135 km radius circle centred on each study location to generate the prey fields. However, as samples were scarce around the Faroes and Iceland, this radius was increased to 207 km for the Faroes, and 244 km for Iceland (see Figure 4.1). These cut-offs were obtained by incrementally increasing the distance until at least 10 years of prey fields could be generated. Plankton dynamics are still expected to show at least weak positive correlations over these scales (Defriez et al. 2016) but the larger radii do introduce additional uncertainty. For temperature, data from the grid-point closest to the location centre points were used. Day lengths and surface irradiance were generated based on the latitude of each location centre point. Again, a constant value of 0.1 was assumed for the diffusive attenuation coefficient a_d (Capuzzo et al. 2018) and a_b was calculated as $5a_d - 0.08$ (Shannon 1975).

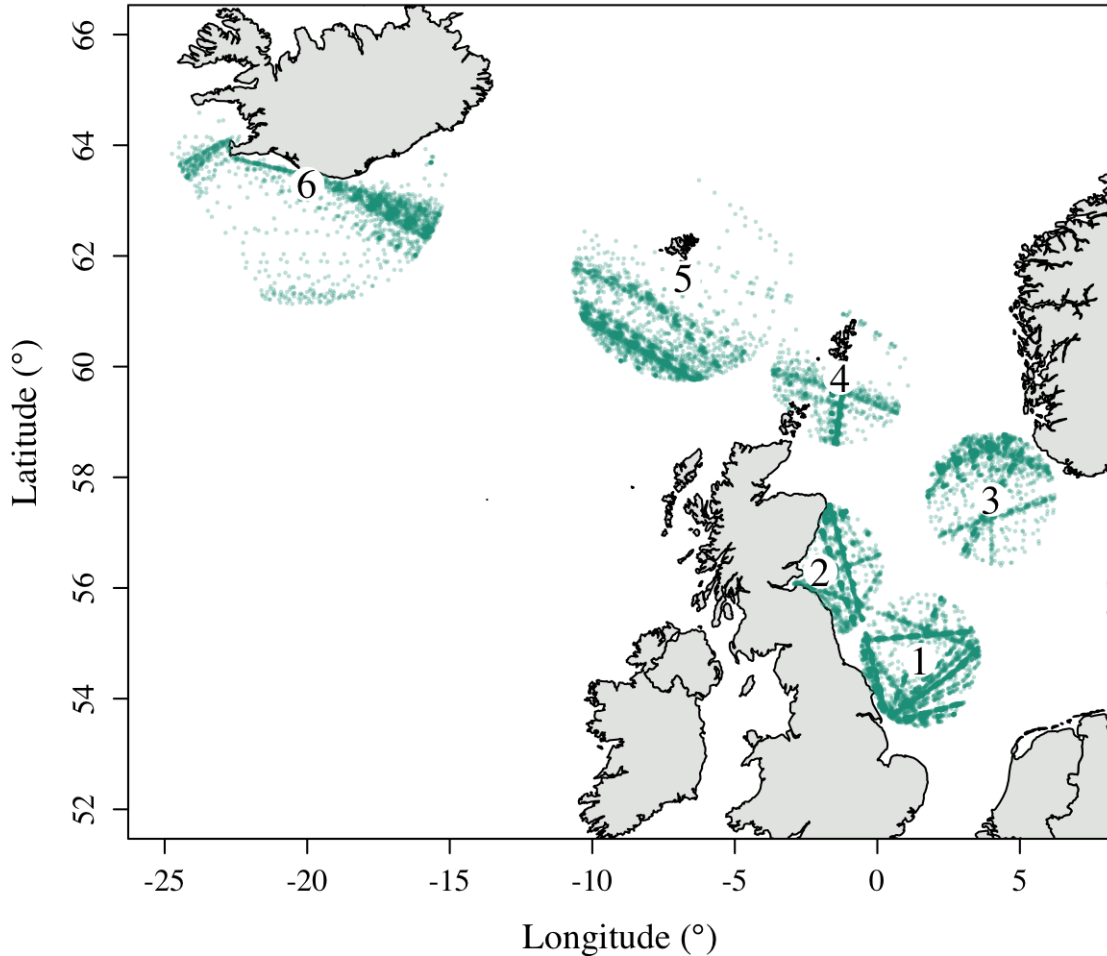


Figure 4.1: Model locations. 1 = Dogger Bank, 2 = Firth of Forth, 3 = East Central Grounds (ECG) 4 = Shetland, 5 = Faroes, 6 = southern Iceland. The CPR samples used to create prey fields for each modelling ground are also shown.

The total number of years with available input data varied between locations (Dogger Bank: $N = 33$, Firth of Forth: $N = 33$, ECG: $N = 23$, Shetland: $N = 36$, Faroes: $N = 10$, Iceland: $N = 10$). When the term ‘location-year’ is used in the following text it refers to a single year in a given location (with ‘location-years’ signifying all possible combinations).

4.2.2 Initial conditions

The starting conditions of the model include the day of year at metamorphosis and size at metamorphosis. Based on studies from a range of locations, length at metamorphosis varies between 35 to 55 mm, with all studies including the length 40 mm (Jensen 2000; Régnier et al. 2017; Wright and Bailey 1996), which is what was used as the starting length here. Based on this length, the structural energy S can be calculated (see Section 3.3.4). For R , as there is no information on weight at metamorphosis, it was assumed that the relationship between S and $R + S$ follows that in Figure 3.7, and R was calculated based on this. The estimated timing of metamorphosis shows large variation between years, but range from beginning of

May (Régnier et al. 2017) to the end of June (Jensen 2000). For the model start date, day 141 (21 May in a regular year, referred to as day_{MM} from hereon) was chosen as this has been observed as the median date of metamorphosis in 2 out of 3 years in Shetland (Wright and Bailey 1996), is close to the average estimated metamorphosis date for the Firth of Forth (133, Régnier et al. 2017), and is within the range of metamorphosis dates observed in the north-east North Sea (Jensen 2000). However, it should be noted that the range of metamorphosis dates is large and while there does not seem to be any marked systematic spatial difference between the separate sandeel stock assessment areas to which Dogger Bank, the Firth of Forth, the ECG and Shetland belong (Lynam et al. 2013), it is unclear whether this is the case for the Faroes and Iceland. To quantify the impact of starting conditions on predicted growth, a sensitivity analysis was conducted (see Section 4.3.3.3).

4.2.3 Sandeel data

Observational datasets exist for comparison with model predictions of length for all locations described in Section 4.2.1.1. Length measurements have been collected by the ICES Herring Assessment Working Group during dredge surveys in December, when the sandeels are overwintering, in Dogger Bank (2004–2019) and the ECG (2006–2019). These lengths are thus representative of the length at which the sandeels initiated overwintering, potentially modified by some size-selective mortality. In the Firth of Forth, lengths have been measured on 0 group sandeels brought back by Atlantic puffins (*Fratercula arctica*, hereafter ‘puffin’) to the colony on the Isle of May in the north-western North Sea (see Wanless et al. 2018). The dataset covers the years 1975 to 2015. The lengths are all standardised to 1 July, and they correspond well with simultaneous estimates from sandeel survey data when available (Wanless et al. 2004). In Shetland, a targeted survey covering three years (1990–1992) was conducted which estimated the age and length of 0 group sandeels in June (see Wright and Bailey 1996). Further, the length of 0 group sandeels has been measured in the Faroes in the second half of June at a range of stations around the Faroe Shelf (see e.g. Jacobsen et al. 2019, for details). This dataset covers the time period 1983 to 2018. Finally, a time series covering the years 2006 to 2017 (excluding 2014 and 2015) from southern Iceland was also obtained, where length was measured in mid-July in most years.

4.2.4 Tuning of handling time and capture success

Three of the DEB model parameters were manually tuned as there were no previous studies or data that could be used to inform these parameters. These parameters included effective handling time (again, not only the time it takes for the sandeel to capture and ingest a given prey, but a general limitation on sandeel ingestion rate, see Equation 3.5) and the parameters controlling the sigmoidal decline of capture success with increasing prey size (b controls the steepness of the decline whereas m controls the point at which the decline occurs, see Equation 3.12).

Capture success was tuned first. To obtain a baseline value to use while tuning capture success, effective handling time was first roughly tuned to achieve a realistic range of predicted sizes (it is tuned more finely below). The baseline values for b and m were obtained from Pepin et al. (1987), and are based on the estimated relationship between the prey/predator size ratio and capture success of fish larvae for a range of predators. b and m were then tuned against the observed ratio of the average prey size in sandeel guts and the average prey size in the water column, which was calculated to be 1.12 based on values reported from simultaneous sandeel stomach sampling and zooplankton sampling (Godiksen et al. 2006). It is possible that this ratio may vary depending on prey types present, but this estimate may still serve as a guideline for achieving a realistic size distribution of ingested prey. For each model location-year with sufficient data, the ratio of average size of ingested prey predicted by the model and the average size of prey available was calculated for each day and the total average over the whole season ($day_{MM}-day_{OW}$) was compared to the value calculated from Godiksen et al. (2006). The default value of b appeared to work well, so m was tuned by sequential decrease until a good agreement between the predicted and observed size ratios was achieved. Based on the size distribution of copepods eaten by Dogger Bank sandeels between day 123 and day 165 reported by van Deurs et al. (2013), the ingested copepods had an average size of 1 mm, and 24% of copepods ingested were >1.3 mm. Using the tuned parameters, the average prey size ingested in Dogger Bank between day_{MM} and day 165 was predicted to be 0.94 mm, and 11% of the prey ingested were >1.3 mm copepods. Considering that the model also covers non-copepod prey and that the modelling period only covers the later part of the date range for which copepod size data were reported, it seems as if the model predicts a plausible diet size composition. The final value of b was 5.095 (again, from Pepin et al. 1987, with the uncertainty range based on reported standard errors: 4.075, 6.115) and the final value of m was -1.9, where the uncertainty interval was based on a range of values that still provided plausible predictions (-2 to -1.8).

Once the final capture success parameters were established, effective handling time was tuned to the Firth of Forth time series on length (see Section 4.2.3). This time series was chosen as the Firth of Forth is a well sampled area in terms of CPR data and the time series covers the full series of model predictions. It should be noted that tuning effective handling time to this time series does not affect the predicted temporal trend or predicted relative differences in sandeel length between locations, only the absolute length. This resulted in a final effective handling time of 50 seconds. Again, the effective handling time also incorporates the fact that the sandeels are not always able to feed actively and most of the time exposed to below average abundances. This is why this is considerably longer than the time it takes to capture and ingest a prey in laboratory conditions (around one second, Christensen 2010; Winslade 1974b). The ratio of ingested prey to available prey was again assessed to confirm that it still agreed with the ratio calculated based on values reported by Godiksen et al. (2006). The uncertainty interval was based on a range that still provided plausible predictions (40–60 seconds).

4.2.5 Spatio-temporal variation in 0 group growth

4.2.5.1 Comparison between observations and predictions

Next, the model was used to hindcast growth for the locations depicted in Figure 4.1: Dogger Bank, the Firth of Forth, the ECG, Shetland, the Faroes and southern Iceland. First, predictions of length were made that aligned with the observational datasets described in Section 4.2.3, so that the ability of the model to predict observed patterns could be established. The Shetland comparison was conducted in a slightly different way and is described below. For the other locations, predictions were produced for dates that aligned with dates of measurements for the observational datasets (Dogger Bank = day_{OW} , Firth of Forth = day 182, ECG = day_{OW} , Faroes = day 174, in Iceland this varied between years and predictions were adjusted accordingly). For Dogger Bank and the ECG, the observational dataset refers to data collected during overwintering in December, meaning that the measured lengths correspond roughly to the length at which overwintering is initiated. Predictions were thus made for day_{OW} , but it should be remembered that timing of overwintering initiation is uncertain and may vary between years (MacDonald 2017; Reeves 1994). When comparing the predicted and measured lengths for each location, only the range of years from the first year in which both predictions and measurements were available to the last year both predictions and measurements were available were considered (except for in Iceland where the full observational dataset was considered due to its short length).

The agreement of predictions and measurements were not considered on a year-by-year basis. As the prey fields used as input contain substantial variability and uncertainty when considered over shorter time scales (see discussions in Chapter 2), and the day of metamorphosis may also vary between years, there is too much uncertainty to expect agreement within a given year, even if the model would be able to correctly predict growth given accurate input. Instead, the agreement of averages and long-term trends was considered. This was done by comparing the 95% confidence intervals for calculated averages for model predictions and observations for each location, as well as the 95% confidence intervals for estimated slopes for linear models using year as an explanatory variables. Linear models were judged to be adequate based on the generally short time series examined as well as linear trend being previously reported in the observational data (Wanless et al. 2018). The presence of nonlinear patterns was still assessed by examining the model residuals.

In Shetland, where length estimates for a range of ages within a given year were available (see Fig. 4 in Wright and Bailey 1996), predictions were instead made for the full range of ages within each survey year. Ages are counted from the day of hatching, so to translate the day of year (which is what the predictions are made for) into age, the average date of hatching for each year was subtracted from each year day. Further, as estimates of timing of metamorphosis were available from the surveys, the model was run using these dates as the starting condition (however, only in 1992 when the median calendar day of metamorphosis was 147 did this differ from day_{MM}). Here, the agreement between model predictions and observations was assessed by calculating the number of observations falling above versus below the predicted line.

4.2.5.2 Spatio-temporal variation in predictions

Following this, the model was run in all location-years where sufficient input data were available. As 1979 was the first year where all types of input data were available, this was the first year predictions were made for. Growth curves were produced for each year, but spatio-temporal patterns in length were also explored in more detail based on predictions for specific days. This included dates corresponding to peak energy demand of some seabird species which have a high proportion of 0 group sandeels in their diet (see Wanless et al. 2018): razorbills (*Alca torda*), puffins and black-legged kittiwakes (*Rissa tridactyla*). Peak energy demand in razorbills and puffins generally occur in the second half of June (day 172, Burthe et al. 2012, hereafter day_{SB1}) and in the first half of July for black-legged kittiwakes (day 189, Burthe et al. 2012, hereafter day_{SB2}). In addition, length on day_{OW} was also examined. This corresponds roughly with the start of overwintering (MacDonald 2017; van Deurs et al. 2011a). Further, the decision whether to invest in reproduction, which is size-dependent (Bergstad et al. 2001; Boulcott et al. 2007), also takes place around this time of the year (Boulcott and Wright 2008). To examine variation over time and between locations, generalised additive models (GAMs) were used, including year as a smoothing term and location as a factor, with an interaction between the trend and the location. GAMs were chosen based on an initial examination of predicted lengths which indicated nonlinear trends in some locations. GAMs were fitted using the function *gam* in the R-package *mgcv* (Wood 2011). The models were fitted with an identity link function, using generalised cross-validation to estimate the smoothing parameter. The adequacy of the smooths were assessed by checking for patterns in the residuals using the function *gam.check*. The full model was compared to its simpler sub-models using AIC_C (Hurvich and Tsai 1989). Models with a maximum ΔAIC_C of 2 were considered to best represent the examined relationship, and if several models had ΔAIC_C values of less than 2, the simplest model was considered to be the most representative, based on the principle of parsimony (Burnham and Anderson 2002). Location-specific smooths were evaluated using p-values, based on a confidence level of 0.05.

4.2.6 Parameter sensitivity analysis

Then, the response of predicted reserve energy R and structural energy S on day_{OW} to variation in parameter values was examined. The range of variation examined included both an increase/decrease in parameter values by 10%, which will indicate which model processes have a particularly large impact on predictions, and an increase/decrease as based on the uncertainty bounds presented in Table 3.1, which will indicate which parameters are the greatest sources of uncertainty through either natural variability or a lack of precise measurement. Only one parameter value was varied at a time with all other parameters kept at their nominal values. The responses of R and S (considered as percentage difference compared to baseline conditions for day_{OW}) were considered here as they are the model state variables and the relationships with some of the parameter values are therefore more straightforward. However, for the other sensitivity analyses in this and following sections, the percentage difference in length as compared to baseline conditions was considered, as the interpretation of this metric is more easily compared to observational data.

The parameter sensitivity analysis was complemented by an assessment of the impact of some of the structural choices made in the model. This included the assumption that sandeels do not feed when food is not present (with the alternative being that they feed each day, whatever the conditions), the assumption that the sandeels follow different allocation rules after a period of starvation (with the alternative being that allocation is always based on total current energy, disregarding the ratio between S and $R + S$), the assumption of optimal foraging (with the alternative being simultaneous feeding on all prey types) and the assumption that when feeding according to optimal foraging rules, large copepods belong to a different search class than small copepods and other small prey (see Section 3.3.1 for details of the default choices). One process was varied at a time, and all parameter values kept at their nominal values. Sensitivity was measured as predicted sandeel length on day_{OW} in relation to predicted length for baseline conditions.

Finally, uncertainty in model input may also introduce substantial error in predictions (Ney 1993). The sensitivity of model output to environmental conditions is examined in Section 4.2.7, but here, the sensitivity of model output to some of the parameter values used when developing the prey fields for the model (see Chapter 2) was examined, as these can also be considered model parameters. This included both the abundance correction factors used (Table 2.3) and the prey trait values, including size, prey image area and energy content (see Table 2.4). In reality, these components vary together, but here the other values were kept at their nominal values as the main purpose was to examine the impact of the choice of value, rather than biological variation. Sensitivity was measured as predicted sandeel length on day_{OW} in relation to predicted length for baseline conditions.

For all sensitivity analyses, all location-years with enough input data were considered. This approach was chosen over one based on a baseline standardised input scenario to get an idea of how sensitivities vary depending on input (for example, the sensitivity to parameters related to digestion rate may depend on the abundance of food, as the sandeels are more likely to be limited by gut space when food is abundant). Similarly, the sensitivity to parameter values/structural choices may depend on the value of other parameters (for example, if digestion rates are slow, the sensitivity to parameters controlling encounter rate may be lower as the sandeels are likely to be gut space-limited). However, it was outside the scope of this chapter to extend the sensitivity analysis to a global analysis.

4.2.7 Drivers of variation in growth

Finally, drivers of variation in sandeel length were explored. This included three components: (1) comparing the length predicted for each location-year with the corresponding environmental input, (2) varying environmental drivers in isolation while keeping the remaining drivers constant to explore the impact on predicted length and finally, (3) examining the impact of varying size at metamorphosis and timing of metamorphosis on predicted length.

4.2.7.1 Environmental input versus predicted length

To explore what has driven the observed variation in sandeel length, the relationship between predicted length on day_{OW} and model input was examined across years for each location. Several input variables were explored: average daily abundance of each prey type (individuals m^{-3}), total daily energy available ($kJ\ m^{-3}$), average daily abundance of small copepods (*Acartia* spp., *Oithona* spp., *Para-Pseudocalanus* spp. and *Temora longicornis*, individuals m^{-3}) and average square root of the image area (mm), thus aligning with the variables examined in Chapter 2. Average daily temperature ($^{\circ}C$) was also included. All variables were averaged over the feeding season (day_{MM} to day_{OW}). Light conditions were not considered as they were kept constant across years in a given location. Note that this analysis was based on the full set of the input as is, so that when estimating the effect of a given variable, the values of the other variables are not controlled for. Linear models of both untransformed and \log_{10} -transformed data were fitted, as it might be expected that growth rates show a saturated relationship with food availability. A confidence level of 0.05 was used to determine whether relationships were present or not. If both linear and log-linear relationships had $p < 0.05$, the model with the highest R^2 was considered to be the most representative model.

4.2.7.2 Environmental driver sensitivity analysis

Then, the sensitivity of length predictions to individual environmental drivers was investigated, quantified as the percentage difference in length on day_{OW} as compared to the baseline scenario. To do this, the model was run for the same location-years as above, varying one driver at a time while keeping the remaining input constant. Through this approach, the effect of drivers can be isolated, but it also provides an idea of how much the impact can vary depending on other environmental conditions. In each case, the impact of the driver was explored over the range of values previously observed in the dataset and/or projected future variation in the variable. Seven drivers were explored: average total daily energy available, prey size composition, prey phenology, the relative proportion of *C. finmarchicus* and *C. helgolandicus*, temperature, turbidity and cloud cover.

For total energy in available prey ($kJ\ m^{-3}$, the energy content of each prey type multiplied by abundance and added together), this was calculated as daily averages over the feeding season and explored over the range from the lowest ($0.4\ kJ\ m^{-3}$) to highest ($10\ kJ\ m^{-3}$) values observed in the dataset (mean value in dataset = $2.8\ kJ\ m^{-3}$). Then, to examine the impact of the size distribution of the prey field, the effect of changing the relative proportion of small prey types (small copepods and other small prey types, equivalent to search class A as described in Section 4.2.1) to large prey types (large copepods, crustaceans and fish larvae, equivalent to search classes B and C as described in Section 4.2.1) was explored. This was also done over the range of values observed in the dataset (23% small prey to 99% small prey, mean observed in the dataset = 92%). To examine the impact of phenological shifts, the simplified scenario that the whole prey field shifts in unison was considered here and the impact of advancements of up to 60 days was examined, which is within the range of change observed and expected in zooplankton (Richardson 2008).

The impact of the presently occurring shift from *C. finmarchicus* to *C. helgolandicus* on predicted growth was explored by examining the impact of shifting from a prey field completely dominated by *C. finmarchicus* to one completely dominated by *C. helgolandicus*. To isolate the impact of trait values and phenology, rather than abundance, the total abundance of *C. finmarchicus* and *C. helgolandicus* in a given year was kept constant, but the relative proportion was varied. First, the baseline phenology of each species in each location was determined by averaging the abundance for each day of the year over all years for which prey field data were available, producing a time series of daily values for each location. While phenology may vary between years, this approach still captures the key differences in phenology between the two species. Then, the time series of *C. helgolandicus* was adjusted so that, in each location, the daily mean as averaged over the whole year was the same for both species. The model was then run on the full range of relative proportions of the two species, keeping the total abundance constant. This was repeated for all location-years, where other environmental input was kept constant but abundances of *C. finmarchicus* and *C. helgolandicus* were replaced by those computed here. However, only Dogger Bank, the Firth of Forth, the ECG and Shetland were considered as abundances of *C. helgolandicus* are still so low in the Faroes and Iceland that no adequate baseline phenology could be established.

To examine the impact of temperature, a baseline temperature climatology was established by averaging the temperature for each day based on all location-years. A range of temperature conditions were then examined by adjusting this baseline climatology, from subtracting 3°C (corresponding roughly to coldest year in dataset) to adding 4.5°C (corresponding to the upper limit of climate-change driven temperature increase by the end of the century, Schrum et al. 2016). Finally, to examine the impact of variation in light conditions, a_d (which is a function of turbidity and also affects beam attenuation a_b) was varied over the range 0 (completely clear waters) to 0.3, based on a range of values commonly observed in the hydrodynamic regions corresponding to sandeel habitat (see supplementary materials in Capuzzo et al. 2018). Cloud cover was varied over a range of $\pm 20\%$ based on the maximum projected changes as a result of climate change (May et al. 2016). To examine the impact latitudinal differences in light might have on growth, the model was run using all location-years with sufficient input but varying light conditions as a function of latitude as based on the range of latitudes from the lowest-latitude site (Dogger Bank) to the highest-latitude site (southern Iceland).

4.2.7.3 Timing of metamorphosis and size at metamorphosis

To assess the impact of pre-metamorphic processes on predicted size (quantified as percentage difference in length at day_{OW} compared to the baseline scenario), the impact of date of metamorphosis and size at metamorphosis was examined. The model was run for all location-years for which input data were available and the model start date (date of metamorphosis) was varied from 121 to 181 and the initial size (length at metamorphosis) was varied from 3.5 to 5.5 cm as based on observed ranges (see Section 4.2.1).

4.3 Results

4.3.1 Spatio-temporal variation in 0 group growth

4.3.1.1 Comparison between observations and predictions

The agreement of observational data on length and model predictions for corresponding dates were examined based on the overlap of the 95% confidence intervals of the estimated means and slopes in all locations apart from Shetland (Figure 4.2, Table 4.1). In Dogger Bank, all model predictions fell within the standard deviation of the length observations and the confidence intervals of the means overlapped. In terms of a temporal trend, there were indications of a similar negative trend in both the observed data and the model predictions, but in both cases the confidence intervals overlapped with zero. In the Firth of Forth, confidence intervals of the estimated means overlapped, and both the predicted and observed lengths showed negative trends, with the confidence intervals of the slope estimates overlapping. In the ECG, the confidence intervals of the means overlapped, although the estimated mean of predictions was 1.1 cm longer. There was no clear indication of a trend. In the Faroes and in Iceland, the predicted values were larger than the observed values, with no overlap in the confidence intervals of the means. There were no clear temporal trends in these two locations, apart from an indication of a negative trend in the observational data from the Faroes. Apart for one outlier (Firth of Forth 1991, Figure 4.2a), the inter-annual range of variation in observations and predictions were similar.

In Shetland, where several observations were available for each year, the magnitude of predictions aligned well (see Figure 4.2d) considering that model predictions are not expected to capture inter-annual variation in size. 22, 55 and 64% of observations were greater than predicted values for the same age in 1990, 1991 and 1992 respectively.

4.3.1.2 Spatio-temporal variation in predictions

Looking at the predicted growth curves, it is clear that these vary between locations (Figure 4.3). In addition to variation in the length on a given day (explored in more detail below), it seems that while length in some locations generally increases throughout the season (Firth of Forth, Dogger Bank), in others it shows signs of levelling off (the ECG and Shetland) whereas in others it levels off completely (the Faroes and Iceland). However, this varied between years. Notable is also that while some locations showed considerable inter-annual variation (in particular Iceland and the ECG), others were more consistent (in particular Dogger Bank). Finally, unlike the other locations, the Firth of Forth was predicted to show very poor growth in a few years, with the predicted length staying at the initial length at metamorphosis for around a month. These growth rates are not realistic, as the sandeels likely would have died of starvation. Only one of the three years with predicted poor growth aligned with observed small sizes (Figure 4.2).

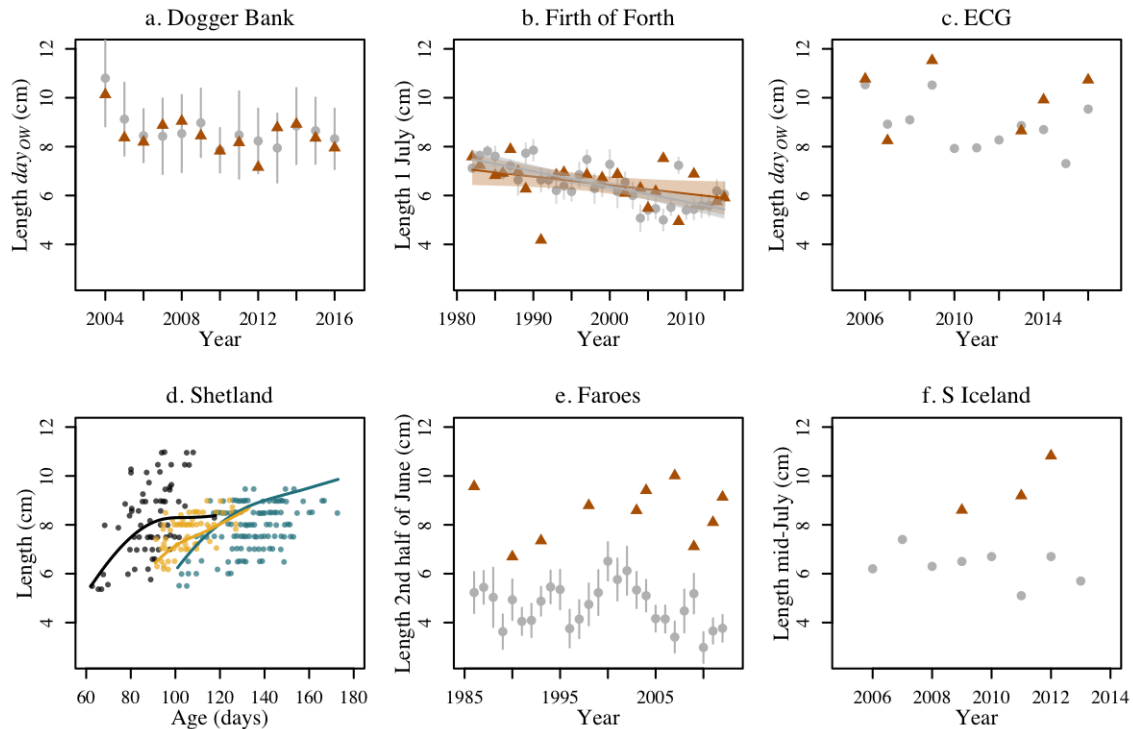


Figure 4.2: For (a)(b)(c)(e)(f) markers show model predictions (red triangles) and corresponding observations (grey circles, with standard deviations indicated by error bars where these were available from the dataset). Predictions were made for days corresponding to dates of observations (see Section 4.2.5) which vary between locations. For the Firth of Forth (b), the only location where the 95% confidence interval of the estimated trend did not overlap with zero, lines show linear trends, with shaded 95% confidence intervals. For (d) (Shetland), markers show observed length for a given age (counted since hatching), and lines show corresponding predictions for 1990 (blue), 1991 (black) and 1992 (yellow). Note the different x-axis for (d).

In terms of predictions of lengths for given days - day_{OW} (roughly the day of overwintering), day_{SB1} (peak chick energy demand razorbills and puffins) and day_{SB2} (peak chick energy demand black-legged kittiwakes) - the GAM with the lowest AIC_C included location and location-specific smoothing terms in all cases (for all other models $\Delta AIC_C > 2$). In terms of spatial differences, the Firth of Forth sandeels were the smallest in all cases (p all < 0.01). Further, while Dogger Bank sandeels were bigger than the Firth of Forth sandeels, they were smaller than the sandeels in all other locations (p all < 0.02).

For the remaining locations, patterns were more muddled. Sandeels at the ECG were indistinguishable from the Faroese sandeels (p all > 0.8). Generally, the Icelandic sandeels were smaller than the ECG sandeels (p all < 0.02 apart from length at day_{OW} when $p = 0.06$), and Shetland and ECG sandeels were indistinguishable (p all > 0.06). There was no difference between Shetland and Iceland (p all > 0.13) apart from on day_{SB1} ($p = 0.047$), when the Icelandic sandeels were smaller. Faroese sandeels were indistinguishable from Shetland sandeels (p all > 0.22). Finally, Ice-

Table 4.1: Comparison between observational data and corresponding predicted lengths, including estimated slopes (mm year⁻¹) with associated confidence intervals, and estimated means with associated confidence intervals.

Location	Observed slope (95% CI)	Predicted slope (95% CI)	Observed mean (95% CI)	Predicted mean (95% CI)
Dogger Bank	-0.10 (-0.21; 0.01)	-0.08 (-0.19; 0.03)	8.7 (8.3; 9.1)	8.5 (8.1; 8.9)
Firth of Forth	-0.06 (-0.08; -0.04)	-0.03 (-0.07; 0.00)	6.5 (6.2; 6.7)	6.5 (6.1; 6.9)
ECG	-0.14 (-0.35; 0.07)	0.01 (-0.43; 0.45)	8.9 (8.3; 9.5)	10.0 (8.9; 11.0)
Faroes	-0.03 (-0.07; 0.01)	0.02 (-0.07; 0.12)	4.7 (4.4; 5.0)	8.5 (7.8; 9.2)
S Iceland	-0.12 (-0.38; 0.13)	0.68 (-3.52; 4.88)	6.3 (5.8; 6.8)	9.5 (8.2; 10.8)

landic sandeels were generally smaller than Faroese sandeels early in the season (day_{SB1} , $p = 0.03$), but this pattern did not last as the season went on (day_{SB2} : $p = 0.06$, day_{OW} : $p = 0.16$).

It was also clear that temporal trends differed between locations (see Figure 4.4 for trends based on day_{OW}). Regardless of day considered, there were no clear trends in Dogger Bank, the ECG or the Faroes (p all > 0.21). Firth of Forth showed linear declines when considering day_{SB1} ($p = 0.01$, 0.4 mm per year) and day_{SB2} ($p = 0.03$, 0.4 mm per year), but this effect was not present by day_{OW} ($p = 0.13$). Shetland instead seemed to show an increase in all cases (p all < 0.02), which appeared to be nonlinear, with a shift towards higher values in around 2000. Finally, Iceland also seemed to show a nonlinear pattern, present in all cases (p all < 0.01). However, the nonlinearity was to a large extent driven by the first data point, which was followed by an overall increase.

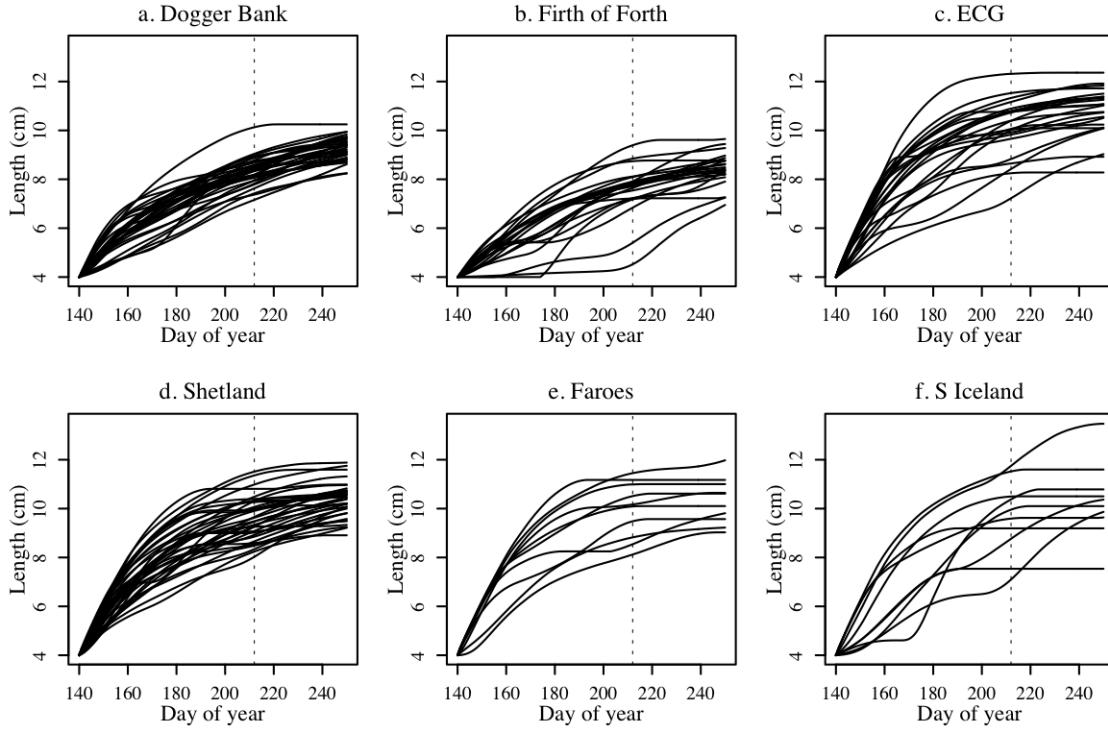


Figure 4.3: Predicted length for each day from metamorphosis (day_{MM}) until the end of the model run (mid-September, day 250) for each location-year with sufficient input data. day_{OW} (beginning of August, approximate day of overwintering) is marked with a vertical dashed line. Each line represents a different year for which predictions were made.

4.3.2 Parameter sensitivity analysis

The sensitivity of predicted S and R to variation in parameter values was examined over both $\pm 10\%$ of the nominal value and the defined uncertainty ranges (Table 3.1) (see Figure 4.5). When considering the impact of increasing/decreasing parameter values by 10%, it was clear that model output was more sensitive to parameters relating to maximum intake rate i_{max} (in particular m , which controls at what prey size capture success declines), than parameters relating to the limitation introduced by limited gut space. Further, output was also sensitive to α_ϵ , which controls assimilation efficiency. In terms of metabolic costs, output was most sensitive to costs associated with swimming activity F , but in general, sensitivity was low to parameters related to metabolic costs as compared to parameters related to intake rate. Sensitivity was moderately high to α_{alloc} , which controls allocation to structural energy S . As expected, the effect was opposite when comparing S and R (as a larger value results in greater allocation to S). Finally, sensitivity to β_{dry} , which controls the relationship between length L and structural dry weight, was high.

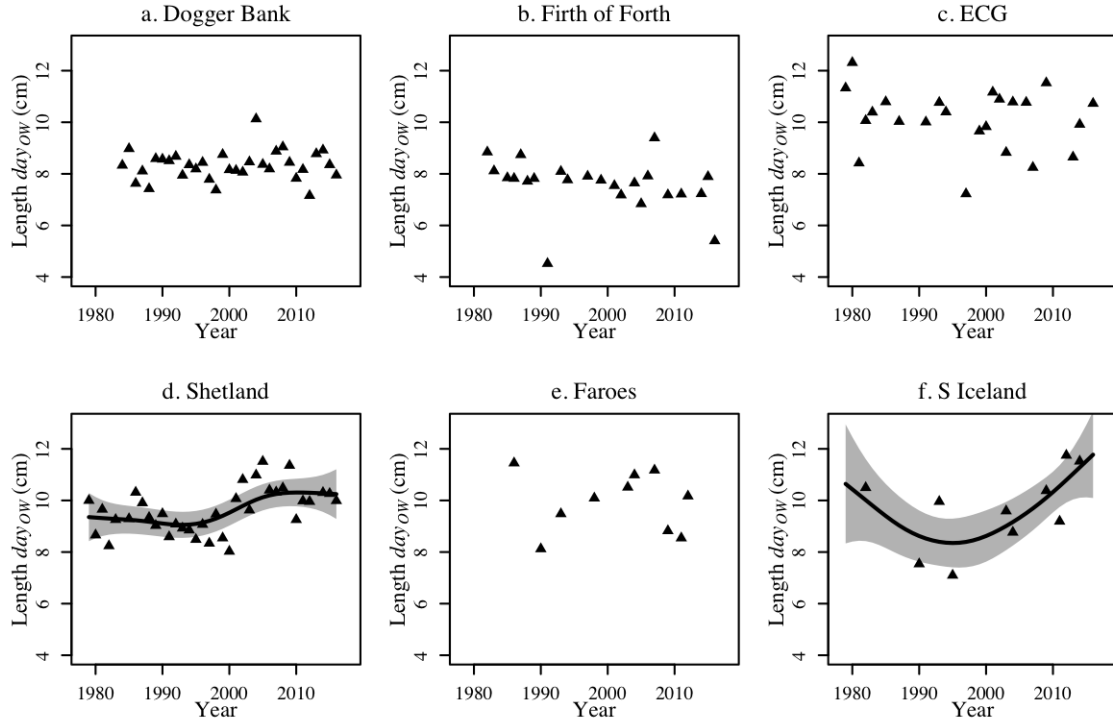


Figure 4.4: Predicted length on day_{ow} for all location-years where sufficient input data were available. Where present, full lines show GAM fits with associated 95% confidence intervals (only included if $p < 0.05$ for the location-specific smooth).

When considering the sensitivity of the output to parameter values when varied within a defined uncertainty range, results were generally similar, in particular for the parameters related to ingestion, although sensitivities to parameters related to i_{max} were generally greater, in particular in the case of speed v , feeding depth z and D_{frac} , which controls visual acuity. Further, ζ_{SDA} , the costs associated with processing food and synthesising tissue, introduced substantial uncertainty. Finally, within the given uncertainty interval, parameters associated with allocation and translation between length/weight and S/R did not introduce much uncertainty.

In general, the estimated sensitivity to the value of a given parameter varied depending on the input data. For example, the sensitivity to parameters related to digestion and gut size was generally low, but in some years (when food conditions were better), sensitivity was higher.

In terms of the structural differences that were tested, the assumption of the sandeels not feeding when food was not present had a very small impact, only resulting in different predicted lengths in 4% of location-years, with a maximum reduction of 1% when assuming that the sandeels feed each day. Assuming the same allocation rules following a period of starvation resulted in a mean increase in length of 7% (ranging from 2 to 11%). In terms of the assumption of optimal foraging, the impact of non-selective feeding ranged from a 28% decrease to a 29% increase (mean = 1% decrease). Results for considering search classes A and B as a single search class were similar, ranging from a 28% decrease to a 28% increase (mean = 2% decrease).

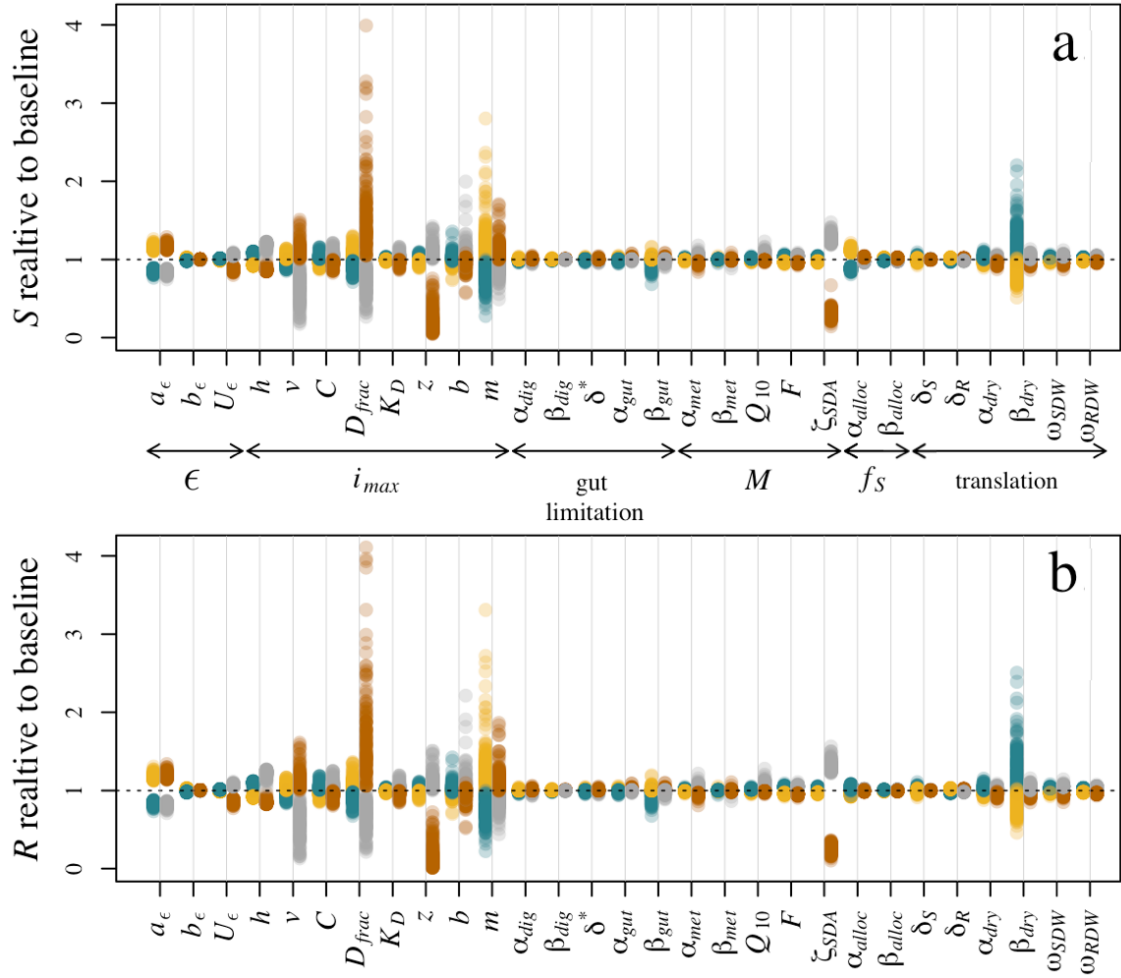


Figure 4.5: Parameter sensitivity analysis based on 10% decrease (blue markers) and increase (yellow markers), as well as the defined lower (grey markers) and upper (red markers) uncertainty boundaries, with each point representing a different location-year. y-axis shows predicted structural energy S (a) and reserve energy R (b) on day_{OW} in proportion to the baseline scenario of all parameters at their nominal value. For the meaning of each parameter, see Table 3.1. The general process each parameter belongs to is indicated under (a), where ϵ is assimilation efficiency, i_{max} is maximum intake rate with no gut space limitation (which is instead covered by ‘gut limitation’), M are metabolic costs, f_s is the allocation of net assimilated energy to S and translation refers to the set of parameters governing the relationship between S/R and L/W .

In terms of the sensitivity of the output to CPR parameters, the impact of varying correction factors and prey image area (which both determine encounter rates) produced very similar results, with predicted lengths being particularly sensitive to variation in parameter values for *Acartia* spp., *C. finmarchicus*, *Calanus* I–IV, Decapoda larvae and *Podon* spp. (see Figure B.1 in Appendix B, only correction factors shown due to high similarity). Still, on average, the effect was less than 1% difference even for these taxa. Generally, the impact of increasing the parameter values was positive, but this was not always the case (see *Evadne* and *Oithona* spp. in particular). The impact of varying individual energy content was also similar (see Figure B.2 in Appendix B), although here the effect of an increase was always pos-

itive, apart from in the case of Euphausiacea. Again, even for the taxa showing the strongest response, this was on average generally less than 1%. Finally, in terms of size, the impact of an increase in size was generally negative, although in the case of Euphausiacea, it had a positive effect (see Figure B.3 in Appendix B). Once again, even the strongest responses were on the order of 1%.

4.3.3 Drivers of variation in growth

4.3.3.1 Environmental input versus predicted length

The relationships between environmental input and predicted length on day_{OW} varied between locations (Figure 4.6, Table B.2 in Appendix B). It was clear that no single variable explained the predicted variation in length fully. One of the most prominent patterns that emerged was a positive relationship with *Calanus* spp. Positive relationships were found between *C. finmarchicus* and predicted length in the ECG ($R^2 = 0.47$), Shetland ($R^2 = 0.42$), the Faroes ($R^2 = 0.89$) and Iceland ($R^2 = 0.69$), whereas positive relationships were identified between *C. helgolandicus* and predicted length in Dogger Bank ($R^2 = 0.27$) and Shetland ($R^2 = 0.51$). Further, positive relationships were identified between *Calanus* I–IV and predicted length in all locations (Dogger Bank $R^2 = 0.45$; Firth of Forth $R^2 = 0.35$; ECG $R^2 = 0.76$; Shetland $R^2 = 0.39$; Faroes $R^2 = 0.69$; Iceland $R^2 = 0.45$). In addition, several prey types showed positive relationships with predicted length in some locations (e.g. *Acartia* spp. in the Firth of Forth, $R^2 = 0.47$). In terms of the composite prey metrics, positive relationships were identified between total energy and predicted length in the ECG ($R^2 = 0.45$), Shetland ($R^2 = 0.38$) and the Faroes ($R^2 = 0.42$), and between abundance of small copepods and predicted length in the Firth of Forth ($R^2 = 0.41$) and Shetland ($R^2 = 0.24$). There were positive relationships with the average square root of the prey image area in Dogger Bank ($R^2 = 0.19$), the ECG ($R^2 = 0.14$) and Iceland ($R^2 = 0.37$) but a negative relationship in the Firth of Forth ($R^2 = 0.22$). Finally, a positive relationship between temperature and predicted length was identified in Shetland ($R^2 = 0.24$).

4.3.3.2 Environmental driver sensitivity analysis

The impact of the drivers examined varied over the ranges explored, and the effect tended to depend on the values of other environmental input (Figure 4.7, see also Table 4.2). The sensitivity to total energy was high, with a reduction to lowest values in the range examined resulting in a reduction of on average 26% and an increase resulting in an increase in length of on average 21%. Sensitivity to the proportion of small prey in the prey field was also high, resulting in an 11% increase in length at the smallest observed prey size ratios and a decrease of on average 1% at the largest observed ratios (most location-years had large observed ratios initially). In terms of a shift in phenology, on average across all location-years, a shift of 60 days did not result in any clear difference in projected size, but it was clear that the effect varied strongly between location-years. For example, in the Firth of Forth, a shift of 60 days resulted in on average 13% longer sandeels compared to the baseline, whereas the same shift for ECG sandeels resulted in 7% shorter sandeels. The effect of a

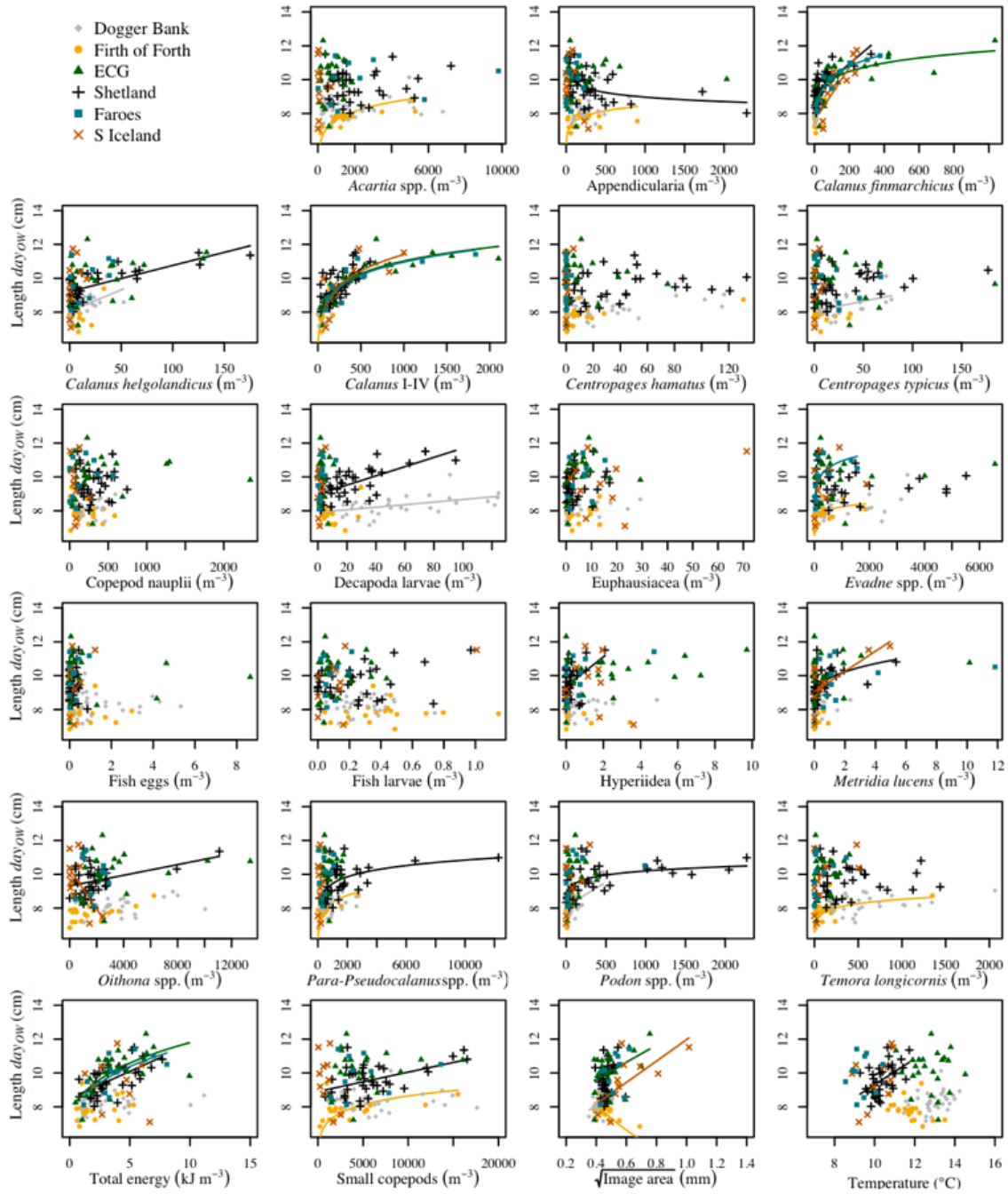


Figure 4.6: Average daily abundance of prey types (individuals m^{-3}), average total daily energy ($kJ m^{-3}$), average daily abundance of small copepods (*Acartia* spp., *Oithona* spp., *Para-Pseudocalanus* spp. and *Temora longicornis*, individuals m^{-3}), average square root of the image area (mm) and average daily temperature ($^{\circ}C$) against predicted growth for day_{OW} . Lines show model predictions of linear or log-linear models.

shift from *C. finmarchicus* to *C. helgolandicus* varied depending on location. In the ECG, the shift resulted in a decrease in predicted length of up to 11% (mean = 3%), in Shetland, a decrease of up to 2% (mean = 1%), whereas in Dogger Bank and the Firth of Forth, the effect was close to zero.

The impact of a shift in temperature was generally smaller than that of the changes in the prey field examined. On average, a decrease in temperature (corresponding to the coldest year in the dataset) resulted in a decrease in predicted length of around 1%, whereas an increase had a close to zero effect. Again, the impact varied between location-years, with a negative effect of increased temperatures in location-years with low maximum intake rates (mainly Firth of Forth, decrease of down to 6%, average = 1% decrease) and positive effect of increased temperatures in location-years with high maximum intake rates (mainly the ECG, increase of up to 3%, average = 1% increase).

Finally, there was a negative effect of poorer light conditions on predicted length. The diffusive light attenuation coefficient a_d had a large impact on predicted length. On average, a decrease in turbidity to completely clear waters resulted in an increase in predicted lengths of on average 3%, whereas an increase resulted in a decrease of on average 54% for the maximum value examined. The levelling off of the curve suggests that at maximum turbidity, intake was reduced to zero at some point for all location-years in the time series. Years with poorer food conditions (again, mainly Firth of Forth) levelled off earlier (with the larger proportional length just being a result of length at no growth - 4 cm - being a larger proportion of predicted length at default values when maximum intake rate is low). In contrast, cloud cover did not have a large impact on predicted length, with a decrease having on average a close to zero effect, and an increase resulting in a decrease in predicted length of on average 1%. Finally, an increase in latitude from 54.7°N (Dogger Bank) to 63.3°N (S Iceland) resulted in an average increase in predicted length of around 4%.

4.3.3.3 Timing of metamorphosis and size at metamorphosis

The timing of metamorphosis had a larger impact on predicted length at day_{OW} than the size at metamorphosis (Figure 4.8). The earliest date of metamorphosis on average resulted in a 4–9% larger size while the latest date resulted in a 11–21% smaller size, depending on size at metamorphosis. The effect varied between location-years. Assuming a length of 4 cm, the effect of metamorphosing at the earliest date varied between 0–14% depending on input, whereas the effect of metamorphosing at the latest date varied between 1–48% depending on input. The average standard deviation as based on the full set of location-year combinations for a given combination of initial size and date was 4 percentage points, increasing to 8 percentage points for the latest metamorphosis and smallest sizes.

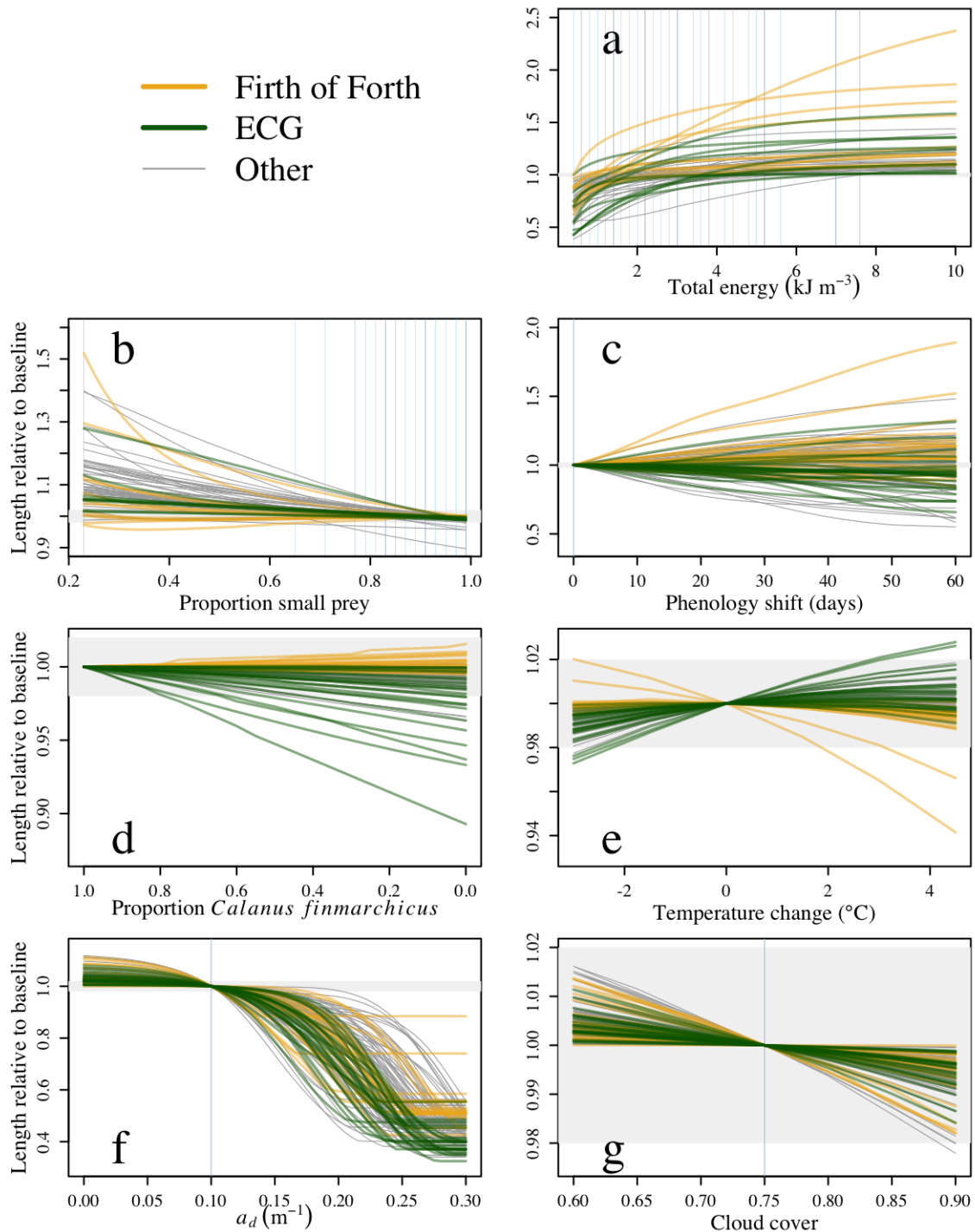


Figure 4.7: Impact on predicted length at day_{ow} relative to baseline conditions of variation in (a) average total daily energy (kJ m^{-3}), (b) proportion of prey field made up of small prey, (c) a shift in phenology (in days), (d) proportion of *C. finmarchicus* in relation to total abundance of *C. finmarchicus* and *C. helgolandicus*, (e) a shift in temperature ($^{\circ}\text{C}$), (f) a change in the diffusive attenuation coefficient a_d (m^{-1}) and (g) a change in cloud cover. Each line represent one location-year, ECG (generally high growth rates) and Firth of Forth (generally low growth rates) are colour-coded whereas others are plotted with thin grey lines to aid interpretation. Vertical blue lines denote nominal values (not included for proportion of *C. finmarchicus* and temperature as these were based on climatological baselines). As plots are on different scales, a grey shaded area covering the same range in each plot is included to give a sense of scale.

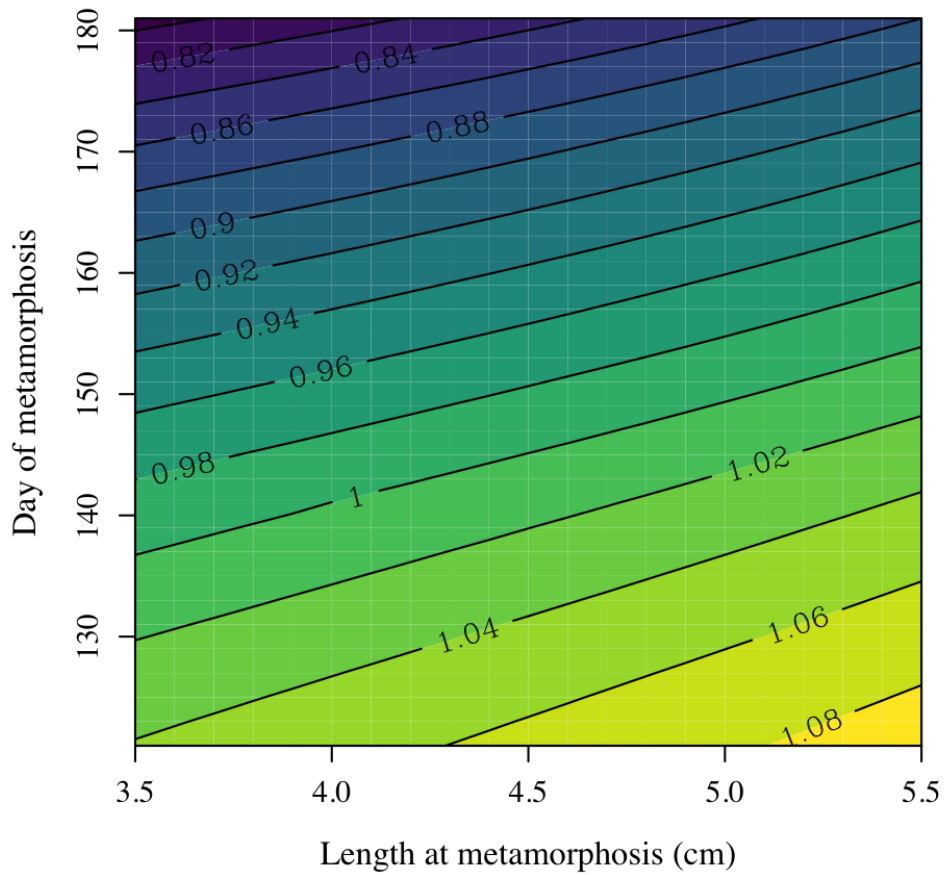


Figure 4.8: Sensitivity to initial conditions. Colours and contour lines indicate predicted length on day_{OW} , as depending on the day of metamorphosis (model start date) and length at metamorphosis (model initial size), in proportion to the length predicted for default values (default $day_{MM} = 141$, default length = 4 cm). Values are averaged over all location-year input combinations.

4.4 Discussion

In this chapter, the DEB model developed in Chapter 3 was used to explore drivers of variation in the growth of lesser sandeels, focusing on the impact of food conditions, temperature, light conditions as well as size at and timing of metamorphosis. Model predictions agreed well with empirical data showing a decline in length over time in the Firth of Forth, and within the North Sea, the predictions aligned in magnitude with observations in all locations. However, the agreement with observations further north was poorer. The model sensitivity analysis suggested that predictions were particularly sensitive to parameters and processes related to ingestion rate. Further, comparing predicted lengths with the environmental input used to drive the model suggested that *Calanus* spp. were important drivers of variation, where *C. helgolandicus* was more strongly related to predicted size further south whereas *C. finmarchicus* was more strongly related to predicted size in the north. The direct effect of temperature, which interacted with food conditions, was negligible. The most extreme increase in temperature considered resulted in a maximum difference in predicted length of 6%, but on average the effect was close to zero. In terms of light conditions, it did not seem as if latitudinal variation in light conditions had a large impact on growth, and neither did cloud cover. However, predictions were sensitive to turbidity, but since spatio-temporal variation in turbidity was not examined, it is not clear what role this played in the variation in growth. Finally, while the impact of size at metamorphosis was small, the impact of timing of metamorphosis was larger, with a shift towards the latest date previously observed resulting in a 19% decrease in length. This suggests that conditions both before and after metamorphosis contribute to observed variation in size at the end of the feeding season.

4.4.1 Agreement between predictions and observations

The extent to which predicted lengths agreed with observational data varied between locations (see Figure 4.2). In Dogger Bank, the Firth of Forth, the ECG and Shetland, predictions agreed well with the magnitude of observed lengths, and in the Firth of Forth the same long-term decline in length was also predicted. Further, in Dogger Bank, both the model predictions and the observational data showed hints of declines, although both of the confidence intervals overlapped with zero. In the more northerly locations of the Faroes and Iceland, the predicted lengths were greater than those observed. Further, in addition to the comparison with empirical data conducted in Section 4.3.1.1, the agreement of model predictions with previously published patterns is also generally good. In the North Sea, it has been observed in both 0 group sandeels (Boulcott et al. 2007) and 1+ group sandeels (Bergstad et al. 2002; Boulcott et al. 2007) that Firth of Forth sandeels are smaller than Dogger Bank sandeels, which in turn are smaller than ECG sandeels. This agrees with the differences found here (see Figure 4.4). Further, based on ICES data from the late 1970s, Bergstad et al. (2002) reported high growth rates in the northern North Sea (corresponding roughly to the ECG) as compared to Shetland, while 0 group sandeels in Shetland in the early 1990s (Wright and Bailey 1996) were larger than those in the Firth of Forth (Wanless et al. 2004). Both of these observations

agree with model predictions. In contrast, a longer term decline in length of 1+ group sandeels at Dogger Bank from the late 1980s to the early 2000s reported by van Deurs et al. (2014) was not visible in model predictions (Figure 4.4). However, it is not clear whether this observed trend, which was reported based on data from older age groups, is also present in 0 group sandeels. In the ECG, larger sizes were reported in the late 1970s as compared to the late 1990s (Bergstad et al. 2002), but due to the large variability in model predictions, and in observed values, it is hard to tell to what extent predictions and observations agree in this case. Further, the predicted increase in length around 2000 in Shetland (see Figure 4.4) does not agree with observations, where measurements of 0 group sandeels caught by puffins on Fair Isle (located south of Shetland) instead suggest a sustained decline in length from the late 1980s to 2010, and if anything, that sandeels were particularly small following 2000 (Harris and Wanless 2011).

There are several reasons for why predictions and observations might not agree. Again, while a generic date was used for timing of metamorphosis, in reality this will vary, and as can be seen from Figure 4.8, this will impact the size of the sandeels on a given date. Timing of metamorphosis varies between years (Jensen 2000; Régnier et al. 2017; Wright and Bailey 1996) and potentially also over space, as timing of larval occurrence varies spatially (Lynam et al. 2013). In the Faroes, sandeels that were measured in the second half of June were in several years close to lengths observed at metamorphosis (see Figure 4.2), suggesting that sandeels are metamorphosing later than the assumed date (second half of May), at least in some years. The sandeels in Iceland, which were measured a couple of weeks after those in Firth of Forth, were of a similar size to the Firth of Forth sandeels in spite of model predictions suggesting that food conditions are better in Iceland. This suggests that the Icelandic sandeels may also metamorphose relatively late.

Further, in terms of reasons for why the observations and predictions may differ, the predicted lengths in a sense represent potential growth of an average individual, whereas the observed sizes will be a full size distribution modified by size-selective mortality, which could be incurred by both fisheries and predators. Fisheries target all age groups, but catches of 0 group sandeels are usually low (ICES 2017; Rindorf et al. 2016). Further, a small mesh-size is used that will reduce selectivity (Rindorf et al. 2016) and observed variation in size has not been found to align with fishery pressure (Bergstad et al. 2002; Wanless et al. 2004). As such, fisheries are unlikely to have a large impact on observed variation in 0 group size. In terms of predation of post-metamorphic stages, Rindorf et al. (2016) argued that while size-dependent mortality might be expected, based on the spatial pattern of sandeel predators, this is unlikely to have caused the observed spatial patterns in size. As discussed in Section 3.4, it is also possible that the presence of predators could impact intake rates and energy expenditure. Increased predator pressure may result in the sandeels spending less time feeding (see van Deurs et al. 2010) or spend more time engaged in costly predator avoidance behaviour (see Pitcher and Wyche 1983), which would both contribute to reduced intake rates and subsequent growth. As sandeel predators are more abundant further north (ICES 2017), this could be another potential contributor to the disparity between observed and predicted length in the more northerly locations. In addition to predators, both intra-specific and inter-specific

competitors could potentially also affect growth rates. While Bergstad et al. (2002) suggested that high local densities may result in food competition, Eliassen (2013) identified a positive relationship between abundance and size and Rindorf et al. (2016) did not find a relationship between sandeel density and growth. This suggests that effects of density dependence are likely not large. Further, at least on greater temporal and spatial scales, the impact of competition from both conspecifics and other species may be partially reflected in the CPR data.

Some of the disparities between observed and modelled length will also be the result of how growth was modelled. The prey field input is one large source of uncertainty. Again, while long-term trends may be captured, the combination of the CPR sampling set-up and the patchiness of the zooplankton means that input on a given day is unlikely to be representative of actual conditions (see discussion in Chapter 2). The input is particularly uncertain in Iceland and the Faroes where CPR data were interpolated over a larger area due to scarce samples. These were also the locations in which model predictions and observations showed the poorest agreement. The sensitivity of the CPR to horizontal patchiness is likely to generate larger inter-annual variability in food conditions than what is actually observed, which may explain some of the outlier prediction years (e.g. Firth of Forth 1991, see Figure 4.4). The sensitivity to patchiness may also be behind the inability of the model to predict observed outlier years. For example, in 2004, the energy content of 9.5–10 cm sandeels in the Firth of Forth was only 26% of what it would normally be at that length (Wanless et al. 2005), but the model did not predict this year to be an outlier in terms of energy content, and there was nothing unusual in the input prey fields either. The model developed by MacDonald et al. (2018), which was also run in the Firth of Forth but using zooplankton data from a point-based sampling scheme with high temporal and taxonomic resolution, did not predict 2004 to be an outlier year either. As such, what might be behind the 2004 observations is still unclear.

Further, while the sensitivity analysis suggested that a 10% change in the correction factors applied to the CPR abundances only resulted in a maximum 4% change in predicted length at day_{OW} , the uncertainty in some of the correction factors is likely larger than this. Further, it is also possible that there could be some systematic variation, such as spatial variation in the diel vertical migration behaviour (see e.g. Beare and McKenzie 1999a). This would render the correction factors less appropriate in some areas and could potentially contribute to some of the discrepancies between predictions and observations. Further, it was assumed that prey trait values were constant within a given prey type over time and space, which is unlikely to be the case (e.g. Bottrell and Robins 1984), and as suggested by the results in this chapter, variation in the trait values chosen have a non-negligible impact on predicted growth. For example, if a 10% larger size would have been used for *C. finmarchicus* (which would still be a plausible size, see e.g. Campbell et al. 2001), this would have resulted in an up to 10% decrease in predicted length at day_{OW} .

The model structure and parameter choices will also have played a role in the deviation of model predictions from observations. The parameter sensitivity analysis suggested that predictions were highly sensitive to parameters governing maximum intake rate as a function of food conditions. Maximum intake rate is arguably the

most difficult process to model as a result of the lack of knowledge of how sandeels interact with prey in the field. For example, it is unclear at what speed *A. marinus* swim when foraging and how it may vary depending on prey type (see Christensen 2010), how much time they actually spend actively foraging (the long tuned effective handling time could suggest that they do not forage full time from sunrise to sunset), how they are impacted by small-scale patchiness in the plankton (which also likely contributed to the long effective handling time) or how capture probability may vary with prey type and size. The model's propensity to over-predict lengths in the more northerly locations where prey generally are larger could potentially reflect a tendency to overestimate the capture probability of larger prey types.

Further, it is also unclear to what extent sandeels exhibit optimal foraging. The findings in this chapter suggest that this is an adaptive behaviour, as growth rates were generally higher when the model included optimal foraging. However, this varied depending on food conditions. This can be explained by the fact that when the sandeels are not limited by prey availability, feeding optimally increases energy intake rates, whereas when prey are scarce, it is better to feed indiscriminately. The inclusion of optimal foraging in the model may also be behind some of the counter-intuitive patterns found when assessing the impact of prey trait values on predicted length (see Section 4.3.2). For example, the positive impact of an increase in the size of Euphausiacea, in spite of this decreasing capture probabilities, could potentially be explained by this increasing the proportional profitability of the prey search class to which Euphausiacea belongs, leading to less time spent in other more profitable search classes. Further, the results also showed that how prey types are grouped into different search classes impacts predicted length, and these groupings are far from certain. All in all, more remains to be understood about optimal foraging in sandeels in order to be able to model it robustly.

4.4.2 Drivers of spatio-temporal variation in growth

While several processes may thus generate differences in predictions and observations, the agreement of observed and predicted spatio-temporal variation in the more southerly grounds, where the CPR input data were more robust and metamorphosis phenology better known, suggests that the model is able to capture at least some of the processes that contribute to observed spatio-temporal growth patterns and can thus be used to explore drivers of variation in size. A summary of the relative impact of the different drivers considered can be seen in Table 4.2.

It was clear that food conditions had a large impact on growth. As expected and in line with previous empirical studies (Eliassen 2013; MacDonald et al. 2019b), the total amount of food available, in terms of kJ m^{-3} , was positively associated with predicted length (Figure 4.7a). In terms of the effect of size composition, a higher proportion of small prey resulted in smaller predicted lengths, when all other factors were kept constant (Figure 4.7b). In contrast with this, while a larger prey image area resulted in larger predicted growth in some locations, in the Firth of Forth, the relationship was instead negative (Figure 4.6). This can be explained by large average image areas in the Firth of Forth generally being associated with a low abundance

Table 4.2: Relative impact of considered drivers of growth as measured by length relative to baseline conditions. It should be noted that the contribution to the averages is proportional to the number of years for each location for which input data exist.

Driver	Range of variation in driver	Difference at lower value mean (range)	Difference at upper value mean (range)
Total energy	0.4–10 kJ m ⁻³	-26 (-61; 0)%	+26 (+1; +137)%
Relative proportion small/large prey	0–1	+11 (-3; +52)%	-1 (-10; 0)%
Phenological shift	0–60 days	-	0 (-45; 89)%
Relative proportion <i>C. finmarchicus</i> / <i>C. helgolandicus</i>	1–0	-	-1 (-11; +2)
Temperature	-3–4.5°C	-1 (-3; +2)%	0 (-6; +3)%
a_d	0–0.3	3 (0; 11)%	-44 (-68; -12)%
Cloud cover	0.6–0.9	0 (0; +2)%	-1 (-2; 0)%
Latitudinal light variation	54.7–63.3	-	+4 (+2; +6)%
Date of metamorphosis	121–181	+5 (0; +14)	-19 (-48; -1)
Size at metamorphosis	3.5–5.5 cm	-1 (-10; 0)	+4 (+1; +28)

of small prey rather than a high abundance of large prey. This suggests that while prey size may have a positive effect in theory, as has been suggested previously for both sandeels (MacDonald et al. 2018; van Deurs et al. 2015, 2014) and other species of fish (e.g. Ljungström et al. 2020), the overall association when other variables are not accounted for will also depend on the abundance and composition of the prey field. In terms of prey phenology, the impact of a shift towards an earlier phenology did not on average have a clear effect in either direction, but for individual location-years, the impact could be large (Figure 4.7c). The effect depends on the shape and timing of food availability and how it aligns with the foraging window. For example, in the Firth of Forth, a shift to an earlier phenology generally had a positive impact, as peak abundances tend to occur later in this location.

The abundance of *Calanus* spp. was strongly related to predicted growth, which aligns with previous work (MacDonald et al. 2018; van Deurs et al. 2015, 2014). The predicted lengths in all locations were clearly associated with the abundance of *Calanus* I-IV, whereas the relationship with adult *Calanus* varied between locations (Figure 4.6). Previously, it has been suggested that the ongoing replacement of *C. finmarchicus* by *C. helgolandicus* could have a negative effect on sandeels due to the different phenology of the two species (Frederiksen et al. 2013; MacDonald et al. 2015). Based on climatological phenologies of the two species with a constant total yearly abundance, this appeared to be the case in the ECG, but not in the Firth of Forth, Shetland or Dogger Bank (Figure 4.7d). This suggests that in locations where *C. finmarchicus* has not generally been very abundant in the past, which is true for the Firth of Forth, Shetland and Dogger Bank, the recent increase in *C. helgolandicus* may instead have a positive impact on size. Interestingly, the increase in *C. helgolandicus* in the Firth of Forth and Dogger Bank in the early 2000s (see Figure 2.13 in Chapter 2) aligns with a slowing of the decline in sandeel length both in the Firth of Forth puffin series (see Wanless et al. 2018, Figure 4.2), as well as in length in 1+ group sandeels in Dogger Bank (van Deurs et al. 2014). In the ECG, the phenologies appear to be more different and a potential shift may have a negative effect, especially as absolute abundances of *C. helgolandicus* do not seem to match those of *C. finmarchicus* (Edwards et al. 2020, Chapter 2).

When isolating the effect of temperature, this had a small impact on predicted length relative to the other drivers, even at maximum projected climate change-driven increases (Figure 4.7e). This is in line with the results presented by MacDonald et al. (2018). Further, the effect of temperature depended on food conditions. Temperature has a positive effect on predicted lengths when intake rates are high, and a negative effect when intake rates are low. This has also been observed empirically in other fish species (Brodersen et al. 2011). Increased temperatures lead to increases in assimilation efficiency and digestion rate, which allows for a higher intake rate if gut capacity is limiting. However, they also result in increased metabolic costs. As such, the impact will depend on whether the increased metabolic costs are balanced by a higher rate of energy assimilation. Comparing temperature input data with model predictions identified a positive relationship in Shetland (Figure 4.6). This relationship is likely largely the result of a positive association with food, as the magnitude of the effect (22% increase in length from a temperature increase of 2.5°C) was greater than that expected by the direct effect of temperature (maximum

increase for same temperature increase = 2%). This may also suggest that the faster growth found in warmer sandeel grounds by Rindorf et al. (2016) is at least not fully explained by a direct impact of temperature, although it could exacerbate the impact of good food conditions.

As for light conditions, model predictions were not strongly affected by cloud cover or latitudinal variation in light, but in contrast, predictions were very sensitive to variation in turbidity (as represented by a_d) (Figure 4.7f,g, Table 4.2). The small effect of latitude suggests that the higher growth rates predicted in the north are not due to a longer feeding window. The lack of sensitivity to cloud cover suggests that even at the most extreme scenarios of projected changes in cloud cover (see May et al. 2016), this is not going to impact the sandeels markedly. It also suggests that the choice of which value to use is not of large importance. In contrast, the large sensitivity to a_d , which is in line with results presented in van Deurs et al. (2015), means that the choice of a_d will have a large impact on predicted growth. Further, it also implies that if the increase in turbidity observed in the North Sea (Capuzzo et al. 2015; Dupont and Aksnes 2013) have also impacted sandeel grounds, this could also have contributed to observed declines in size. However, it is unclear to what extent these large-scale patterns are representative of sandeel grounds. The findings here thus echo those for visually foraging fish in general (Aksnes 2007; Ljungström et al. 2020) as well as for *A. marinus* (van Deurs et al. 2015) in particular, that visual conditions may have a large impact on intake rates and subsequent growth, with the caveat that the turbidity levels required to have a substantial impact on predicted intake rates may not commonly occur in sandeel grounds.

While size at metamorphosis generally did not have a large impact on predicted length, the timing of metamorphosis did (Figure 4.8). It has previously been suggested that variation in hatch date and growth rate both contribute to the observed variation in size in the Firth of Forth (Frederiksen et al. 2011; MacDonald et al. 2019a). Here, the model predicts that over the range of metamorphosis dates observed in the Firth of Forth (Régnier et al. 2017, median hatching date plus average age at settlement in Table 2), this results in a length difference of around 12%, which means that even if the sandeels would have shifted between the two extremes, this would not explain the decline in length of 28% observed in the Firth of Forth during the study period (see Figure 4.2). As such, while pre-metamorphic processes may contribute to some of the observed variation, they are not sufficient for explaining the observed decline. Further, the large variation between location-years in the effect of a shift in date of metamorphosis (see Table 4.2) suggests that favourable environmental conditions during the feeding season may be able to compensate for late metamorphosis. Still, on average, a delay in the timing of metamorphosis had a negative impact on predicted length. With increased temperatures, studies from the Firth of Forth suggest that larval sandeels will become increasingly mismatched with their prey, leading to reduced recruitment (Régnier et al. 2019). Likely, this will also lead to slower larval growth and thus later metamorphosis (which may be exacerbated by a delay in spawning caused by increased temperatures, Wright et al. 2017b). Based on the results presented here, this could further contribute to a decline in the size of sandeels. However, the impact of this will also depend on the phenology of the prey of the settled sandeels. An earlier phenology in prey has

the same impact as a delay in the phenology of the sandeel, which implies that the impact of a delay in sandeel phenology will depend on the local prey phenology (see Figure 4.6c).

4.4.3 Climate change-driven decreases in size

As timing of metamorphosis and light conditions (apart from latitudinal variation, which had a small impact) were kept constant when making predictions for given location-years and temperature had a very small impact, the spatio-temporal variation predicted by the model, which generally agreed with observed spatio-temporal variation, was mainly driven by variation in food conditions. As the decline in size in the Firth of Forth was adequately captured by the model, this suggests that changes in food conditions were sufficient to explain this decline. This supports the hypothesis that a change in food conditions is one of the mechanisms behind the widespread declines in size observed in many organisms (Gardner et al. 2011). While these observed declines are often hypothesised to be linked to climate change, the extent to which the decline in the Firth of Forth is actually associated with climate change depends on whether the change in food conditions is driven by climate change (discussed further in Chapter 6). The small direct impact of temperature on predicted size suggests that increased metabolic costs as a result of increased temperatures, which has been proposed as one of the mechanisms behind climate change-associated body size declines (Sheridan and Bickford 2011) are not the cause of the decline. Beyond the impact on metabolism, there may also be other mechanisms through which increased temperature, or temperature-associated changes in oxygen content, may impact size (Atkinson 1994; Audzijonyte et al. 2019), but their role cannot be deduced from this study. While sufficient information was not available to assess the extent to which changes in turbidity or phenology of metamorphosis have contributed to observed variation, both of these variables were capable of generating large variation in size. Further, both phenology (Régnier et al. 2019) and turbidity (Capuzzo et al. 2015) may be expected to respond to climate change. This points to the importance of considering more subtle drivers.

4.4.4 Future studies

The findings of this study suggest several interesting future research avenues. Due to the strong link between size and demographic rates (Boulcott and Wright 2011; Boulcott et al. 2007; MacDonald et al. 2018), extending the model to further age groups could provide a better understanding of how processes impacting growth rates also result in variation in abundances. The model developed by MacDonald et al. (2018) already includes older age groups, but there are several aspects that could be developed further. First, the growth curves produced here (Figure 4.3) appear to level off around the time of overwintering, where this levelling off (where food conditions cannot further sustain growth) could potentially be incorporated as a mechanism for when overwintering is initiated. Further, recent experimental work (Wright et al. 2017a,b) has provided new insight into the process of gonad investment and how it depends on temperature, which would allow the exploration

of the impact of both summer feeding conditions and overwintering temperatures on fecundity and also timing of spawning. Together with an improved understanding of the effect of temperature on the incubation period (Régner et al. 2018) and of processes governing larval growth (e.g. Henriksen et al. 2018; Régner et al. 2017, 2019), it would potentially be possible to close the gap between spawning and metamorphosis in the model by MacDonald et al. (2018). Size-dependent maturation rates (Bergstad et al. 2001; Boulcott et al. 2007) and overwintering mortality (MacDonald et al. 2018) could also be incorporated into the model to further improve the understanding of size-mediated bottom-up effects.

With the results from the sensitivity analysis in place it is also worth to now return to the question of the complexity of the model, and discuss uncertainties as well as potential simplifications. Again, much of the uncertainty comes from variables and processes governing encounter rate and capture probability. The results of the sensitivity analysis suggest that to reduce the uncertainty of these processes, better information is required on sandeel visual acuity, how capture success varies between prey types as well as at what depth and with which speed the sandeels forage. However, the effort required to accurately estimate these parameters is daunting. Instead, a better way forward may be to, as also suggested by MacDonald et al. (2018), make use of simultaneous samples of sandeel guts and zooplankton. While several studies have conducted simultaneous samples (Eliassen 2013; Gómez García et al. 2012; van Deurs et al. 2014), the study conducted by Godiksen et al. (2006) is exemplary in that it also considers the size distribution of the sandeels as well as of the prey in the guts and in the water column. This type of information can be used to determine how the composition of a given prey field translates into the composition of prey actually eaten by the sandeels. This would make it possible to tune predictions from the visual foraging model, or be sufficient on its own through computing attack rate estimates for a given prey type. Further, the lack of sensitivity to parameters governing digestion and maximum gut size suggests that a simplified model could exclude this step. Two processes that may be interesting to obtain better estimates of are assimilation efficiency and metabolic costs of feeding and synthesising tissue. These values are highly uncertain but important for an improved understanding of energy flow through the system. Further, considering the large impact of turbidity on predicted length, a better understanding of to what extent this shows spatio-temporal variation in sandeel grounds of the magnitude needed to generate a non-negligible difference in growth would also be useful. Finally, in a slightly larger perspective, considering that a 10% change in prey trait values could generate an up to 10% difference in predicted sandeel length, the development of a prey trait database would be highly useful for modellers, not only saving time, but also encouraging different studies to use the same values, which would increase the comparability across studies.

Part III

Spatio-temporal patterns in the dynamics of a sandeel predator in relation to the spatial structure of their sandeel prey

Chapter 5

Spatial synchrony of breeding success in the black-legged kittiwake (*Rissa tridactyla*) reflects the spatial dynamics of its sandeel prey

5.1 Introduction

A wide variety of taxa show spatial synchrony, defined as “coincident changes in the abundance or other time-varying characteristics of geographically disjunct populations” (Liebhold et al. 2004). Synchrony is an important aspect of population dynamics as the degree to which populations show synchronised dynamics is a key determinant of long-term metapopulation persistence (Engen et al. 2002) and may have important implications for community dynamics and ecosystem function (Stenseth et al. 2002). Several mechanisms may act to generate synchrony, including trophic interactions with other species that show spatial synchrony (e.g. Haynes et al. 2009; Ims and Andreassen 2000; Ripa and Ranta 2007), mixing between close-by populations through dispersal (e.g. Schwartz et al. 2002; Sutcliffe et al. 1996) or dependence on some spatially autocorrelated external factor such as weather conditions (e.g. Grenfell et al. 1998; Grøtan et al. 2005; Moran 1953; Post and Forchhammer 2002). The patterns of synchrony may be further modified by spatial variation in the dynamics of density dependence (e.g. Liebhold et al. 2004). Different mechanisms may be expected to generate different geographical patterns of synchrony. Comparing these expected patterns with observed spatial patterns in population synchrony, including detailed geographic patterns (Walter et al. 2017) as well as how between-population synchrony declines with distance (Bjørnstad and Falck 2001), can thus help to identify factors that drive population dynamics and at what spatial scale they operate (Walter et al. 2017). This approach has, for example, been used previously to identify large-scale climate fluctuations as a driver of population dynamics in caribou (*Rangifer tarandus*) and muskoxen (*Ovibos moschatus*) in Greenland (Post

and Forchhammer 2002). As such, it can provide useful information for species conservation by identifying causes of population declines and the spatial scales over which management efforts may be needed (O’Hanlon and Nager 2018).

One species in which spatial synchrony has been investigated is the black-legged kittiwake (*Rissa tridactyla*, hereafter ‘kittiwake’), a colonial, pelagic seabird species that has recently shown such steep declines that it was globally red listed (BirdLife International 2018). Over the scale of its full distribution across the Northern Hemisphere, synchrony in the fluctuations of colony sizes has generally been non-existent or very low, apart from a synchronised decline during a period of rapid ocean warming (Descamps et al. 2017). Similarly, a study looking at smaller scale synchrony, using colonies along the coast of Norway, found no evidence that colony sizes fluctuated in unison (Sandvik et al. 2014). However, synchrony has been identified in kittiwake breeding success in the UK and Ireland, where colonies formed geographically distinct clusters in which breeding success fluctuated in unison (Frederiksen et al. 2005; Furness et al. 1996). Furness et al. (1996) hypothesised that the observed clusters were the result of a response to the independent dynamics of aggregations of lesser sandeels (*Ammodytes marinus*, hereafter ‘sandeels’), the main prey of kittiwakes in large parts of the UK. The sandeel is also an important prey for many other top predators in this area (Furness and Tasker 2000), and climate-driven declines in the abundance and size of the sandeel are thought to be an important contributing factor to declines of kittiwakes and other sandeel-eating seabirds in large parts of the UK (MacDonald et al. 2015). In line with the hypothesis developed by Furness et al. (1996), Frederiksen et al. (2005) found that the kittiwake breeding success synchrony clusters corresponded roughly to distinct aggregations of larval and settled sandeels. While this provides support for the hypothesis, this is a coarse way of representing sandeel dynamics compared to what is now known about sandeel spatial structure. Furthermore, no alternative mechanisms that could potentially generate similar patterns were examined and ruled out.

Of the potential mechanisms that could generate the observed spatial patterns in kittiwake breeding success synchrony, spatial patterns in the synchrony of a trophically interacting species or spatial patterns in the synchrony of environmental conditions appear most plausible. There is no evidence of any density-dependent effects acting on kittiwake breeding success in this area (Frederiksen et al. 2005), and this is thus unlikely to contribute to the observed synchrony patterns. Further, while dispersal may synchronise fluctuations in abundance through dispersers from one population spreading to multiple other populations and thus creating a synchronised increase (e.g. Schwartz et al. 2002), dispersal would not be expected to have a similar effect on a demographic rate such as breeding success. In terms of trophic interactions and environmental conditions, there are multiple alternative drivers. Weather conditions, primarily wind (e.g. Christensen-Dalsgaard et al. 2018a,b) and rain (Alvestad 2015) may impact breeding success through effects on thermoregulation and foraging conditions. More extreme weather events may also result in nests being washed away or dislodged (e.g. Newell et al. 2015). As a result, weather, which shows strong spatial autocorrelation, could be capable of generating spatial patterns in kittiwake breeding success synchrony. Another driver of kittiwake breeding success is predation. Kittiwake eggs and chicks are targeted by a range of predators (e.g. Collins et al.

2014; Galbraith 1983), but great skuas (*Stercorarius skua*, hereafter ‘skua’) are likely the only ones able to have a substantial impact on productivity (see Heubeck 2002; Votier et al. 2004). Skuas are only present in the north of the UK and this spatial variation in presence, together with the ability of predation to induce synchrony (e.g. Ims and Andreassen 2000), means that skua dynamics could potentially generate spatial patterns in kittiwake breeding success synchrony. Finally, as hypothesised by Furness et al. (1996) and Frederiksen et al. (2005), it is possible that sandeels, which show clear spatial patterns in synchrony, are responsible for the observed patterns. Sandeels have a strong preference for a certain depth and sediment type which shows a patchy distribution (Holland et al. 2005; Wright et al. 2000), and as a result, aggregations of sandeels have a patchy distribution themselves (e.g. Jensen et al. 2011). As sandeels show very low levels of post-settlement movement, dispersal of larvae is the main process connecting sandeel grounds (Wright et al. 2019). This, together with external drivers of sandeel demographic rates such as zooplankton conditions (e.g. MacDonald et al. 2018; Régnier et al. 2017), temperature (e.g. Rindorf et al. 2016; Wright et al. 2017a) and predation (e.g. Frederiksen et al. 2007b), likely act as driving forces of synchrony in sandeel dynamics. Synchrony in sandeel abundances has been shown to decline with distance (Wright et al. 2019). However, likely largely as a result of patterns of larval transport, this decline is not uniform, and areas that are not hydrographically well-connected show low levels of synchrony (ICES 2017; Wright et al. 2019).

The aim of this study is to examine spatial patterns in the synchrony of breeding success in British kittiwakes and to revisit the hypothesis of Furness et al. (1996) and Frederiksen et al. (2005) that synchrony in kittiwake breeding success in the UK is driven by the spatial structure of their sandeel prey. The study builds on previous work by utilising recent advancements in the understanding of sandeel spatial structure, by adding 15 further years of data on kittiwake breeding success and by also examining alternative hypotheses. To characterise spatial patterns in kittiwake breeding success synchrony, the study (1) examines the relationship between breeding success synchrony and between-colony geographical distance, (2) maps out the spatial configuration of colony pairs showing stronger or weaker synchrony than expected based on distance and (3) examines geographical patterns in synchrony further using a cluster analysis. Following this, (4) potential mechanisms for generating the observed spatial patterns in kittiwake breeding success synchrony are investigated, focusing on sandeel spatial structure, skua predation and weather conditions. This is done using two different metrics of synchrony, focusing mainly on one reflecting synchrony in inter-annual fluctuations only (r_{diff}) but also looking at one reflecting synchrony in both inter-annual fluctuations and long-term trends (r). The study will help to identify large-scale drivers of breeding success in the rapidly declining population of British kittiwakes, and the spatial scales over which they may be acting. On a broader scale, the study, having access to long-term spatially resolved data, also helps to further understand what drivers may act to generate spatial patterns in synchrony.

5.2 Methods

5.2.1 Kittiwake breeding success data

The study area covered the part of the UK where sandeel is an important prey item for kittiwakes (based on Furness and Tasker 2000) and it was possible to make well-founded predictions for sandeel synchrony patterns (see Section 5.2.4). This area included the north and east coast of mainland UK, as well as Shetland and Orkney (Figure 5.1a). For this area, data on breeding success (average number of fledglings produced per nest per year in each colony) were accessed from the Seabird Monitoring Programme website (<http://jncc.defra.gov.uk/smp>, accessed 27 January 2019) and from the Centre for Ecology and Hydrology (data from the Isle of May Newell et al. 2016). The same protocol (Walsh et al. 1995) was used at all colonies to estimate breeding success. Estimates based on fewer than 40 nests were excluded as smaller samples may not be representative as a result of demographic stochasticity. The study period covered the years 1986 to 2018, as breeding success was not monitored in many colonies before 1986.

5.2.2 Synchrony in breeding success

Synchrony can be measured with different metrics that emphasise different aspects (Buonaccorsi et al. 2001). Here, synchrony was measured as the Pearson correlation of the differences in breeding success between consecutive years, r_{diff} . This metric is good at capturing the degree to which two time series move together on an annual scale, closely following the textbook definition of synchrony (Buonaccorsi et al. 2001). As such, it does not reflect synchrony in long-term trends, which reduces the risk to infer high synchrony between colonies that show similar long-term trends for different reasons. However, similar long-term signals may also say something about mutual drivers (Pyper and Peterman 1998), and this is not picked up by r_{diff} . For this reason, a parallel analysis was also run where the Pearson correlation r of the untransformed breeding success time series for each colony pair was used as an alternative measure of synchrony.

Only colonies that had a minimum average of 15 occasions of overlapping estimates of breeding success in two consecutive years with all other colonies were included (see Table C.1 in Appendix C for values for each colony pair). This cut-off value was based on an examination of how much the estimated r_{diff} changed as data points were removed (see Figure C.1 in Appendix C) balanced against the number of colonies that could be included and their geographical spread. In total, 22 colonies spread out over the entire area of interest (Figure 5.1a) had sufficient data (average 27.1 years of data per colony, range 17 to 31). Most colonies had missing years distributed throughout the time period, but a few colonies had a longer sequence (maximum 10 years) missing at the start (Colony 22) or at the end (Colonies 9, 14, 15, 18, 19, see Figure 5.1a and Table 5.1 to identify colonies).

5.2.3 Spatial patterns in synchrony

5.2.3.1 Effect of geographical distance on synchrony

To establish the spatial scale of synchrony, the relationship between the between-colony geographical distance and the between-colony breeding success synchrony was determined. As similarity in conditions and connectivity between colonies is more likely to depend on distance along the coast rather than the distance across landmasses, along-coast distance was used as a distance metric. This was calculated as the shortest path between colonies without allowing the crossing of landmasses, using the function *gridDistance* in the package *raster* (Hijmans 2018) in R 3.5.2 (R Core Team 2018, used for all analyses). To assess how synchrony declined with distance, a cubic smoothing spline was fitted, thus making no prior assumptions about the shape of the relationship (Bjørnstad and Falck 2001). This was done using the *Sncf* function from the R-package *ncf* (Bjørnstad 2019), where uncertainty was estimated with a bootstrapping approach based on 10,000 resamples.

5.2.3.2 Deviations from the distance-synchrony relationship

Next, the spatial patterns of colony pairs showing stronger or weaker synchrony in breeding success than what was expected based on distance were examined. To do this, colony pairs falling above (positive residuals) and below (negative residuals) the 99% bootstrapping confidence interval of the estimated distance-synchrony spline were identified and these higher-than-expected and lower-than-expected linkages were then visualised on a map. Only colony pairs separated by a distance for which there was a clear relationship between synchrony and distance were used.

5.2.3.3 Cluster analysis

A cluster analysis was carried out to further examine spatial patterns in breeding success synchrony. Colonies were clustered based on the similarity distance between each colony pair, calculated as $1 - \text{synchrony}$ (perfect synchrony gives a distance of 0, no correlation a distance of 1 and perfect asynchrony a distance of 2). As the final cluster structure can be sensitive to the choice of clustering algorithm, several different algorithms were used to obtain a more robust understanding of the cluster structure. Using functions from the R-package *cluster* (Maechler et al. 2018), hierarchical agglomerative clustering (*agnes*), using the Ward (1963) method to measure similarity between clusters, divisive hierarchical clustering (*diana*), partitional clustering (*pam*), and fuzzy clustering (*fanny*) were all conducted. In *fanny*, the degree of belonging to each of a defined number of clusters is calculated, thus providing a better understanding of which colonies may form the core of a cluster, and which colonies are instead showing similarities with several clusters.

All algorithms require the number of clusters, k , to be specified. To do this, three metrics were used to assess the strength of the cluster structure for different values of k for each algorithm, the within-cluster sum of squares, which measures within-cluster variation, the gap statistic, which compares the within-cluster variation for each value of k with the expected values under a null reference distribution, and

the average silhouette width, which compares the average similarity of colonies to other colonies within their own cluster with the average similarity to colonies in the most similar neighbouring cluster (see Figure C.2 in Appendix C). All were implemented with the function *fviz_nbclust* from the R-package *factoextra* (Kassambara and Mundt 2017).

Finally, the strength of the final cluster structure was assessed for each algorithm using the silhouette width as described above. Values close to 0 indicate that a colony lies in between clusters and values around and above 0.5 indicate a “reasonable” to “strong” cluster structure (Kaufman and Rousseeuw 2005). The stability of the cluster structure was also assessed using the average proportion of non-overlap, which measures the proportion of colonies that would be assigned to a different cluster if a random colony were to be removed from the data. Values close to zero suggest a stable structure. Both the silhouette widths and the proportion of non-overlap were calculated using the R-package *clValid* (Brock et al. 2008).

5.2.4 Inferring causes of synchrony

In order to investigate potential drivers of synchrony, matrix regression was used (see Lichstein 2007 and references therein). Here, the response variable is the matrix representing between-colony synchrony, and potential drivers are all also formulated as matrices. In this case, these alternative drivers include sandeel spatial structure, weather conditions and skua predation, as outlined in Section 5.1. In addition to this, an effect of distance was included, which could be a result of these drivers, but also other spatially autocorrelated drivers.

For sandeels, each colony was assigned to a sandeel sub-population, expecting colonies assigned to the same sub-population (1 in the matrix) to be more synchronous than colonies assigned to different sub-populations (0 in the matrix). Sub-population boundaries were based on current knowledge of sandeel spatial structure (Figure 5.1a). Along the North Sea coast of the British mainland, there are two distinct sandeel sub-populations that are managed as separate ICES stock assessment areas (ICES 2017), delineated based on larval transport patterns (Christensen et al. 2008). This delineation is supported by both otolith microchemistry (Wright et al. 2018) and genetic structure (Jiménez-Mena et al. 2020). ICES has not considered the evidence for structuring north of mainland UK, but based on evidence from distribution (Wright 1996), larval transport modelling (Proctor et al. 1998) and otolith microchemistry (Gibb et al. 2017), Orkney and Shetland were divided into two separate sub-populations. Handa Island (Colony 9) and North Sutor (Colony 16) were also assigned to the Orkney sub-population, based on evidence from otolith microchemistry (Gibb et al. 2017) and recent larval drift simulations (Wright et al. 2019), respectively. It should be noted that as these sub-population boundaries are to a large degree based on larval transport they are not fixed, as transport varies between years, or absolute, meaning that aggregations near a boundary may be expected to display similar dynamics (Wright et al. 2019). Whether a colony pair belonged to the same sub-population or not is strongly related to the distance between them, and for this reason all sandeel models also included a distance effect to control for this. This

also, to some extent, accounts for the fact that synchrony in sandeel dynamics also declines with distance, even within sandeel sub-populations (Wright et al. 2019).

The knowledge of synchrony in skua predation pressure between colonies is poor. As a simple way to represent this driver, an area in which kittiwake colonies are susceptible to predation by skuas was defined based on knowledge of the distribution (Mitchell et al. 2004) and foraging distance (Wade et al. 2014) of skuas. This area included Handa Island (Colony 9) as well as colonies in Shetland and Orkney. Colony pairs both located within this area or both located outside this area are given a value of 1 in the matrix, whereas other pairs are given a value of 0. Again, these values will be confounded with distance, and so a distance effect was always included in the skua models. Similarly, while it is not known how the impact of skuas may be synchronised across space, it is reasonable to assume that it will decline with distance, and this will also be picked up by the distance effect.

As outlined in the Section 5.1, weather (primarily rain and wind conditions) can also impact the breeding success of kittiwakes. In this analysis, weather was represented as a matrix of between-colony synchrony in daily total precipitation (mm) during the breeding season (May to August), measured as the Pearson correlation coefficient. This was based on data covering the full study period from the HadUK-Grid dataset, which provides data on a 1×1 km grid, interpolated from the network of weather stations (Hollis et al. 2019, downloaded December 2019). Wind speed was not used as it is only available as monthly averages from this dataset, which is not at a fine enough scale to capture how similar conditions are for a given part of the kittiwake breeding cycle. However, the correlation between between-colony synchrony in monthly wind speed and between-colony synchrony in daily precipitation was high ($r = 0.85$, $p < 0.001$), suggesting that this variable will be representative of similarity in weather conditions in general. Finally, as weather shows strong spatial autocorrelation, this may cause multicollinearity issues when included in the same model as the general distance effect. For this reason, residuals from a smoothing spline of between-colony synchrony in precipitation as a function of between-colony distance were used to represent the effect of synchrony in weather conditions.

Both distance and weather were translated into similarities, so that the most similar colony pair were given a value of 1, and the most dissimilar colony pair a value of 0. Examining the residuals from the full linear model, it was clear that the effect of distance was not linear. This is common (e.g. Liebhold et al. 2004), and was also expected based on the findings presented here (see Section 5.3.1.1). To deal with this, the effect of distance was modelled using a spline. The degrees of freedom were increased until the pattern in the residuals disappeared, stopping at 3. A set of candidate models were then created as subsets of the full model (see Table 5.2). The model selection was based on the leave-n-out cross-validation approach outlined in Walter et al. (2017), where models are ranked based on their predictive power. An n of 4 was used (18% of total number of colonies, similar to percentages as reported in the supplementary material of Walter et al. 2017), where the predictive power is defined as the mean of the sum of squared errors between predicted and measured synchrony over all possible combinations of test sets of 4 colonies. In order to compare the support for the different models, a bootstrapping approach was

used where colonies were resampled with replacement 250 times, model ranks were calculated for each resample and model weights were determined as the proportion of resamples where the model was ranked as the top model. Further, p-values were calculated with a permutation approach using the function *MRM* in the package *ecodist* (Goslee and Urban 2007).

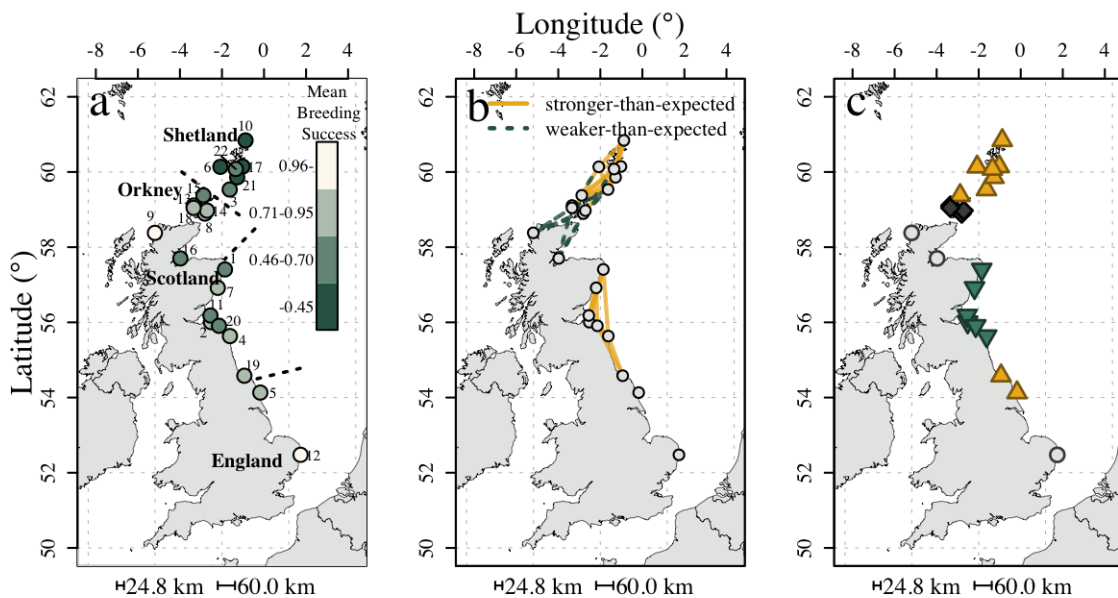


Figure 5.1: (a) Black-legged kittiwake colonies included in the study, colour-coded by the mean breeding success during the study period (1986–2018). Place names referred to in the text are included for reference. The numbers correspond to colonies listed in Table 5.1. Dashed lines: approximate borders between sandeel sub-populations regions (see Section 5.2.4). (b) Weaker (negative residuals from relationship in Figure 5.2) and stronger (positive residuals from relationship in Figure 5.2) synchrony than expected based on distance for colonies closer than 200 km apart (the synchrony-distance relationship was unclear beyond this distance, see Section 5.3.1.1). (c) Combined results from the cluster analysis. Round grey symbols: colonies assigned to different clusters by the different algorithms (see Table C.2 in Appendix C). The other coloured symbols indicate clusters that were consistently identified by all algorithms. All maps were produced with the R-package *rworldmap* (South 2011). The scale bars correspond to the average length (24.8 km) and the average estimated maximum length (60.0 km) of a kittiwake foraging trip based on a meta-analysis of foraging ranges (Thaxter et al. 2012).

5.3 Results

5.3.1 Spatial patterns in synchrony

5.3.1.1 Effect of geographical distance on synchrony

Between-colony synchrony (r_{diff} , correlation in the difference in breeding success between consecutive years) was high (~ 0.75) for close-by colony pairs and declined with along-coast distance until around 300 km, followed by a temporary increase centred around 600 km (Figure 5.2), although the 99% confidence interval remained close to zero. The 99% confidence interval intersected with $r_{diff} = 0$ at just over 200 km, which can thus be considered to be the scale of spatial synchrony (Bjørnstad and Falck 2001). A similar pattern was found when synchrony was measured as r (correlation in untransformed time series of breeding success, Figure C.3 in Appendix C).

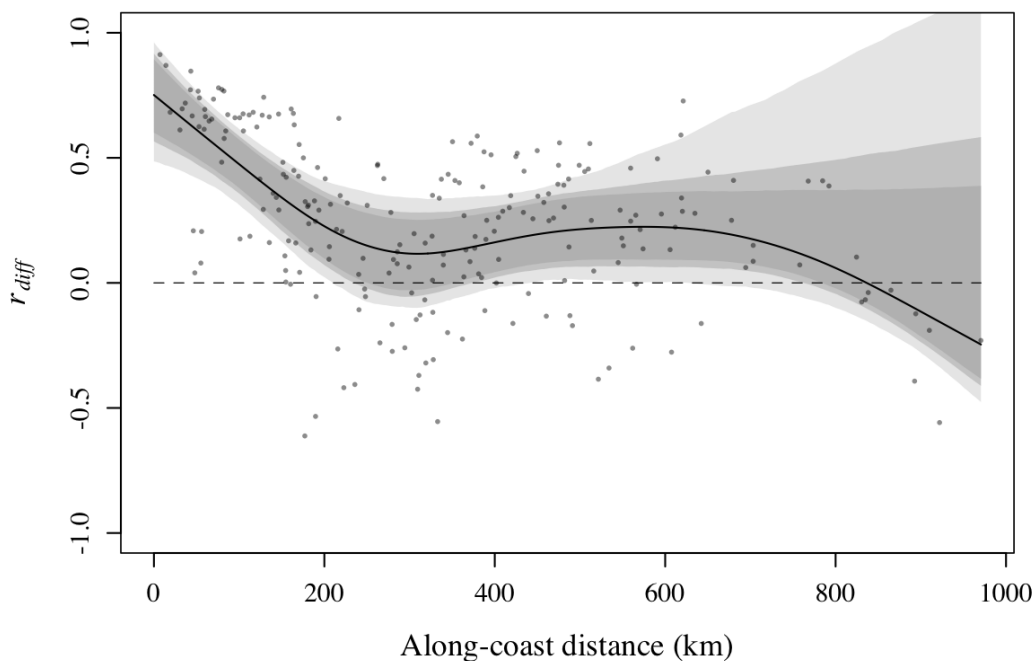


Figure 5.2: Cubic smoothing spline fitted between the along-coast distance and synchrony in inter-annual fluctuations (r_{diff}) for each black-legged kittiwake colony pair (black line). Each point shows the r_{diff} of a colony pair against the along-coast distance between the two colonies. Dashed line: $r_{diff} = 0$. Grey shading shows 99, 95 and 90% confidence intervals as estimated from boot-strapping.

5.3.1.2 Deviations from the distance-synchrony relationship

When synchrony was measured as r_{diff} , several colony pairs showed either stronger or weaker synchrony than expected based on distance (restricted to distances below which there was a clear relationship with synchrony, around 200 km, Figure 5.2). On the Scottish east coast, many colony pairs showed stronger-than-expected synchrony, and this was also the case in Shetland (Figure 5.1b). The four southernmost

colonies in Orkney (Colonies 8, 13, 14 and 18) showed weaker-than-expected synchrony both with the more southerly colonies Handa Island (Colony 9) and North Sutor (Colony 16) as well as several colonies in Shetland. Unlike the other Orkney colonies, North Hill (Colony 15) showed stronger-than-expected synchrony with several colonies in Shetland, and also weaker-than-expected synchrony with the other Orkney colonies. There was a clear difference in the corresponding results when synchrony was measured as r (Figure C.4a in Appendix C), in that the synchrony of the four southernmost colonies in Orkney with Handa Island and North Sutor were stronger-than-expected rather than weaker-than-expected.

5.3.1.3 Cluster analysis

Colonies were first clustered based on synchrony measured as r_{diff} . While the optimal k was slightly different for the different algorithms (Figure C.2 in Appendix C), they all identified the same three core clusters (Figure 5.1c), although a few colonies were assigned less consistently (see Table C.2 in Appendix C for the final cluster structure for each algorithm). Starting from the north, the colonies in Shetland formed one cluster which was consistent across algorithms (Figure 5.1c, yellow cluster), with Shetland colonies showing affinities of close to 50 or above with this cluster (Table 5.1). Outside Shetland, the English colonies Saltburn Cliffs (Colony 19) and Flamborough Head (Colony 5) as well as the Orkney colony North Hill (Colony 15) were consistently assigned to this cluster across algorithms. While all these colonies showed the highest affinity with this cluster, the affinity of North Hill was higher than those of the English colonies and similar to those of the Shetland colonies (Table 5.1). Apart from North Hill, all other colonies in Orkney were consistently assigned to the same cluster by all algorithms (Figure 5.1c, black cluster). Going further south, both Handa Island (Colony 9) and North Sutor (Colony 16), were assigned inconsistently (Figure 5.1c, grey), and showed similar affinities to all clusters (Table 5.1). The colonies on the Scottish east coast formed a consistent cluster (Figure 5.1c, green), with affinities centred around 50 (Table 5.1). Finally, the southernmost colony of Lowestoft was assigned inconsistently (Figure 5.1c, grey) but showed the strongest affinity with the Orkney cluster (Table 5.1). All algorithms had similar average silhouette widths of around 0.40, indicating a weak to moderate cluster structure. Based on the calculated average proportion of non-overlap, clusters appeared to be moderately stable, where on average 29, 26 and 38% of colonies would be re-assigned if a random colony were to be removed from the dataset for each of the three algorithms *agnes*, *diana* and *pam*, respectively.

When clustering was based on synchrony measured as r rather than r_{diff} , both Handa Island and North Sutor were consistently clustered with Orkney, and this was also the case for the two southernmost English colonies, Saltburn Cliffs and Lowestoft (Figure C.4b in Appendix C). Looking at the time series of breeding success for the different clusters (Figure 5.3), the difference between using r and r_{diff} becomes clear. While Handa Island and North Sutor do not seem to show similar inter-annual fluctuations to Orkney, they show a similar drop in breeding success in the early 2000s, and as such show correlated long-term patterns. Figure 5.3 also illustrates how colonies within each core cluster generally show clear synchrony in their fluctuations.

5.3.2 Inferring causes of synchrony

The model with the highest weight when synchrony was measured as r_{diff} only included an effect of distance (Table 5.2). The model with the highest weight when synchrony was measured as r also included distance, but contained an effect of sandeel sub-population as well, where colony pairs assigned to the same sandeel sub-population showed a synchrony of 0.24 units higher than colony pairs assigned to different sandeel sub-populations after accounting for the effect of distance ($p = 0.003$). The model weights indicated that there was no support for skua predation or weather conditions driving the observed synchrony patterns, regardless of whether synchrony was measured as r or r_{diff} .

Table 5.1: Results of the fuzzy clustering (*fanny*) showing the affinities (expressed as rounded percentages) of each colony to each of the three clusters in Figure 5.1c (colours used in Figure 5.1c are also indicated). Colony numbers correspond to numbers in Figure 5.1a. The cluster with the highest affinity is shown in **bold** for each colony. Three clusters were considered for the fuzzy clustering, based on the identification of three core clusters by all algorithms (see Section 5.3.1.3).

Colony number	Colony name	Cluster		
		Scottish east coast (green)	Orkney (black)	Shetland (yellow)
1	Buchan Ness	48	31	20
2	Dunbar Coast	47	31	20
3	Fair Isle	20	21	59
4	Farne Islands	44	31	25
5	Flamborough Head	31	34	35
6	Foula	24	25	51
7	Fowlsheugh	51	26	23
8	Gultak	27	49	23
9	Handa Island	36	29	34
10	Hermaness	23	28	49
11	Isle of May	55	24	21
12	Lowestoft	29	42	29
13	Marwick Head	30	47	23
14	Mull Head	27	52	22
15	North Hill	22	25	53
16	North Sutor	31	40	29
17	Noss	21	23	56
18	Row Head	26	49	25
19	Saltburn Cliffs	32	32	37
20	St Abb's Head	52	26	22
21	Sumburgh Head	25	28	47
22	Whale Wick	25	21	54

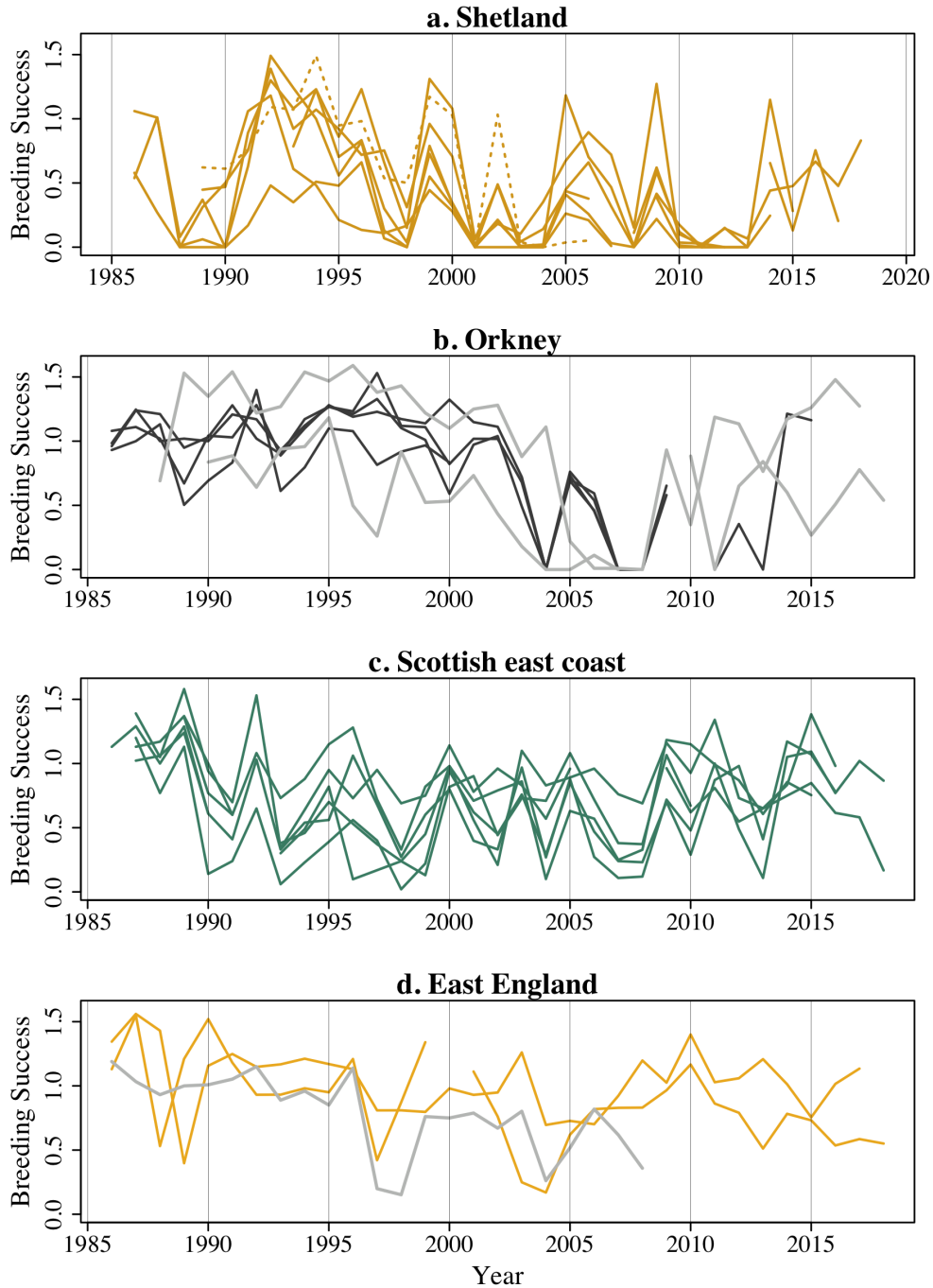


Figure 5.3: Time series of black-legged kittiwake breeding success. (a) All colonies in Shetland assigned to the yellow Shetland cluster (see Figure 5.1c), as well as the Orkney colony North Hill (Colony 15, dotted line) that was also assigned to this cluster. (b) All colonies in Orkney assigned to the black Orkney cluster (see Figure 5.1c), as well as (grey) colonies Handa Island (Colony 9) and North Sutor (Colony 16). (c) All colonies included in the green Scottish east coast cluster (see Figure 5.1c). Note that this also includes the English colony Farne Islands (Colony 4). (d) Rest of the English colonies. Yellow: Flamborough Head (Colony 5) and Saltburn Cliffs (Colony 19), which were assigned to the yellow Shetland cluster; grey: Lowestoft (Colony 12), which was assigned to different clusters by the different algorithms. The cluster structure is based on synchrony measured as synchrony in inter-annual fluctuations (r_{diff}).

Table 5.2: Model weights for all candidate models from the matrix regression. Model weights were calculated as the proportion of times the given model was ranked as the top model based on 250 resamples. Weights are given for models where synchrony was measured as synchrony in inter-annual fluctuations (r_{diff}) and models where it was measured as synchrony in both inter-annual fluctuations and long-term trends (r). The largest model weight for each synchrony measure is indicated in **bold**.

Explanatory variables	Model weights	
	r_{diff}	r
distance + weather + skuas + sandeels	2	2.4
distance + weather + skuas	6.8	3.2
distance + weather + sandeels	4.8	16.4
distance + sandeels + skuas	2.8	5.6
distance + weather	25.2	5.6
distance + sandeels	10	41.6
distance + skuas	7.6	6.8
distance	32.4	15.6
weather	1.6	0.4
null	6.8	2.4

5.4 Discussion

In this study, there was clear evidence of geographical patterns in the synchrony of breeding success in the examined British kittiwake colonies. As expected, the distance between colonies was an important determinant of between-colony synchrony. However, some colony pairs showed stronger or weaker synchrony than expected based on distance and this was also reflected in the configuration of spatially coherent clusters of colonies with synchronous breeding success. There was some evidence that the spatial structure of the kittiwakes' sandeel prey has played a role in generating the observed patterns, but this depended on how synchrony was measured. As such, the results lend some support to the hypothesis developed by Furness et al. (1996) and Frederiksen et al. (2005) that spatial synchrony in kittiwake breeding success in the UK is driven by the spatial structure of sandeel populations, but also show that the story is potentially more complex. On a broader scale, the findings show that examining spatial patterns in synchrony can provide useful information on potential demographic drivers and also highlight that different stories can emerge depending on how synchrony is measured.

The negative effect of distance on synchrony, with synchrony declining up to a distance of just over 200 km, aligns with previous studies of spatial synchrony (Liebhold et al. 2004). However, patterns were less clear beyond this initial decline. Centred at around 600 km, there was a temporary increase, and although the confidence intervals remained close to zero, it is possible that this weak positive synchrony at long distances reflects large-scale drivers that may generate synchrony in kittiwake breeding success, such as carry-over effects from shared wintering areas (see Frederiksen et al. 2012). Centred at around 300 km, there are multiple negative correlations. This dip may not necessarily have any biological meaning, but may instead be the result of multiple negative correlations between colonies on the Scottish east coast and colonies in Shetland and Orkney, with many colony-pairs being separated by similar distances. Even at shorter distances, the large residuals indicated that the spatial pattern in synchrony was more complex than a simple decline with distance. The distribution of colony pairs showing weaker-than-expected or stronger-than-expected synchrony showed a clear spatial pattern and this was also reflected in the spatial configuration of clusters showing synchronous breeding success. The geographical structure, with Shetland, southern Orkney and the Scottish east coast each forming consistent clusters, was similar but more spatially coherent than that found in Furness et al. (1996) and Frederiksen et al. (2005), and also aligned with the strong correlations on the Scottish east coast observed by Harris and Wanless (1997).

There was some evidence that this geographical structure was driven by sandeel spatial structure, where the three identified core clusters were situated in separate sandeel sub-population regions. In particular, the sandeel sub-population on the Scottish east coast can be clearly distinguished from other sub-populations (Jiménez-Mena et al. 2020; Wright et al. 2019, 2018) and this was reflected in a strong cluster of colonies with synchronous breeding success. The information on sandeel spatial structure is less complete in Shetland and Orkney, and patterns of kittiwake breeding success synchrony were also less clear here. For example, North Hill (Colony 15) in

the north of Orkney consistently clustered with the Shetland colonies (Figure 5.1c) even though this colony was assigned to the Orkney sandeel sub-population. This could reflect the incomplete knowledge of sub-population borders, but may also reflect the ability of kittiwakes to cross these borders, where Shetland sandeel grounds are within reach for North Hill kittiwakes. Interestingly, when examining the support for different drivers of synchrony, sandeel sub-population structure was included in the most well-supported model when synchrony was measured as r (reflecting both correlated long-term signals and correlated inter-annual differences) but not when synchrony was measured as r_{diff} (reflecting correlated inter-annual differences only). This suggests that synchrony in long-term patterns align better with sandeel spatial structure than synchrony in inter-annual fluctuations. To a large extent, the difference is likely driven by Handa Island (Colony 9) and North Sutor (Colony 16) showing similar long-term patterns to Orkney, but not similar inter-annual fluctuations. In particular, a synchronised drop in breeding success in the 2000s could be seen in all colonies assigned to the Orkney sandeel sub-population. It is possible that this drop is the result of a collapse of the sandeel sub-population around Orkney, which includes an extensive spawning ground (Lynam et al. 2013). This is further supported by a concurrent drop in the breeding success of other sandeel-eating seabirds in Orkney (JNCC 2016) and could potentially be linked to large-scale shifts in environmental conditions occurring around this time impacting sandeel recruitment (see Alvarez-Fernandez et al. 2012). This shows how looking at different metrics of synchrony can be useful, where synchrony in long-term patterns can potentially point to mutual responses to large-scale processes, such as the potential collapse of a sandeel spawning stock in this case. However, caution should be observed when inferring drivers from similar long-term patterns, as they could be the result of separate processes.

Some other features of the data also provide circumstantial evidence supporting sandeel dynamics as a governing force. The scale of synchrony, just over 200 km, is similar to the scale of sandeel synchrony (Wright et al. 2019), where similar scales of synchrony in the hypothesised driver and the target population can be used to infer a causal relationship (Bjørnstad and Falck 2001). However, it should be noted that different mechanisms can generate similar patterns of distance-decay (Abbott 2007) and that between-colony distance is not exactly equal to the distance between the sandeel grounds in which the kittiwakes may be feeding, as they may forage in several directions from the colony (Christensen-Dalsgaard et al. 2018b; Robertson et al. 2014) and at various distances (Thaxter et al. 2012), with differences potentially exacerbated by colonies generally showing segregated foraging areas (e.g. Bolton et al. 2019). In addition to this, in many colonies, in particular in Shetland and on the Scottish east coast, breeding success fluctuated on a biannual time-scale (see Figure 5.3), which fits with similar biannual fluctuations in sandeel recruitment (e.g. Arnott and Ruxton 2002; van Deurs et al. 2009) and thus provides additional support for sandeels as a potential driver of synchrony. Taking all the evidence together, it seems as if the independent and disparate dynamics of sandeel sub-populations filter up to the level of kittiwakes. The role played by sandeels is likely larger further north where sandeel is a more important prey item. In Shetland and Orkney there is an almost total lack of alternative prey for kittiwakes (e.g. Furness and Tasker 2000; Hamer et al. 1993), but the importance appears to decline the further south along

the coast you go (Carter 2014; Furness and Tasker 2000; Wanless et al. 2018).

While the support for sandeel as the main driver was not conclusive, there was even less support for the alternative drivers that were examined: weather conditions and skua predation. When it comes to the role of weather conditions, it is not possible to rule out that the distance effect to some extent is the result of synchrony in weather conditions. However, the lack of support for including additional variation in weather synchrony suggests that it is not a major driver. One minor caveat is that while data on a highly resolved spatial scale were used, the possibility that the direction and exposure of a colony could to some extent determine the impact of weather conditions was not taken into account (Newell et al. 2015). Similarly, there was no evidence suggesting that skua predation was a key driver of the observed synchrony patterns. It should be noted that skua predation was only captured as a driving force in a simplistic way and it is thus not possible to exclude it as a driver of synchrony, at least locally. Further, the vulnerability of kittiwake colonies to skuas will depend to a large extent on how accessible they are (Heubeck 2002), and this was not accounted for in this study. However, the strong synchrony on the Scottish east coast, where skua predation pressure is low, clearly shows that skua predation cannot be the only driver of synchrony.

The spatial independence in breeding success that was identified could have important consequences for the long-term trajectory of the UK kittiwake population as a whole, as uncorrelated fluctuations in population dynamics tend to have a positive impact on long-term persistence (Engen et al. 2002; Heino et al. 1997; Palmqvist and Lundberg 1998). It is clear that the different clusters have shown quite different patterns in breeding success over time (Figure 5.1a, Figure 5.3) and, as expected from the fact that breeding success is an important driver of changes in colony sizes in the UK (Coulson 2017), this spatial variation in breeding success is mirrored by variation in colony size trajectories. In Shetland, breeding success has been variable but often low, with frequent cluster-wide breeding failures, and along these lines, Shetland colonies have experienced substantial declines since the late 1980s (see JNCC 2016). In the Orkney cluster, breeding success was generally high until the early 2000s before dropping and becoming more variable, and this also coincided with a steep drop in colony sizes (see JNCC 2016). On the Scottish east coast, breeding success has generally been quite low and variable, but the cluster has rarely shown cluster-wide failure. While colony sizes have declined here as well, the declines have been more variable and not as steep as further north (see JNCC 2016). The English colonies have generally maintained relatively high levels of breeding success and as a result, declines in colony size have been slower or absent (see JNCC 2016). As such, it is clear that there are spatial patterns both in synchrony and in long-term trajectories.

If the spatial patterns in breeding success that were identified are driven by sandeel spatial structure, this would support the more general hypothesis that trophic interactions with prey displaying spatial synchrony can drive spatial synchrony in predators in some systems (see Liebold et al. 2004). This is in line with previous theoretical studies finding that synchrony can propagate through food webs (Ripa and Ranta 2007), as well as empirical studies finding that synchrony in predators

can be driven by synchrony in their prey (e.g. Haynes et al. 2009), even to the extent that studying the patterns of synchrony in predators can say something about a less well-studied prey population (e.g. Fay et al. 2020). In particular, interactions with prey as a driver of synchrony is likely to be expected where bottom-up effects are strong, such as in this case, where breeding success and food conditions are closely linked in kittiwakes (e.g. Gill and Hatch 2002) and bottom-up effects have been identified as a strong governing force (Frederiksen et al. 2006). In addition, the sedentary behaviour and thus relatively permanent and fine-scale spatial structure of the sandeel population may mean that in this case the prey spatial structure plays an unusually large role in generating synchrony. Still, similar conditions may be found in other systems. For example, a closely related species of the lesser sandeel, the Pacific sandeel (*Ammodytes hexapterus*, now recognised as *Ammodytes personatus*, von Biela et al. 2019), is an important prey for several species of seabirds in a large area of the north Pacific (e.g. Hedd et al. 2006; Litzow et al. 2000), and being very similar to *A. marinus*, it likely also displays clear spatial structure, which seem to filter up to the level of seabirds (Litzow et al. 2000) and is likely to impact their breeding success (see Hedd et al. 2006). Other important forage fish species used by seabirds also tend to show increasingly independent dynamics over space (e.g. Marquez et al. 2019; Östman et al. 2017), which likely impacts spatial patterns of breeding success and long-term population trajectories of seabirds. This work adds to other seabird studies (e.g. Descamps et al. 2017; O’Hanlon and Nager 2018) showing that spatial patterns of population synchrony can provide useful information on ecosystem drivers of population dynamics and over which spatial scale they are acting.

Part IV

General discussion

Chapter 6

Discussion and conclusions

In this chapter, the key results of the thesis are briefly summarised before the results from the different chapters are threaded together and put into the context of some of the larger questions raised in Chapter 1, including what the results tell us about bottom-up energy flow in the zooplankton-sandeel-seabird food chain and how the lesser sandeels (*Ammodytes marinus*, hereafter generally referred to as ‘sandeel’) might respond to future environmental change. Further, the application of the findings to other systems are discussed, and the chapter finishes with pointing to remaining open questions.

Chapter 2 addressed the lack of high-resolution data for exploring the role of food conditions in sandeel dynamics by developing an approach based on temporal interpolation of spatially aggregated Continuous Plankton Recorder (CPR) data corrected for taxon-specific sampling efficiency. While the resulting prey fields do not represent actual conditions on a given day due to the high sensitivity of the CPR to plankton patchiness, uncertainty in correction factors and variability in prey traits, it still goes a long way to producing prey fields of the necessary resolution that capture long-term and large-scale trends. The generated prey fields were then used to examine spatio-temporal patterns in sandeel food conditions, focusing mainly on the North Sea and covering the time period 1975 to 2016. Due to the differences in the timing of the feeding seasons, it was clear that 0 group and 1+ group sandeels experienced different prey fields, with, for example, a larger abundance of smaller copepods during the 0 group feeding season. In the western North Sea, there have been clear declines both in the total amount of energy available to sandeels, especially during the 0 group feeding season, and in the abundance of small copepods, with abundances decreasing by more than 50% during the 0 group feeding season. In terms of *Calanus* spp., there was no clear change in *Calanus finmarchicus* in the examined locations, while *Calanus helgolandicus* showed a clear increase in most of the study area around 2000. The average prey size generally increased over time in the western North Sea, whereas it instead declined in the north-east. However, this was only visible during the 1+ group feeding season.

To be able to determine to what extent this variation in food conditions can explain spatio-temporal variation in sandeel size, a dynamic energy budget growth model was then developed in Chapter 3, which estimates size daily throughout the first sandeel growth season as a function of food conditions, temperature, light conditions as well as size at and timing of metamorphosis. In Chapter 4, the model was then run in six locations: southern Iceland, the Faroes, Shetland and three locations further south in the North Sea, including Dogger Bank, the Firth of Forth and the East Central Grounds (ECG). In the more southerly locations considered, model predictions agreed well with observations in terms of long-term mean lengths, spatial differences in length and the model also reproduced a previously observed decline in length in the north-western North Sea. Agreement with observations in the Faroes and Iceland was poorer, which could potentially be partly explained by the sandeels here metamorphosing later than what was assumed in the model. Food conditions played the main role in driving predicted variation in size, with *Calanus* spp. being particularly important. Timing of metamorphosis also had a substantial impact on predicted sandeel size, with a shift towards the latest date previously observed resulting in a 19% decrease in length. In contrast, the direct effect of temperature was negligible, even at extreme temperature increases.

Finally, in Chapter 5, the extent to which processes occurring in the sandeel population are reflected in the populations of their seabird predators was explored. To do this, geographical patterns in the synchrony of breeding success in black-legged kittiwake (*Rissa tridactyla*, hereafter 'kittiwake') colonies were examined in parts of the UK where sandeels are an important part of the diet. The distance between colonies was a strong determinant of between-colony synchrony but colonies also formed clusters with synchronous breeding success with a clear spatial pattern, which generally aligned with the spatial structure of the kittiwakes' sandeel prey. This suggests that processes occurring at the level of the sandeel propagate up to the level of their seabird predators. The spatial scale of synchrony (around 200 km) also aligns well with previously established scales of synchrony in sandeels.

6.1 Bottom-up energy flow in the sandeel food chain and its implications

The overall aim of the thesis was to contribute to the mechanistic understanding of bottom-up effects in the zooplankton-sandeel-seabird food chain. The focus was mainly on how sandeel growth responds to food conditions. This will directly determine energy availability to upper trophic levels, but through the relationship between size and demographic rates, this may also result in the more traditional interpretation of bottom-up effects in the form of correlated abundances. In this section, findings relating to the response of the sandeel to food and other environmental conditions are discussed first, followed by a discussion of knock-on effects on demographic rates, seabirds and fisheries.

The modelling results suggested that food conditions are the main driver of observed spatial variation in size, confirming a long-standing hypothesis (Bergstad et al. 2002; Boulcott et al. 2007; Macer 1966), and are also likely behind the observed decline in size in the Firth of Forth. Further, the findings support the hypothesis that *Calanus* spp. likely play a particularly large role in explaining spatio-temporal variation, as suggested by Bergstad et al. (2002) (and supported by MacDonald et al. 2018; van Deurs et al. 2015, 2014). While the abundance of *C. finmarchicus* was strongly related to predicted length further north, the relationship was stronger with abundances of *C. helgolandicus* in Dogger Bank and Shetland (Figure 4.6). Several studies have pointed to importance of *C. finmarchicus* for sandeels in the North Sea (Frederiksen et al. 2013; van Deurs et al. 2014, 2009), but recent evidence from Dogger Bank (Henriksen et al. 2018) and the Firth of Forth (MacDonald et al. 2018; Régnier et al. 2017) suggests that the role of *C. finmarchicus* may have been exaggerated and that at least in the Firth of Forth, *C. helgolandicus* may play a larger role both for recruitment and post-metamorphic stages. The findings in this thesis bring further support to this claim.

Further, while the strong dependence on *Calanus* and the finding that an increase in the proportion of larger prey had a positive impact on predicted length (Figure 4.7) both support the idea that prey size has a positive impact on growth, the findings in this thesis also add nuance to this picture. The sandeels in the Firth of Forth have declined in size in spite of the average prey size increasing, at least during the 1+ group feeding season (Figure 2.15), which is in contrast with earlier suggestions that a decline in copepod size may be behind observed declines in sandeel size (MacDonald et al. 2015; van Deurs et al. 2014). In line with this, it was also found that the abundance of small copepods and other small prey types such as appendicularians were strongly related to predicted length in some locations, in particular in the Firth of Forth (Figure 4.6). This points to how the most important aspect of the prey field may vary depending on local conditions, where variation in the abundance of small prey types play a large role in the Firth of Forth where larger prey are scarce, and food conditions are poor overall.

Given the important role of food conditions, a crucial question is then what drives the variation in the sandeel prey field. In terms of *Calanus*, the gradual northward shift of both *C. finmarchicus* and *C. helgolandicus* is likely temperature-driven (Edwards et al. 2020). For North Sea *C. finmarchicus*, which are replenished each year through advective transport from more northerly waters, part of the observed decline may have been caused by a change in current patterns (Heath et al. 1999). In terms of the declining abundances of small zooplankton seen in both the Firth of Forth and the Dogger Bank (Figure 2.9), this has been linked to a decline in primary productivity, which in turn appears to be associated with an increase in temperature in conjunction with decreased nutrient input (Capuzzo et al. 2018). As such, food conditions of sandeels are likely to a large extent linked to temperature, suggesting that indirect effects of temperature could be important.

These indirect effects likely explain the positive correlation between temperature and predicted sandeel length in Shetland (Figure 4.4), where warmer temperatures were associated with the improved food conditions occurring around 2000, which

included an increase in the abundance of *C. helgolandicus* (Figure 2.13). No other location showed a positive relationship between temperature and predicted sandeel length, even though this may have been expected in, for example, the Firth of Forth, where the decline in small copepods may be associated with an increase in temperature (Capuzzo et al. 2018). The lack of a relationship may be partly down to the inability of the CPR dataset to capture inter-annual variability (see Chapter 2 for detailed discussions). Further, it is possible that prey respond to temperature at a very specific part of the year, which is not fully reflected by the average temperature during the sandeel feeding season. Combining this with the marked spatial variation in prey composition, one might thus not expect the indirect relationship between temperature and sandeel growth to be the same across space, and likely not across time either. This idea could potentially at least partly explain why when correlating kittiwake breeding success with temperature, as a proxy for sandeel availability, relationships generally vary between colonies (Carroll et al. 2015; Frederiksen et al. 2007a). Likely, the impact of temperature on recruitment (Régner et al. 2017), which may also vary depending on prey composition, could also play a role in this.

In contrast, the direct effects of temperature on sandeel size were small, which aligns with previous findings (MacDonald et al. 2018). It is possible that not all direct temperature effects were accounted for. Winslade (1974b) found a strong relationship between ingestion rates and temperature (an increase in temperature from 5°C to 15°C resulted in a doubling of ingestion rates). This was suggested to act largely through the impact of temperature on digestion rates, which was incorporated into the model (Equation 3.14), but did not appear to translate into an effect of temperature on predicted length (or predicted ingestion rate, results not shown). Potentially, this could be explained by the sandeels rarely being limited by gut space, either in the model (as suggested by the low sensitivity to parameters related to digestion rate and maximum gut size, Figure 4.5) or in the field (Figure 3.4). However, other direct temperature effects may also contribute to the increased ingestion rate observed by Winslade (1974b), such as an increased detection distance (Gliwicz et al. 2018). Still, along with potential positive effects of increased temperature on net energy gain that may be unaccounted for, there are also negative effects that are unaccounted for, such as the increased loss of energy through nitrogenous excretion (Cui and Wootton 1988; Elliott 1976), which may partly cancel out the positive effects. As such, even if not all potential effects were accounted for, it still seems that, over the range of inter-annual variation experienced by the sandeels, the effect is not likely to be large.

It was also clear that considering variation in phenology is important. Predicted sandeel length was sensitive to both timing of metamorphosis and shifts in the phenology of their prey. The spatial difference in the impact of shifting the phenology of the prey field (Figure 4.7) is in line with the timing and shape of peak food conditions varying spatially (Planque and Fromentin 1996). Further, the difference in the prey field between 0 group and 1+ group sandeels further points to the importance of considering phenology. For example, as abundances were lower and the decline less steep in small copepods during the 1+ group feeding season as compared to the 0 group season in the Firth of Forth (Figure 2.9), the role small copepods have played in observed declines could potentially differ between the two

feeding seasons. As a match between the sandeel foraging season and food abundance is related to sandeel fitness (van Deurs et al. 2010), understanding variation in the phenology of both sandeels and their prey is clearly important.

Finally, the net energy gain was also sensitive to light conditions, in particular turbidity. While a shift towards completely clear waters only resulted in an increase in predicted length of on average 3% (maximum 11%), an increase in turbidity, which was still within values commonly observed in parts of the North Sea inhabited by sandeels (Capuzzo et al. 2018), resulted in a decrease in predicted length by on average 44% (Figure 4.7). As discussed in Chapter 4, it is unclear to what extent larger-scale spatio-temporal patterns in turbidity apply specifically to sandeel grounds. Still, it is clear that at least suspended particulate matter concentrations are not zero in areas of dense sandeel grounds (Wilson and Heath 2019), and primary productivity is also likely to vary over a range that impacts visual conditions for sandeels (van Deurs et al. 2015). van Deurs et al. (2015) suggested that the impact of changes in turbidity will be larger when the sandeel is feeding on smaller prey types. This aligns with the findings here, where the impact was much larger in locations dominated by small prey, such as the Firth of Forth. There are also further pathways through which changes in turbidity may impact sandeels. Increased turbidity may result in a delay of the timing of the spring bloom as a result of reduced light availability (Opdal et al. 2019), which could have knock-on effects on the sandeels through bottom-up effects. At the same time it is possible that predation pressure is reduced as the sandeel predators have a harder time spotting their prey (see e.g. Aksnes 2007). The overall effect of potential changes in turbidity is thus still unclear.

6.1.1 Knock-on effects on sandeel demographic rates

One of the main motivating factors for using a growth model to improve the mechanistic understanding of bottom-up effects in the zooplankton-sandeel-seabird food chain was the strong link between sandeel size and several demographic rates regulating productivity and survival. As a result of this link, the predicted spatio-temporal variation in length presented in Chapter 4 is likely to have knock-on effects on abundance. The energy reserves available at the end of the feeding season have a large impact on overwinter survival (MacDonald et al. 2018; van Deurs et al. 2011a). van Deurs et al. (2011a) suggested a body length of 9.5 cm on 1 August as a threshold for surviving the winter. Although this threshold is approximate and will vary depending on overwintering temperature, the condition of the sandeel and the actual timing of overwintering, the model predictions often fall below this threshold, in particular in the Firth of Forth and Dogger Bank. This suggests that the poor growth in these locations may result in higher rates of overwinter starvation. Along these lines, MacDonald et al. (2018) suggested that inter-annual variation in summer feeding conditions have played a large role in generating inter-annual variation in overwintering mortality in the Firth of Forth.

Based on a one-off survey conducted after overwintering was initiated but before spawning in 1999, Boulcott et al. (2007) found clear spatial differences in 0 group maturation rates, with an estimate of 22% in Fisher Bank, which is close to the

East Central Grounds (average length = 10.9 cm), but 0% in both the Firth of Forth (average length = 8.3 cm) and two Dogger Bank grounds (average length NW Rough = 9.3 cm, Elbow Spit = 9.9 cm). The model predictions align well with the observed spatial variation in size and as the predicted variation was largely the result of variation in food conditions, this suggests that food conditions may play a large role in generating spatial variation in maturation rates. Further, through the strong dependency of maturation rates on size (Bergstad et al. 2001; Boulcott et al. 2007), food-driven inter-annual variation in size will likely also result in variability in the proportion of the 0 group maturing and contributing to the spawning stock. Considering the skew towards younger age groups in the sandeel population, an increase in the maturation rate of 0 group sandeels may have a non-negligible impact on spawning-stock biomass (Boulcott et al. 2007). For those that do mature, their fecundity will also be length-dependent (Boulcott and Wright 2011). In 1 group sandeels, the fecundity of 12 cm sandeels is more than 50% greater than that of 10 cm sandeels (Boulcott and Wright 2011), suggesting that the inter-annual variability in length predicted in the ECG would likely have substantial consequences for the fecundity of potentially maturing 0 group sandeels.

As the relationships between size and both maturation rate and fecundity are non-linear (Boulcott and Wright 2011; Boulcott et al. 2007), it may be that the greatest effect of variation in 0 group size on reproductive rates acts through carry-over effects to the second growth season. Further, as maturation rates respond not only to available reserves but also resource acquisition rates (Boulcott and Wright 2008), it is likely that the change in food conditions documented in Chapter 2 during both the 1+ group and the 0 group feeding seasons not only affects maturation rates via the impact on sandeel size, but also through a more direct effect on maturation rates.

6.1.2 Knock-on effects on seabirds

These knock-on effects on demographic rates may impact the number of sandeels available to seabirds, but variation in size will also have a more direct impact through the amount of energy contained in a single sandeel. In the Firth of Forth, the model predicted a decline in sandeel length by 0.4 mm per year during both the period of peak chick energy demand in razorbills (*Alca torda*) and Atlantic puffins (*Fratercula arctica*, hereafter ‘puffin’) and the period of peak chick energy demand in kittiwakes (based on estimated time of peak demand from Burthe et al. 2012) over the study period (1982-2016). This corresponds to a decline in energy content of individual 0 group sandeels of about 60% at the time of razorbill and puffin peak energy demand, and a decline of 51% at the time of kittiwake peak energy demand. This decline will have consequences for the number of sandeels that need to be caught to fulfil the energetic demands of the seabirds. For example, based on the energy demand of kittiwake chicks (490 kJ at 15 days; Galbraith 1983), this decline translates into an increase from 87 to 177 sandeels needed to fulfil the requirements of the chick. The absolute difference may be even larger as kittiwakes may raise several chicks. For puffins, which have an earlier phenology and thus feed on smaller sandeel, the required catch per day by each puffin parent to meet their own metabolic costs

and to provide their share of chick-feeding (1193 kJ; Harris and Wanless 2011) increased from 316 to 778 sandeels over the study period. This difference may be further exacerbated by the need of the puffin to meet increased energetic demands associated with the increased foraging effort of catching more sandeels.

This increased effort could be expected to be reflected in seabird breeding success. In line with this, several sandeel-eating species on the Isle of May in the Firth of Forth have shown a sustained decline in breeding success (Lahoz-Monfort et al. 2013) alongside the observed and predicted decline in sandeel size. Further, the breeding success of kittiwakes at Flamborough Head, which have a foraging range that includes Dogger Bank (Carroll et al. 2015), is generally higher than that in Firth of Forth colonies (Figure 5.3), which aligns with both observed and predicted differences in size between these two locations (Figure 4.4). However, it was clear that predicted patterns of size do not fully align with patterns of breeding success. For example, in Shetland, the model predicted an increase in length just after 2000 as food conditions became better for the sandeel, for example through an increase in *C. helgolandicus* abundances (see Figure 2.13). However, the predicted increase in length does not agree with observations (see Harris and Wanless 2011), suggesting that the changes seen in post-metamorphic food conditions were not reflected in sandeel growth. One possible explanation is that the observed small sandeel sizes after 2000 (Harris and Wanless 2011) were the result of low larval growth rates, as a study by Alvarez-Fernandez et al. (2012) found that a decline in the abundance of fish larval food occurred around this time in the North Sea, which aligned with a decline in sandeel recruitment and could possibly have extended up to Shetland. Interestingly, the predicted shift in sandeel size coincides with poorer seabird breeding success in this region (Figure 5.3, JNCC 2016), potentially as a result of the low sandeel recruitment rates. Whatever the mechanism, it is clear that something changed substantially in Shetland and Orkney around 2000.

From the perspective of the seabirds, changes in sandeel growth rates are to some extent similar to a shift in the timing of metamorphosis, as both results in the size on a given day being smaller. On the Isle of May, the date the 0 group sandeels reach a given threshold size has become increasingly later since the beginning of the 1980s (Burthe et al. 2012). The study by Burthe et al. (2012) reports concurrent delays in seabird phenology that may reduce this effect, and so far, the mismatch does not seem to have had an impact on seabird breeding success. In terms of phenology, another potential mechanism that may impact seabirds is the tendency of sandeels to initiate overwintering earlier when food conditions are good and they have accumulated sufficient reserves (e.g. MacDonald et al. 2018). This earlier overwintering may impact several species of seabirds through 1+ groups disappearing from the water column earlier (Rindorf et al. 2000). If overwintering is initiated when growth curves level off (see Figure 4.3), the results in this thesis suggest that the time of year when the sandeels disappear from the water column may vary both over space and time. If this finding also applies to 1+ group sandeels, this may have knock-on effects for seabirds. An interesting observation is that in 2008, kittiwakes on the Isle of May, which switch from feeding on 1+ group early on in the season to feeding on 0 group (Lewis et al. 2001), stopped feeding on 1+ group sandeel so early that monitoring missed it (Francis Daunt, pers. comm.), and this coincided with model

predictions by MacDonald et al. (2018) suggesting that the sandeels overwintered particularly early in this year as a result of good food conditions (there were not sufficient CPR data to make a prediction for this year in Chapter 3). This year was also associated with poor kittiwake breeding success (Figure 5.3). Contrary to traditional linear bottom-up effects, this thus suggests that kittiwake breeding success may decrease in years when the food conditions for sandeels are particularly good.

Finally, the findings of Chapter 5 suggest that sandeels play a role in structuring the dynamics of at least their kittiwake predators. Further, there was no evidence to suggest that weather or predation by great skuas (*Stercorarius skua*) drove the dynamics of the kittiwakes, supporting the view of the sandeel-mediated bottom-up regulation of seabirds in this region (Frederiksen et al. 2006). The lack of an impact of weather conditions also suggests that any impacts of climate change on kittiwakes are likely to act through their sandeel prey, rather than via direct impacts, thus supporting both the prevailing view in this system (MacDonald et al. 2015) and the general conclusion that the impact of climate change on top predators is most likely to act through their prey (Sydeman et al. 2015).

6.1.3 Implications for fisheries

While no sandeel fishery ever operated in Iceland (Vigfúsdóttir 2012) or the Faroes (Eliassen 2013), there is a fishery operating in the North Sea. The management of the North Sea fishery is divided into stock assessment areas that are defined mainly based on larval dispersal patterns (ICES 2017), but which are also reflected in studies of otolith chemistry (Gibb et al. 2017; Wright et al. 2018), to some degree in genetic studies (Jiménez-Mena et al. 2020) and in the degree of synchrony in abundances (Wright et al. 2019). To a large extent, the spatial configuration of clusters of kittiwake colonies with synchronous breeding success (Chapter 5) mirrors the spatial structure of the sandeel population, suggesting that this spatial management aligns well with a management approach that considers the fished species in its full ecosystem context.

The sandeels in the different stock assessment areas are of very different sizes, which was reproduced by the model. Sandeels in SA4 (which includes the Firth of Forth) are smaller than sandeels in SA1 (which includes Dogger Bank), which in turn are smaller than those in SA3 (which includes the ECG) (Bergstad et al. 2002; Boulcott et al. 2007; ICES 2017; Rindorf et al. 2016). As catches tend to be measured in biomass, understanding variation in size over space and time is important for estimating population sizes and setting fishery targets. For example, Rindorf et al. (2016) found that over space, the variation in the weight of age 2 sandeels resulted in a four-fold difference in the number of sandeels per kg, which would have large implications for the number of sandeels a certain biomass target corresponds to. Further, due to the link with demographic rates, pinpointing drivers of growth contributes to the understanding natural variability in non-fishing mortality and recruitment, which is also important for understanding the dynamics of the fished populations. In addition, sandeels provide an important food source for several species of piscivorous fish, which themselves are fished (Engelhard et al. 2014). Engelhard et al. (2013)

found that in Dogger Bank, the body condition of several commercially important species fished for human consumption was linked to the availability of sandeels. This suggests that improving the understanding of the drivers of sandeel dynamics may also have implications for understanding the dynamics of their fish predators.

6.2 How may sandeels be affected by projected environmental change?

A major motivating force of this work were the rapid environmental changes that have been observed in the study system, and the consequences these might have on all levels of the food chain. So based on the findings of this thesis, what might be expected to occur as the environment continues to change?

One of the most prominent consequences of climate change is an increase in temperature, which is also expected to continue to occur in the study system (Schrum et al. 2016). As the response to the direct effects of temperature on predicted sandeel length was close to zero on average, this is not likely to have a strong impact on future growth patterns. However, through the interaction with food, which is a result of the balance between the positive effects of temperature on assimilation and digestion rate and the positive effect on metabolic rates, the negative impact of poor food conditions could be exacerbated (Figure 4.7). For example, in the Firth of Forth in 2016, when food conditions were poor, an increase in temperature by 2°C resulted in a decrease in the predicted sandeel energy content by 1 August from 1.8 to 1.7 kJ, whereas the more extreme temperature scenario of a 4.5°C increase resulted in an energy content of 1.6 kJ. In contrast, looking at the ECG in the year 2009, when food conditions were good, an increase in temperature by 2°C resulted in an increase in the predicted energy content by 1 August from 27.2 to 27.8 kJ, whereas the more extreme temperature scenario of a 4.5°C increase resulted in an energy content of 28.0 kJ, indicating that impact of good food conditions may be amplified. This means that if the spatial differences in food conditions are maintained, the spatial variation size may be strengthened as temperatures increase. However, the effect is very small compared to the existing spatial differences.

Likely, indirect effects of increased temperatures will have a bigger impact. One of the most common responses to increasing temperatures in marine ecosystems is a shift in phenology (Poloczanska et al. 2013). As larval sandeels and their prey become increasingly mismatched as temperatures increase (Régner et al. 2019), a shift towards a later date of metamorphosis may be expected. This is likely to have a negative impact on size, with a shift from the default date of metamorphosis (day 141) to the latest observed date (end of June) resulting in an average decrease in predicted length on 1 August of 19%. Due to the nonlinear growth curve, the impact is even more dramatic earlier on in the growth season. At the same time, the sandeel's zooplankton prey is likely to shift towards an earlier phenology (Richardson 2008). The model results show that the impact of this depends on the current shape of the prey abundance peak. For example, a shift towards an earlier phenology is beneficial in the Firth of Forth where peak abundances generally occur later.

Northward shifts is another common response to increased temperatures (Poloczanska et al. 2013). The distribution of several zooplankton taxa are expected to shift rapidly northwards in the study system (Edwards et al. 2020). As part of this, the shift from a system dominated by *C. finmarchicus* to one dominated by *C. helgolandicus* is will likely to continue. In the ECG, this shift was predicted to have a negative impact on length as a result of the different phenologies of the two species, even if the total yearly abundance was kept constant (Figure 4.7). The effect may be further exacerbated by the fact that peak abundances of *C. helgolandicus* are unlikely to match those of *C. finmarchicus* previously observed in the ECG (Edwards et al. 2020). However, in the case of the more westerly locations where abundances of *C. finmarchicus* have generally been low compared to the ECG (Figure 2.10), the increase in *C. helgolandicus* may instead be beneficial. In terms of Iceland and the Faroes, the environmental suitability for *C. finmarchicus* is expected to decline (Frederiksen et al. 2013) while abundances of *C. helgolandicus* are still low (Figure 2.12). This does not seem promising considering the strong link in both locations between predicted length and abundances of *C. finmarchicus* and younger stages of *Calanus* (Figure 4.7).

Finally, in addition to shifts in phenology and distribution, zooplankton, like the sandeels, will likely show a shift to smaller sizes (Daufresne et al. 2009). If all else is kept constant, a shift to smaller prey is likely to have a negative impact on sandeel length (Figure 4.7), but as is seen in the Firth of Forth and discussed above, the impact will depend on what actually drives the change in size, a decline in small taxa or an increase in large taxa. As such, as the decline in small copepods may be expected to continue with further temperature-linked decreases in primary productivity (Capuzzo et al. 2018), this may result in a continued increase in the average size of prey in the Firth of Forth, but sustained declines in sandeel size unless other prey types increase. In the ECG, the average prey size has instead decreased over time (Figure 2.15), and may continue to do so if the declines in the abundance of *C. finmarchicus* continues further, which may similarly be the case up towards Iceland and the Faroes. A potential decline in prey size could interact with changes in turbidity. Turbidity may increase with climate change through changed hydrodynamic conditions (Capuzzo et al. 2015), but at the same time, further declines in primary productivity (Capuzzo et al. 2018) may instead result in a decrease in turbidity. If on the whole it results in an increase in turbidity, any negative effects of a reduced prey size may be exacerbated.

Although this is not an exhaustive review, it is evident that the overall effect of climate change on sandeel growth is not clear. It is clear however that the impact is likely to vary by location, which is a general pattern in changes in size as a response to climate change (Ohlberger 2013). Locations that depend strongly on *C. finmarchicus*, in particular the ECG, are likely to be negatively impacted by its continued decline. Instead, more southerly locations such as Dogger Bank and the Firth of Forth could potentially benefit from an increase in *C. helgolandicus* and a better match with peak food conditions. Further, impacts of ongoing environmental change on sandeels are not limited to impacts on growth rates. While the impact of food conditions on energy reserves is likely to be the most important driver of both overwinter survival (MacDonald et al. 2018) and reproductive investment (Boul-

cott and Wright 2008), increased temperatures during the overwintering period may still have an additional, negative, impact (MacDonald et al. 2018; Wright et al. 2017a). Temperature increases are also expected to increase the mismatch between the timing of hatching and availability of larval food, leading to lower recruitment (Régner et al. 2019). Importantly, as sandeels are restricted by very particular habitat requirements, this reduces their ability to respond to increased temperatures by shifting their distribution (Heath et al. 2012). Finally, changes that are not necessarily connected to climate change, such as the ongoing increase in predation mortality in the southern North Sea (ICES 2017), will likely also have a big impact on sandeel abundances. This trend may be expected to continue as sandeel predators recover from over-fishing (Frederiksen et al. 2007b).

6.2.1 Implications for seabirds

These expected changes in the sandeel populations are likely to have knock-on effects on seabirds through the mechanisms discussed above (Section 6.1.1), resulting in indirect effects of climate change. However, in addition to previously identified patterns, it is also possible that tipping points will be crossed. For example, while the decline in sandeel size-at-date so far has not had a large impact on the Isle of May seabirds (Burthe et al. 2012), it is possible that continued poor growth rates in conjunction with a possible delay in the timing of metamorphosis will eventually result in a sharper drop in breeding success.

The availability of alternative prey is likely an important determinant of how seabirds may respond to future changes in the sandeel populations. Even in locations where sandeels have made up the majority of the diet in the past couple of decades, there have been increases in the proportion of non-sandeel prey in the diet of several seabird species. On the Isle of May, this increase has mainly been in the form of sprat (*Sprattus sprattus*) (Wanless et al. 2018). The shift aligns both with a decline in the local sandeel population and a recovery of the sprat population, which collapsed in the 1980s but appears to be favoured by the increasing temperatures (Wanless et al. 2018). This expansion of alternative prey could potentially have contributed to the slightly more encouraging trends in breeding success and abundance seen in several British seabird populations in recent years (JNCC 2020). However, while sprat may provide a good alternative food source, the continued northward shift of the forage fish community as a result of increasing temperatures means that it may only be a short-term solution (MacDonald et al. 2015).

6.3 Implications for the understanding of other zooplankton-forage fish-seabird food chains

The zooplankton-forage fish-seabird food chain is one replicated in many marine ecosystems, and so are several of the patterns observed in this study system (for example, a decline in forage fish size, an increase in temperature). This suggests that some of the insights from this work can be transferred to other food chains of similar structure.

6.3.1 Other *Ammodytes* spp.

Other species of the same genus as *A. marinus* have a similar life-cycle and play a similar role in other food webs (Robards et al. 1999a), suggesting that some of the findings here could also apply to these other species. As is the case for *A. marinus*, several studies of other *Ammodytes* spp. have identified relationships between sandeel dynamics and temperature. Robards et al. (2002) found that *Ammodytes hexapterus* (now recognised as *Ammodytes personatus*, von Biela et al. 2019) in the Gulf of Alaska showed a positive correlation between growth and temperature within sites whereas across sites it was instead found that the sandeels in the warmest grounds showed the slowest growth. Further, von Biela et al. (2019), also in the Gulf of Alaska, showed that a heatwave reduced the length and condition of *A. personatus*, even though the sandeels in this region are normally do well in warmer years, as found by Robards et al. (2002). Both studies suggested that the relationship with temperature was the result of indirect effects acting via the prey of the sandeel. This conclusion is supported by results in this thesis, which suggest that direct effects of temperature are small in *A. marinus*. As such, the key to understanding the impact of increasing temperatures on growth in *Ammodytes* spp. likely lies in understanding the impact of temperature on their prey. However, experimental work on *A. personatus* by Tomiyama and Yanagibashi (2004) found that the body condition of *A. personatus* was reduced when temperatures exceeded 20°C, even though food was not limiting. It is unclear whether this effect is the result of the standard nonlinear effect of temperature on metabolic rate, or an elevated response to extreme temperatures. Nevertheless, the finding suggests that at temperature extremes, direct effects may still be important.

The results in this thesis also suggest that turbidity is able to have a large impact on sandeel ingestion rates through obstructing their visual field. While this may not have a substantial impact on offshore species, such as *A. marinus*, it is possible that the impact may be larger in other *Ammodytes* spp, such as *Ammodytes tobianus*, which inhabit nearshore waters that may be more turbid (Robards et al. 1999a). One study of larval *Ammodytes* spp. found that in Hudson Bay, Canada, foraging was at times limited by the turbidity introduced by river discharge (Gilbert et al. 1992), but in general, few studies have examined the role of turbidity in limiting intake rates in *Ammodytes* spp.

6.3.2 Lessons learnt about understanding variation in size and bottom-up effects in forage fish

A decline in size, which is considered to be one of the universal responses to climate change (Daufresne et al. 2009), has been observed in several species of forage fish (Baudron et al. 2014; Daufresne et al. 2009). The results of this thesis suggest that changes in food conditions are sufficient to explain the decline in size observed in the Firth of Forth, and that direct effects of temperature do not play a large role. A change in food conditions is often not considered as an explanation for observed declines (Sheridan and Bickford 2011), but these results suggest that it is an important mechanism to investigate. Further, this thesis also highlights that more subtle impacts, such as the effect of turbidity on ingestion rates in visual foragers, should be considered in future studies. Along these lines, an increase in turbidity has previously been linked to a decline in fish biomass in the Black Sea (Aksnes 2007). Further, phenology was identified as having a large impact on predicted size, and considering that shifts in phenology is another common response to climate change (Poloczanska et al. 2013), this is another driver that may be useful to consider.

In terms of the impact of food conditions, this thesis highlights the importance of considering the correct scale. Absolute abundances and trends in food conditions may vary widely over space, and this may also depend on which part of the year is considered (see Chapter 2). As such, trends based on data aggregated over large areas, or aggregated over a large part of the year, may not necessarily be informative. For example, *C. finmarchicus* has been reported to decline in the North Sea (Beaugrand 2004; Beaugrand et al. 2003; Planque and Fromentin 1996), but this effect is mainly driven by the decline in the north-eastern North Sea, with very minor changes visible in, for example, Dogger Bank and the Firth of Forth. The importance of considering the correct spatial scale is further emphasised by the clear spatial independence in the breeding success of kittiwakes (Figure 5.2), which suggests that any drivers examined need to be resolved on this scale (around 200 km).

Further, the taxonomic resolution of the prey field may also be important. The results in Chapter 4 suggest that the abundances of several different prey types are related to predicted growth, and that the impact of variation in the prey field as well as in other environmental conditions to a large extent depends on the relative abundances of different prey types. The use of a prey field with high taxonomic resolution may also explain why some expected relationships, such as the positive relationship between prey size and intake rate (van Deurs et al. 2015, 2014), do not always come through in the correlation between input data and model results. For example, as discussed above, years of larger average sandeel sizes in the Firth of Forth were generally the result of a low abundance of small prey rather than an increase in the abundance of large prey, which resulted in a negative relationship between average prey size and predicted lengths in the Firth of Forth (Figure 4.6). This suggests that, while prey size may have a positive effect on growth rates in theory (Ljungström et al. 2020; MacDonald et al. 2018; van Deurs et al. 2015, 2014), the overall association will also depend on the abundance and composition of the prey field.

The results of the thesis also highlight the usefulness of mechanistic modelling and how it complements observational datasets. For instance, it was clear that growth cannot be directly deduced from food conditions, as, for example, the decline in energy availability in Dogger Bank seen in Chapter 2 did not translate into a predicted decline in size in Chapter 4. In addition, the dynamic energy budget model also made it possible to quantify the direct impact of temperature on sandeels, and its interaction with food conditions, leading to the conclusion that temperature effects are more likely to be indirect. The mechanistic modelling approach thus helps to understand the mechanisms underlying associations between temperature and size, and makes it possible to extrapolate to future scenarios.

6.4 Potential directions for future work

As food conditions are the main driver of sandeel growth, and are likely also the main driver of recruitment (Henriksen et al. 2018; Régnier et al. 2017), focusing the attention on the interaction between sandeel and their prey and drivers of prey dynamics is likely to prove most fruitful. For example, Chapter 4 showed that predicted sandeel lengths were strongly related to the abundance of *Calanus* I-IV, suggesting that further exploring the impact of earlier copepodite stages of *Calanus* on sandeel growth and abundance may be useful. In the CPR, *C. finmarchicus* and *C. helgolandicus* are not separated in their earlier stages. However, considering the different phenology of the two species, understanding how the shift towards an increased domination of *C. helgolandicus* impacts changes in the abundance and phenology of earlier copepodite stages may be key for predicting the impact of the shift on sandeel growth rates. Further, the results of the comparison between modelled and observed sandeel length (Figure 4.2) suggest that sandeels may be metamorphosing earlier further north. Exploring this further would be useful as it would help to delineate the time window in which potential impacts of food conditions would be acting. This could potentially be done, at least at a coarse temporal scale, using records of sandeel larvae collected by the CPR (see Lynam et al. 2013).

While questions still remain regarding bottom-up effects, the relative importance of top-down versus bottom-up effects may make up a larger gap in knowledge. The results of this thesis suggest that variation in food conditions result in variation in sandeel size, which is likely to have knock-on effects on abundance. However, after accounting for top-down effects, as well as drivers of variation in recruitment not related to the energy reserves of the spawners, are the impacts of these bottom-up effects on the amount of energy available to top predators still visible?

In terms of the relationship between sandeels and their seabird predators, one of the largest unknowns is what factor(s) constitute the biggest driver(s) of breeding success, and how this may vary between seabird species. Identifying the most important driver of seabird breeding success is important as environmental drivers may differ. For example, if abundance of 0 group is the key driver, the timing and abundance of larval food may be of large importance (e.g. Henriksen et al. 2018; Régnier et al. 2017) whereas food conditions during the 1+ group feeding season are likely to be more important if the timing of overwintering of 1+ group plays a large

role (MacDonald 2017). At the Isle of May, several studies examining the relationship between different sandeel metrics and seabird breeding success were conducted in the early 2000s (e.g. Daunt et al. 2008; Frederiksen et al. 2006; Rindorf et al. 2000; Wanless et al. 2007). Since then, datasets have been extended and new types of data have become available, and a re-examination of these relationships could prove fruitful. Available datasets include annual abundance estimates from Marine Scotland Science December dredge surveys (1999-2003, 2008-present), estimates of hatching dates based on larval samples from Stonehaven (2000-present, Régnier et al. 2019), estimates of metamorphosis dates (7 years 1999-2013, Régnier et al. 2017) and length estimates of both 0 group and 1+ group sandeels from the long-term puffin survey (Wanless et al. 2018). These data can be supplemented by and validated against data from more intensive short-term surveys (e.g. Greenstreet et al. 2006). Further, the model presented here, in unison with the model developed by MacDonald et al. (2018) or a refined merge of the two (see developments suggested in Chapter 4), could provide time series of daily size estimates and overwintering dates. Using the puffin time series, it would also be possible to obtain a longer time series of metamorphosis dates through predicting the day on which the sandeels must have metamorphosed to achieve the observed length on the given day. To reduce the impact of the variability in the CPR prey fields, the model could be run on the Stonehaven dataset (as in MacDonald et al. 2018, but with increased resolution of prey types).

Finally, as seabird colonies with a diet previously dominated by sandeels may be shifting to a larger proportion of non-sandeel prey such as sprat (Wanless et al. 2018), understanding the dynamics of these alternative food sources will be necessary to understand potential future bottom-up effects in this system. Even if different species of forage fish may be able to replace each other in terms of their role in the food web, the response to lower trophic levels and to environmental conditions may vary significantly (Cury et al. 2003). For example, sprat usually occurs in warmer waters than the sandeel and, unlike the winter-spawning capital-breeding sandeel, sprats are spring-spawning income-breeders (Heath et al. 2012), suggesting that critical periods of the annual cycle as well as responses to environmental change may differ.

6.5 Conclusions

Like sandeels and their seabird predators, populations of forage fish and seabirds are showing rapid declines in several marine ecosystems (Hutchings et al. 2010; Paleczny et al. 2015; Sydeman et al. 2015). Seabirds, which are endothermic and have high energy requirements, are highly sensitive to changes in their forage fish prey (Sydeman et al. 2015). As indicated by the findings in this thesis, the response of the forage fish to environmental change is likely to vary depending on factors such as the timing of the annual cycle, the degree to which they rely on visual foraging and what type of prey they depend on in a given location. As such, obtaining a mechanistic understanding of the response to environmental change based on the biology of the forage fish is key for teasing apart the key pathways of impact. This mechanistic understanding makes it possible to improve our predictions of the impact of expected environmental change on both forage fish and seabirds. Ideally, this will allow us to identify vulnerable populations and locations, enabling us to reduce additional stressors – through for example reducing fishing pressure or establishing marine reserves – ahead of time to minimise the overall impact as much as possible.

Appendix A

Appendix for Chapter 2

Table A.1: Corresponding taxa in the Continuous Plankton Recorder (CPR) and Stonehaven datasets used when developing correction factors. Copepods in the CPR dataset are generally adults (stages V and VI, Richardson et al. 2006).

CPR taxa	Stonehaven taxa
<i>Acartia</i> spp.	<i>Acartia clausi</i> V–VI <i>Acartia longiremis</i> VI
Appendicularia	Appendicularia
<i>Calanus finmarchicus</i>	<i>Calanus finmarchicus</i> V–VI
<i>Calanus helgolandicus</i>	<i>Calanus helgolandicus</i> V–VI
<i>Calanus</i> I–IV	<i>Calanus</i> spp. I–IV
<i>Calanus</i> V–VI (unidentified)	No equivalent
<i>Centropages hamatus</i>	<i>Centropages hamatus</i> V–VI
<i>Centropages typicus</i>	<i>Centropages typicus</i> V–VI
<i>Centropages</i> spp. (unidentified)	
Copepod nauplii	Copepod nauplii
Decapoda larvae	Decapoda larvae <i>Nephrops norvegicus</i> larvae
Euphausiacea	<i>Nyctiphanes couchii</i> juvenile <i>Nyctiphanes couchii</i> adult <i>Thysanoessa inermis</i> adult <i>Thysanoessa longicaudata</i> adult
<i>Evadne</i> spp.	<i>Evadne nordmanni</i>

Fish eggs	Pisces eggs
Fish larvae	Ammodytidae larvae Clupeidae larvae Gadiformes larvae Pisces larvae
Hyperiidia	<i>Hyperia</i> spp. <i>Themisto</i> spp.
<i>Metridia lucens</i>	<i>Metridia lucens</i> V–VI
<i>Oithona</i> spp.	<i>Oithona</i> spp. IV–VI
<i>Para-Pseudocalanus</i> spp. (also includes unidentified small copepods)	<i>Paracalanus parvus</i> V–VI <i>Pseudocalanus elongatus/minutus</i> V–VI <i>Ctenocalanus vanus</i> V–VI <i>Microcalanus pusillus</i> I–VI <i>Para-/Pseudo-/Cteno-/Clausocalanus</i> I–IV
<i>Podon</i> spp.	<i>Podon</i> spp. <i>Podon leuckartti</i> <i>Podon intermedius</i>
<i>Temora longicornis</i>	<i>Temora longicornis</i> V–VI

Appendix B

Appendix for Chapter 4

Table B.1: Based on the arguments outlined in Section 4.2.1, there are three search classes, each associated with specific prey characteristics. Search class A include small copepods (<1.3 mm) and other small prey, search class B include large copepods (>1.3 mm) and search class C include large crustaceans and fish larvae.

Taxon	Search class	Motivation
<i>Acartia</i> spp.	A	Small copepod < 1.3 mm
Appendicularia	A	Small zooplankton (~ 1 mm)
<i>Calanus finmarchicus</i>	B	Large copepod > 1.3 mm
<i>Calanus helgolandicus</i>	B	Large copepod > 1.3 mm
<i>Calanus</i> I–IV	B	Large copepod > 1.3 mm
<i>Calanus</i> V–VI	B	Large copepod > 1.3 mm
<i>Centropages hamatus</i>	B	Large copepod > 1.3 mm
<i>Centropages typicus</i>	B	Large copepod > 1.3 mm
<i>Centropages</i> spp.	B	Large copepod > 1.3 mm
Copepod nauplii	A	Small zooplankton (< 1 mm)
Decapoda larvae	A	Small zooplankton (~ 1 mm)
Euphausiacea spp.	C	Large crustacean (~ 17 mm)
<i>Evadne</i> spp.	A	Small zooplankton (< 1 mm)
Fish eggs	A	Small zooplankton (~ 1 mm)
Fish larvae	C	Fish larvae (~ 12 mm)
Hyperiidia spp.	C	Large crustacean (~ 16 mm)
<i>Metridia lucens</i>	B	Large copepod > 1.3 mm
<i>Oithona</i> spp.	A	Small copepod < 1.3 mm
<i>Para-Pseudocalanus</i> spp.	A	Small copepod < 1.3 mm
<i>Podon</i> spp.	A	Small zooplankton (< 1 mm)
<i>Temora longicornis</i>	A	Small copepod < 1.3 mm

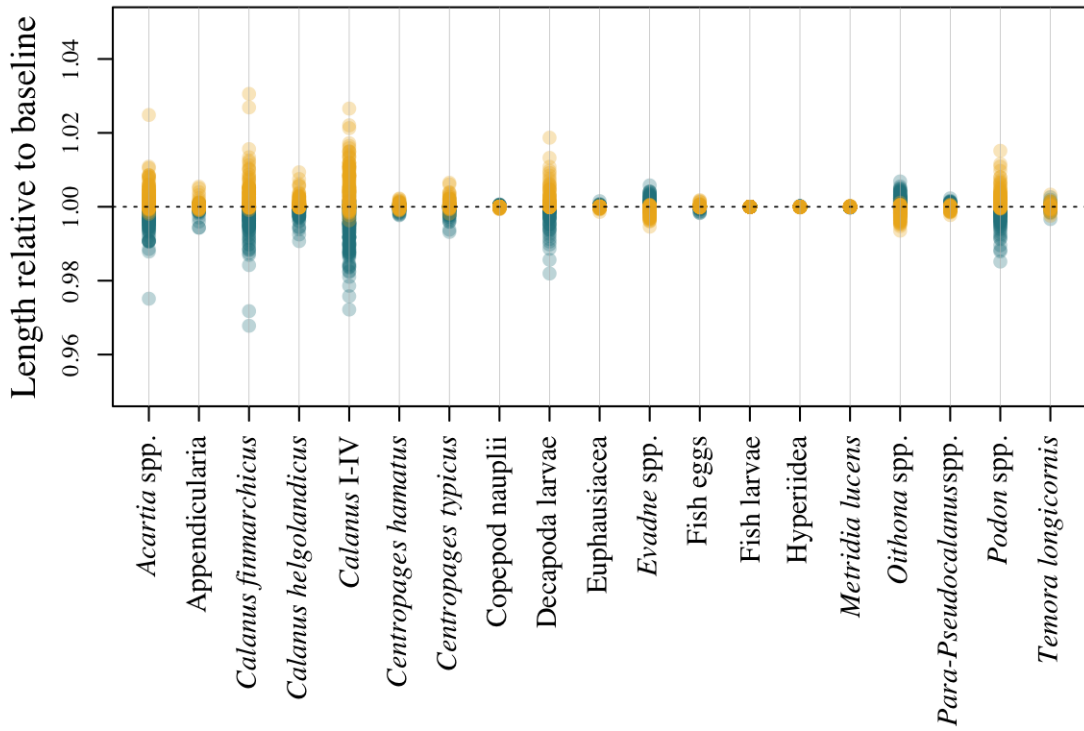


Figure B.1: Sensitivity analysis based on 10% decrease (blue markers) and increase (yellow markers) in the **correction factors** applied to each prey type (see Table 2.3 for nominal values), with each point representing a different location-year combination. y-axis shows predicted length on day_{OW} in proportion to the baseline scenario of the correction factors of all prey types being at their nominal values.

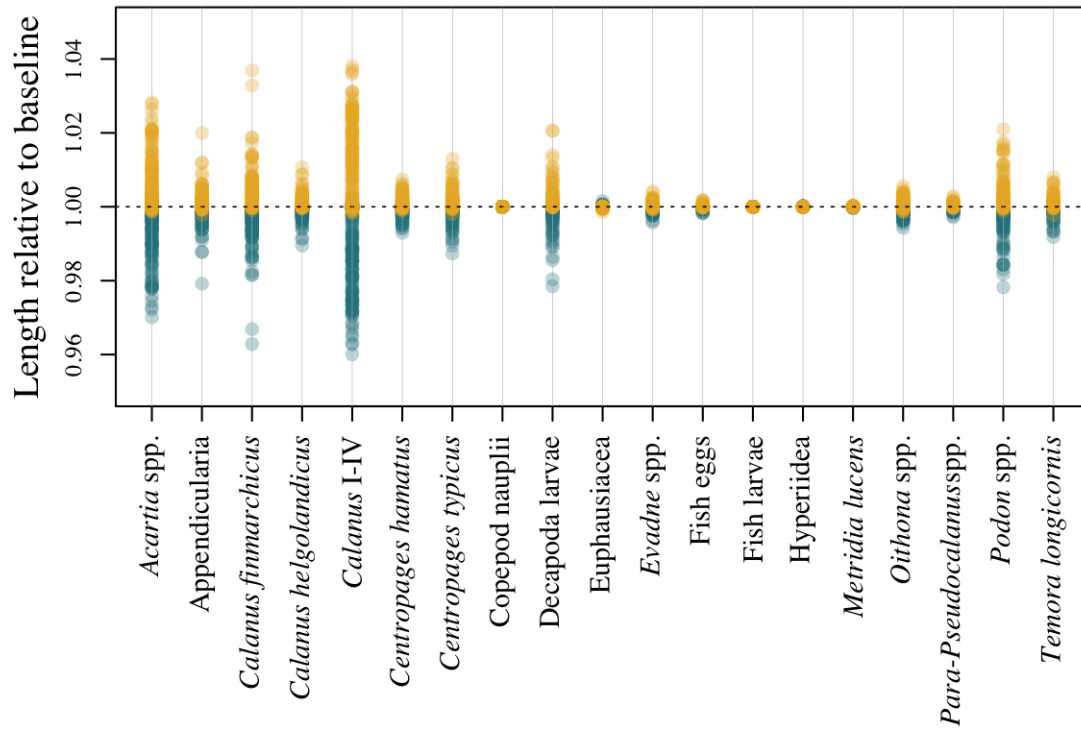


Figure B.2: Sensitivity analysis based on 10% decrease (blue markers) and increase (yellow markers) in the **energy content** of each prey type (see Table 2.4 for weight and energy density used to calculate nominal values), with each point representing a different location-year combination. y-axis shows predicted length on day_{OW} in proportion to the baseline scenario of the energy content of all prey types being at their nominal values.

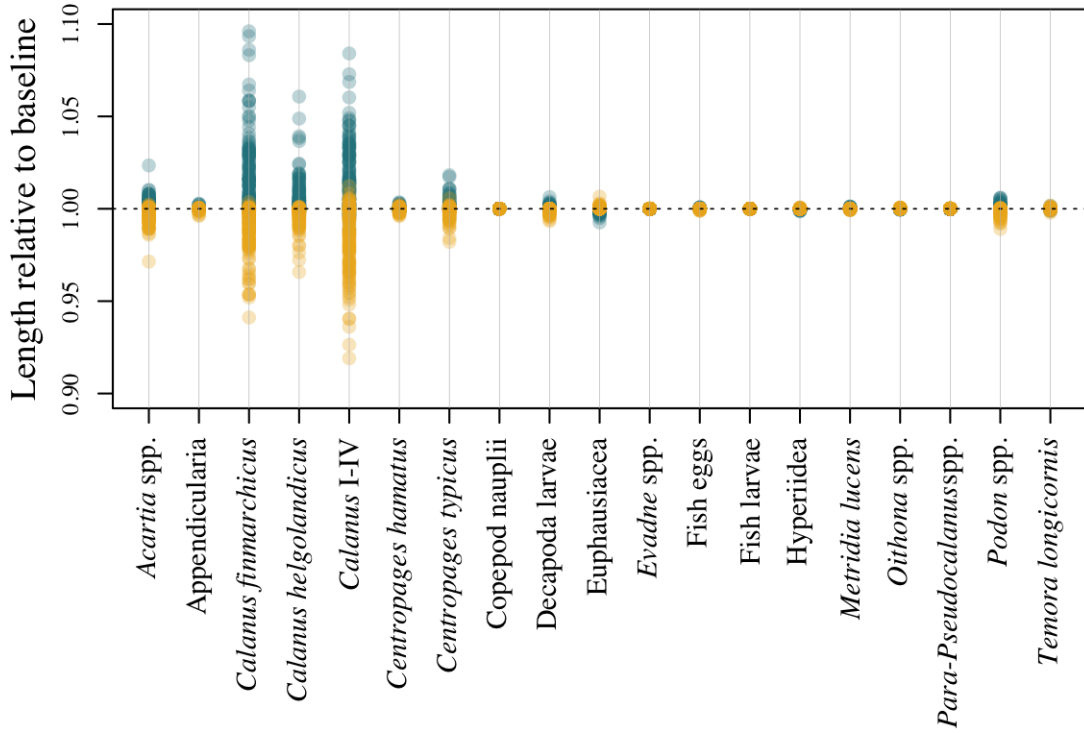


Figure B.3: Sensitivity analysis based on 10% decrease (blue markers) and increase (yellow markers) in the **size** of each prey type (see Table 2.4 for nominal values), with each point representing a different location-year combination. y-axis shows predicted length on *day_{OW}* in proportion to the baseline scenario of the size of all prey types being at their nominal values.

Table B.2: Output from models fit between environmental drivers and predicted length on *day_{OW}*. lm denotes linear models of untransformed data and log denotes linear models of log₁₀-transformed data. Relationships are depicted in Figure 4.6. FoF = Firth of Forth, DB = Dogger Bank, Shet = Shetland, ECG = East Central Grounds, Ice = Iceland, Faro = Faroes (see Figure 4.1 for locations).

Driver	Loca- tion	lm slope	lm p	lm R ² (%)	log slope	log p	log R ² (%)
<i>Acartia</i> spp.	FoF	3.3×10^{-4}	0.02	18	9.4×10^{-2}	<0.01	47
<i>Acartia</i> spp.	DB	7.1×10^{-5}	0.19	2	1.9×10^{-2}	0.05	9
<i>Acartia</i> spp.	Shet	7.8×10^{-5}	0.41	-1	4.4×10^{-3}	0.84	-3
<i>Acartia</i> spp.	ECG	6.7×10^{-5}	0.90	-5	1.6×10^{-2}	0.57	-3
<i>Acartia</i> spp.	Ice	-5.2×10^{-5}	0.98	-12	4.9×10^{-3}	0.86	-12
<i>Acartia</i> spp.	Faro	4.7×10^{-5}	0.74	-11	1.1×10^{-2}	0.62	-9
Appendicularia	FoF	5.9×10^{-4}	0.60	-3	5.1×10^{-2}	0.02	18
Appendicularia	DB	4.9×10^{-3}	0.43	-1	-5.0×10^{-3}	0.67	-3
Appendicularia	Shet	-7.9×10^{-4}	0.01	14	-4.3×10^{-2}	0.01	18
Appendicularia	ECG	2.5×10^{-4}	0.69	-4	4.4×10^{-3}	0.76	-4
Appendicularia	Ice	-9.0×10^{-3}	0.06	28	-1.4×10^{-2}	0.58	-8
Appendicularia	Faro	4.2×10^{-3}	0.42	-3	1.9×10^{-2}	0.33	1

<i>C. finmarchicus</i>	FoF	-6.5×10^{-3}	0.66	-4	-3.9×10^{-2}	0.22	3
<i>C. finmarchicus</i>	DB	7.9×10^{-3}	0.24	1	2.1×10^{-4}	0.06	8
<i>C. finmarchicus</i>	Shet	8.7×10^{-3}	<0.01	42	4.7×10^{-2}	<0.01	39
<i>C. finmarchicus</i>	ECG	3.0×10^{-3}	<0.01	36	6.7×10^{-2}	<0.01	47
<i>C. finmarchicus</i>	Ice	1.6×10^{-2}	<0.01	69	1.8×10^{-1}	<0.01	63
<i>C. finmarchicus</i>	Faro	8.0×10^{-3}	<0.01	75	9.3×10^{-2}	<0.01	89
<i>C. helgolandicus</i>	FoF	3.0×10^{-2}	0.27	1	1.2×10^{-2}	0.70	-4
<i>C. helgolandicus</i>	DB	2.5×10^{-2}	<0.01	27	3.2×10^{-2}	<0.01	24
<i>C. helgolandicus</i>	Shet	1.5×10^{-2}	<0.01	51	4.4×10^{-2}	<0.01	43
<i>C. helgolandicus</i>	ECG	1.0×10^{-2}	0.12	7	2.3×10^{-2}	0.22	3
<i>C. helgolandicus</i>	Ice	1.0×10^{-1}	0.28	4	6.8×10^{-2}	0.17	13
<i>C. helgolandicus</i>	Faro	3.1×10^{-2}	0.19	10	2.8×10^{-2}	0.40	-2
<i>Calanus</i> I-IV	FoF	1.0×10^{-2}	0.01	28	8.5×10^{-2}	<0.01	35
<i>Calanus</i> I-IV	DB	5.0×10^{-3}	<0.01	45	4.1×10^{-2}	<0.01	28
<i>Calanus</i> I-IV	Shet	3.8×10^{-3}	<0.01	39	6.3×10^{-2}	<0.01	28
<i>Calanus</i> I-IV	ECG	1.6×10^{-3}	<0.01	48	1.0×10^{-1}	<0.01	76
<i>Calanus</i> I-IV	Ice	3.3×10^{-3}	0.02	44	1.3×10^{-1}	0.02	45
<i>Calanus</i> I-IV	Faro	1.5×10^{-3}	0.02	48	1.0×10^{-1}	<0.01	69
<i>Centropages hamatus</i>	FoF	1.0×10^{-2}	0.21	3	3.1×10^{-2}	0.21	3
<i>Centropages hamatus</i>	DB	3.0×10^{-3}	0.35	0	1.8×10^{-3}	0.86	-3
<i>Centropages hamatus</i>	Shet	2.1×10^{-3}	0.61	-2	-2.6×10^{-3}	0.80	-3
<i>Centropages hamatus</i>	ECG	-1.3×10^{-3}	0.93	-5	1.4×10^{-2}	0.45	-2
<i>Centropages hamatus</i>	Ice	4.2×10^{-1}	0.18	12	1.1×10^{-1}	0.25	6
<i>Centropages hamatus</i>	Faro	6.7×10^{-2}	0.84	-12	2.1×10^{-2}	0.81	-12
<i>Centropages typicus</i>	FoF	1.4×10^{-2}	0.51	-3	3.1×10^{-2}	0.25	2
<i>Centropages typicus</i>	DB	1.1×10^{-2}	0.01	17	1.1×10^{-2}	0.22	2
<i>Centropages typicus</i>	Shet	7.2×10^{-3}	0.07	7	1.9×10^{-2}	0.05	8
<i>Centropages typicus</i>	ECG	-5.2×10^{-3}	0.41	-1	-1.8×10^{-2}	0.31	0
<i>Centropages typicus</i>	Ice	9.2×10^{-2}	0.59	-8	4.8×10^{-2}	0.44	-4
<i>Centropages typicus</i>	Faro	-2.1×10^{-2}	0.23	7	-4.0×10^{-2}	0.13	17
Copepod nauplii	FoF	1.1×10^{-3}	0.42	-2	2.7×10^{-2}	0.36	-1
Copepod nauplii	DB	-1.7×10^{-4}	0.79	-3	-1.0×10^{-2}	0.43	-1
Copepod nauplii	Shet	1.3×10^{-4}	0.88	-3	3.3×10^{-3}	0.88	-3
Copepod nauplii	ECG	1.5×10^{-4}	0.75	-4	1.1×10^{-2}	0.58	-3
Copepod nauplii	Ice	-5.7×10^{-3}	0.45	-4	-7.6×10^{-2}	0.21	9
Copepod nauplii	Faro	2.0×10^{-3}	0.36	-1	1.5×10^{-2}	0.41	-3
Decapoda larvae	FoF	3.3×10^{-2}	0.25	2	5.9×10^{-2}	0.20	3
Decapoda larvae	DB	7.6×10^{-3}	0.01	20	3.5×10^{-2}	0.02	13
Decapoda larvae	Shet	2.7×10^{-2}	<0.01	43	5.2×10^{-2}	<0.01	34
Decapoda larvae	ECG	-3.4×10^{-2}	0.73	-4	-2.2×10^{-2}	0.62	-3
Decapoda larvae	Ice	5.0×10^{-1}	0.11	19	1.2×10^{-2}	0.20	10
Decapoda larvae	Faro	1.7×10^{-1}	0.14	16	1.0×10^{-1}	0.08	26
Euphausiacea spp.	FoF	3.2×10^{-2}	0.53	-3	1.4×10^{-2}	0.72	-4
Euphausiacea spp.	DB	3.4×10^{-4}	0.98	-3	2.9×10^{-3}	0.82	-3
Euphausiacea spp.	Shet	3.3×10^{-2}	0.28	1	2.2×10^{-2}	0.22	2
Euphausiacea spp.	ECG	3.0×10^{-2}	0.44	-2	5.3×10^{-2}	0.06	12
Euphausiacea spp.	Ice	2.1×10^{-2}	0.43	-3	5.9×10^{-3}	0.93	-12
Euphausiacea spp.	Faro	8.4×10^{-2}	0.34	0	5.8×10^{-2}	0.28	4

<i>Evadne</i> spp.	FoF	7.7×10^{-4}	0.13	6	3.3×10^{-2}	0.01	22
<i>Evadne</i> spp.	DB	1.2×10^{-4}	0.25	1	1.3×10^{-3}	0.88	-3
<i>Evadne</i> spp.	Shet	-3.5×10^{-5}	0.74	-3	5.9×10^{-4}	0.95	-3
<i>Evadne</i> spp.	ECG	2.3×10^{-5}	0.90	-5	-7.6×10^{-3}	0.69	-4
<i>Evadne</i> spp.	Ice	7.2×10^{-4}	0.44	-4	2.7×10^{-2}	0.22	8
<i>Evadne</i> spp.	Faro	1.0×10^{-3}	0.15	15	5.5×10^{-2}	0.02	48
Fish eggs	FoF	1.6×10^{-1}	0.57	-3	6.0×10^{-2}	0.47	-2
Fish eggs	DB	-9.9×10^{-3}	0.89	-3	-1.3×10^{-3}	0.95	-3
Fish eggs	Shet	-3.0×10^{-1}	0.69	-2	-3.4×10^{-2}	0.73	-3
Fish eggs	ECG	-6.1×10^{-2}	0.63	-4	-2.1×10^{-2}	0.62	-4
Fish eggs	Ice	1.5	0.28	3	2.1×10^{-1}	0.35	0
Fish eggs	Faro	1.6	0.24	6	2.1×10^{-1}	0.27	4
Fish larvae	FoF	5.9×10^{-1}	0.49	-2	1.4×10^{-1}	0.45	-2
Fish larvae	DB	-4.5×10^{-1}	0.52	-2	-6.2×10^{-2}	0.58	-2
Fish larvae	Shet	1.1	0.09	5	1.3×10^{-1}	0.16	3
Fish larvae	ECG	1.0	0.63	-4	1.6×10^{-1}	0.54	-3
Fish larvae	Ice	2.5	0.16	14	3.7×10^{-1}	0.18	11
Fish larvae	Faro	4.5	0.46	-5	4.9×10^{-1}	0.49	-5
Hyperiidia spp.	FoF	-2.7×10^{-1}	0.35	0	-1.0×10^{-1}	0.25	2
Hyperiidia spp.	DB	3.3×10^{-2}	0.75	-3	8.1×10^{-3}	0.77	-3
Hyperiidia spp.	Shet	8.7×10^{-1}	0.01	16	1.3×10^{-1}	0.02	12
Hyperiidia spp.	ECG	1.3×10^{-1}	0.17	4	4.9×10^{-2}	0.16	5
Hyperiidia spp.	Ice	-4.7×10^{-1}	0.35	0	-7.2×10^{-2}	0.55	-7
Hyperiidia spp.	Faro	4.1×10^{-1}	0.13	16	1.1×10^{-1}	0.14	16
<i>Metridia lucens</i>	FoF	-6.2×10^{-1}	0.51	-3	-1.0×10^{-1}	0.58	-3
<i>Metridia lucens</i>	DB	6.1×10^{-2}	0.74	-3	1.4×10^{-2}	0.71	-3
<i>Metridia lucens</i>	Shet	3.1×10^{-1}	0.02	12	9.1×10^{-2}	0.01	18
<i>Metridia lucens</i>	ECG	1.0×10^{-1}	0.40	-1	4.3×10^{-2}	0.32	0
<i>Metridia lucens</i>	Ice	6.0×10^{-1}	0.03	41	1.6×10^{-1}	0.04	36
<i>Metridia lucens</i>	Faro	6.6×10^{-2}	0.58	-8	3.8×10^{-2}	0.55	-7
<i>Oithona</i> spp.	FoF	2.1×10^{-4}	0.10	8	3.1×10^{-2}	0.11	8
<i>Oithona</i> spp.	DB	-3.0×10^{-5}	0.49	-2	-1.6×10^{-2}	0.22	2
<i>Oithona</i> spp.	Shet	1.6×10^{-4}	0.03	11	1.8×10^{-2}	0.10	5
<i>Oithona</i> spp.	ECG	8.2×10^{-5}	0.34	0	4.9×10^{-2}	0.19	4
<i>Oithona</i> spp.	Ice	-1.2×10^{-3}	0.05	33	-2.8×10^{-2}	0.11	19
<i>Oithona</i> spp.	Faro	-6.2×10^{-5}	0.90	-12	1.4×10^{-2}	0.85	-12
<i>Para-Pseudocalanus</i>	FoF	6.7×10^{-4}	0.06	12	6.8×10^{-2}	<0.01	33
<i>Para-Pseudocalanus</i>	DB	1.0×10^{-4}	0.50	-2	1.4×10^{-2}	0.32	0
<i>Para-Pseudocalanus</i>	Shet	1.9×10^{-4}	0.01	18	5.9×10^{-2}	<0.01	29
<i>Para-Pseudocalanus</i>	ECG	5.8×10^{-4}	0.30	1	5.1×10^{-2}	0.21	3
<i>Para-Pseudocalanus</i>	Ice	-1.9×10^{-3}	0.75	-11	1.3×10^{-2}	0.67	-10
<i>Para-Pseudocalanus</i>	Faro	9.6×10^{-4}	0.38	-2	8.7×10^{-3}	0.85	-12
<i>Podon</i> spp.	FoF	1.9×10^{-2}	0.01	24	5.5×10^{-2}	0.02	20
<i>Podon</i> spp.	DB	2.8×10^{-3}	0.01	18	6.5×10^{-3}	0.48	-2
<i>Podon</i> spp.	Shet	7.8×10^{-4}	<0.01	25	3.5×10^{-2}	<0.01	41
<i>Podon</i> spp.	ECG	4.4×10^{-4}	0.85	-5	3.9×10^{-3}	0.82	-5
<i>Podon</i> spp.	Ice	6.4×10^{-3}	0.23	7	3.6×10^{-2}	0.18	11
<i>Podon</i> spp.	Faro	1.2×10^{-3}	0.36	-1	3.0×10^{-2}	0.13	17

<i>Temora longicornis</i>	FoF	1.3×10^{-3}	0.10	8	4.4×10^{-2}	0.04	14
<i>Temora longicornis</i>	DB	2.6×10^{-4}	0.29	0	9.8×10^{-3}	0.56	-2
<i>Temora longicornis</i>	Shet	1.4×10^{-4}	0.73	-3	4.6×10^{-3}	0.72	-3
<i>Temora longicornis</i>	ECG	8.8×10^{-4}	0.68	-4	8.8×10^{-3}	0.57	-3
<i>Temora longicornis</i>	Ice	4.1×10^{-3}	0.12	19	2.3×10^{-2}	0.34	0
<i>Temora longicornis</i>	Faro	4.1×10^{-3}	0.21	9	3.4×10^{-2}	0.05	32
Total energy	FoF	2.4×10^{-1}	0.09	9	1.2×10^{-2}	0.07	10
Total energy	DB	3.3×10^{-2}	0.43	-1	2.7×10^{-2}	0.25	1
Total energy	Shet	3.2×10^{-1}	<0.01	38	1.4×10^{-2}	<0.01	35
Total energy	ECG	3.0×10^{-1}	0.01	28	1.8×10^{-2}	<0.01	45
Total energy	Ice	1.0×10^{-1}	0.32	1	5.5×10^{-2}	0.57	-8
Total energy	Faro	3.4×10^{-1}	0.04	35	1.8×10^{-1}	0.02	42
Small copepods	FoF	1.2×10^{-4}	0.04	15	8.9×10^{-2}	<0.01	41
Small copepods	DB	8.7×10^{-6}	0.71	-3	3.4×10^{-3}	0.84	-3
Small copepods	Shet	1.1×10^{-4}	<0.01	24	6.3×10^{-2}	0.01	18
Small copepods	ECG	7.5×10^{-5}	0.31	0	5.8×10^{-2}	0.16	5
Small copepods	Ice	-1.1×10^{-3}	0.1	22	-7.1×10^{-2}	0.13	16
Small copepods	Faro	4.5×10^{-5}	0.70	-10	3.8×10^{-2}	0.57	-8
Image area	FoF	-6.4	0.02	19	-1.6	0.01	22
Image area	DB	6.4	0.01	19	1.1	0.01	19
Image area	Shet	3.2	0.44	-1	4.5×10^{-1}	0.48	-1
Image area	ECG	5.0	0.04	14	7.6×10^{-1}	0.06	12
Image area	Ice	5.6	0.04	35	1.1	0.04	37
Image area	Faro	7.3	0.24	7	1.1	0.26	5
Temperature	FoF	-2.9×10^{-1}	0.40	-1	-4.9×10^{-1}	0.48	-2
Temperature	DB	2.8×10^{-1}	0.07	7	4.8×10^{-1}	0.07	7
Temperature	Shet	7.1×10^{-1}	<0.01	19	8.7×10^{-1}	0.01	18
Temperature	ECG	2.6×10^{-1}	0.38	-1	-4.2×10^{-1}	0.36	0
Temperature	Ice	6.9×10^{-1}	0.29	3	8.3×10^{-1}	0.31	2
Temperature	Faro	1.5×10^{-1}	0.84	-12	1.6×10^{-1}	0.85	-12

Appendix C

Appendix for Chapter 5

Table C.1: The number of overlapping estimates of breeding success in two consecutive years for all colony pairs, which is the sample size for calculating synchrony in the form of r_{diff} . Numbers in the first column correspond to the colony numbers in the first row. Note that the values in the diagonal are the number of between-year differences in breeding success that could be estimated for each colony. When calculating synchrony as the correlation between untransformed time series of breeding success (r) the sample size is larger as it does not require consecutive estimates.

	1.	2.	3.	4.	5.	6.	7.	8.	9.	10.	11.	12.	13.	14.	15.	16.	17.	18.	19.	20.	21.	22.
1.	19	15	19	19	17	17	18	13	19	17	19	19	18	17	15	15	19	18	17	19	19	17
2.		27	24	24	25	21	22	15	25	25	25	26	22	18	16	23	23	18	18	27	24	14
3.			29	26	27	22	25	18	27	24	27	29	25	22	17	22	26	23	22	28	27	18
4.				28	26	23	25	17	27	24	28	28	26	21	17	22	27	22	21	28	28	18
5.					30	21	25	17	27	25	27	29	25	20	15	23	26	21	20	29	27	16
6.						23	20	16	23	21	23	23	21	19	17	20	23	19	18	23	23	16
7.							27	15	25	22	26	27	24	19	14	20	25	20	19	26	26	18
8.								18	16	14	17	18	18	18	14	14	18	18	18	17	18	11
9.									29	26	28	29	25	20	17	24	26	21	20	29	27	18
10.										27	25	26	22	17	17	24	23	18	17	27	24	16
11.											29	29	26	21	17	23	27	22	21	29	28	18
12.												31	27	22	17	24	28	23	22	30	29	18
13.													27	22	17	21	26	23	22	26	27	16
14.														22	17	17	22	22	22	21	22	15
15.															17	16	17	17	17	17	17	13
16.																25	21	17	17	25	22	15
17.																	28	23	22	27	28	18
18.																		23	22	22	23	16
19.																			22	21	22	15
20.																					31	18
21.																						29
22.																						18

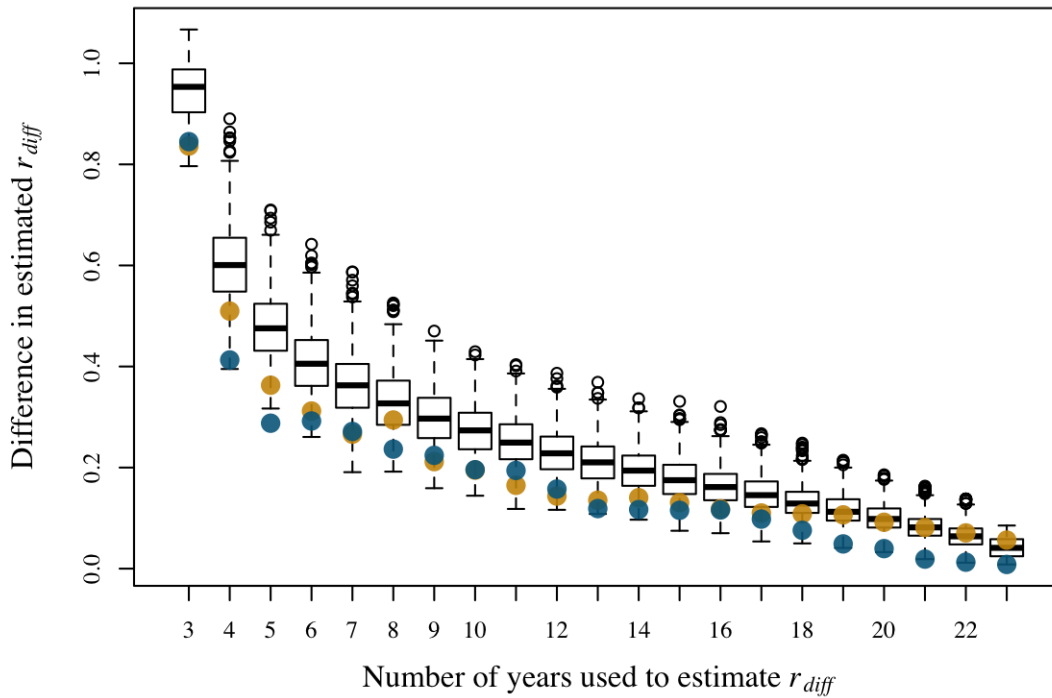


Figure C.1: In order to investigate the role of sample size, the 11 UK colonies with the most complete time series were picked out, which had a total of 24 years of estimated breeding success in common, and it was determined how the estimated r_{diff} changed as years were randomly removed from the data. This process was repeated 1000 times, where the order in which the years were removed was randomised each time. The plot shows the number of years used to estimate r_{diff} against the distribution of the 1000 estimated average absolute differences between the estimated r_{diff} and the r_{diff} estimated from the complete 24 year time series for the different colonies. It is clear that as the number of years increase, the difference decreases, being 0.180 (95% CI: 0.177; 0.183) on average at the cut-off of 15 (see Section 5.2) (but it should be noted that the estimate based on 24 years is not a “true” estimate of correlation strength). When synchrony was measured as r rather than r_{diff} , differences were generally smaller than shown here. If a longer sequence of years is missing at the beginning or the end of the time series, which is the case in some of the colonies (see Section 5.2), this could potentially have a different impact on the estimated synchrony if synchrony patterns has changed over time. For this reason, the effect on the estimated synchrony of removing years sequentially from the beginning or the end of the time series (yellow and blue dots, respectively). There was no evidence that this resulted in larger differences in the estimated correlation strength when synchrony was measured as r_{diff} . However, when synchrony was measured as r , the differences when years were removed sequentially were generally slightly larger than the average for when years were removed randomly, which is to be expected as this measure also reflects synchrony in long-term trends.

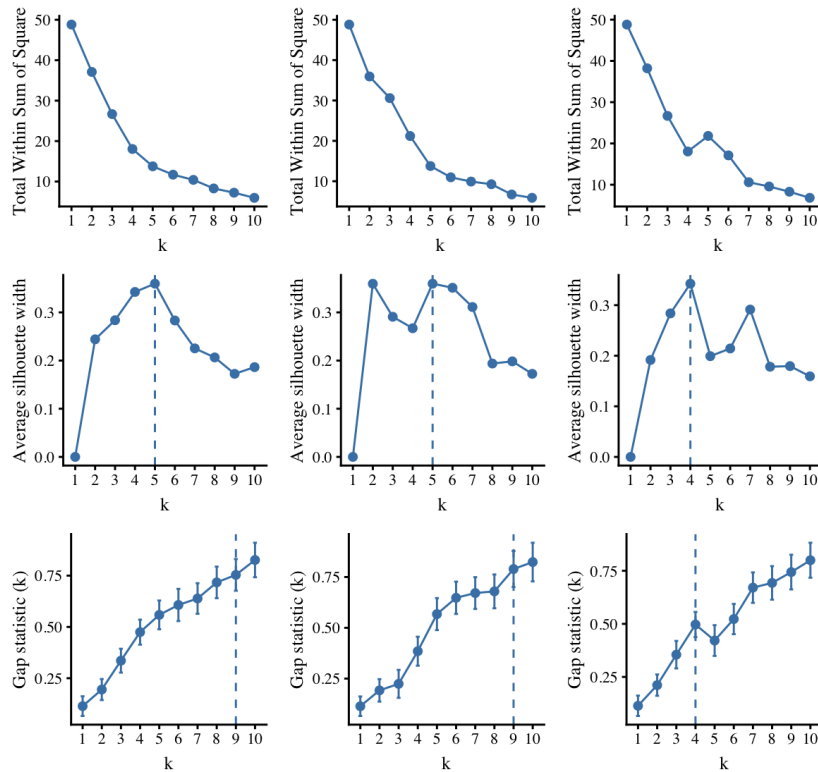


Figure C.2: Results for the three metrics used to determine the appropriate number of clusters k to use when synchrony was measured as r_{diff} . Each row represents a different metric and each column a different clustering algorithm (*agnes*, *diana* and *pam* – note that *fanny* was used primarily to look at affinities and for that reason not included). The first metric is the total within sum of squares, which shows how within-cluster variation decreases as the number of clusters increase, where the appropriate number of clusters is often considered to be point where the decrease in the total within sum of squares shows a marked change in the rate of decline, known as the “elbow criterion”. Here, this seems to suggest a k of 4 for *pam*, while it is less clear for *agnes* and *diana*, but around 4–5. The next metric is the average silhouette width, which measures the strength of within-cluster similarity as compared to the similarity with the next-closest cluster, which here suggests a k of 5 for *agnes* and *diana* and a k of 4 for *pam*. Finally, the gap statistic was assessed, which compares the intra-cluster variation for each value of k with their expected values under a null reference distribution. The optimal k is taken to be the smallest k for which the gap-statistic is not more than one standard error away from the first local maximum (standard errors are indicated by error bars). This method suggested the optimal values 9 for *agnes* and *diana* and 4 for *pam*. All methods thus suggest a k of 4 for *pam*, which is what was used for this algorithm. The values to use for *agnes* and *diana* were less obvious. Since the focus was on large-scale patterns rather than fine-scale structure, the lower values suggested by the total within sum of squares and the average silhouette width were more relevant than the higher values suggested by the gap-statistic. A k of 5 was chosen for both as this was suggested as optimal based on the total within sum of squares and also seemed reasonable for the average silhouette width. Again k in itself is not of interest, but rather the spatial configuration of the clusters. Based on a similar reasoning to the one outlined here, a k of 3 was used for all algorithms when synchrony was measured as r .

Table C.2: Final cluster structure for each algorithm when synchrony was measured as r_{diff} . (1 = Scottish east coast, 2 = Shetland, 3 = Orkney, see Figure 5.1c). Colonies that were not consistently assigned to the same cluster are indicated in bold (these are shown in grey in Figure 5.1c). Colony numbers correspond to numbers in Figure 5.1a.

Colony number	Colony name	<i>agnes</i>	<i>diana</i>	<i>pam</i>
1	Buchan Ness	1	1	1
2	Dunbar Coast	1	1	1
3	Fair Isle	2	2	2
4	Farne Islands	1	1	1
5	Flamborough Head	2	2	2
6	Foula	2	2	2
7	Fowlsheugh	1	1	1
8	Gultak	3	3	3
9	Handa Island	4	4	1
10	Hermaness	2	2	2
11	Isle of May	1	1	1
12	Lowestoft	5	5	4
13	Marwick Head	3	3	3
14	Mull Head	3	3	3
15	North Hill	2	2	2
16	North Sutor	5	5	4
17	Noss	2	2	2
18	Row Head	3	3	3
19	Saltburn Cliffs	2	2	2
20	St Abb's Head	1	1	1
21	Sumburgh Head	2	2	2
22	Whale Wick	2	2	2

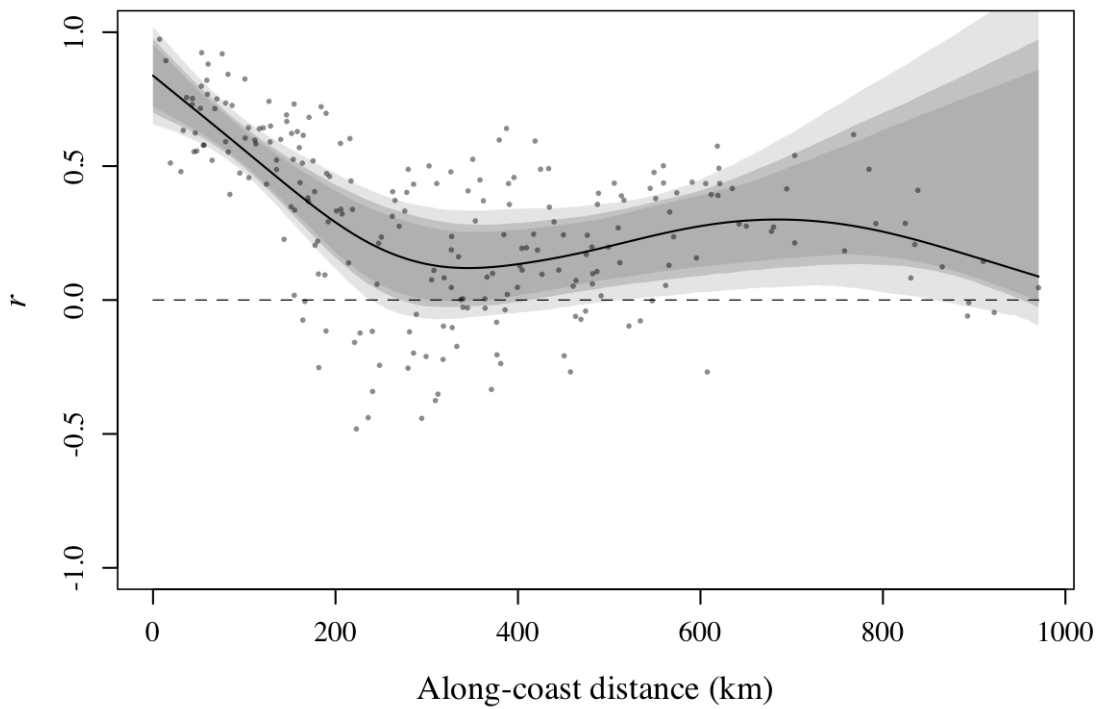


Figure C.3: This plot is equivalent to Figure 5.2 but measuring synchrony as the strength of the correlation between the untransformed time series of breeding success (r), rather than the correlation of the differences between consecutive years (r_{diff}). The black line shows the cubic smoothing spline fitted between the along-coast distance and synchrony for each colony pair. The dashed line indicates $r = 0$. Grey shading shows 99%, 95% and 90% confidence intervals as estimated from bootstrapping. Each point shows the synchrony of a colony pair against the along-coast distance between the two colonies.

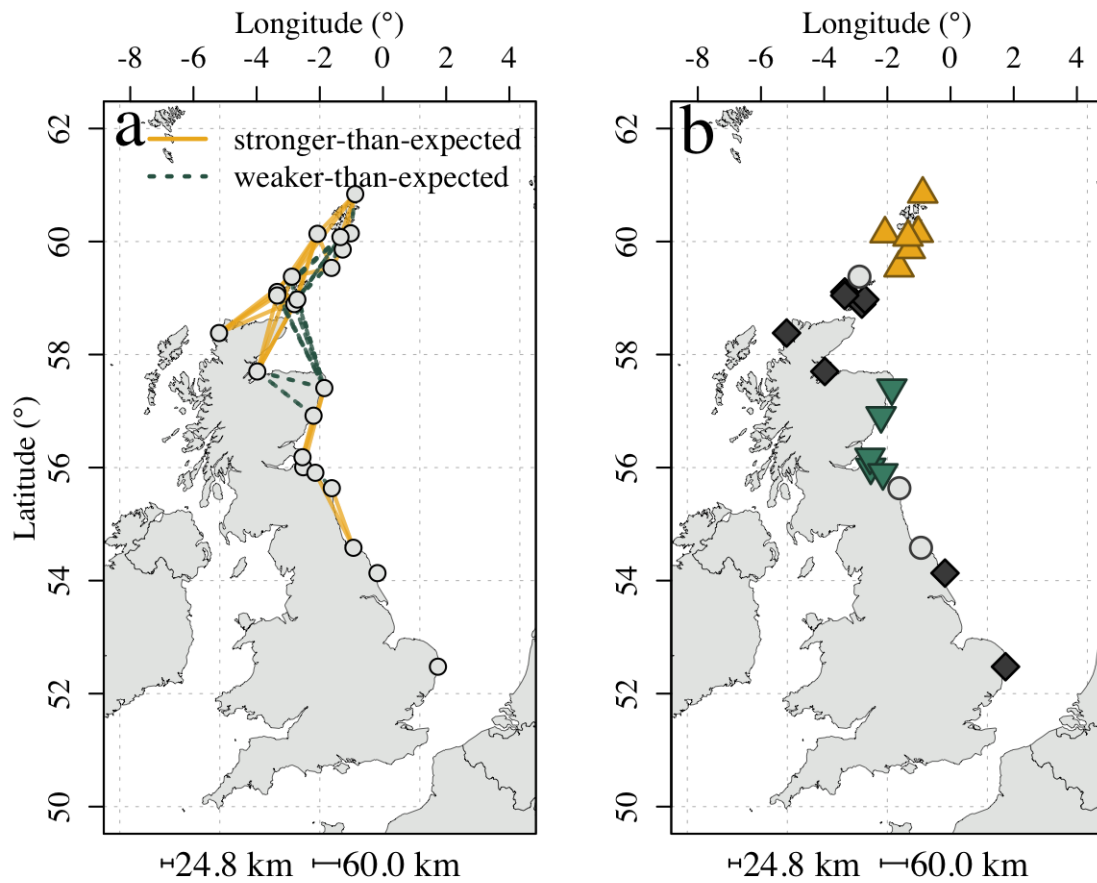


Figure C.4: These plots are equivalent to Figure 5.1b and Figure 5.1c but measuring synchrony as the strength of the correlation between the untransformed time series of breeding success (r), rather than the correlation of the differences between consecutive years (r_{diff}). (a) Green dashed lines indicate weaker synchrony than expected based on distance (negative residuals from the relationship between r and between-colony distance, Figure C.3) whereas yellow lines indicate stronger correlations than expected based on distance (positive residuals from the relationship between r and between-colony distance, Figure C.3). (b) Combined results from the cluster analysis. Round grey symbols indicate colonies that were assigned to different clusters by the different algorithms, whereas the other coloured symbols indicate clusters that were consistently identified by all algorithms. The average silhouette widths for all algorithms were around 0.36–0.37, indicating a slightly weaker cluster structure compared to when clustering was based on synchrony measured as r_{diff} . The average proportion of non-overlap ranged from 2 to 18%, indicating a more stable cluster structure compared to when clustering was based on synchrony measured as r_{diff} .

Bibliography

- Abbott, K. C. (2007). Does the pattern of population synchrony through space reveal if the Moran effect is acting? *Oikos*, *116*, 903–912.
- Aksnes, D. L. (2007). Evidence for visual constraints in large marine fish stocks. *Limnology and Oceanography*, *52*, 198–203.
- Aksnes, D. L., & Utne, A. C. W. (1997). A revised model of visual range in fish. *Sarsia*, *82*, 137–147.
- Alvarez-Fernandez, S., Lindeboom, H., & Meesters, E. (2012). Temporal changes in plankton of the North Sea: community shifts and environmental drivers. *Marine Ecology Progress Series*, *462*, 21–38.
- Alvestad, R. J. (2015). *Effects of climate on chick growth in the black-legged kittiwake (Rissa tridactyla)* (MSc Thesis, Norwegian University of Science and Technology).
- Andersen, N. G. (1999). The effects of predator size, temperature, and prey characteristics on gastric evacuation in whiting. *Journal of Fish Biology*, *54*, 287–301.
- Andersen, N. G. (2001). A gastric evacuation model for three predatory gadoids and implications of using pooled field data of stomach contents to estimate food rations. *Journal of Fish Biology*, *59*, 1198–1217.
- Arnott, S. A., & Ruxton, G. D. (2002). Sandeel recruitment in the North Sea: demographic, climatic and trophic effects. *Marine Ecology Progress Series*, *238*, 199–210.
- Arrhenius, F., & Hansson, S. (1996). Growth and seasonal changes in energy content of young Baltic Sea herring (*Clupea harengus* L.). *ICES Journal of Marine Science*, *53*, 792–801.
- Atkinson, D. (1994). Temperature and organism size — a biological law for ectotherms? *Advances in Ecological Research*, *25*, 1–58.
- Audzijonyte, A., Barneche, D. R., Baudron, A. R., Belmaker, J., Clark, T. D., Marshall, C. T., Morrongiello, J. R., & van Rijn, I. (2019). Is oxygen limitation in warming waters a valid mechanism to explain decreased body sizes in aquatic ectotherms? *Global Ecology and Biogeography*, *28*, 64–77.
- Ayón, P., Swartzman, G., Bertrand, A., Gutiérrez, M., & Bertrand, S. (2008). Zooplankton and forage fish species off Peru: Large-scale bottom-up forcing and local-scale depletion. *Progress in Oceanography*, *79*, 208–214.
- Bailey, R. S., Furness, R. W., Gauld, J. A., & Kunzlik, P. A. (1991). Recent changes in the population of the sandeel (*Ammodytes marinus* Raitt) at Shetland in relation to estimates of seabird predation. *ICES mar. Sci. Symp.* *193*, 209–216.

- Bainbridge, V. (1958). Some observations on *Evadne nordmanni* Lovén. *Journal of the Marine Biological Association of the United Kingdom*, *37*, 349–370.
- Barneche, D. R., Robertson, D. R., White, C. R., & Marshall, D. J. (2018). Fish reproductive-energy output increases disproportionately with body size. *Science*, *360*, 642–645.
- Barton, A. D., Finkel, Z. V., Ward, B. A., Johns, D. G., & Follows, M. J. (2013). On the roles of cell size and trophic strategy in North Atlantic diatom and dinoflagellate communities. *Limnology and Oceanography*, *58*, 254–266.
- Batten, S. D., Clark, R., Flinkman, J., Hays, G., John, E., John, A. W. G., Jonas, T., Lindley, J. A., Stevens, D. P., & Walne, A. (2003). CPR sampling: the technical background, materials and methods, consistency and comparability. *Progress in Oceanography*, *58*, 193–215.
- Baudron, A. R., Needle, C. L., Rijnsdorp, A. D., & Marshall, T. C. (2014). Warming temperatures and smaller body sizes: synchronous changes in growth of North Sea fishes. *Global Change Biology*, *20*, 1023–1031.
- Beare, D. J., Batten, S. D., Edwards, M., McKenzie, E., Reid, P. C., & Reid, D. G. (2003). Summarising spatial and temporal information in CPR data. *Progress in Oceanography*, *58*, 217–233.
- Beare, D., & McKenzie, E. (1999a). Continuous Plankton Recorder data and diel vertical migration in stage V and VI *Calanus finmarchicus*: a statistical analysis. *Fisheries Oceanography*, *8*, 126–137.
- Beare, D., & McKenzie, E. (1999b). The multinomial logit model: a new tool for exploring Continuous Plankton Recorder data. *Fisheries Oceanography*, *8*, 25–39.
- Beaugrand, G. (2004). The North Sea regime shift: evidence, causes, mechanisms and consequences. *Progress in Oceanography*, *60*, 245–262.
- Beaugrand, G., Brander, K. M., Lindley, J. A., Souissi, S., & Reid, P. C. (2003). Plankton effect on cod recruitment in the North Sea. *Nature*, *426*, 661–664.
- Beaugrand, G., Edwards, M., Brander, K., Luczak, C., & Ibanez, F. (2008). Causes and projections of abrupt climate-driven ecosystem shifts in the North Atlantic. *Ecology Letters*, *11*, 1157–1168.
- Beaugrand, G., Ibañez, F., & Lindley, J. A. (2001). Geographical distribution and seasonal and diel changes in the diversity of calanoid copepods in the North Atlantic and North Sea. *Marine Ecology Progress Series*, *219*, 189–203.
- Beaugrand, G., Reid, P. C., Ibanez, F., & Planque, B. (2000). Biodiversity of North Atlantic and North Sea calanoid copepods. *Marine Ecology Progress Series*, *204*, 299–303.
- Behrens, J. W., Petersen, J. K., Ærtebjerg, G., & Steffensen, J. F. (2010). Influence of moderate and severe hypoxia on the diurnal activity pattern of lesser sandeel *Ammodytes tobianus*. *Journal of Fish Biology*, *77*, 538–551.
- Behrens, J. W., Præbel, K., & Steffensen, J. F. (2006). Swimming energetics of the Barents Sea capelin (*Mallotus villosus*) during the spawning migration period. *Journal of Experimental Marine Biology and Ecology*, *331*, 208–216.
- Belkin, I. M. (2009). Rapid warming of Large Marine Ecosystems. *Progress in Oceanography*, *81*, 207–213.
- Bergstad, O. A., Høines, Å. S., & Jørgensen, T. (2002). Growth of sandeel, *Ammodytes marinus*, in the northern North Sea and Norwegian coastal waters. *Fisheries Research*, *56*, 9–23.

- Bergstad, O. A., Hoines, Å. S., & Krüger-Johnsen, E. M. (2001). Spawning time, age and size at maturity, and fecundity of sandeel, *Ammodytes marinus*, in the north-eastern North Sea and in unfished coastal waters off Norway. *Aquatic Living Resources*, *14*, 293–301.
- BirdLife International. (2018). *Rissa tridactyla*. In *The IUCN Red List of threatened species 2018: Et22694497a132556442*.
- Bivand, R. S., Pebesma, E. J., & Gómez-Rubio, V. (2013). *Applied spatial data analysis with R, 2nd edition*. Springer, NY.
- Bjørnstad, O. (2019). *Ncf: Spatial covariance functions*. R package version 1.2-8. Retrieved from <https://CRAN.R-project.org/package=nfc>
- Bjørnstad, O., & Falck, W. (2001). Nonparametric spatial covariance functions: Estimation and testing. *Environmental and Ecological Statistics*, *8*, 53–70.
- Blaxter, J. H. S., & Dickson, W. (1959). Observations on the swimming speeds of fish. *ICES Journal of Marine Science*, *24*, 472–479.
- Boldt, J. L., Thompson, M., Rooper, C. N., Hay, D. E., Schweigert, J. F., Quinn, T. J., Cleary, J. S., & Neville, C. M. (2019). Bottom-up and top-down control of small pelagic forage fish: factors affecting age-0 herring in the Strait of Georgia, British Columbia. *Marine Ecology Progress Series*, *617-618*, 53–66.
- Bolton, M., Conolly, G., Carroll, M., Wakefield, E. D., & Caldow, R. (2019). A review of the occurrence of inter-colony segregation of seabird foraging areas and the implications for marine environmental impact assessment. *Ibis*, *161*, 241–259.
- Bonnet, D., Richardson, A., Harris, R., Hirst, A., Beaugrand, G., Edwards, M., Ceballos, S., Diekman, R., López-Urrutia, A., Valdes, L., Carlotti, F., Molinero, J. C., Weikert, H., Greve, W., Lucic, D., Albaina, A., Yahia, N. D., Umani, S. F., Miranda, A., dos Santos, A., Cook, K., Robinson, S., & Fernandez de Puelles, M. L. (2005). An overview of *Calanus helgolandicus* ecology in European waters. *Progress in Oceanography*, *65*, 1–53.
- Bottrell, H. H., & Robins, D. B. (1984). Seasonal variations in length, dry weight, carbon and nitrogen of *Calanus helgolandicus* from the Celtic Sea. *Marine Ecology Progress Series*, *14*, 259–268.
- Boulcott, P., Clarke, J., & Wright, P. J. (2017). Effect of size on spawning time in the lesser sandeel *Ammodytes marinus*. *Journal of Fish Biology*, *91*, 362–367.
- Boulcott, P., & Wright, P. J. (2008). Critical timing for reproductive allocation in a capital breeder: evidence from sandeels. *Aquatic Biology*, *3*, 31–40.
- Boulcott, P., & Wright, P. J. (2011). Variation in fecundity in the lesser sandeel: implications for regional management. *Journal of the Marine Biological Association of the UK*, *91*, 1273–1280.
- Boulcott, P., Wright, P. J., Gibb, F. M., Jensen, H., & Gibb, I. M. (2007). Regional variation in maturation of sandeels in the North Sea. *ICES Journal of Marine Science*, *64*, 369–376.
- Bresnan, E., Cook, K. B., Hughes, S. L., Hay, S. J., Smith, K., Walsham, P., & Webster, L. (2015). Seasonality of the plankton community at an east and west coast monitoring site in Scottish waters. *Journal of Sea Research*, *105*, 16–29.
- Bresnan, E., Hay, S., Hughes, S. L., Fraser, S., Rasmussen, J., Webster, L., Slesser, G., Dunn, J., & Heath, M. R. (2009). Seasonal and interannual variation in

- the phytoplankton community in the north east of Scotland. *Journal of Sea Research*, *61*, 17–25.
- Brett, J. R. (1965). The relation of size to rate of oxygen consumption and sustained swimming speed of sockeye salmon (*Oncorhynchus nerka*). *Journal of the Fisheries Research Board of Canada*, *22*, 1491–1501.
- Brett, J. R., & Groves, T. D. D. (1979). Physiological energetics. In W. Hoar, D. Randall, & J. Brett (Eds.), *Fish Physiology Vol. VIII* (pp. 279–352). London: Academic Press.
- Brock, G., Pihur, V., Datta, S., & Datta, S. (2008). clValid: An R package for cluster validation. *Journal of Statistical Software*, *25*, 1–22.
- Brodersen, J., Rodriguez-Gil, J. L., Jönsson, M., Hansson, L.-A., Brönmark, C., Nilsson, P. A., Nicolle, A., & Berglund, O. (2011). Temperature and resource availability may interactively affect over-wintering success of juvenile fish in a changing climate. *PLoS ONE*, *6*, e24022.
- Broekhuizen, N., Gurney, W. S. C., Jones, A., & Bryant, A. D. (1994). Modelling compensatory growth. *Functional Ecology*, *8*, 770–782.
- Buonaccorsi, J. P., Elkinton, J. S., Evans, S. R., & Liebhold, A. M. (2001). Measuring and testing for spatial synchrony. *Ecology*, *82*, 1668–1679.
- Burnham, K. P., & Anderson, D. R. (2002). *Model selection and multimodel inference*. New York: Springer.
- Burthe, S., Daunt, F., Butler, A., Elston, D. A., Frederiksen, M., Johns, D., Newell, M., Thackeray, S. J., & Wanless, S. (2012). Phenological trends and trophic mismatch across multiple levels of a North Sea pelagic food web. *Marine Ecology Progress Series*, *454*, 119–133.
- Burton, T., Killen, S. S., Armstrong, J. D., & Metcalfe, N. B. (2011). What causes intraspecific variation in resting metabolic rate and what are its ecological consequences? *Proceedings of the Royal Society B: Biological Sciences*, *278*, 3465–3473.
- Butler, J. L., & Pickett, D. (1988). Age-specific vulnerability of Pacific sardine, *Sardinops sagax*, larvae to predation by northern anchovy, *Engraulis mordax*. *Fishery Bulletin U.S.* *86*, 163–167.
- Campbell, R. G., Wagner, M. M., Teegarden, G. J., Boudreau, C. A., & Durbin, E. G. (2001). Growth and development rates of the copepod *Calanus finmarchicus* reared in the laboratory. *Marine Ecology Progress Series*, *221*, 161–183.
- Capuzzo, E., Lynam, C. P., Barry, J., Stephens, D., Forster, R. M., Greenwood, N., McQuatters-Gollop, A., Silva, T., van Leeuwen, S. M., & Engelhard, G. H. (2018). A decline in primary production in the North Sea over 25 years, associated with reductions in zooplankton abundance and fish stock recruitment. *Global Change Biology*, *24*, e352–e364.
- Capuzzo, E., Painting, S. J., Forster, R. M., Greenwood, N., Stephens, D. T., & Mikkelsen, O. A. (2013). Variability in the sub-surface light climate at ecohydrodynamically distinct sites in the North Sea. *Biogeochemistry*, *113*, 85–103.
- Capuzzo, E., Stephens, D., Silva, T., Barry, J., & Forster, R. M. (2015). Decrease in water clarity of the southern and central North Sea during the 20th century. *Global Change Biology*, *21*, 2206–2214.
- Carroll, M. J., Butler, A., Owen, E., Ewing, S. R., Cole, T., Green, J. A., Soanes, L. M., Arnould, J. P. Y., Newton, S. F., Baer, J., Daunt, F., Wanless, S.,

- Newell, M. A., Robertson, G. S., Mavor, R. A., & Bolton, M. (2015). Effects of sea temperature and stratification changes on seabird breeding success. *Climate Research*, *66*, 75–89.
- Carter, C. (2014). The success of a small East Anglian colony of kittiwakes may be due to a diet supplemented by clupeids. *Seabird Group Newsletter*, *126*, 8–10.
- Chivers, L. S., Lundy, M. G., Colhoun, K., Newton, S. F., & Reid, N. (2012). Diet of black-legged kittiwakes (*Rissa tridactyla*) feeding chicks at two Irish colonies highlights the importance of clupeids. *Bird Study*, *59*, 363–367.
- Christensen-Dalsgaard, S., May, R. F., Barrett, R. T., Langset, M., Sandercock, B. K., & Lorentsen, S.-H. (2018a). Prevailing weather conditions and diet composition affect chick growth and survival in the black-legged kittiwake. *Marine Ecology Progress Series*, *604*, 237–249.
- Christensen-Dalsgaard, S., May, R. F., & Lorentsen, S.-H. (2018b). Taking a trip to the shelf: Behavioral decisions are mediated by the proximity to foraging habitats in the black-legged kittiwake. *Ecology and Evolution*, *8*, 866–878.
- Christensen, A., Jensen, H., Mosegaard, H., St. John, M., & Schrum, C. (2008). Sandeel (*Ammodytes marinus*) larval transport patterns in the North Sea from an individual-based hydrodynamic egg and larval model. *Canadian Journal of Fisheries and Aquatic Sciences*, *65*, 1498–1511.
- Christensen, V. (2010). Behavior of sandeels feeding on herring larvae. *The Open Fish Science Journal*, *3*, 164–168.
- Ciannelli, L. (1997). Winter dormancy in the Pacific sand lance (*Ammodytes hexapterus*) in relation to gut evacuation time. In *Forage fishes in marine ecosystems* (pp. 95–104).
- Clark, R. A., Frid, C. L. J., & Batten, S. (2001). A critical comparison of two long-term zooplankton time series from the central-west North Sea. *Journal of Plankton Research*, *23*, 27–39.
- Clarke, A., & Johnston, N. M. (1999). Scaling of metabolic rate with body mass and temperature in teleost fish. *Journal of Animal Ecology*, *68*, 893–905.
- Collins, P. M., Green, J. A., Dodd, S., Shaw, P. J. A., & Halsey, L. G. (2014). Predation of black-legged kittiwake chicks *Rissa tridactyla* by a peregrine Falcon *Falco peregrinus*: insights from time-lapse cameras. *The Wilson Journal of Ornithology*, *126*, 158–161.
- Confer, J. L., & Blades, P. I. (1975). Omnivorous zooplankton and planktivorous fish. *Limnology and Oceanography*, *20*, 571–579.
- Conti, S. G., Demer, D. A., & Brierley, A. S. (2005). Broad-bandwidth, sound scattering, and absorption from krill (*Meganyctiphanes norvegica*), mysids (*Praunus flexuosus* and *Neomysis integer*), and shrimp (*Crangon crangon*). *ICES Journal of Marine Science*, *62*, 956–965.
- Cook, R. M. (2004). Estimation of the age-specific rate of natural mortality for Shetland sandeels. *ICES Journal of Marine Science*, *61*, 159–164.
- Copernicus Climate Change Service C3S. (2017). ERA5: Fifth generation of ECMWF atmospheric reanalyses of the global climate. Retrieved August 2019, from <https://cds.climate.copernicus.eu/cdsapp#!/home>
- Coulson, J. C. (2017). Productivity of the black-legged kittiwake *Rissa tridactyla* required to maintain numbers. *Bird Study*, *64*, 84–89.

- Crisp, D. J. (1971). Energy flow measurements. In N. A. Holme & A. D. McIntyre (Eds.), *Methods for the study of marine benthos. IBP Handbook No. 16* (pp. 197–279). Oxford: Blackwell Scientific Publications.
- Crowder, L. B. (1985). Optimal foraging and feeding mode shifts in fishes. *Environmental Biology of Fishes*, *12*, 57–62.
- Cui, Y., & Wootton, R. J. (1988). Bioenergetics of growth of a cyprinid, *Phoxinus phoxinus*: the effect of ration, temperature and body size on food consumption, faecal production and nitrogenous excretion. *Journal of Fish Biology*, *33*, 431–443.
- Cury, P., Shannon, L., & Shin, Y.-J. (2003). The functioning of marine ecosystems: a fisheries perspective. In M. Sinclair & G. Valdimarsson (Eds.), *Responsible fisheries in the marine ecosystem* (pp. 103–123). Wallingford, UK: CABI Publishing.
- Cury, P. M., Boyd, I. L., Bonhommeau, S., Anker-Nilssen, T., Crawford, R. J. M., Furness, R. W., Mills, J. A., Murphy, E. J., Österblom, H., Paleczny, M., Piatt, J. F., Roux, J.-P., Shannon, L., & Sydeman, W. J. (2011). Global seabird response to forage fish depletion – one-third for the birds. *Science*, *334*, 1703–1706.
- Cushing, D. H. (1990). Plankton production and year-class strength in fish populations: an update of the match/mismatch hypothesis. *Advances in Marine Biology*, *26*, 249–293.
- Danielsen, N. S. T., Hedeholm, R. B., & Grønkjær, P. (2016). Seasonal changes in diet and lipid content of northern sand lance *Ammodytes dubius* on Fyllas Bank, West Greenland. *Marine Ecology Progress Series*, *558*, 97–113.
- Daufresne, M., Lengfellner, K., & Sommer, U. (2009). Global warming benefits the small in aquatic ecosystems. *Proceedings of the National Academy of Sciences*, *106*, 12788–12793.
- Daunt, F., Wanless, S., Greenstreet, S. P. R., Jensen, H., Hamer, K. C., & Harris, M. P. (2008). The impact of the sandeel fishery closure on seabird food consumption, distribution, and productivity in the northwestern North Sea. *Canadian Journal of Fisheries and Aquatic Sciences*, *65*, 362–381.
- Defriez, E. J., Sheppard, L. W., Reid, P. C., & Reuman, D. C. (2016). Climate change-related regime shifts have altered spatial synchrony of plankton dynamics in the North Sea. *Global Change Biology*, *22*, 2069–2080.
- Descamps, S., Anker-Nilssen, T., Barrett, R. T., Irons, D. B., Merkel, F., Robertson, G. J., Yoccoz, N. G., Mallory, M. L., Montevicchi, W. A., Boertmann, D., Artukhin, Y., Christensen-Dalsgaard, S., Erikstad, K. E., Gilchrist, H. G., Labansen, A. L., Lorentsen, S.-H., Mosbech, A., Olsen, B., Petersen, A., Rail, J.-F., Renner, H. M., Strøm, H., Systad, G. H., Wilhelm, S. I., & Zelenskaya, L. (2017). Circumpolar dynamics of a marine top-predator track ocean warming rates. *Global Change Biology*, *23*, 3770–3780.
- Dessier, A., Dupuy, C., Kerric, A., Mornet, F., Authier, M., Bustamante, P., & Spitz, J. (2018). Variability of energy density among mesozooplankton community: New insights in functional diversity to forage fish. *Progress in Oceanography*, *166*, 121–128.
- Devlin, M. J., Barry, J., Mills, D. K., Gowen, R. J., Foden, J., Sivyer, D., Greenwood, N., Pearce, D., & Tett, P. (2009). Estimating the diffuse attenuation coefficient

- from optically active constituents in UK marine waters. *Estuarine, Coastal and Shelf Science*, 82, 73–83.
- Dupont, N., & Aksnes, D. L. (2013). Centennial changes in water clarity of the Baltic Sea and the North Sea. *Estuarine, Coastal and Shelf Science*, 131, 282–289.
- Durant, J. M., Hjermmann, D. Ø., Ottersen, G., & Stenseth, N. C. (2007). Climate and the match or mismatch between predator requirements and resource availability. *Climate Research*, 33, 271–283.
- Dwyer, W. P., & Kramer, R. H. (1975). The influence of temperature on scope for activity in cutthroat trout, *Salmo clarki*. *Transactions of the American Fisheries Society*, 104, 552–554.
- Economou, A. N. (1991). Food and feeding ecology of five gadoid larvae in the northern North Sea. *ICES Journal of Marine Science*, 47, 339–351.
- Edwards, M., Helaouet, P., Halliday, N., Beaugrand, G., Fox, C., Johns, D. G., Licandro, P., Lynam, C., Pitois, S., Stevens, D., Coombs, S., & Fonesca, L. (2011). *Fish larvae atlas of the NE Atlantic. Results from the Continuous Plankton Recorder survey 1948-2005*. Plymouth: Sir Alister Hardy Foundation for Ocean Science.
- Edwards, M., Atkinson, A., Bresnan, E., Hélaouët, P., McQuatters-Gollop, A., Ostle, C., Pitois, S., & Widdicombe, C. (2020). Plankton, jellyfish and climate in the North-East Atlantic. *MCCIP Science Review 2020*, 322–353.
- Edwards, M., & Richardson, A. J. (2003). Impact of climate change on marine pelagic phenology and trophic mismatch. *Nature*, 430, 881–884.
- Eggers, D. M. (1976). Theoretical effect of schooling by planktivorous fish predators on rate of prey consumption. *Journal of the Fisheries Research Board of Canada*, 33, 1964–1971.
- Eggers, D. M. (1977). The nature of prey selection by planktivorous fish. *Ecology*, 58, 46–59.
- Ehrlich, K. F., Blaxter, J. H. S., & Pemberton, R. (1976). Morphological and histological changes during the growth and starvation of herring and plaice larvae. *Marine Biology*, 35, 105–118.
- Eigaard, O. R., van Deurs, M., Behrens, J. W., Bekkevold, D., Brander, K., Plambech, M., Plet-Hansen, K. S., & Mosegaard, H. (2014). Prey or predator – expanding the food web role of sandeel *Ammodytes marinus*. *Marine Ecology Progress Series*, 516, 267–273.
- Eliassen, K. (2013). *Sandeel, Ammodytes spp., as a link between climate and higher trophic levels on the Faroe shelf* (PhD Thesis, University of Aarhus).
- Elliott, J. M. (1976). Energy losses in the waste products of brown trout (*Salmo trutta* L.) *Journal of Animal Ecology*, 45, 561–580.
- Elliott, J. M. (1991). Rates of gastric evacuation in piscivorous brown trout, *Salmo trutta*. *Freshwater Biology*, 25, 297–305.
- Embling, C. B., Armstrong, E., Illian, J., & Scott, B. E. (2008). Topographic & tidal influenced foraging behaviour of top predators and prey. *ICES CM 2008/M:16*.
- Engelhard, G. H., Blanchard, J. L., Pinnegar, J. K., van der Kooij, J., Bell, E. D., Mackinson, S., & Righton, D. A. (2013). Body condition of predatory fishes linked to the availability of sandeels. *Marine Biology*, 160, 299–308.
- Engelhard, G. H., Peck, M. A., Rindorf, A., Smout, S. C., van Deurs, M., Raab, K., Andersen, K. H., Garthe, S., Lauerburg, R. A. M., Scott, F., Brunel, T., Aarts, G., van Kooten, T., & Dickey-Collas, M. (2014). Forage fish, their fisheries,

- and their predators: who drives whom? *ICES Journal of Marine Science*, 71, 90–104.
- Engelhard, G. H., van der Kooij, J., Bell, E. D., Pinnegar, J. K., Blanchard, J. L., Mackinson, S., & Righton, D. A. (2008). Fishing mortality versus natural predation on diurnally migrating sandeels *Ammodytes marinus*. *Marine Ecology Progress Series*, 369, 213–227.
- Engen, S., Lande, R., & Saether, B.-E. (2002). The spatial scale of population fluctuations and quasi-extinction risk. *American Naturalist*, 160, 439–451.
- Everett, J. D., Baird, M. E., Buchanan, P., Bulman, C., Davies, C., Downie, R., Griffiths, C., Heneghan, R., Kloser, R. J., Laiolo, L., Lara-Lopez, A., Lozano-Montes, H., Matear, R. J., McEnnulty, F., Robson, B., Rochester, W., Skerratt, J., Smith, J. A., Strzelecki, J., Suthers, I. M., Swadling, K. M., van Ruth, P., & Richardson, A. J. (2017). Modeling what we sample and sampling what we model: Challenges for zooplankton model assessment. *Frontiers in Marine Science*, 4, 77.
- Fall, J., & Fiksen, Ø. (2019). No room for dessert: A mechanistic model of prey selection in gut-limited predatory fish. *Fish and Fisheries*, 21, 63–79.
- Fauchald, P., Anker-Nilssen, T., Barrett, R. T., Bustnes, J. O., Bårdsen, B., Christensen-Dalsgaard, S., Descamps, S., Engen, S., Erikstad, K. E., Hanssen, S. A., Lorentsen, S.-H., Moe, B., Reiertsen, T. K., Strøm, H., & Systad, G. H. (2015). *The status and trends of seabirds breeding in Norway and Svalbard - NINA Report 1151*.
- Fay, R., Michler, S., Laesser, J., Jeanmonod, J., & Schaub, M. (2020). Large-scale vole population synchrony in central Europe revealed by kestrel breeding performance. *Frontiers in Ecology and Evolution*, 7, 512.
- Folkvord, A., & Hunter, J. R. (1986). Size-specific vulnerability of northern anchovy, *Engraulis mordax*, larvae to predation by fishes. *Fishery Bulletin U.S.* 84, 859–869.
- Fossum, P. (1996). A study of first-feeding herring (*Clupea harengus* L.) larvae during the period 1985–1993. *ICES Journal of Marine Science*, 53, 51–59.
- Frederiksen, M., Edwards, M., Mavor, R. A., & Wanless, S. (2007a). Regional and annual variation in black-legged kittiwake breeding productivity is related to sea surface temperature. *Marine Ecology Progress Series*, 350, 137–143.
- Frederiksen, M., Furness, R. W., & Wanless, S. (2007b). Regional variation in the role of bottom-up and top-down processes in controlling sandeel abundance in the North Sea. *Marine Ecology Progress Series*, 337, 279–286.
- Frederiksen, M., Edwards, M., Richardson, A. J., Halliday, N. C., & Wanless, S. (2006). From plankton to top predators: bottom-up control of a marine food web across four trophic levels. *Journal of Animal Ecology*, 75, 1259–1268.
- Frederiksen, M., Elston, D. A., Edwards, M., Mann, A. D., & Wanless, S. (2011). Mechanisms of long-term decline in size of lesser sandeels in the North Sea explored using a growth and phenology model. *Marine Ecology Progress Series*, 432, 137–147.
- Frederiksen, M., Wright, P. J., Harris, M. P., Mavor, R. A., Heubeck, M., & Wanless, S. (2005). Regional patterns of kittiwake *Rissa tridactyla* breeding success are related to variability in sandeel recruitment. *Marine Ecology Progress Series*, 300, 201–211.

- Frederiksen, M., Anker-Nilssen, T., Beaugrand, G., & Wanless, S. (2013). Climate, copepods and seabirds in the boreal Northeast Atlantic – current state and future outlook. *Global Change Biology*, *19*, 364–372.
- Frederiksen, M., Moe, B., Daunt, F., Phillips, R. A., Barrett, R. T., Bogdanova, M. I., Boulinier, T., Chardine, J. W., Chastel, O., Chivers, L. S., Christensen-Dalsgaard, S., Clément-Chastel, C., Colhoun, K., Freeman, R., Gaston, A. J., González-Solís, J., Goutte, A., Grémillet, D., Guilford, T., Jensen, G. H., Krasnov, Y., Lorentsen, S.-H., Mallory, M. L., Newell, M., Olsen, B., Shaw, D., Steen, H., Strøm, H., Systad, G. H., Thórarinnsson, T. L., & Anker-Nilssen, T. (2012). Multicolony tracking reveals the winter distribution of a pelagic seabird on an ocean basin scale. *Diversity and Distributions*, *18*, 530–542.
- Freeman, S., Mackinson, S., & Flatt, R. (2004). Diel patterns in the habitat utilisation of sandeels revealed using integrated acoustic surveys. *Journal of Experimental Marine Biology and Ecology*, *305*, 141–154.
- Fritsch, F. N., & Carlson, R. E. (1980). Monotone piecewise rational cubic interpolation. *SIAM Journal on Numerical Analysis*, *17*, 238–246.
- Fuiman, L. A. (1989). Vulnerability of Atlantic herring larvae to predation by yearling herring. *Marine Ecology Progress Series*, *51*, 291–299.
- Furness, R. W. (2002). Management implications of interactions between fisheries and sandeel-dependent seabirds and seals in the North Sea. *ICES Journal of Marine Science*, *59*, 261–269.
- Furness, R. W., Greenstreet, S. P. R., & Walsh, P. M. (1996). Spatial and temporal variability in the breeding success of seabirds around the British Isles: evidence for distinct sandeel stocks? *ICES Cooperative Research Report*, *216*, 63–65.
- Furness, R. W., & Tasker, M. L. (2000). Seabird-fishery interactions: quantifying the sensitivity of seabirds to reductions in sandeel abundance, and identification of key areas for sensitive seabirds in the North Sea. *Marine Ecology Progress Series*, *202*, 253–264.
- Galbraith, H. (1983). The diet and feeding ecology of breeding kittiwakes *Rissa tridactyla*. *Bird Study*, *30*, 109–120.
- Garber, K. J. (1983). Effect of fish size, meal size and dietary moisture on gastric evacuation of pelleted diets by yellow perch, *Perca flavescens*. *Aquaculture Research*, *34*, 41–49.
- Gardner, J. L., Peters, A., Kearney, M. R., Joseph, L., & Heinsohn, R. (2011). Declining body size: a third universal response to warming? *Trends in Ecology and Evolution*, *26*, 285–291.
- Gibb, F. M., Régnier, T., Donald, K., & Wright, P. J. (2017). Connectivity in the early life history of sandeel inferred from otolith microchemistry. *Journal of Sea Research*, *119*, 8–16.
- Gieskes, W. W. C. (1971). Ecology of the Cladocera of the North Atlantic and the North Sea. *Netherlands Journal of Sea Research*, *5*, 342–376.
- Giggenbach, D., Moll, F., Fuchs, C., & Brechtelsbauer, M. (2010). Direct optical high speed downlinks and ground station networks for small Leo missions. *16th Ka-and Broadband Communication Conference*, 1–8.
- Gilbert, M., Fortier, L., Ponton, D., & Drolet, R. (1992). Feeding ecology of marine fish larvae across the Great Whale River plume in seasonally ice-covered southeastern Hudson Bay. *Marine Ecology Progress Series*, *84*, 19–30.

- Gill, A. B., & Hart, P. J. B. (1998). Stomach capacity as a directing factor in prey size selection of three-spined stickleback. *Journal of Fish Biology*, *53*, 897–900.
- Gill, V. A., & Hatch, S. A. (2002). Components of productivity in black-legged kittiwakes *Rissa tridactyla*: response to supplemental feeding. *Journal of Avian Biology*, *33*, 113–126.
- Gilman, S. L. (1994). An energy budget for northern sand lance, *Ammodytes dubius*, on Georges Bank, 1977–1986. *Fishery Bulletin*, *92*, 647–654.
- Gislason, A., Petursdottir, H., & Gudmundsson, K. (2014). Long-term changes in abundance of *Calanus finmarchicus* south and north of Iceland in relation to environmental conditions and regional diversity in spring 1990–2013. *ICES Journal of Marine Science*, *71*, 2359–2549.
- Gliwicz, Z. M., Babkiewicz, E., Kumar, R., Kunjiappan, S., & Leniowski, K. (2018). Warming increases the number of apparent prey in reaction field volume of zooplanktivorous fish. *Limnology and Oceanography*, *63*, S30–S43.
- Gliwicz, Z. M., & Maszczyk, P. (2016). Heterogeneity in prey distribution allows for higher food intake in planktivorous fish, particularly when hot. *Oecologia*, *180*, 383–399.
- Godiksen, J. A., Hallfredsson, E. H., & Pedersen, T. (2006). Effects of alternative prey on predation intensity from herring *Clupea harengus* and sandeel *Ammodytes marinus* on capelin *Mallotus villosus* larvae in the Barents Sea. *Journal of Fish Biology*, *69*, 1807–1823.
- Godø, O. R., Handegard, N. O., Browman, H. I., Macaulay, G. J., Kaartvedt, S., Giske, J., Ona, E., Huse, G., & Johnsen, E. (2014). Marine ecosystem acoustics (MEA): quantifying processes in the sea at the spatio-temporal scales on which they occur. *ICES Journal of Marine Science*, *71*, 2357–2369.
- Gómez García, G., Demain, D., Drewery, H., & Gallego, A. (2012). The distribution of zooplankton prey of forage fish in the Firth of Forth Area, East Coast of Scotland. *Scottish Marine and Freshwater Science*, *3*, 1–23.
- Goslee, S. C., & Urban, D. L. (2007). The ecodist package for dissimilarity-based analysis of ecological data. *Journal of Statistical Software*, *22*, 1–19.
- Greenstreet, S. P. R., Armstrong, E., Mosegaard, H., Jensen, H., Gibb, I. M., Fraser, H. M., Scott, B. E., Holland, G. J., & Sharples, J. (2006). Variation in the abundance of sandeels *Ammodytes marinus* off southeast Scotland: an evaluation of area-closure fisheries management and stock abundance assessment methods. *ICES Journal of Marine Science*, *63*, 1530–1550.
- Grenfell, B. T., Wilson, K., Finkenstädt, B. F., Coulson, T. N., Murray, S., Albon, S. D., Pemberton, J. M., Clutton-Brock, T. H., & Crawley, M. J. (1998). Noise and determinism in synchronized sheep dynamics. *Nature*, *394*, 674–677.
- Grøtan, V., Sæther, B.-E., Engen, S., Solberg, E. J., Linnell, J. D. C., Andersen, R., Brøseth, H., & Lund, E. (2005). Climate causes large-scale spatial synchrony in population fluctuations of a temperate herbivore. *Ecology*, *86*, 1472–1482.
- Gurkan, Z., Christensen, A., Maar, M., Møller, E. F., Madsen, K. S., Munk, P., & Mosegaard, H. (2013). Spatio-temporal dynamics of growth and survival of lesser sandeel early life-stages in the North Sea: Predictions from a coupled individual-based and hydrodynamic-biogeochemical model. *Ecological Modelling*, *250*, 294–306.

- Hamer, K. C., Monaghan, P., Uttley, J. D., Walton, P., & Burns, M. D. (1993). The influence of food supply on the breeding ecology of kittiwakes *Rissa tridactyla* in Shetland. *Ibis*, *135*, 255–263.
- Harris, M. P., & Wanless, S. (1997). Breeding success, diet, and brood neglect in the kittiwake (*Rissa tridactyla*) over an 11-year period. *ICES Journal of Marine Science*, *54*, 615–623.
- Harris, M. P., & Wanless, S. (2011). *The Puffin*. London: T & AD Poyser.
- Harvey, H. R., Pleuthner, R. L., Lessard, E. J., Bernhardt, M. J., & Shaw, C. T. (2012). Physical and biochemical properties of the euphausiids *Thysanoessa inermis*, *Thysanoessa raschii*, and *Thysanoessa longipes* in the eastern Bering Sea. *Deep-Sea Research Part II: Topical Studies in Oceanography*, *65-70*, 173–183.
- Hay, S. J., Kiørboe, T., & Matthews, A. (1991). Zooplankton biomass and production in the North Sea during the Autumn Circulation Experiment, October 1987–March 1988. *Continental Shelf Research*, *11*, 1453–1476.
- Hayes, J. W., Stark, J. D., & Shearer, K. A. (2000). Development and test of a whole-lifetime foraging and bioenergetics growth model for drift-feeding brown trout. *Transactions of the American Fisheries Society*, *129*, 315–332.
- Haynes, K. J., Liebhold, A. M., Fearer, T. M., Wang, G., Norman, G. W., & Johnson, D. M. (2009). Spatial synchrony propagates through a forest food web via consumer-resource interactions. *Ecology*, *90*, 2974–2983.
- Heath, M. R., Backhaus, J. O., Richardson, K., McKenzie, E., Slagstad, D., Beare, D., Dunn, J., Fraser, J. G., Gallego, A., Hainbucher, D., Hay, S., Jónasdóttir, S., Madden, H., Mardaljevic, J., & Schacht, A. (1999). Climate fluctuations and the spring invasion of the North Sea by *Calanus finmarchicus*. *Fisheries Oceanography*, *8*, 163–176.
- Heath, M. R., Neat, F. C., Pinnegar, J. K., Reid, D. G., Sims, D. W., & Wright, P. J. (2012). Review of climate change impacts on marine fish and shellfish around the UK and Ireland. *Aquatic Conservation: Marine and Freshwater Ecosystems*, *22*, 337–367.
- Hedd, A., Bertram, D. F., Ryder, J. L., & Jones, I. L. (2006). Effects of interdecadal climate variability on marine trophic interactions: rhinoceros auklets and their fish prey. *Marine Ecology Progress Series*, *309*, 263–278.
- Heino, M., Kaitala, V., Ranta, E., & Lindstrom, J. (1997). Synchronous dynamics and rates of extinction in spatially structured populations. *Proceedings of the Royal Society B: Biological Sciences*, *264*, 481–486.
- Hélaouët, P., Beaugrand, G., & Reygondeau, G. (2016). Reliability of spatial and temporal patterns of *C. finmarchicus* inferred from the CPR survey. *Journal of Marine Systems*, *153*, 18–24.
- Hempel, G., & Blaxter, J. H. S. (1967). Egg weight in Atlantic herring. *ICES Journal of Marine Science*, *31*, 170–195.
- Henriksen, O., Christensen, A., Jónasdóttir, S., MacKenzie, B. R., Nielsen, K. E., Mosegård, H., & van Deurs, M. (2018). Oceanographic flow regime and fish recruitment: reversed circulation in the North Sea coincides with unusually strong sandeel recruitment. *Marine Ecology Progress Series*, *607*, 187–205.
- Heubeck, M. (2002). The decline of Shetland's kittiwake population. *British Birds*, *95*, 118–122.

- Hijmans, R. J. (2017). *geosphere: Spherical trigonometry*. R package version 1.5-7. Retrieved from <https://CRAN.R-project.org/package=geosphere>
- Hijmans, R. J. (2018). *raster: geographic data analysis and modeling*. R package version 3.0-2. Retrieved from <https://CRAN.R-project.org/package=raster>
- Hislop, J. R. G., Harris, M. P., & Smith, J. G. M. (1991). Variation in the calorific value and total energy content of the lesser sandeel (*Ammodytes marinus*) and other fish preyed on by seabirds. *Journal of Zoology*, *224*, 501–517.
- Hjort, J. (1914). Fluctuations in the great fisheries of Northern Europe. *Rapports et Procès-Verbaux*, *20*, 1–228.
- Hobson, E. S. (1986). Predation on the Pacific sand lance, *Ammodytes hexapterus* (Pisces: Ammodytidae), during the transition between day and night in south-eastern Alaska. *Copeia*, *1986*, 223–226.
- Holland, G. J., Greenstreet, S. P. R., Gibb, I. M., Fraser, H. M., & Robertson, M. R. (2005). Identifying sandeel *Ammodytes marinus* sediment habitat preferences in the marine environment. *Marine Ecology Progress Series*, *303*, 269–282.
- Holling, C. S. (1959). Some characteristics of simple types of predation and parasitism. *The Canadian Entomologist*, *91*, 385–398.
- Hollis, D., McCarthy, M., Kendon, M., Legg, T., & Simpson, I. (2019). HadUK-Grid—A new UK dataset of gridded climate observations. *Geoscience Data Journal*, *6*, 151–159.
- Holt, J., Polton, J., Huthnance, J., Wakelin, S., O’Dea, E., Harle, J., Yool, A., Artioli, Y., Blackford, J., Siddorn, J., & Inall, M. (2018). Climate-driven change in the North Atlantic and Arctic Oceans can greatly reduce the circulation of the North Sea. *Geophysical Research Letters*, *45*, 11827–11836.
- Hopcroft, R. R., Roff, J. C., & Bouman, H. A. (1998). Zooplankton growth rates: the larvaceans *Appendicularia*, *Fritillaria* and *Oikopleura* in tropical waters. *Journal of Plankton Research*, *20*, 539–555.
- Hunt, B. P. V., & Hosie, G. W. (2003). The Continuous Plankton Recorder in the Southern Ocean: a comparative analysis of zooplankton communities sampled by the CPR and vertical net hauls along 140°E. *Journal of Plankton Research*, *25*, 1561–1579.
- Hurst, T. P., & Conover, D. O. (2003). Seasonal and interannual variation in the allometry of energy allocation in juvenile striped bass. *Ecology*, *84*, 3360–3369.
- Hurvich, C., & Tsai, C.-L. (1989). Regression and time series model selection in small samples. *Biometrika*, *76*, 297–307.
- Hutchings, J. A., Minto, C., Ricard, D., Baum, J. K., & Jensen, O. P. (2010). Trends in the abundance of marine fishes. *Canadian Journal of Fisheries and Aquatic Sciences*, *67*, 1205–1210.
- ICES. (2017). Report of the Benchmark Workshop on Sandeel (WKSand 2016), 31 October - 4 November 2016, Bergen, Norway., ICES CM 2016/ACOM:33.
- ICES. (2020a). Sandeel (*Ammodytes* spp.) in divisions 4.a–b and Subdivision 20, Sandeel Area 3r (northern and central North Sea, Skagerrak), Report of the ICES Advisory Committee, 2020. Retrieved from <https://doi.org/10.17895/ices.advice.4722>
- ICES. (2020b). Sandeel (*Ammodytes* spp.) in divisions 4.a–b, Sandeel Area 4 (northern and central North Sea), Report of the ICES Advisory Committee, 2020. Retrieved from <https://doi.org/10.17895/ices.advice.4723>

- ICES. (2020c). Sandeel (*Ammodytes* spp.) in divisions 4.b and 4.c, Sandeel Area 1r (central and southern North Sea, Dogger Bank), Report of the ICES Advisory Committee, 2020. Retrieved from <https://doi.org/10.17895/ices.advice.5760>
- Ims, R. A., & Andreassen, H. P. (2000). Spatial synchronization of vole population dynamics by predatory birds. *Nature*, *408*, 194–196.
- Irigoien, X., Conway, D. V. P., & Harris, R. P. (2004). Flexible diel vertical migration behaviour of zooplankton in the Irish Sea. *Marine Ecology Progress Series*, *267*, 85–97.
- Jacobsen, S., Gaard, E., Hátún, H., Steingrund, P., Larsen, K. M. H., Reinert, J., Ólafsdóttir, S. R., Poulsen, M., & Vang, H. B. M. (2019). Environmentally driven ecological fluctuations on the Faroe Shelf revealed by fish juvenile surveys. *Frontiers in Marine Science*, *6*, 559.
- Jensen, H. (2000). *Settlement dynamics in the lesser sandeel *Ammodytes marinus* in the North Sea* (PhD Thesis, University of Aberdeen).
- Jensen, H., Rindorf, A., Wright, P. J., & Mosegaard, H. (2011). Inferring the location and scale of mixing between habitat areas of lesser sandeel through information from the fishery. *ICES Journal of Marine Science*, *68*, 43–51.
- Jiménez-Mena, B., Le Moan, A., Christensen, A., van Deurs, M., Mosegaard, H., Hemmer-Hansen, J., & Bekkevold, D. (2020). Weak genetic structure despite strong genomic signal in lesser sandeel in the North Sea. *Evolutionary Applications*, *13*, 376–387.
- JNCC. (2016). *Seabird population trends and causes of change: 1986-2015 Report*. Retrieved from <http://jncc.defra.gov.uk/page-3201>
- JNCC. (2020). *Seabird population trends and causes of change: 1986-2018 Report*. Retrieved from <https://jncc.gov.uk/our-work/smp-report-1986-2018>
- Jobling, M. (1981). The influences of feeding on the metabolic rate of fishes: a short review. *Journal of Fish Biology*, *18*, 385–400.
- Jobling, M. (1993). Bioenergetics: feed intake and energy partitioning. In J. C. Rankin & F. B. Jensen (Eds.), *Fish ecophysiology* (pp. 1–44). Dordrecht: Springer.
- Johannessen, T., & Johnsen, E. (2015). *Demographically disconnected subpopulations in lesser sandeel (*Ammodytes marinus*) as basis of a high resolution spatial management system*. *ICES CM 2015/E:12*.
- John, E. H., Batten, S. D., Harris, R. P., & Hays, G. C. (2001). Comparison between zooplankton data collected by the Continuous Plankton Recorder survey in the English Channel and by WP-2 nets at station L4, Plymouth (UK). *Journal of Sea Research*, *46*, 223–232.
- John, E. H., Batten, S. D., Stevens, D., Walne, A. W., Jonas, T., & Hays, G. C. (2002). Continuous Plankton Records stand the test of time: evaluation of flow rates, clogging and the continuity of the CPR time-series. *Journal of Plankton Research*, *24*, 941–946.
- Johnsen, E., Pedersen, R., & Ona, E. (2009). Size-dependent frequency response of sandeel schools. *ICES Journal of Marine Science*, *66*, 1100–1105.
- Johnsen, E., Rieucan, G., Ona, E., & Skaret, G. (2017). Collective structures anchor massive schools of lesser sandeel to the seabed, increasing vulnerability to fishery. *Marine Ecology Progress Series*, *573*, 229–236.
- Jones, W. (2001). *Modelling the growth and resource allocation dynamics of juvenile salmonids* (PhD Thesis, University of Strathclyde).

- Kaiser, M. J., Westhead, A. P., Hughes, R. N., & Gibson, R. N. (1992). Are digestive characteristics important contributors to the profitability of prey? A study of diet selection in the fifteen-spined stickleback, *Spinachia spinachia* (L.) *Oecologia*, *90*, 61–69.
- Kane, J. (2009). A comparison of two zooplankton time series data collected in the Gulf of Maine. *Journal of Plankton Research*, *31*, 249–259.
- Kassambara, A., & Mundt, F. (2017). *factoextra: extract and visualize the results of multivariate data analyses*. R package version 1.0.5. Retrieved from <https://CRAN.R-project.org/package=factoextra>
- Kaufman, L., & Rousseeuw, P. J. (2005). *Finding groups in data: An introduction to cluster analysis*. Hoboken: John Wiley.
- King, K. R., I, Hoilibaugh, J. T., & Azam, F. (1980). Predator-prey interactions between the larvacean *Oikopleura dioica* and bacterioplankton in enclosed water columns. *Marine Biology*, *56*, 49–57.
- Kjørboe, T. (2013). Zooplankton body composition. *Limnology and Oceanography*, *58*, 1843–1850.
- Koenker, R. (2018). *quantreg: quantile Regression*. R package version 5.38. Retrieved from <https://CRAN.R-project.org/package=quantreg>
- Kooijman, S. A. L. M. (2000). *Dynamic energy and mass budgets in biological systems* (2nd ed.). Cambridge: Cambridge University Press.
- Kraft, A., Nöthig, E.-M., Bauerfeind, E., Wildish, D. J., Pohle, G. W., Bathmann, U. V., Beszczynska-Möller, A., & Klages, M. (2013). First evidence of reproductive success in a southern invader indicates possible community shifts among Arctic zooplankton. *Marine Ecology Progress Series*, *493*, 291–296.
- Krogdahl, Å., & Bakke-McKellep, A. M. (2005). Fasting and refeeding cause rapid changes in intestinal tissue mass and digestive enzyme capacities of Atlantic salmon (*Salmo salar* L.) *Comparative Biochemistry and Physiology, Part A*, *141*, 450–460.
- Kulka, D. W., & Corey, S. (2006). Length and weight Relationships of euphausiids and caloric values of *Meganycitiphanes Norvegica* (M. Sars) in the Bay of Fundy. *Journal of Crustacean Biology*, *2*, 239–247.
- Lahoz-Monfort, J. L., Morgan, B. J. T., Harris, M. P., Daunt, F., Wanless, S., & Freeman, S. N. (2013). Breeding together: modeling synchrony in productivity in a seabird community. *Ecology*, *94*, 3–10.
- Lalli, C., & Parsons, T. R. (1997). *Biological oceanography: an introduction* (2nd ed.). Elsevier.
- Langsdale, T. R. M. (1993). Developmental changes in the opacity of larval herring, *Clupea harengus*, and their implications for vulnerability to predation. *Journal of the Marine Biological Association of the United Kingdom*, *73*, 225–232.
- Larimer, S. (1992). *Aspects of the bioenergetics and ecology of sand lance of Georges Bank* (PhD Thesis, University of Rhode Island).
- Laurence, G. (1976). Caloric values of some North Atlantic calanoid copepods. *Fishery Bulletin*, *74*, 218–220.
- Lewis, S., Wanless, S., Wright, P. J., Harris, M. P., Bull, J., & Elston, D. A. (2001). Diet and breeding performance of black-legged kittiwakes *Rissa tridactyla* at a North Sea colony. *Marine Ecology Progress Series*, *221*, 277–284.
- Lichstein, J. W. (2007). Multiple regression on distance matrices: a multivariate spatial analysis tool. *Plant Ecology*, *188*, 117–131.

- Liebold, A., Koenig, W. D., & Bjørnstad, O. N. (2004). Spatial synchrony in population dynamics. *Annual Review of Ecology, Evolution, and Systematics*, *35*, 467–490.
- Lika, K., & Nisbet, R. M. (2000). A Dynamic Energy Budget model based on partitioning of net production. *Journal of Mathematical Biology*, *41*, 361–386.
- Lilliendahl, K., Hansen, E. S., Bogason, V., Sigursteinsson, M., Magnúsdóttir, M. L., Jónsson, P. M., Helgason, H. H., Óskarsson, G. J., Óskarsson, P. F., & Sigursson, Ó. J. (2013). Vikomubrestur lunda og sandsílis við Vestmannaeyjar. *Náttúrufræingurinn*, *83*, 65–79.
- Lindgren, M., van Deurs, M., MacKenzie, B. R., Worsoe Clausen, L., Christensen, A., & Rindorf, A. (2017). Productivity and recovery of forage fish under climate change and fishing: North Sea sandeel as a case study. *Fisheries Oceanography*, *27*, 212–221.
- Lindley, J. A. (1977). Continuous Plankton Records: the distribution of the Euphausiacea (Crustacea: Malacostraca) in the North Atlantic and the North Sea, 1966–1967. *Journal of Biogeography*, *4*, 121.
- Lindley, J. A. (1998). Dry weights, carbon and nitrogen content of decapod larvae from the plankton. *Journal of the Marine Biological Association of the United Kingdom*, *78*, 341–344.
- Lindley, J. A., Beaugrand, G., Luczak, C., Dewarumez, J., & Kirby, R. R. (2010). Warm-water decapods and the trophic amplification of climate in the North Sea. *Biology Letters*, *6*, 773–776.
- Lindley, J. A., John, A. W. G., & Robins, D. B. (1997). Dry weight, carbon and nitrogen content of some calanoid copepods from the seas around southern Britain in winter. *Journal of the Marine Biological Association of the United Kingdom*, *77*, 249–252.
- Lindley, J. A., Robins, D. B., & Williams, R. (1999). Dry weight carbon and nitrogen content of some euphausiids from the north Atlantic Ocean and the Celtic Sea. *Journal of Plankton Research*, *21*, 2053–2066.
- Lindley, J. A., & Williams, R. (1980). Plankton of the Fladen Ground during FLEX 76 II. Population dynamics and production of *Thysanoessa inermis* (Crustacea: Euphausiacea). *Marine Biology*, *57*, 79–86.
- Link, J. (1996). Capture probabilities of Lake Superior zooplankton by an obligate planktivorous fish — the lake herring. *Transactions of the American Fisheries Society*, *125*, 139–142.
- Litzow, M. A., Piatt, J. F., Abookire, A. A., Prichard, A. K., & Robards, M. D. (2000). Monitoring temporal and spatial variability in sandeel (*Ammodytes hexapterus*) abundance with pigeon guillemot (*Cepphus columba*) diets. *ICES Journal of Marine Science*, *57*, 976–986.
- Ljungström, G., Claireaux, M., Fiksen, Ø., & Jørgensen, C. (2020). Body size adaptations under climate change: zooplankton community more important than temperature or food abundance in model of a zooplanktivorous fish. *Marine Ecology Progress Series*, *636*, 1–18.
- Luecke, C., Rice, J. A., Crowder, L. B., Yeo, S. E., & Binkowski, F. P. (1990). Recruitment mechanisms of bloater in Lake Michigan: an analysis of the predatory gauntlet. *Canadian Journal of Fisheries and Aquatic Sciences*, *47*, 524–532.

- Lynam, C. P., Halliday, N. C., Höffle, H., Wright, P. J., van Damme, C. J. G., Edwards, M., & Pitois, S. G. (2013). Spatial patterns and trends in abundance of larval sandeels in the North Sea: 1950–2005. *ICES Journal of Marine Science*, *70*, 540–553.
- Lynam, C. P., Llope, M., Möllmann, C., Helaouët, P., Bayliss-Brown, G. A., & Stenseth, N. C. (2017). Interaction between top-down and bottom-up control in marine food webs. *Proceedings of the National Academy of Sciences*, *114*, 1952–1957.
- Maar, M., Saurel, C., Landes, A., Dolmer, P., & Petersen, J. K. (2015). Growth potential of blue mussels (*M. edulis*) exposed to different salinities evaluated by a Dynamic Energy Budget model. *Journal of Marine Systems*, *148*, 48–55.
- MacDonald, A. (2017). *Modelling the impact of environmental change on the physiology and ecology of sandeels* (PhD Thesis, University of Strathclyde).
- MacDonald, A., Heath, M. R., Edwards, M., Furness, R. W., Pinnegar, J. K., Wanless, S., Speirs, D. C., & Greenstreet, S. P. R. (2015). Climate driven trophic cascades affecting seabirds around the British Isles. *Oceanography and Marine Biology: An Annual Review*, *53*, 55–79.
- MacDonald, A., Heath, M. R., Greenstreet, S. P. R., & Speirs, D. C. (2019a). Timing of sandeel spawning and hatching off the east coast of Scotland. *Frontiers in Marine Science*, *6*, 70.
- MacDonald, A., Speirs, D. C., Greenstreet, S. P. R., & Heath, M. R. (2018). Exploring the influence of food and temperature on North Sea sandeels using a new Dynamic Energy Budget model. *Frontiers in Marine Science*, *5*, 339.
- MacDonald, A., Speirs, D. C., Greenstreet, S. P. R., Boulcott, P., & Heath, M. R. (2019b). Trends in sandeel growth and abundance off the east coast of Scotland. *Frontiers in Marine Science*, *6*, 201.
- Macer, C. T. (1966). Sand eels (Ammodytidae) in the south-western North Sea; their biology and fishery. *Fisheries Investigations. London Series 2*, *24*, 1–55.
- Mackas, D. L., Denman, K. L., & Abbott, M. R. (1985). Plankton patchiness: biology in the physical vernacular. *Bulletin of Marine Science*, *37*, 652–674.
- Mackinson, S. (2007). Multi-species fisheries management: a comprehensive impact assessment of the sandeel fishery along the English east coast, Cefas M0323/02.
- Maechler, M., Rousseeuw, P., Struyf, A., Hubert, M., & Hornik, K. (2018). *cluster: cluster analysis basics and extensions*. R package version 2.0.7-1.
- Margulies, D. (1989). Size-specific vulnerability to predation and sensory system development of white seabass, *Atractoscion nobilis*, larvae. *Fishery Bulletin*, *87*, 537–552.
- Marine Scotland Science. (2018). Scottish Coastal Observatory - Stonehaven site data. Retrieved from <https://data.marine.gov.scot/dataset/scottish-coastal-observatory-stonehaven-site>
- Marquez, J. F., Lee, A. M., Aanes, S., Engen, S., Herfindal, I., Salthaug, A., & Sæther, B.-E. (2019). Spatial scaling of population synchrony in marine fish depends on their life history. *Ecology Letters*, *22*, 1787–1796.
- May, W., Ganske, A., Leckebusch, G. C., Rockel, B., Tinz, B., & Ulbrich, U. (2016). Projected change-atmosphere. In M. Quante & F. Colijn (Eds.), *North Sea Region climate change assessment* (pp. 149–173). Springer.
- McGinty, N., Power, A. M., & Johnson, M. P. (2011). Variation among northeast Atlantic regions in the responses of zooplankton to climate change: Not all areas

- follow the same path. *Journal of Experimental Marine Biology and Ecology*, *400*, 120–131.
- McHardy, R. A. (1970). *Distribution and abundance of hyperiid amphipods in near-surface water of the North Atlantic Ocean and North Sea* (PhD Thesis, University of Edinburgh).
- Meyer, T. L., Cooper, R. A., & Langton, R. W. (1979). Relative abundance, behavior, and food habits of the American sand lance, *Ammodytes americanus*, from the Gulf of Maine. *Fishery Bulletin*, *77*, 243–253.
- Miller, T. J., Crowder, L. B., & Rice, J. A. (1993). Ontogenetic changes in behavioural and histological measures of visual acuity in three species of fish. *Environmental Biology of Fishes*, *37*, 1–8.
- Mills, E. L., Confer, J. L., & Ready, R. C. (1984). Prey selection by young yellow perch: The influence of capture success, visual acuity, and prey choice. *Transactions of the American Fisheries Society*, *113*, 579–587.
- Mitchell, P. I., Newton, S. F., Ratcliffe, N., & Dunn, T. E. (2004). *Seabird populations of Britain and Ireland: results of the Seabird 2000 census (1998-2002)*. London: T & AD Poyser.
- Moran, P. A. P. (1953). The statistical analysis of the Canadian lynx cycle. *Australian Journal of Zoology*, *1*, 291–298.
- Newell, M., Harris, M. P., Wanless, S., Burthe, S., Bogdanova, M., M, G. C., & Daunt, F. (2016). *The Isle of May long-term study (IMLOTS) seabird annual breeding success 1982-2016 NERC Environmental Information Data Centre*. Retrieved from <https://doi.org/10.5285/02c98a4f-8e20-4c48-8167-1cd5044c4afe>
- Newell, M., Wanless, S., Harris, M. P., & Daunt, F. (2015). Effects of an extreme weather event on seabird breeding success at a North Sea colony. *Marine Ecology Progress Series*, *532*, 257–268.
- Ney, J. J. (1993). Bioenergetics modeling today: growing pains on the cutting edge. *Transactions of the American Fisheries Society*, *122*, 736–748.
- Nisbet, R. M., Jusup, M., Klanjscek, T., & Pecquerie, L. (2012). Integrating dynamic energy budget (DEB) theory with traditional bioenergetic models. *Journal of Experimental Biology*, *215*, 892–902.
- Nishikawa, T., Nakamura, Y., Okamoto, S., & Ueda, H. (2020). Interannual decrease in condition factor of the western sand lance *Ammodytes japonicus* in Japan in the last decade: Evidence for food-limited decline of the catch. *Fisheries Oceanography*, *29*, 52–55.
- O’Hanlon, N. J., & Nager, R. G. (2018). Identifying habitat-driven spatial variation in colony size of herring gulls *Larus argentatus*. *Bird Study*, *65*, 306–316.
- Odum, E. P. (1968). American Zoologist. *Integrative and Comparative Biology*, *8*, 11–18.
- Ohlberger, J. (2013). Climate warming and ectotherm body size - from individual physiology to community ecology. *Functional Ecology*, *27*, 991–1001.
- Olin, A. B., Banas, N. S., Wright, P. J., Heath, M. R., & Nager, R. G. (2020). Spatial synchrony of breeding success in the black-legged kittiwake *Rissa tridactyla* reflects the spatial dynamics of its sandeel prey. *Marine Ecology Progress Series*, *638*, 177–190.

- Opdal, A. F., Lindemann, C., & Aksnes, D. L. (2019). Centennial decline in North Sea water clarity causes strong delay in phytoplankton bloom timing. *Global Change Biology*, *25*, 3946–3953.
- Oro, D., & Furness, R. W. (2002). Influences of food availability and predation on survival of kittiwakes. *Ecology*, *83*, 2516–2528.
- Österblom, H., Olsson, O., Blenckner, T., & Furness, R. W. (2008). Junk-food in marine ecosystems. *Oikos*, *117*, 967–977.
- Ostle, C., Artigas, L. F., Atkinson, A., Aubert, A., Budria, A., Graham, G., Helaouët, P., Johns, D., Padegimas, B., Rombouts, I., Widdicombe, C., & McQuatters-Gollop, A. (2017). Spatial representivity of plankton indicators, EcApRHA1.3/2017.
- Östman, Ö., Olsson, J., Dannewitz, J., Palm, S., & Florin, A.-B. (2017). Inferring spatial structure from population genetics and spatial synchrony in demography of Baltic Sea fishes: implications for management. *Fish and Fisheries*, *18*, 324–339.
- Owen, R. W. (1989). Microscale and finescale variations of small plankton in coastal and pelagic environments. *Journal of Marine Research*, *47*, 197–240.
- Owens, N. J. P., Hosie, G. W., Batten, S. D., Edwards, M., Johns, D. G., & Beaugrand, G. (2013). All plankton sampling systems underestimate abundance: Response to “Continuous Plankton Recorder underestimates zooplankton abundance” by J.W. Dippner and M. Krause. *Journal of Marine Systems*, *128*, 240–242.
- Paleczny, M., Hammill, E., Karpouzi, V., & Pauly, D. (2015). Population trend of the world’s monitored seabirds, 1950–2010. *PLoS ONE*, *10*, e0129342.
- Palmqvist, E., & Lundberg, P. (1998). Population extinctions in correlated environments. *Oikos*, *83*, 359–367.
- Pebesma, E. J., & Bivand, R. S. (2005). Classes and methods for spatial data in R. *R News*, *5*, 9–13. Retrieved from <https://CRAN.R-project.org/doc/Rnews/>
- Pecquerie, L., Petitgas, P., & Kooijman, S. A. L. M. (2009). Modeling fish growth and reproduction in the context of the Dynamic Energy Budget theory to predict environmental impact on anchovy spawning duration. *Journal of Sea Research*, *62*, 93–105.
- Pepin, P., Pearre, S., & Koslow, J. A. (1987). Predation on larval fish by Atlantic mackerel, *Scomber scombrus*, with a comparison of predation by zooplankton. *Canadian Journal of Fisheries and Aquatic Sciences*, *44*, 2012–2018.
- Persson, L. (1979). The effects of temperature and different food organisms on the rate of gastric evacuation in perch *Perca fluviatilis*. *Freshwater Biology*, *9*, 99–104.
- Persson, L. (1981). The effects of temperature and meal size on the rate of gastric evacuation in perch (*Perca fluviatilis*) fed on fish larvae. *Freshwater Biology*, *11*, 131–138.
- Persson, L. (1982). Rate of food evacuation in roach (*Rutilus rutilus*) in relation to temperature, and the application of evacuation rate estimates for studies on the rate of food consumption. *Freshwater Biology*, *12*, 203–210.
- Pikitch, E. K., Rountos, K. J., Essington, T. E., Santora, C., Pauly, D., Watson, R., Sumaila, U. R., Boersma, P. D., Boyd, I. L., Conover, D. O., Cury, P., Heppell, S. S., Houde, E. D., Mangel, M., Plagányi, É., Sainsbury, K., Steneck, R. S., Geers, T. M., Gownaris, N., & Munch, S. B. (2014). The global contribution of forage fish to marine fisheries and ecosystems. *Fish and Fisheries*, *15*, 43–64.

- Pirhonen, J., Muuri, L., Kalliokoski, S. M., Puranen, M. M., & Marjomäki, T. J. (2019). Seasonal and ontogenetic variability in stomach size of Eurasian perch (*Perca fluviatilis* L.) *Aquaculture International*, *27*, 1125–1135.
- Pitcher, T. J., & Wyche, C. J. (1983). Predator-avoidance behaviours of sand-eel schools: why schools seldom split. In D. L. G. Noakes, D. G. Lindquist, G. S. Helfman, & J. A. Ward (Eds.), *Predators and prey in fishes* (pp. 193–204). Dordrecht: Springer.
- Pitois, S. G., & Fox, C. J. (2006). Long-term changes in zooplankton biomass concentration and mean size over the Northwest European shelf inferred from Continuous Plankton Recorder data. *ICES Journal of Marine Science*, *63*, 785–798.
- Planque, B., & Fromentin, J.-M. (1996). *Calanus* and environment in the eastern North Atlantic. I. Spatial and temporal patterns of *C. finmarchicus* and *C. helgolandicus*. *Marine Ecology Progress Series*, *134*, 101–109.
- Poloczanska, E. S., Brown, C. J., Sydeman, W. J., Kiessling, W., Schoeman, D. S., Moore, P. J., Brander, K., Bruno, J. F., Buckley, L. B., Burrows, M. T., Duarte, C. M., Halpern, B. S., Holding, J., Kappel, C. V., O'Connor, M. I., Pandolfi, J. M., Parmesan, C., Schwing, F., Thompson, S. A., & Richardson, A. J. (2013). Global imprint of climate change on marine life. *Nature Climate Change*, *3*, 919–925.
- Poloczanska, E. S., Cook, R. M., Ruxton, G. D., & Wright, P. J. (2004). Fishing vs. natural recruitment variation in sandeels as a cause of seabird breeding failure at Shetland: a modelling approach. *ICES Journal of Marine Science*, *61*, 788–797.
- Post, E., & Forchhammer, M. C. (2002). Synchronization of animal population dynamics by large-scale climate. *Nature*, *420*, 168–171.
- Post, J. R., & Parkinson, E. A. (2001). Energy allocation strategy in young fish: allometry and survival. *Ecology*, *82*, 1040–1051.
- Proctor, R., Wright, P. J., & Everitt, A. (1998). Modelling the transport of larval sandeels on the north-west European shelf. *Fisheries Oceanography*, *7*, 347–354.
- Purcell, J. E., & Sturdevant, M. V. (2001). Prey selection and dietary overlap among zooplanktivorous jellyfish and juvenile fishes in Prince William Sound, Alaska. *Marine Ecology Progress Series*, *210*, 67–83.
- Pyper, B. J., & Peterman, R. M. (1998). Comparison of methods to account for autocorrelation in correlation analyses of fish data. *Canadian Journal of Fisheries and Aquatic Sciences*, *55*, 2127–2140.
- Quinn, T., & Schneider, D. E. (1991). Respiration of the teleost fish *Ammodytes hexapterus* in relation to its burrowing behavior. *Comparative Biochemistry and Physiology – Part A: Physiology*, *98*, 71–75.
- R Core Team. (2018). *R: A language and environment for statistical computing*. R Foundation for Statistical Computing. Vienna, Austria. Retrieved from <https://www.R-project.org/>
- Raab, K., Nagelkerke, L. A. J., Boérée, C., Rijnsdorp, A. D., Temming, A., & Dickey-Collas, M. (2012). Dietary overlap between the potential competitors herring, sprat and anchovy in the North Sea. *Marine Ecology Progress Series*, *470*, 101–111.

- Rankine, P. W., & Morrison, J. A. (1989). Predation on herring larvae and eggs by sand-eels *Ammodytes marinus* (Raitt) and *Hyperoplus lanceolatus* (Lesauvage). *Journal of the Marine Biological Association of the United Kingdom*, *69*, 493–498.
- Razouls, C., de Bovée, F., Kouwenberg, J., & Desreumaux, N. (2020). Diversity and geographic distribution of marine planktonic copepods. Retrieved March 20, 2020, from <http://copepodes.obs-banyuls.fr/en>
- Reay, P. J. (1970). Synopsis of the biological data on North Atlantic sand eels of the genus *Ammodytes*. *FAO Fisheries Synopsis*, *82*.
- Reeves, S. A. (1994). Seasonal and annual variation in catchability of sandeels at Shetland. *ICES CM*, *1994/D:19*.
- Régnier, T., Gibb, F. M., & Wright, P. J. (2017). Importance of trophic mismatch in a winter-hatching species: evidence from lesser sandeel. *Marine Ecology Progress Series*, *567*, 185–197.
- Régnier, T., Gibb, F. M., & Wright, P. J. (2018). Temperature effects on egg development and larval condition in the lesser sandeel, *Ammodytes marinus*. *Journal of Sea Research*, *134*, 34–41.
- Régnier, T., Gibb, F. M., & Wright, P. J. (2019). Understanding temperature effects on recruitment in the context of trophic mismatch. *Scientific Reports*, *9*, 15179.
- Reid, P. C., Colebrook, J. M., Matthews, J. B. L., & Aiken, J. (2003a). The Continuous Plankton Recorder: concepts and history, from Plankton Indicator to undulating recorders. *Progress in Oceanography*, *58*, 117–173.
- Reid, P. C., Edwards, M., Beaugrand, G., Skogen, M., & Stevens, D. (2003b). Periodic changes in the zooplankton of the North Sea during the twentieth century linked to oceanic inflow. *Fisheries Oceanography*, *12*, 260–269.
- Ren, J. S., & Ross, A. H. (2001). A dynamic energy budget model of the Pacific oyster *Crassostrea gigas*. *Ecological Modelling*, *142*, 105–120.
- Rice, J. A., Crowder, L. B., & Binkowski, F. P. (1987). Evaluating potential sources of mortality for larval bloater (*Coregonus hoyi*): starvation and vulnerability to predation. *Canadian Journal of Fisheries and Aquatic Sciences*, *44*, 467–472.
- Richardson, A. J. (2008). In hot water: zooplankton and climate change. *ICES Journal of Marine Science*, *65*, 279–295.
- Richardson, A. J., John, E. H., Irigoien, X., Harris, R. P., & Hays, G. C. (2004). How well does the Continuous Plankton Recorder (CPR) sample zooplankton? A comparison with the Longhurst Hardy Plankton Recorder (LHPR) in the northeast Atlantic. *Deep-Sea Research Part I: Oceanographic Research Papers*, *51*, 1283–1294.
- Richardson, A. J., Walne, A. W., John, A. W. G., Jonas, T. D., Lindley, J. A., Sims, D. W., Stevens, D., & Witt, M. (2006). Using Continuous Plankton Recorder data. *Progress in Oceanography*, *68*, 27–74.
- Riis-Vestergaard, J. (2002). Energy density of marine pelagic fish eggs. *Journal of Fish Biology*, *60*, 1511–1528.
- Rindorf, A., Wanless, S., & Harris, M. P. (2000). Effects of changes in sandeel availability on the reproductive output of seabirds. *Marine Ecology Progress Series*, *202*, 241–252.
- Rindorf, A., Henriksen, O., & van Deurs, M. (2019). Scale-specific density dependence in North Sea sandeel. *Marine Ecology Progress Series*, *619*, 97–110.

- Rindorf, A., Wright, P. J., Jensen, H., & Maar, M. (2016). Spatial differences in growth of lesser sandeel in the North Sea. *Journal of Experimental Marine Biology and Ecology*, *479*, 9–19.
- Ripa, J., & Ranta, E. (2007). Biological filtering of correlated environments: towards a generalised Moran theorem. *Oikos*, *116*, 783–792.
- Robards, M. D., Willson, M. F., Armstrong, R. H., & Piatt, J. F. (1999a). Sand lance: a review of biology and predator relations and annotated bibliography, PNW-RP-521.
- Robards, M. D., Anthony, J. A., Rose, G. A., & Piatt, J. F. (1999b). Changes in proximate composition and somatic energy content for Pacific sand lance (*Ammodytes hexapterus*) from Kachemak Bay, Alaska relative to maturity and season. *Journal of Experimental Marine Biology and Ecology*, *242*, 245–258.
- Robards, M. D., Rose, G. A., & Piatt, J. F. (2002). Growth and abundance of Pacific sand lance, *Ammodytes hexapterus*, under differing oceanographic regimes. *Environmental Biology of Fishes*, *64*, 429–441.
- Robertson, G. S., Bolton, M., Grecian, W. J., & Monaghan, P. (2014). Inter- and intra-year variation in foraging areas of breeding kittiwakes (*Rissa tridactyla*). *Marine Biology*, *161*, 1973–1986.
- Rodhouse, P. G., & Roden, C. M. (2007). Carbon budget for a coastal inlet in relation to intensive cultivation of suspension-feeding bivalve mollusks. *Marine Ecology Progress Series*, *36*, 225–236.
- Roessingh, M. (1957). Problems arising from the expansion of the industrial fishery for sandeel, *Ammodytes marinus* Raitt, towards the Dutch coastal area, ICES CM 1957.
- Ryland, J. S. (1964). The feeding of plaice and sand-eel larvae in the southern North Sea. *Journal of the Marine Biological Association of the United Kingdom*, *44*, 343–364.
- Salonen, K., Sarvala, J., Hakala, I., & Viljanen, M.-L. (1976). The relation of energy and organic carbon in aquatic invertebrates. *Limnology and Oceanography*, *21*, 724–730.
- Sameoto, D., Cochrane, N., & Herman, A. (1993). Convergence of acoustic, optical, and net-catch estimates of euphausiid abundance: use of artificial light to reduce net avoidance. *Canadian Journal of Fisheries and Aquatic Sciences*, *50*, 334–346.
- Sandvik, H., Reiertsen, T. K., Erikstad, K. E., Anker-Nilssen, T., Barrett, R. T., Lorentsen, S.-H., Systad, G. H., & Myksvoll, M. S. (2014). The decline of Norwegian kittiwake populations: modelling the role of ocean warming. *Climate Research*, *60*, 91–102.
- Schmidt, K., Birchill, A. J., Atkinson, A., Brewin, R. J., Clark, J. R., Hickman, A. E., Johns, D. G., Lohan, M. C., Milne, A., Pardo, S., Polimene, L., Smyth, T. J., Tarran, G. A., Widdicombe, C. E., Woodward, E. M. S., & Ussher, S. J. (2020). Increasing picocyanobacteria success in shelf waters contributes to long-term food web degradation. *Global Change Biology*, 1–14.
- Schrum, C., Lowe, J., Meier, H. E. M., Graebmann, I., Holt, J., Mathis, M., Pohlmann, T., D, S. M., Sterl, A., & Wakelin, S. (2016). Projected change — North Sea. In M. Quante & F. Colijn (Eds.), *North Sea Region climate change assessment* (pp. 175–218). Springer.

- Schwartz, M. K., Mills, L. S., McKelvey, K. S., Ruggiero, L. F., & Allendorf, F. W. (2002). DNA reveals high dispersal synchronizing the population dynamics of Canada lynx. *Nature*, *415*, 520–522.
- Scopel, L., Diamond, A., Kress, S., & Shannon, P. (2019). Varied breeding responses of seabirds to a regime shift in prey base in the Gulf of Maine. *Marine Ecology Progress Series*, *626*, 177–196.
- Scott, J. S. (1973). Food and inferred feeding behavior of Northern Sand Lance (*Ammodytes dubius*). *Journal of the Fisheries Research Board of Canada*, *30*, 451–454.
- Secor, S. M. (2009). Specific dynamic action: a review of the postprandial metabolic response. *Journal of Comparative Physiology B: Biochemical, Systemic, and Environmental Physiology*, *179*, 1–56.
- Sekiguchi, H. (1977). Further observation on the feeding habits of planktivorous fish sand-eel in Ise Bay. *Bulletin of the Japanese Society of Scientific Fisheries*, *43*, 417–422.
- Sekiguchi, H., Nagoshi, M., Horiuchi, K., & Nakanishi, N. (1976). Feeding, fat deposits and growth of sand-eels in Ise bay, central Japan. *Bulletin of the Japanese Society of Scientific Fisheries*, *42*, 831–835.
- Shannon, J. G. (1975). Correlation of beam and diffuse attenuation coefficients measured in selected ocean waters. *SPIE*, *64*, 3–11.
- Sheridan, J. A., & Bickford, D. (2011). Shrinking body size as an ecological response to climate change. *Nature Climate Change*, *1*, 401–406.
- Signal Developers. (2014). *signal: signal processing*. Retrieved from <http://r-forge.r-project.org/projects/signal/>
- Simonsen, C. S., Munk, P., Folkvord, A., & Pedersen, S. A. (2006). Feeding ecology of Greenland halibut and sandeel larvae off West Greenland. *Marine Biology*, *149*, 937–952.
- Sogard, S. M. (1997). Size-selective mortality in the juvenile stage of teleost fishes: a review. *Bulletin of Marine Science*, *60*, 1129–1157.
- South, A. (2011). rworldmap: a new R package for mapping global data. *The R Journal*, *3*, 35–43. Retrieved from http://journal.r-project.org/archive/2011-1/RJournal_2011-1_South.pdf
- Stenseth, N. C., Mysterud, A., Ottersen, G., Hurrell, J. W., Chan, K.-S., & Lima, M. (2002). Ecological effects of climate fluctuations. *Science*, *297*, 1292–1296.
- Stroud, G. D. (2011). The herring. *Torry Advisory Note*, *57*.
- Sun, Y., Liu, Y., Liu, X., & Tang, O. (2010). The influence of particle size of dietary prey on food consumption and ecological conversion efficiency of young-of-the-year sand lance, *Ammodytes personatus*. *Deep-Sea Research Part II: Topical Studies in Oceanography*, *57*, 1001–1005.
- Suryan, R. M., Irons, D. B., & Benson, J. (2000). Prey switching and variable foraging strategies of black-legged kittiwakes and the effect on reproductive success. *The Condor*, *102*, 374–384.
- Sutcliffe, O. L., Thomas, C. D., & Moss, D. (1996). Spatial synchrony and asynchrony in butterfly population dynamics. *The Journal of Animal Ecology*, *65*, 85–95.
- Svensson, J.-E. (1995). Predation risk increases with clutch size in a copepod. *Functional Ecology*, *9*, 774–777.

- Sydeman, W. J., Poloczanska, E., Reed, T. E., & Thompson, S. A. (2015). Climate change and marine vertebrates. *Science*, *350*, 772–777.
- Tanskanen, S. (1994). Seasonal variability in the individual carbon content of the calanoid copepod *Acartia bifilosa* from the northern Baltic Sea. *Hydrobiologia*, *292-293*, 397–403.
- Thaxter, C. B., Lascelles, B., Sugar, K., Cook, A. S. C. P., Roos, S., Bolton, M., Langston, R. H. W., & Burton, N. H. K. (2012). Seabird foraging ranges as a preliminary tool for identifying candidate Marine Protected Areas. *Biological Conservation*, *156*, 53–61.
- Thayer, J. A., & Sydeman, W. J. (2007). Spatio-temporal variability in prey harvest and reproductive ecology of a piscivorous seabird, *Cerorhinca monocerata*, in an upwelling system. *Marine Ecology Progress Series*, *329*, 253–265.
- Thieurmel, B., & Elmarhraoui, A. (2019). *suncalc: compute sun position, sunlight phases, moon position and lunar phase*. R package version 0.5.0. Retrieved from <https://CRAN.R-project.org/package=suncalc>
- Thomas, Y., Mazurié, J., Alunno-Bruscia, M., Bacher, C., Bouget, J.-F., Gohin, F., Pouvreau, S., & Struski, C. (2011). Modelling spatio-temporal variability of *Mytilus edulis* (L.) growth by forcing a dynamic energy budget model with satellite-derived environmental data. *Journal of Sea Research*, *66*, 308–317.
- Thompson, G., Dinofrio, E. O., Alder, V. A., Takahashi, K. T., & Hosie, G. W. (2012). Copepod distribution in surface waters of the Drake Passage using Continuous Plankton Recorder and a Pump-Net onboard system. *Brazilian Journal of Oceanography*, *60*, 367–380.
- Tien, N. S. H., Craeymeersch, J., van Damme, C., Couperus, A. S., Adema, J., & Tulp, I. (2017). Burrow distribution of three sandeel species relates to beam trawl fishing, sediment composition and water velocity, in Dutch coastal waters. *Journal of Sea Research*, *127*, 194–202.
- Tomiyama, M., & Yanagibashi, S. (2004). Effect of temperature, age class, and growth on induction of aestivation in Japanese sandeel (*Ammodytes personatus*) in Ise Bay, central Japan. *Fisheries Oceanography*, *13*, 81–90.
- Utne-Palm, A. C. (1999). The effect of prey mobility, prey contrast, turbidity and spectral composition on the reaction distance of *Gobiusculus flavescens* to its planktonic prey. *Journal of Fish Biology*, *54*, 1244–1258.
- Uye, S.-i. (1982). Length-weight relationships of important zooplankton from the Inland Sea of Japan. *Journal of Oceanographical Society of Japan*, *38*, 149–158.
- van Couwelaar, M. (2003). Zooplankton and micronekton of the North Sea. Retrieved July 10, 2019, from <http://species-identification.org/index.php>
- van der Kooij, J., Scott, B. E., & Mackinson, S. (2008). The effects of environmental factors on daytime sandeel distribution and abundance on the Dogger Bank. *Journal of Sea Research*, *60*, 201–209.
- van Deurs, M., Hartvig, M., & Steffensen, J. F. (2011a). Critical threshold size for overwintering sandeels (*Ammodytes marinus*). *Marine Biology*, *158*, 2755–2764.
- van Deurs, M., Behrens, J. W., Warnar, T., & Steffensen, J. F. (2011b). Primary versus secondary drivers of foraging activity in sandeel schools (*Ammodytes tobianus*). *Marine Biology*, *158*, 1781–1789.

- van Deurs, M., Christensen, A., Frisk, C., & Mosegaard, H. (2010). Overwintering strategy of sandeel ecotypes from an energy/predation trade-off perspective. *Marine Ecology Progress Series*, *416*, 201–214.
- van Deurs, M., Christensen, A., & Rindorf, A. (2013). Patchy zooplankton grazing and high energy conversion efficiency: ecological implications of sandeel behavior and strategy. *Marine Ecology Progress Series*, *487*, 123–133.
- van Deurs, M., Jørgensen, C., & Fiksen, Ø. (2015). Effects of copepod size on fish growth: a model based on data for North Sea sandeel. *Marine Ecology Progress Series*, *520*, 235–243.
- van Deurs, M., Koski, M., & Rindorf, A. (2014). Does copepod size determine food consumption of particulate feeding fish? *ICES Journal of Marine Science*, *71*, 35–43.
- van Deurs, M., van Hal, R., Tomczak, M. T., Jónasdóttir, S. H., & Dolmer, P. (2009). Recruitment of lesser sandeel *Ammodytes marinus* in relation to density dependence and zooplankton composition. *Marine Ecology Progress Series*, *381*, 249–258.
- Varpe, Ø., & Fiksen, Ø. (2010). Seasonal plankton–fish interactions: light regime, prey phenology, and herring foraging. *Ecology*, *91*, 311–318.
- Verkuil, Y., Dekinga, A., Koolhaas, A., van der Winden, J., van der Have, T. M., & Chernichko, I. I. (2006). Migrating broad-billed sandpipers achieve high fuelling rates by taking a multi-course meal. *Wader Study Group Bulletin*, *110*, 15–20.
- Vigfúsdóttir, F. (2012). *Drivers of productivity in a subarctic seabird: Arctic Terns in Iceland* (PhD Thesis, University of East Anglia).
- Visser, A. W., & Fiksen, Ø. (2013). Optimal foraging in marine ecosystem models: selectivity, profitability and switching. *Marine Ecology Progress Series*, *473*, 91–101.
- von Biela, V. R., Arimitsu, M. L., Piatt, J. F., Heflin, B., Schoen, S. K., Trowbridge, J. L., & Clawson, C. M. (2019). Extreme reduction in nutritional value of a key forage fish during the pacific marine heatwave of 2014–2016. *Marine Ecology Progress Series*, *613*, 171–182.
- Votier, S. C., Bearhop, S., Ratcliffe, N., Phillips, R. A., & Furness, R. W. (2004). Predation by great skuas at a large Shetland seabird colony. *Journal of Applied Ecology*, *41*, 1117–1128.
- Wade, H. M., Masden, E. A., Jackson, A. C., Thaxter, C. B., Burton, N. H. K., Bouten, W., & Furness, R. W. (2014). Great skua (*Stercorarius skua*) movements at sea in relation to marine renewable energy developments. *Marine Environmental Research*, *101*, 69–80.
- Walsh, P. M., Halley, D. J., Harris, M. P., del Nevo, A., Sim, I. M. W., & Tasker, M. L. (1995). *Seabird monitoring handbook for Britain and Ireland: a compilation of methods for survey and monitoring of breeding birds*. Peterborough: Joint Nature Conservation Committee.
- Walter, J. A., Sheppard, L. W., Anderson, T. L., Kastens, J. H., Bjørnstad, O. N., Liebhold, A. M., & Reuman, D. C. (2017). The geography of spatial synchrony. *Ecology Letters*, *20*, 801–814.
- Wanless, S., Wright, P. J., Harris, M. P., & Elston, D. A. (2004). Evidence for decrease in size of lesser sandeels *Ammodytes marinus* in a North Sea aggregation over a 30-yr period. *Marine Ecology Progress Series*, *279*, 237–246.

- Wanless, S., Frederiksen, M., Daunt, F., Scott, B. E., & Harris, M. P. (2007). Black-legged kittiwakes as indicators of environmental change in the North Sea: Evidence from long-term studies. *Progress in Oceanography*, *72*, 30–38.
- Wanless, S., Harris, M. P., Newell, M. A., Speakman, J. R., & Daunt, F. (2018). Community-wide decline in the occurrence of lesser sandeels *Ammodytes marinus* in seabird chick diets at a North Sea colony. *Marine Ecology Progress Series*, *600*, 193–206.
- Wanless, S., Harris, M. P., Redman, P., & Speakman, J. R. (2005). Low energy values of fish as a probable cause of a major seabird breeding failure in the North Sea. *Marine Ecology Progress Series*, *294*, 1–8.
- Ward, J. J. (1963). Hierarchical grouping to optimize an objective function. *Journal of the American Statistical Association*, *58*, 236–244.
- Warner, A. J., & Hays, G. C. (1994). Sampling by the Continuous Plankton Recorder survey. *Progress In Oceanography*, *34*, 237–256.
- Watanuki, Y., Daunt, F., Takahashi, A., Newell, M., Wanless, S., Sato, K., & Miyazaki, N. (2008). Microhabitat use and prey capture of a bottom-feeding top predator, the European shag, shown by camera loggers. *Marine Ecology Progress Series*, *356*, 283–293.
- Werner, E. E., & Hall, D. J. (1974). Optimal foraging and the size selection of prey by the bluegill sunfish (*Lepomis Macrochirus*). *Ecology*, *55*, 1042–1052.
- Wiebe, P. H., Boyd, S. H., Davis, B. M., & Cox, J. L. (1982). Avoidance of towed nets by the euphausiid *Nematoscelis megalops*. *Fishery Bulletin*, *80*, 75–91.
- Wiebe, P. H., Lawson, G. L., Lavery, A. C., Copley, N. J., Horgan, E., & Bradley, A. (2013). Improved agreement of net and acoustical methods for surveying euphausiids by mitigating avoidance using a net-based LED strobe light system. *ICES Journal of Marine Science*, *70*, 650–664.
- Williams, R., & Robins, D. (1979). Calorific, ash, carbon and nitrogen content in relation to length and dry weight of *Parathemisto gaudichaudi* (Amphipoda: Hyperiidea) in the North East Atlantic Ocean. *Marine Biology*, *52*, 247–252.
- Wilson, R. J., & Heath, M. R. (2019). Increasing turbidity in the North Sea during the 20th century due to changing wave climate. *Ocean Science*, *15*, 1615–1625.
- Winberg, G. (1960). Rate of metabolism and food requirements of fishes. *Fisheries Research Board of Canada Translation Series*, *194*.
- Winslade, P. (1974a). Behavioural studies on the lesser sandeel *Ammodytes marinus* (Raitt) II. The effect of light intensity on activity. *Journal of Fish Biology*, *6*, 577–586.
- Winslade, P. (1974b). Behavioural studies on the lesser sandeel *Ammodytes marinus* (Raitt) III. The effect of temperature on activity and the environmental control of the annual cycle of activity. *Journal of Fish Biology*, *6*, 587–599.
- Winslade, P. (1974c). Behavioural studies on the lesser sandeel *Ammodytes marinus* (Raitt) I. The effect of food availability on activity and the role of olfaction in food detection. *Journal of Fish Biology*, *6*, 565–576.
- Wood, S. N. (2011). Fast stable restricted maximum likelihood and marginal likelihood estimation of semiparametric generalized linear models. *Journal of the Royal Statistical Society (B)*, *73*, 3–36.
- Wright, P. J., & Bailey, M. C. (1993). Biology of sandeels in the vicinity of seabird colonies at Shetland. *Marine Laboratory Aberdeen Fisheries Research Report*, *15/93*.

- Wright, P. J., & Bailey, M. C. (1996). Timing of hatching in *Ammodytes marinus* from Shetland waters and its significance to early growth and survivorship. *Marine Biology*, *126*, 143–152.
- Wright, P. J., Christensen, A., Régnier, T., Rindorf, A., & van Deurs, M. (2019). Integrating the scale of population processes into fisheries management, as illustrated in the sandeel, *Ammodytes marinus*. *ICES Journal of Marine Science*, *76*, 1453–1463.
- Wright, P. J., Jensen, H., & Tuck, I. (2000). The influence of sediment type on the distribution of the lesser sandeel, *Ammodytes marinus*. *Journal of Sea Research*, *44*, 243–256.
- Wright, P. J., Orpwood, J. E., & Scott, B. E. (2017a). Impact of rising temperature on reproductive investment in a capital breeder: The lesser sandeel. *Journal of Experimental Marine Biology and Ecology*, *486*, 52–58.
- Wright, P. J., Orpwood, J. E., & Boulcott, P. (2017b). Warming delays ovarian development in a capital breeder. *Marine Biology*, *164*, 80.
- Wright, P. J., Régnier, T., Gibb, F. M., Augley, J., & Devalla, S. (2018). Identifying stock structuring in the sandeel, *Ammodytes marinus*, from otolith microchemistry. *Fisheries Research*, *199*, 19–25.
- Xie, S., Zhu, X., Cui, Y., Wootton, R. J., Lei, W., & Yang, Y. (2001). Compensatory growth in the gibel carp following feed deprivation: temporal patterns in growth, nutrient deposition, feed intake and body composition. *Journal of Fish Biology*, *58*, 999–1009.
- Zhu, X., Xie, S., Lei, W., Cui, Y., Yang, Y., & Wootton, R. J. (2005). Compensatory growth in the Chinese longsnout catfish, *Leiocassis longirostris* following feed deprivation: Temporal patterns in growth, nutrient deposition, feed intake and body composition. *Aquaculture*, *248*, 307–314.